THE ASTROPHYSICAL JOURNAL

AN INTERNATIONAL REVIEW OF SPECTROSCOPY AND ASTRONOMICAL PHYSICS

VOLUME 100 NOVEMBER 1944 NUMBER 3

THE ECLIPSING SYSTEM SX CASSIOPEIAE

SERGEI GAPOSCHKIN

Harvard College Observatory

Received July 15, 1944

ABSTRACT

The eclipsing system SX Cassiopeiae has been studied on the basis of 2046 photographic observations, in addition to the 537 visual observations published by Dugan and to the spectrographic results of Struve. The relative dimensions are as follows:

Mean radius: G6, 0.200 (pg), 0.250 (vis); A6, 0.044 (pg), 0.118 (vis)
Luminosity: G6, 0.36 (pg), 0.46 (vis); A6, 0.64 (pg), 0.54 (vis)
Ratio of surface brightnesses (A6/G6): 36.9 (pg), 5.3 (vis)
Ratio of radii (A6/G6): 0.22 (pg), 0.47 (vis)
Inclination of orbit: 87.7° (pg), 88.3° (vis)
Masses of both components (adopted): 5 ⊙
Radii: G6, 19 ⊙ (pg), 22 ⊙ (vis); A6, 4 ⊙ (pg), 10 ⊙ (vis)
M_{vis}: G6, +0.09 (pg), −0.23 (vis); A6, +0.60 (pg), −1.39 (vis)

The writer's photographic dimensions agree exactly with those determined by Gerasimovič in 1927.

The chief result of the investigation is that the radius of the blue component is smaller, the shorter the wave length. SX Cassiopeiae provides the first conspicuous example of this phenomenon. A comparison with Struve's spectroscopic observations suggests that the peculiarity of the bluer component is associated with a thick atmosphere, which surrounds not only the A6 star but probably the whole system and is asymmetrical in distribution.

I. INTRODUCTION

The eclipsing stars have been chiefly responsible for our knowledge of the radii and temperatures of stars in general. They have also been responsible for fostering our ideas concerning the internal constitution of stars. It now appears that the eclipsing stars compel us to conclude that our conception of the radius of a star should be, if not greatly modified, at least more precisely defined.

During the last decade the scope of the study of eclipsing stars has been greatly extended by the recognition of such systems as RY Scuti,[1] the Wolf-Rayet eclipsing stars HV 11086,[2] HV 11111 (V 444 Cygni[3]), W Serpentis,[4] and the supergiant systems VV

[1] S. Gaposchkin, *Harvard Ann.*, **105**, 509, 1937; D. Popper, *Ap. J.*, **97**, 394, 1943.

[2] S. Gaposchkin, *Ap. J.*, **100**, 242, 1944.

[3] S. Gaposchkin, *Ap. J.*, **93**, 202, 1941; O. C. Wilson, *Ap. J.*, **91**, 379, 1940.

[4] S. Gaposchkin, *Harvard Ann.*, **105**, 511, 1937.

Cephei,[5] ϵ Aurigae,[6] and S Doradus.[7] But the system of SX Cassiopeiae is the first (and that of RX Cassiopeiae the second) in which the radius of a star is found to be different in different wave lengths. It seems, therefore, that these stars open a new and promising field in the heterochromatic study of eclipsing stars for the purpose not of determining color indices but of examining the dependence of apparent dimensions on wave length.

Struve[8] has recently published a detailed paper on the spectroscopic behavior of the system SX Cassiopeiae. He finds that, in order to harmonize most of the peculiarities of the system, an extensive gaseous envelope must be supposed to surround one or both components. The results of our photographic work, combined with the visual studies of Dugan, seem not only to confirm the work of Struve but to go further.

II. HISTORICAL REVIEW

The variability of SX Cassiopeiae was discovered by Mme W. Ceraski[9] on Moscow photographic plates in 1909, and the eclipsing nature of the star was suggested by the discoverer and confirmed by S. Blažko and S. Enebo[10] in 1908. Since that time, many visual observations have been made sporadically by several observers, and the first set of relative dimensions was given in 1913 by H. Shapley[11] on the basis of the visual observations of Luizet, whose observations, though not numerous (98), were on a scale consistent with the international scale, as was later confirmed by Dugan. Later the relative dimensions were computed by M. Fowler and B. W. Sitterly,[12] by B. P. Gerasimovič[13] (on the basis of his photographic light-curve), and by R. S. Dugan.[14] Detailed bibliographies will be found in the papers of Dugan,[14] Gaposchkin,[15] and Struve.[8]

III. THE PHOTOGRAPHIC OBSERVATIONS

The brightness of the star was estimated on 2046 Harvard patrol plates. Most of the estimates were made by Miss Virginia Brenton, and about 300 were made by the writer. The greater part of the reduction was carried out by Dr. Richard Prager, who confirmed Dugan's period (36.56757 days), which was not very different from the one obtained from Harvard plates by Gerasimovič (36.5668 days). In agreement with the two latter investigators, Prager found no appreciable change of period during the interval studied.

The comparison stars were those used by Gerasimovič, with a few additional stars included as a check. Since the results derived from the photographic light-curve seem to be important, the author undertook a redetermination of the magnitudes of the comparison stars with reference to the North Polar Sequence. Since no new plates were available for the purpose, several intermediate sequences were used to bridge the interval between the North Polar Sequence and the variable, referring to the NPS stars Nos. 8, 9, 10, 11, 12, 13, 15, 17, and 18.

Since the comparison of the photographic and the visual light-curves is an important part of the present paper, the writer has also determined the photovisual magnitude of the star used by Dugan as a comparison star in his photometric work. The stars used in this comparison were NPS Nos. 10, 11, 12, 13. In addition, the magnitudes were referred

[5] S. Gaposchkin, *Harvard Circ.*, No. 421, 1937; V. Goedicke, *Pub. Obs. U. Michigan*, Vol. 8, No. 1, 1939; O. Struve, *Ap. J.*, 99, 70, 1944.

[6] G. Kuiper, O. Struve, and B. Strömgren, *Ap. J.*, 86, 575, 1937.

[7] S. Gaposchkin, *Ap. J.*, 97, 166, 1943.

[8] *Ap. J.*, 99, 89, 1944.

[9] *A.N.*, 176, 218, 1907. [10] *A.N.*, 177, 221, 1908.

[11] *Pop. Astr.*, 21, 142, 1913; *Princeton Contr.*, No. 3, 1915.

[12] *Ap. J.*, 53, 165, 1921.

[13] *Harvard Bull.*, No. 852, p. 18, 1927. [14] *Princeton Contr.*, No. 13, 1933.

[15] *Veröff. U. Sternw. Berlin-Babelsberg*, Vol. 9, Part V, 1932.

to the near-by photovisual sequence for RY Cassiopeiae.[16] The magnitudes of the comparison stars are summarized in Table 1. They are in good agreement, except for a small difference in zero point, with those used by Gerasimovič.

Table 2 contains the photographic light-curve, derived from 2046 observations. It is represented in Figure 1. The characteristics of the light-curve may be summarized as

TABLE 1

COMPARISON STARS FOR SX CASSIOPEIAE

Designation (Gerasimovič)	IPg	IPv
b	$9^m12 \pm 0^m08$ (m.e.)	.....
c	9.91± .07	.....
d	10.31± .08	.....
e*	10.63± .06	$10^m12 \pm 0^m06$
f	11.18±0.06	.....

* Dugan's comparison star.

TABLE 2

PHOTOGRAPHIC LIGHT-CURVE OF SX CASSIOPEIAE

Phase*	IPg	No. of Obs.	Phase	IPg	No. of Obs.	Phase	IPg	No. of Obs.	Phase	IPg	No. of Obs.
0.010	9^m55	41	0.411	9^m58	27	0.748	9^m72	6	0.815	10^m24	5
.030	9.55	36	.430	9.57	31	.750	9.74	3	.817	9.82	4
.049	9.54	40	.451	9.55	31	.751	9.91	3	.821	9.63	2
.071	9.54	46	.470	9.55	47	.753	10.20	2	.823	9.58	9
.090	9.53	46	.490	9.56	39	.754	10.30	3	.828	9.58	3
.111	9.53	40	.509	9.56	46	.755	10.37	3	.832	9.55	9
.130	9.54	38	.530	9.55	45	.756	10.61	6	.840	9.57	19
.151	9.54	44	.550	9.55	39	.759	10.69	13	.852	9.58	28
.169	9.55	40	.571	9.55	43	.763	10.71	15	.871	9.59	47
.190	9.57	30	.590	9.56	43	.768	10.72	10	.890	9.57	43
.211	9.59	57	.609	9.58	39	.773	10.76	6	.911	9.57	40
.230	9.60	39	.630	9.59	40	.778	10.74	12	.930	9.58	47
.250	9.61	46	.651	9.59	30	.784	10.71	16	.950	9.57	36
.272	9.62	38	.670	9.58	39	.788	10.69	11	.971	9.56	44
.288	9.62	26	.690	9.59	40	.793	10.71	12	0.990	9.55	48
.318	9.62	42	.711	9.60	33	.798	10.71	18			
.330	9.61	43	.728	9.61	30	.803	10.74	8	Total	.....	2046
.349	9.61	46	.736	9.62	11	.806	10.73	13			
.370	9.59	48	.742	9.64	10	.810	10.66	3			
0.390	9.59	38	0.747	9.65	6	0.812	10.65	6			

* Reckoned from JD 2,400,000 as zero. Throughout this paper, phases are expressed in terms of the period, not in days.

follows: (1) the eclipse at the primary minimum is total; (2) the secondary minimum is definitely present and falls almost exactly between primary minima; (3) there are indications of a small ellipticity; (4) the maxima differ in height by 0.02 mag.; (5) there is a small fluctuation during totality, apparently of about two days' duration; and (6) there is a small "flash" just after primary minimum. If we compare our light-curve with that of Gerasimovič, we shall see that the two are identical in points 1, 2, 3, 4, and probably 5.

[16] S. Gaposchkin, *Harvard Ann.*, Vol. **108**, No. 1, 1939.

IV. COMPARISON WITH DUGAN'S VISUAL LIGHT-CURVE

It is easy to see that the steepness of the ascending and descending branches of the photographic light-curve and the well-defined durations of eclipse and totality define the ratio of the radii within narrow limits. Before computing the radii it is necessary to correct for ellipticity; the effective ellipticity, z, was found to be 0.05. The relative dimensions were then computed for uniform brightness, since, for this star, as for HV 11086,[3] ordinary limb darkening needs modification and the theory of S. Kosirev[17] for extended and ejected atmospheres seems to be more applicable. The computations with ordinary

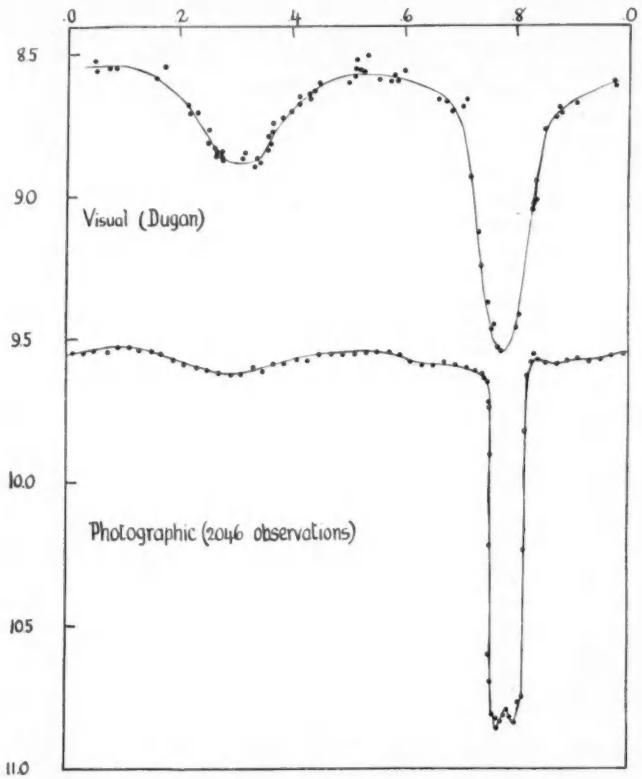

FIG. 1.—Mean light-curves for SX Cassiopeiae: visual above, photographic below. Ordinate and abscissa are magnitude and phase (reckoned from JD 2,400,000).

limb darkening were made by Gerasimovič in connection with his photographic light-curve, with the result that the agreement is as good as with the uniform solution—a result that we shall confirm later. Dugan[14] found that for his visual light-curve the ordinary darkened solution is less satisfactory than the uniform solution. Therefore, in comparing the results of the various solutions we have selected the uniform solutions only.

Table 3 gives a comparison of the results obtained by Dugan from his visual light-curve (537 observations) with those of Gerasimovič (990 photographic observations) and the wholly independent light-curve of the writer (2046 observations). The zero point of Dugan's magnitudes is referred to star "e" of Table 1; any uncertainty in the magnitude of this star will affect the color indices and the deduced distance of the star but not, of

[17] *M.N.*, **94**, 430, 1934.

course, the elements of the system, since Dugan's scale is correct. The duration of totality for Dugan's curve was taken not from his original paper but from his "Finding List for Eclipsing Variables."[18] It may be mentioned that Dugan made an arbitrary correction to the observations on different nights to eliminate the large scatter, with the result that the duration of eclipse, given here, may be regarded as a minimal value.

As has already been reported in *Popular Astronomy*[19] and as may be seen from Figure 1, the outstanding difference between photographic and visual light-curves is in the duration of eclipse and of totality, and also the ellipticity. These differences cause the differences of relative radii shown by Table 3. All possible sources of error, including those of

TABLE 3

COMPARISON OF PHOTOGRAPHIC AND VISUAL RESULTS FOR SX CASSIOPEIAE

	Visual	Photographic	
	Dugan	Gerasimovič	Gaposchkin
Period	$36^d.56756$	$36^d.5668$	$36^d.56756$
Maximum	$8^m.55$	$9^m.84$	$9^m.54$
Minimum$_1$	9.54	10.95	10.70
Minimum$_2$	8.87	9.92	9.62
Range$_1$	0.99	1.11	1.16
Range$_2$	0.32	0.08	0.08
l_1-l_2	$0^p.5$	$0^p.5$	$0^p.5$
Duration of eclipse	$3^d.4=0^p.1022$	$2^d.6=0^p.0711$	$2^d.7=0^p.0749$
Duration of totality	$1^d.3=0^p.0355$	$1^d.8=0^p.0492$	$1^d.8=0^p.0492$
Type of eclipse	Total	Total-Central	Total
Inclination	88.3°	90.0°	87.7°
Luminosity$_1$	0.46*	0.38	0.36
Luminosity$_2$	0.54	0.62	0.64
Radius$_1$	0.250	0.200	0.200
Radius$_2$	0.118	0.044	0.044
Ellipticity (b/a)	0.85	0.95	0.96
Radius, A6 component	10 ⊙	.....	4 ⊙
Radius, G6 component	22 ⊙	.....	19 ⊙
Mass, A6 component	5 ⊙	.....	5 ⊙
Mass, G6 component	5 ⊙	.....	5 ⊙
Density, A6 component	0.050 ⊙	.....	0.080 ⊙
Density, G6 component	0.0005 ⊙	.....	0.0007 ⊙

* Star in front at primary minimum.

magnitude scale and of zero point, are inadequate to change appreciably the results given in Table 3. It is noteworthy that the results of Gerasimovič, obtained in 1927 from an independently determined photographic light-curve, are so nearly identical with those obtained by the writer from a greater amount of material. It is perhaps surprising that Dugan did not discuss more thoroughly the well-determined light-curve of Gerasimovič when he published his own visual observations. The inclinations determined by Gerasimovič, Dugan, and the writer are almost identical.

V. INTERPRETATION OF THE RESULTS

The difference in the computed radii for the A6 star poses an interesting physical problem. Struve has found this star to have many spectroscopic peculiarities, which he interprets in terms of a great surrounding mass of gas. We may picture a simple model in which the A6 component is imbedded in an extensive atmosphere—so extensive as to in-

[18] *Princeton Contr.*, No. 15, 1934. [19] L. Campbell, *Pop. Astr.*, **52**, 200, 1944.

clude the G6 component and, accordingly, the whole system. The distribution of density is such that the apparent limb of the star is farther from the center in visual than in photographic light, so that the apparent radii are different in different wave lengths. The light-curves, visual and photographic, are the integrated effects of two gaseous configurations with indefinite boundaries. We conventionally interpret light-curves only in terms of sharply bounded disks, whose sizes are not appreciably modified by the ordinary conception of limb darkening. However, the theory of Kosirev for stars with thick atmospheres leads to an exaggerated law of darkening,[20] which may considerably affect the apparent radius of the star.

Struve finds that there are streams of gas around the A6 component and, to a lesser extent, around the G6 component; and this seems to justify us in applying the Kosirev[17] theory to SX Cassiopeiae. Starting with a ratio of radii 0.5 (close to that of Dugan), an inclination of 90°, and a center-limb ratio of 500 for the A6 component, we determined the form of the eclipse by graphical methods. The effect is to shorten the apparent duration of the eclipse and to increase the steepness of the branches. The direction of the effect on the form of the light-curve seems to be in agreement with the observations; but the problem is still complicated, and we shall not consider it further here.

Our conclusions are of wider scope than a comparison of Dugan's visual with our photographic results. A new approach to the study of eclipsing stars is suggested. They should be studied in a variety of colors, not only from the standpoint of color indices—in itself a small problem—but as an approach to the study of the structure of the outer layers of the stars and the envelopes of the eclipsing systems. It is probable that for many eclipsing stars, such as Algol, the conception of a sharply defined radius is legitimate. But there are many other systems in which this will probably prove not to be the case, and such systems may have been missed in the past. Such a classical eclipsing system as U Cephei, for example, may furnish an illustration. From H. Rosenberg's[21] heterochromatic study of this star one might obtain confirmation if the observations had been published in detail. In a comparison of the visual light-curve by Dugan[22] and the photographic light-curves determined by R. H. Baker,[23] N. Tchudovischev,[24] and the writer, we find that the duration of the photographic eclipse is about $0^{p}.02$ shorter than the visual. The difference is small and may be accidental, but it is at least interesting that it has the same sign as that found for SX Cassiopeiae. Struve[8] has suggested that the distortion of the velocity-curve of the A star in U Cephei is indicative of an atmospheric layer that does not extend to so great a height as the envelope of the A6 star in SX Cassiopeiae (whose velocity-curve is similarly distorted); the former is a main-sequence star, the latter a supergiant, and the difference of the effect that is detected from the light-curves is in accordance with these dimensions.

VI. DERIVATION OF ABSOLUTE DIMENSIONS

Struve has not observed the velocity-curve for the G6 component and gives only the mass function for the A6 component. Therefore, the masses are undetermined from the spectroscopic point of view. We shall therefore make use of the relation derived by the writer[25] to evaluate them. We shall adopt the same effective temperature for both visual and photographic elements. The masses are determined as follows:

$$\text{A6 component: } 7.3\ \odot\ (\text{vis}); \quad 3.5\ \odot\ (\text{pg}),$$

$$\text{G6 component: } 6.0\ \odot\ (\text{vis}); \quad 5.2\ \odot\ (\text{pg}).$$

[20] F. L. Whipple and C. Payne-Gaposchkin, *Harvard Circ.*, No. 314, 1937.

[21] *Ap. J.*, **83**, 67, 1936.

[22] *Princeton Contr.*, No. 5, 1920.

[23] *Laws Obs. Bull.*, No. 30, 1921.

[24] *Bul. Engelhardt Obs., Kasan U.*, No. 17, 1939.

[25] *Harvard Rept.*, No. 201, 1940.

The fainter component is photographically heavier than the brighter—a possibility already suggested by Struve. Since the difference is not great, we adopt the masses of both to be equal to 5 ⊙. This value is smaller than would be deduced from Struve's mass function. But a small change in the mass ratio produces a considerable change in the mass computed from the mass function, and the adopted mass is well within the possible values for its spectral type. If we adopt a mass ratio in accordance with the ratio of luminosities, the mass of the brighter component is about 5 ⊙.

VII. REDETERMINATION OF THE PHOTOGRAPHIC ELEMENTS

We derived the above results in the usual manner. Z. Kopal[26] has suggested some modifications in the computation; his method is similar in many respects to that of J. Fetlaar.[27] We have used 46 equations outside the eclipse, of the form:

$$l = a - b \cos \theta - c \cos^2 \theta ,$$

where l is the observed intensity, a is the brightness at maximum, b is the constant of the reflection effect (previously adopted to be zero), and c is the constant of ellipticity (usually designated z). The values of the constants were determined as

$$a = 0.9874 \pm 0.0008 ; \qquad b = -0.0042 \pm 0.0025 ; \qquad c = 0.0433 \pm 0.0024 .$$

In other words, the reflection effect is practically zero, and the ellipticity is 0.043—in close agreement with the value (0.05) adopted earlier.

The rectified ranges then are 1.13 mag. and 0.03 mag. Using, then, the well-known formula expressing the loss of light at minima and ratio of radii, k, we find that the ratio of radii is 0.28, close to the adopted one (0.22). In addition, the value of k was computed with a coefficient of limb darkening 0.6, in the manner suggested by Kopal:

$$k^2 (1 - x)\, qx = 1 - \frac{\lambda_2}{\lambda_1},$$

where k is the ratio of radii, x is $\frac{1}{2}$, and q is a function tabulated by J. Ferrari.[28] After several approximations we find a value of 0.28 for k, identical with that for the undarkened solution. The computation of the relative radii followed at once with this value of k: the additional function, p, necessary for the inclusion of limb darkening, was taken from the tables of W. Zessewitsch;[29] and the computed radii are as follows:

Radius, G6 component: 0.174 (U); 0.189 (D),

Radius, A6 component: 0.044 (U); 0.045 (D).

Both values are close to those given in Table 3.

VIII. COLOR INDICES OF THE COMPONENTS

It is interesting to compute the theoretical color indices of the system during totality, since in SX Cassiopeiae both radii and surface brightnesses are different in different wave

[26] *Harvard Reprint.*, No. 229, 1941.

[27] *Utrecht Obs. Pub.*, No. 9, 1923.

[28] *Acad. Sci., Vienna*, **148**, 221, 1939.

[29] W. Zessewitsch, *Acad. Sci. U.S.S.R. Bull.*, No. 50, 1941.

lengths. The author derived a simple relation for computing the color index at any phase;[30] the color index during totality is

$$\mathrm{CI} = 2.51 \log \frac{r_{\mathrm{vis}}^2 J_{\mathrm{vis}}}{r_{\mathrm{pg}}^2 J_{\mathrm{pg}}}.$$

Adopting[25] the ratio of surface brightness ($J_{\mathrm{vis}}/J_{\mathrm{pg}}$) to be 2, we find the predicted color index during totality to be 1.25 mag., while the observed one is 1.27 mag. This agreement tends to confirm the zero point of the magnitudes, though the uncertainty not only of observations but of computations must not be forgotten.

IX. COMPARISON WITH SPECTROSCOPIC RESULTS

The spectroscopic phenomena are more numerous and more difficult to interpret than the photometric ones, which refer to an integrated effect. Struve's outstanding result was

TABLE 4

COMPARISON OF SPECTROSCOPIC AND PHOTOGRAPHIC PHENOMENA FOR SX CASSIOPEIAE

Phase	Spectroscopic	Photographic	Inference
−0.08	Red emission strengthened	1.5 days before beginning of eclipse	Violet emission extends over $10R_A$
−0.04	Red emission 3.5 times stronger than violet	Eclipse begins	Most of violet eclipsed
−0.02–0.00	Red emission equal to violet emission	From beginning of totality to mid-eclipse	Violet emission extends higher above A component than red
0.00–0.02	Violet emission 5.5 times red emission	From mid-eclipse to end of totality	
0.025	Red emission disappears	Just at end of totality	Red emission extends to less distance than violet, not more than $6R_A$
0.05	Violet still stronger than red emission	Out of eclipse, but close to its end	Red emission begins to be visible between stars
0.12	Violet emission is equal to red emission	Quite out of eclipse	

that the apparent orbit of the A6 component is far from the circular form that all the photometric data would lead us to expect. In fact, the apparent eccentricity is 0.5—the largest ever reported for an eclipsing system. Struve has explained this glaring inconsistency by the suggestion that the motion of the A6 star is distorted by the additional motion of some gases surrounding it. The photographic results do not throw any light on these motions, but the photographic light-curve seems to be in better accord with the spectroscopic results than the visual light-curve. The correspondence is shown in Table 4.

There are two photometric phenomena that should be mentioned in connection with Table 4. The first is a small increase of brightness during the second half of totality, that is, when the violet emission is strengthening. The other is the "flash," a slight increase of brightness just after the total eclipse. This is perhaps associated with the spectroscopic

[30] *Pub. A.A.S.*, **9**, 122, 1938.

observation that the red emission is again visible at the corresponding phase and with the appearance of the "hot stream" described by Struve. In addition, the brighter of the two maxima is associated with the fact that the red emission is equal to, if not stronger than, the violet emission, while the fainter of the two maxima corresponds to a much stronger violet emission. These observations imply that the distribution of the gaseous envelope is unsymmetrical, as has already been suggested by Struve.

The secondary minimum is photographically inconspicuous and does not lend itself to detailed comparison with the spectroscopic observations. But the visual minimum is well marked, and Dugan's observations show that it is by no means symmetrical. The question of the symmetry of the primary minimum cannot be settled from the photographic light-curve, because individual minima are not observed; but it can be said that, because the period seems to be quite constant, any considerable asymmetry should be easily detectable. The observed small difference in slope of the rising and falling branches of the primary minimum would indicate that the violet emission extends to a higher level than the red emission, in agreement with the spectroscopic conclusions.

X. GENERAL CONCLUSIONS

The most significant result of the present paper is the conclusion that the radii of the components, especially the bluer one, depend on the wave length. If we were to assume that the change of radius is a linear function of the wave length, we should conclude that at wave length 10,000 A the radii would be equal and the components in contact. The ellipticity would clearly also increase; but, since most probably the two components differ in ellipticity, it is difficult to predict the progress of the effect with wave length. Heterochromatic studies are strongly indicated for this and similar stars.

If the results for SX Cassiopeiae are confirmed in other systems (as they seem to be for RX Cassiopeiae[31]), the conclusions on internal constitution, which have been drawn so extensively from eclipsing variables,[32] may require some modification in view of the necessary redefinition of the dimensions of the stars.

[31] S. Gaposchkin, *Ap. J.*, **100**, 230, 1944.

[32] C. Payne-Gaposchkin and S. Gaposchkin, *Harvard Reprint.*, Ser. 2, No. 2, 1943.

THE ECLIPSING SYSTEM RX CASSIOPEIAE

SERGEI GAPOSCHKIN
Harvard College Observatory
Received July 15, 1944

ABSTRACT

The photographic light-curve (2037 observations) and visual light-curve (324 observations) are combined with Struve's spectroscopic results to determine the relative and absolute dimensions. The whole light-curve undergoes a variation of range 0.46 mag. and period 517.6 days. The photographic light-curve shows a difference of 0.16 mag. between the maxima—the largest ever observed. An additional drop of brightness, of 0.08 mag., occurs just before primary minimum. The visual light-curve shows a much larger ellipticity of the components than the photographic light-curve. The relative dimensions are as follows:

Major axis: G3, 0.39 (pg), 0.36 (vis); A5, 0.17 (pg), 0.28 (vis)
Luminosity: G3, 0.43 (pg), 0.36 (vis); A5, 0.57 (pg), 0.64 (vis)
Ratio of surface brightnesses (A5/G3): 7.2 (pg), 2.8 (vis)
Ratio of radii (A5/G3): 0.43 (pg), 0.8 (vis)
Inclination of orbit: 78.8° (pg)

The masses of both components are about 7 ⊙.

Radii: G3, 37 ⊙ (pg), 32 ⊙ (vis); A5, 16 ⊙ (pg), 26 ⊙ (vis)
M_{vis}: G3, −1.4 (pg), −1.4 (vis); A5, −1.9 (pg), −1.7 (vis)

As in the system of SX Cassiopeiae, the existence of a considerable gaseous envelope around both components seems to be indicated and is probably responsible for the different apparent radii deduced from the photographic and visual light-curves.

I. GENERAL

The system of RX Cassiopeiae (period 32 days, spectra A5 and G3) is very similar to that of SX Cassiopeiae[1] (period 36 days, spectra A5 and G6). But it seems that the relative physical development of the components is not exactly the same. The components of RX Cassiopeiae are more similar to each other than those of SX Cassiopeiae, and the A component of the latter is probably denser than that of the former. On the other hand, there is a strong similarity in the presence of an extensive envelope around the blue component, as has been shown in O. Struve's spectroscopic studies of the two systems.[2] As in the case of SX Cassiopeiae, the photometric results are in full accordance with the spectroscopic conclusions and also permit us to extend them. The envelope of the bluer star, together with the less dense and less extensive atmosphere of the G star, appears to produce a difference of radii in yellow and blue light and is probably responsible for the distortion of the spectrographic orbit of the A star from circular to eccentric form.

II. THE OBSERVATIONS

The author has estimated the brightness of RX Cassiopeiae on 2037 plates in the Harvard collection. The comparison stars were selected from the visual sequence determined by L. Campbell[3] for the star. All the observations were reduced by Mrs. Payne-Gaposchkin with the assistance of Mr. Paul Deutschkron. The photographic magnitudes of the comparison stars were determined by the writer with reference to the photographic sequences for SX Cassiopeiae[1] and XX Cassiopeiae.[4] The photovisual magnitudes of

[1] S. Gaposchkin, *Ap. J.*, **100**, 221, 1944.

[2] *Ap. J.*, **99**, 295, 1944.

[3] *Harvard Ann.*, **63**, 153, 1913.

[4] S. Gaposchkin, *Harvard Bull.*, No. 900, 13, 1935.

the comparison stars were not determined independently; they were checked by reference to the photovisual magnitudes for SX Cassiopeiae and XX Cassiopeiae, with which they were found to be consistent. The photovisual magnitudes determined for Harvard plates were later combined with the visual measures of O. C. Wendell[5] and of D. Martinoff,[6] both of which are essentially on the visual system of *Harvard Annals*, Volume 63. The photographic magnitude and the visual magnitudes of Campbell and Martinoff are given in Table 1. The probable error of the photographic magnitudes is ± 0.05 mag.

The period given by S. Blažko,[7] 32.315 days, was tested by means of all available minima from JD 24,150,000 to 2,431,000 and found to be correct and constant. Similarly,

TABLE 1

COMPARISON STARS FOR RX CASSIOPEIAE

DESIGNATION	IPG	VISUAL	
		Campbell	Martinoff
d	9^m10	8^m77	8^m76
e	9.88	9.30	9.41
f	10.53	9.84	9.76
g	11.17	10.42	.....
h	11.42	.....	.....

it will be recalled that the period of SX Cassiopeiae has remained constant over an interval of 50 years. The elements of RX Cassiopeiae, derived from our observations, are

$$\text{Minimum} = 2422907.750 + 32^d.315\,E.$$

III. THE INTRINSIC VARIATIONS

All the observations were reduced with the period just given. It was apparent at once that the variation is not perfectly regular, the deviations being such as to suggest that the whole light-curve is at times brighter than at other times. All previous observers had noted a large scatter of the observations about the mean light-curve, and Struve[2] remarked that "it is possible .... that the individual curves do not exactly repeat themselves." In order to detect and examine this effect, the deviations of all the individual observations from the mean light-curve were determined (excluding only the 400 estimations, of lower weight than the rest, made with the small-scale 1¼-inch [AI] camera). The mean deviation was determined separately for each cycle of 32.315 days. The resulting curve of residuals plotted against cycles (reckoned from JD 2,400,000 as zero point) is shown in Figure 1. A rather regular fluctuation in the mean light-curve is apparent from the figure; its period is found to be 517.6 days and its range about 0.45 mag. (both these values being the mean of independent determinations by Mrs. Payne-Gaposchkin and the writer). The observations cover 515 eclipsing cycles; and, as the figure shows, each long-period cycle is covered by sufficient observations to establish the reality and periodicity of the changes. Several other eclipsing stars are known in which an intrinsic variation is superimposed on the eclipsing light-curve, notably ϵ Aurigae, ζ Aurigae, VV Cephei, and S Doradus. None of these, however, has shown a variation of such large range and long period. The peculiar eclipsing variable W Serpentis,[8] which

[5] *Harvard Ann.*, **69**, 190, 1913.

[6] *Trudi Obs. U. Kasan*, No. 26, 18, 1930.

[7] *A.N.*, **172**, 57, 1906.

[8] S. Gaposchkin, *Harvard Ann.*, **105**, 511, 1937.

bears a strong resemblance to RX Cassiopeiae, both in light-curve and spectrum, has an additional variation of about the same range and a period of about 270 days. The RV Tauri stars are known to display a similar change in mean brightness, a notable example being DF Cygni, which has been shown by Miss M. Harwood[9] to display a double periodicity of 49.9 and 790 days. The photometric elements of the intrinsic variation of RX Cassiopeiae are:

$$\text{Maximum} = 2422864.8 + 517^{d}.6\ E\ ;$$

$$\text{Maximum} = 9^{m}.82\ ; \qquad \text{Minimum} = 10^{m}.28\ .$$

The rise is apparently rather steeper than the fall of brightness, and the variation suggests that of a Great Sequence variable. The possibility of attributing the variation to one or other of the components is discussed in a later section.

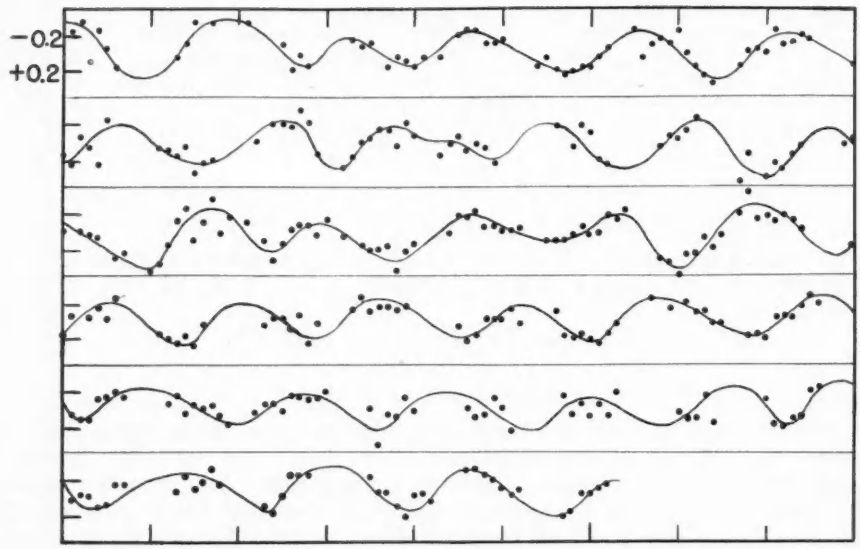

FIG. 1—Long-period variation for RX Cassiopeiae. Abscissas are epochs of the eclipsing light-curve, reckoned from JD 2,400,000 as zero. The first recorded epoch is No. 451; the last, No. 962. Short vertical lines mark intervals of ten epochs (323.15 days). Ordinates are photographic magnitudes, reckoned from mean brightness.

IV. THE PHOTOGRAPHIC LIGHT-CURVE

The observations from 1631 AC plates were combined into the normal points given in Table 2.

Figure 2 shows the mean light-curve in the photographic wave length. The form of the curve is quite extraordinary for an eclipsing star. There are two outstanding characteristics that render it unusual: there is a great difference in the brightness of the two maxima, and there is a peculiar drop in brightness just before the beginning of the primary minimum.

The difference in brightness of the two maxima is so remarkable that confirmation of its reality is desirable. About 400 additional observations were made from plates taken with the $1\frac{1}{4}$-inch AI camera; and these were reduced independently, forming the mean light-curve given in Table 3. There can be no doubt that this light-curve shows the same

[9] *Harvard Ann.*, **105**, 521, 1937.

effect as the other; the AI normal points are shown by circles in Figure 2. It is worth mentioning that some unpublished photographic observations of RX Cassiopeiae, found among Miss H. S. Leavitt's papers, show exactly the same effect. Many eclipsing variables are known to show the so-called "periastron effect," but this usually amounts to two or three hundredths of a magnitude; in RX Cassiopeiae the difference is 0.16 mag. In all our photographic studies of eclipsing stars we have not encountered anything like this difference, except perhaps with W Serpentis. It is not possible to deduce the relative dimensions of the components of the system by ordinary methods without making an arbitrary adjustment of the maximal brightness in the light-curve.

The drop of brightness before primary minimum is not so conspicuous and seems to be an unstable and temporary feature of the light-curve. It is shown also by the light-curve from the AI plates, as may be seen from Figure 2. It resembles the "flash" in the

TABLE 2

PHOTOGRAPHIC MEAN LIGHT-CURVE OF RX CASSIOPEIAE (AC PLATES)

Phase*	IPg	No. of Obs.	Phase	IPg	No. of Obs.	Phase	IPg	No. of Obs.
0.012	10m14	50	0.559	10m27	50	0.867	10m85	10
.042	10.10	50	.586	10.22	50	.876	10.99	10
.078	10.11	50	.612	10.18	50	.884	11.06	10
.108	10.04	50	.642	10.21	50	.890	11.09	10
.137	10.03	50	.672	10.21	50	.897	11.13	10
.167	10.06	50	.699	10.24	50	.901	11.09	10
.201	10.06	50	.725	10.28	50	.909	11.04	10
.232	10.04	50	.750	10.33	50	.914	10.78	10
.264	10.08	50	.777	10.26	50	.918	10.71	10
.290	10.11	50	.809	10.22	50	.923	10.61	10
.315	10.16	50	.829	10.37	10	.930	10.53	10
.350	10.26	50	.834	10.38	10	.937	10.39	10
.388	10.30	50	.839	10.31	10	.942	10.37	10
.427	10.32	50	.843	10.44	10	.962	10.24	50
.452	10.29	50	.847	10.56	10	0.988	10.14	31
.486	10.30	50	.852	10.56	10			
0.525	10.19	50	0.859	10.96	10	Total		1631

* Reckoned from JD 2,400,000 as zero. Throughout this paper, phases are expressed in terms of the period, not in days.

light-curve of SX Cassiopeiae just after the minimum. It has a depth of 0.08 mag.; and it, also, must be arbitrarily removed before the photometric solution can be carried out.

In order to examine the effect of the intrinsic variation upon the light-curve, the observations were divided into four sections, by reference to the long-period light-curve of Figure 1: *I*, maximum brightness; *II*, falling brightness; *III*, minimum brightness; *IV*, rising brightness. The four resulting mean light-curves are shown in Figure 3. In curve *I* the secondary minimum is very shallow, and the drop before primary minimum almost disappears; in curve *III* the secondary minimum is deepest; and in curves *II*, *III*, and *IV*, separately, the drop before primary minimum is conspicuous, though it differs somewhat in phase in the three curves. Table 4 gives the magnitudes of maxima and minima for the four mean light-curves.

The light-curve shows well-known features common to many eclipsing systems: a marked ellipticity (more or less the same from both maxima), and a somewhat asymmetric primary minimum, the rising branch being slightly steeper than the falling one. The maxima are consistent with a constant period. The determination of the dimensions of the system will be carried out by means of the modified mean light-curve in Section VI.

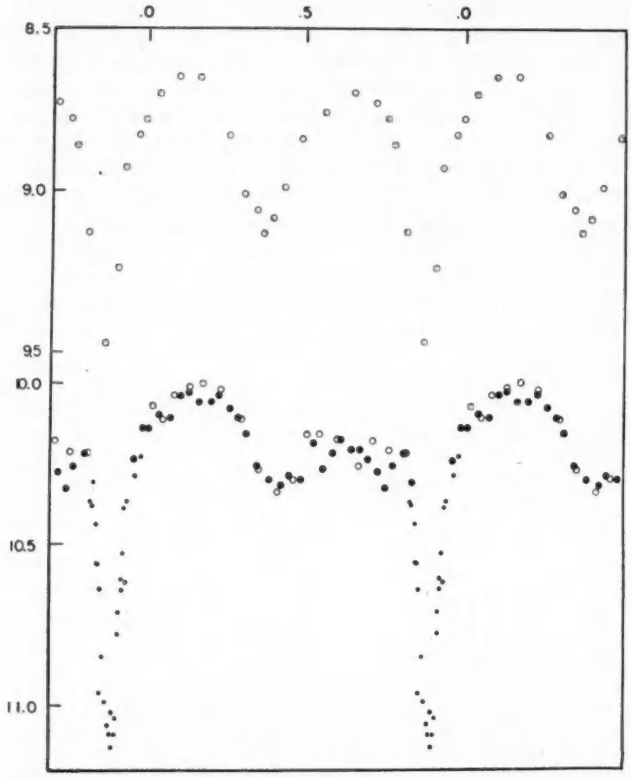

FIG. 2—Mean light-curves for RX Cassiopeiae. *Above*, the visual observations of Wendell and Martinoff and the Harvard photovisual estimates combined into one light-curve. *Below*, photographic curve from Harvard plates. Dots, AM plates (50-point and 10-point means); circles, AI plates (20-point and 10-point means).

TABLE 3

PHOTOGRAPHIC MEAN LIGHT-CURVE OF RX CASSIOPEIAE (AI PLATES)

Phase*	IPg	No. of Obs.	Phase	IPg	No. of Obs.	Phase	IPg	No. of Obs.
0.022.....	10m07	20	0.461.....	10m30	20	0.898.....	11m02	10
.055.....	10.11	20	.504.....	10.16	20	.926.....	10.64	10
.092.....	10.04	20	.541.....	10.16	20	.942.....	10.62	10
.138.....	10.01	20	.605.....	10.18	20	.969.....	10.29	10
.182.....	10.00	20	.670.....	10.26	20	0.988.....	10.23	6
.236.....	10.02	20	.717.....	10.18	20			
.303.....	10.11	20	.763.....	10.21	20	Total....	.....	406
.357.....	10.27	20	.818.....	10.22	20			
0.418.....	10.34	20	0.862.....	10.64	20			

* Reckoned from JD 2,400,000 as zero.

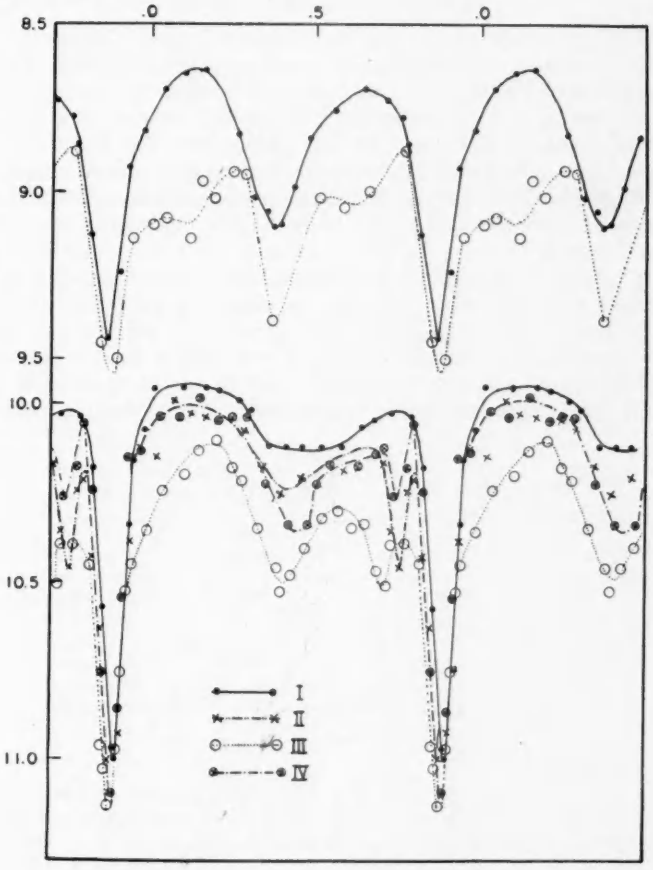

FIG. 3.—Light-curves of RX Cassiopeiae at four stages of the long-period fluctuation: *I*, maximum; *II*, falling brightness; *III*, minimum; *IV*, rising brightness. Symbols are indicated in the figure. Visual curves above; photographic curves below.

TABLE 4

MAGNITUDES FOR INDIVIDUAL MEAN LIGHT-CURVES

Curve	Max_1	Min_2	Max_2	Min_1	A_1	A_2
I	$9^m.97$	$10^m.14$	$10^m.02$	$11^m.17$:	$1^m.20$	$0^m.17$
II	10.01	10.25	10.13	11.17	1.16	0.24
III	10.14	10.52	10.30	11.18	1.04	0.38
IV	10.00	10.36	10.14	11.09	1.09	0.36
Mean	10.04	10.32	10.20	11.13	1.01	0.20

V. THE VISUAL LIGHT-CURVE

The 31 photovisual observations made on Harvard plates showed a considerable scatter; and this, together with their small number, precluded their use in forming a photovisual light-curve. I have therefore combined them with the visual observations of Wendell[5] (123 observations) and Martinoff[6] (170 observations). The same comparison stars and practically the same magnitudes were used for all. The visual mean light-curve is given in Table 5 and in Figure 2. The observations were combined with equal weight.

Like the photographic light-curve, the visual light-curve shows intrinsic fluctuations. This may be seen from the great scatter of Martinoff's observations, which are distributed over a considerable interval. Wendell's observations show less scatter, but it appears that almost all of them were made at the maximum of the long-period fluctuations. In order to examine the effect of the intrinsic variations on the light-curve, the observations were subdivided in the same groups as were formed for the photographic light-curve, the photographic long-period light-curve being again used to decide whether an observation should be assigned to curve *I*, *II*, *III*, or *IV*. It was found that curves *I* (bright) and *III* (faint) were sufficiently represented, and the mean curves for these two

TABLE 5

VISUAL MEAN LIGHT-CURVE OF RX CASSIOPEIAE

Phase*	Vis. Mag.	Phase	Vis. Mag.	Phase	Vis. Mag.
0.038	$8^m.70$	0.395	$9^m.09$	0.775	$8^m.86$
.099	8.65	.432	8.99	.818	9.13
.163	8.65	.484	8.84	.870	9.47
.259	8.83	.557	8.76	.907	9.24
.305	9.01	.646	8.70	.930	8.93
.345	9.06	.715	8.73	.975	8.83
0.367	9.13	0.758	8.78	0.994	8.78

* Reckoned from JD 2,400,000 as zero.

groups are shown in Figure 3. The effects of the intrinsic variation are corroborated; but the small number of visual observations makes it impossible to compare the curves directly, since it cannot be assumed that the curves are truly "synchronized." A special, simultaneous study of the photographic and visual light-curves, a cycle at a time, would be necessary to do this.

The visual light-curve shows two minima, agreeing in phase with those of the photographic light-curve. The secondary minimum is relatively more pronounced than in the photographic curve. The maxima show a difference of only 0.06 mag., as compared with 0.16 mag. for the photographic curve. The minima are of longer duration, and the ellipticities greater, than those obtained from the photographic curve. These conditions are a repetition of those found for SX Cassiopeiae. It is unfortunate that there is for RX Cassiopeiae no visual light-curve comparable in accuracy with the visual light-curve determined for SX Cassiopeiae by R. S. Dugan. The mean visual light-curve suggests that the primary minimum occurs slightly earlier than for the photographic light-curve; it gives an eccentricity equal to zero, which does not contradict the results from the photographic curve. Both photographic and visual light-curves are in full agreement with the spectroscopic observations of the G3 component by Struve, and the whole situation is similar to that found for SX Cassiopeiae. The adopted values for the visual light-curve are as follows:

Max_1	Max_2	Min_1	Min_2	A_1	A_2
$8^m.64$	$8^m.70$	$9^m.47$	$9^m.14$	$0^m.80$	$0^m.47$

VI. THE PHOTOGRAPHIC DIMENSIONS

Since the discovery of RX Cassiopeiae on Moscow plates by Mme L. Ceraski[10] in 1904, only two photometric solutions have been carried out. H. Shapley[11] used the few visual observations of O. C. Wendell[5] to compute the relative dimensions of the system, which he assigned to the third-class orbits of considerable uncertainty. Recently Struve[2] has used the visual light-curve of Martinoff,[6] in combination with his own spectroscopic observations, in deriving the relative dimensions. The important quantities deduced by Shapley and by Struve are tabulated below. Since we have added little material to the mean visual light-curve, our final visual dimensions are similar to those shown in Table 6 (see Sec. VII).

The photographic light-curve was "corrected" in respect to the two peculiarities mentioned in Section IV. Between phases 0.48 and 0.69 a constant correction of 0.162 mag. was added to the magnitudes, thus removing the great difference between the maxima. To remove the dip before primary minimum, the five points at phases 0.699, 0.725, 0.750, 0.777, and 0.809 were combined into one mean, with magnitude 10.26. After making these corrections, the ellipticity of the components (assumed similar for the two) was

RELATIVE DIMENSIONS IN THE SYSTEM OF RX CASSIOPEIAE

	Shapley (U)	Struve
Inclination (i)	83°	75°
Major axis, G3 component	0.27	0.50
Major axis, A5 component	0.27	0.13
Luminosity, G3 component	0.57	0.67
Luminosity, A5 component	0.43	0.33
Ratio of surface brightnesses	1.3	7.3
Ellipticity of components	0.81	0.67

determined, in the usual manner, to be 0.21. The light-curve was then rectified, and the rectified ranges were found to be

$$A_1 = 10^{m}.96 - 10^{m}.02 = 0^{m}.94 ,$$

$$A_2 = 10^{m}.11 - 10^{m}.02 = 0^{m}.09 .$$

It appears that the eclipse at primary minimum is total, with a duration of totality about $0^{p}.02$. The asymmetry of the minimum and the raggedness of the slopes (which are probably results of the intrinsic variation and are difficult to remove) persist in the rectified light-curve.

It has already been shown for SX Cassiopeiae that the conventional correction for darkening does not give significantly better results than the uniform solution. It is probable that for stars with extensive and dense atmospheres the law of darkening will differ from the simple form usually adopted. With these considerations in mind, an undarkened solution has been adopted for RX Cassiopeiae.

For minima of the depths given above and for a total eclipse the ratio of radii is found to be 0.43. The major axis of the G3 component (in front during primary minimum) is 0.391; the inclination of the orbit, 78.8°. The major axis of the smaller (A5) component is 0.168; the ratio of surface brightnesses, 7.2; and the ratio of luminosities, 1.31.

[10] *A.N.*, **164**, 218, 1904.

[11] *Princeton Contr.*, No. 3, 1915; *Ap. J.*, **38**, 158, 1913.

VII. THE VISUAL DIMENSIONS

Our visual light-curve combines all the available observations, and it seems to be worth while to re-examine the visual dimensions. We have proceeded exactly as with the photographic observations, except that there was no need to make arbitrary "corrections" to the maxima. Adopting the mean light-curve that refers to the maximum of the intrinsic variation, we find for the ellipticity a value of 0.30, larger than that derived from the photographic light-curve. As for SX Cassiopeiae, it seems, therefore, that the G component shows the greater effect of ellipticity.

The rectified light-curve gives the following minima:

$$A_1 = 9^m.17 - 8^m.68 = 0^m.49 ,$$

$$A_2 = 8^m.83 - 8^m.68 = 0^m.15 .$$

The rectified light-curve gives no indication of totality; and, as the ranges are small, the ratio of radii is difficult to determine. Therefore we shall use the photographic light-curve as the basis of further discussion. There seems to be no contradiction in assuming that, though radii and effective temperature may differ in visual and photographic light, the inclination of the orbit will be the same for both. We assume that the photographic inclination is applicable to the visual curve. Then we can compute several values of the relative radius of the larger component—the ratio of radii, the eclipsed area, and the function p—as given by Russell and Shapley in 1912, in order to see which ratio of radii is consistent with the photographic inclination. After several trials the ratio 0.8 seemed to be the most satisfactory, as compared with the values 0.4, 0.6, 0.7, and 0.9. The value 0.8 is close to that adopted for the visual observations by Shapley.[11]

VIII. COMPARISON OF PHOTOGRAPHIC AND VISUAL DIMENSIONS

The results obtained in Sections VI and VII are collected in Table 6. It is seen that the blue component is much smaller in photographic light than it is in visual light—a result that recalls the conspicuous difference found for SX Cassiopeiae.[1] Another interesting result is that the smaller component is brighter, both visually and photographically, even though Struve finds that the G spectrum predominates at all phases.

IX. THE ABSOLUTE DIMENSIONS

Although Struve has observed both components, he does not consider that the velocity-curve of the A5 component can be treated as the true orbital velocity, from analogies with SX Cassiopeiae and U Cephei. The velocity-curve of the G3 component is, however, assumed to reflect the orbital motion; it is circular in agreement with the photometric results. It should be noted that the mass function for the G component is rather small for a giant star if the components are assumed of approximately equal mass, in conformity with the observed similarity of range of the velocity-curves. If, on the other hand (as seems likely), the distortion of the velocity-curve of the A5 component has increased the semiamplitude, the actual range is smaller, and the mass of the A5 component is accordingly greater than that of the G3, both being very small (smaller than the sun). Because of this uncertainty, we shall appeal to an indirect method of arriving at the absolute dimensions, to see whether the results are compatible with those derived by Struve. In general, the agreement is satisfactory.

The masses are computed by the method developed by the author,[12] which reposes on Kepler's third law, the Stefan-Boltzmann law, and an adopted mass-luminosity rela-

[12] S. Gaposchkin, *Harvard Reprint*, No. 201, 1940.

tion. The temperatures were adopted according to a table compiled by the writer:[13] for the A5 and G3 spectra the values of temperature used were 7000° and 4500°, not far from the 8000° and 5000° used by Struve.

Since the photographic light-curve is far better observed than the visual, we assume that the "photographic" results are the more correct. If the computation is reversed, so as to calculate what effective temperatures, used in conjunction with the "visual" results, would give the same masses as the photographic curve, we find 5400° for the A5 star and 4800° for the G3. In other words, the energy distribution for the blue star must be greatly distorted.

TABLE 6

RELATIVE DIMENSIONS FOR RX CASSIOPEIAE
PHOTOGRAPHIC AND VISUAL

	Photographic	Visual
Maximum	10^m02	8^m68
Minimum$_1$	11^m13	9^m47
Minimum$_2$	10^m32	9^m14
Major axis, G3 component	0.39	0.36
Major axis, A5 component	0.17	0.28
Ratio of radii	0.43	0.8
Ratio of surface brightnesses	7.2	2.8
Duration of eclipse	$0^p160=5^d2$	$0^p178=5^d7$
Duration of totality	$0^p011=0^d35$	.....
Inclination	78.8°	78.8° (adopted)
Luminosity, G3 component	0.43	0.36
Luminosity, A5 component	0.57	0.64

TABLE 7

ABSOLUTE DIMENSIONS FOR RX CASSIOPEIAE

	Photographic	Visual
Mass, A5 component	6.8 ⊙	10.1 ⊙
Mass, G3 component	6.6 ⊙	5.8 ⊙
Mean radius, A5 component	16 ⊙	26 ⊙
Mean radius, G3 component	37 ⊙	32 ⊙
M_{vis}, A5 component	− 1.9	− 1.7
M_{vis}, G3 component	− 1.4	− 1.4

We adopt the approximate value of 7 ⊙ for the masses of both stars and compute the mean radii. The other dimensions follow in the usual manner, and the results are summarized in Table 7.

The chief result of physical importance is that the earlier component has a much smaller photographic than visual radius. An exactly similar result was obtained for SX Cassiopeiae. In other words, we have here another illustration of the principle that "radius," at least for some stars, must be precisely defined and the simple conception of a definitely bounded disk modified.

The distance between the centers of the stars is determined to be 103.2 ⊙, or 7.17×10^7 kilometers.

[13] C. Payne-Gaposchkin and S. Gaposchkin, *Variable Stars*, p. 50, 1938.

X. ANALYSIS OF THE INTRINSIC VARIATION

In attempting to discover which of the two components is responsible for the intrinsic variation, it is necessary to determine how great must be the variation of one component in order to produce the observed effect on the mean light-curve. From a comparison of curves *I* and *III* for visual and photographic light (Secs. IV and V) the ranges in brightness at the maxima and minima were determined (see Table 8).

Probably the photographic values, based on more reliable light-curves, are more significant than the visual. From Table 8 it is difficult to say which component is respon-

TABLE 8

INTRINSIC VARIATION FOR RX CASSIOPEIAE

	Mean Pg. Mag.	Range Pg. Mag.	Mean Vis. Mag.	Range Vis. Mag.	Photographic Change of Mag.		Visual Change of Mag.	
					A Var.	G Var.	A Var.	G Var.
$Maximum_1$	10.04	±0.17	8.84	±0.34	0.28	0.36	0.50	0.82:
$Maximum_2$	10.18	.27	8.82	.28	.42	.56	.40	.70
$Minimum_1$	11.13	.21	.....	.....	.....	.50	.....	.....
$Minimum_2$	10.33	±0.40	9.11	±0.29	0.64	0.82	0.40	0.70
Mean	.....	.....	.....	.....	0.41	0.56	0.43	0.74

TABLE 9

PRINCIPAL MINIMUM—PHOTOMETRIC AND SPECTROSCOPIC PHENOMENA

Phase*	Spectroscopic	Photometric	Conclusion
−0.13	H lines appear normal	Small drop of 0.1 mag.	
−0.08	Red emission stronger	Beginning of eclipse	Violet side eclipsed
−0.005	Red seven times violet, violet almost gone; red much brighter than blue continuum	Beginning of photographic totality	Most of the violet eclipsed
+0.004	Violet begins to protrude; emissions are single	The end of totality	Red begins to be eclipsed
+0.06	Violet much stronger than red but not in ratio 7:1	Eclipse almost over	Red extends to larger height than violet
+0.09	Spectrum almost normal	Out of eclipse	
$Maximum_1$	Lines of A spectrum weakened; cores of Hβ missing	Much brighter than $Maximum_2$	Asymmetrical distribution of material

* Reckoned from minimum.

sible for the intrinsic variation. The photographic light-curve suggests that the A5 star is variable, because the intrinsic variation seems largest during secondary minimum. This is in line with the statement of Struve that it is the A component and its envelope that undergoes changes (during the eclipsing cycle), not the G component. On the other hand, variability of this type and period has never been found for an A supergiant, whereas for a G supergiant it would not be particularly abnormal. Further observations are needed to decide the question. It is, of course, possible that the intrinsic variation affects the whole system and that the components affect one another, as those of R Aquarii appear to do.[14]

[14] C. Payne Gaposchkin, unpublished.

XI. COMPARISON WITH SPECTROSCOPIC RESULTS

In conclusion, we shall summarize the relation between some of the photometric and spectroscopic phenomena. The observations during eclipse are summarized in Table 9.

It is interesting that Struve finds the G component always visible, while the A is strengthened only during secondary minimum. All of Struve's observations, it should be noted, were made during the maximum of the intrinsic variation. Observations at the minimum would be of interest in the study of the relative strength of the two spectra. At wave length 4000 Struve found that the intensities of the components are approxi-

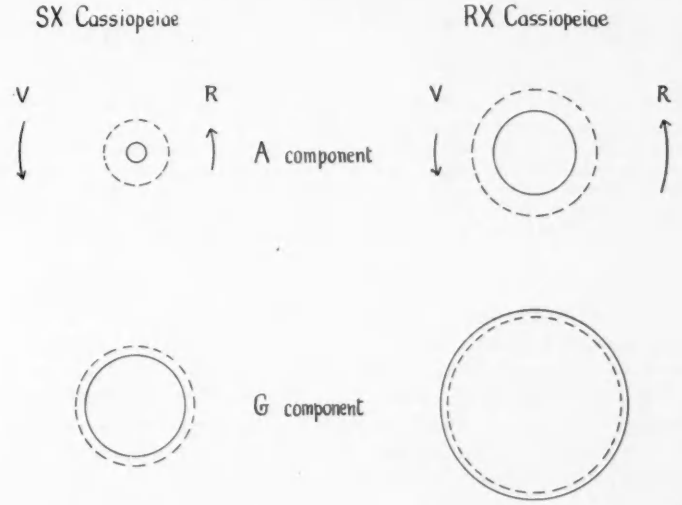

FIG. 4.—Comparison of the systems SX Cassiopeiae and RX Cassiopeiae. Sizes of the systems and the stars are drawn to scale. The continuous lines show the photographic dimensions; the broken lines, the visual dimensions. Arrows show the motion and approximate extent of the gaseous envelopes of the A components.

mately equal. This is not in contradiction with our photometric results. The fact that the G absorption spectrum does not disappear during secondary minimum is also compatible with the inclination and relative dimensions derived in this paper. The seemingly contradictory fact of a total eclipse for the photographic and of a partial eclipse for the visual light-curve is explained by the difference in the relative apparent radii. In the system of SX Cassiopeiae this apparently contradictory situation did not arise, in spite of the difference in photographic and visual radii, because the inclination is nearly 90° and the eclipses are in both cases total.

The dimensions of the two systems are compared in Figure 4.

THE WOLF-RAYET ECLIPSING VARIABLE HV 11086 = HD 214419

SERGEI GAPOSCHKIN
Harvard College Observatory
Received July 15, 1944

ABSTRACT

The star HD 214419, recently studied as a spectroscopic binary by Hiltner, is found to be an eclipsing binary, with a period of 1.641272 days and a β-Lyrae light-curve. The elements are: Min. = JD 2422287.501 + 1.641272 days. The ranges are 0.342 and 0.300 mag. on the IPg scale; the Wolf-Rayet component is eclipsed at primary minimum. The second spectrum is not seen but is computed to be B1. The dimensions are: W star: major axis, 0.323 (= 5.92 ⊙); minor axis, 0.293 (= 5.37 ⊙); mass, 13.9 ⊙; $M_{vis} = -2.5$. B star: major axis, 0.359 (= 6.58 ⊙); minor axis, 0.326 (= 5.97 ⊙); mass, 16.7 ⊙; $M_{vis} = -2.6$. Ratios of surface brightnesses and of luminosities (W : B) are 1.14 and 0.92. The W component of this system has a striking similarity, in its physical properties, to the W component of the system V 444 Cygni. The inconsistency between the spectrum and effective temperature of the latter is shown to be removed by the theory of Kosirev for stars with deep envelopes.

I. INTRODUCTION

The star discussed in the present paper (BD+56° 2818; $\alpha = 22^h31^m15^s$, $\delta = +56°9'.4$, 8.9 mag., 1855) was brought to attention by D. B. McLaughlin and W. A. Hiltner,[1] who found it to be a spectroscopic binary. While engaged in a general survey of the possible variability of Wolf-Rayet stars, I found that the star is variable.[2] Dr. Hiltner was so kind as to send me the manuscript of his paper on the spectroscopic study of the star before publication.[3] The present paper contains an account of my observations on the Harvard patrol plates, which reveal the star as an eclipsing variable, the second of its kind to be detected.

OBSERVATIONAL MATERIAL

THE PERIOD AND ITS VARIATION

Hiltner derives a period of 1.6410 days. In order to verify this period, use was made of 214 observations of minima, obtained from single plates. A discussion of these minima has resulted in a small correction to the period, which is found to be 1.641272 days. All the observations were reduced with this period; and 15 independent light-curves, each covering 1000 days, were formed from the 1795 photographic estimates. The phase of minimum (primary and secondary) was determined independently by two persons for each light-curve, and an unweighted mean of the two estimates was adopted. Table 1 gives the phases of minima for the 15 light-curves. Figure 1 shows the results fo Table 1. The mean interval from primary to secondary minimum is $0^p.5172$ instead of $0^p.5000$, as it would be if the minima were equally spaced. There is no relative shift of the minima during the interval, so that it may be that we have here the case of a "third body" rather than that of "apsidal motion." The excess over half a period may be interpreted as a sign of a small eccentricity, which (if real) would be about 0.03, too small to be detected by ordinary spectroscopic means. Hiltner's assumption that the eccentricity is zero seems, therefore, to be justified.

If the change of the period be supposed to be periodic, our observations show that the period must be at least 80 years. The change of the period, whatever its cause, adds to the

[1] *Pub. A.S.P.*, **53**, 328, 1941.

[2] *Pub. A.A.S.*, **10**, 251, 1942.

[3] *Ap. J.*, **99**, 256, 1944; *McDonald Obs. Contr.*, No. 91, 1944.

TABLE 1

PHASES OF MINIMUM FOR HV 11086

Mean JD	Phase of Primary Minimum*	Phase of Secondary Minimum*	No. of Obs. in Light-Curve
15,500	0.370±0.003	0.898±0.002	59
16,500	.398± .002	.910± .004	146
17,500	.392± .002	.918± .002	145
18,500	.420± .000	.945± .004	116
19,500	.421± .001	.950± .000	57
20,500	.430± .005	.955± .004	78
21,500	.428± .002	.960± .000	124
23,000†	.399± .000	.920± .000	232
24,500	.412± .002	.920± .000	195
25,500	.408± .002	.908± .002	114
26,500	.398± .002	.900± .004	128
27,500	.403± .005	.902± .002	86
28,500	.352± .005	.865± .004	120
29,500	.360± .000	.885± .003	92
30,500	0.342±0.002	0.855±0.002	103
Total	.....	.....	1795
Mean	0.3955	0.9127	.....

* Reckoned from JD 2,400,000 as zero and expressed in terms of the period.

† Standard curve, with which others were compared.

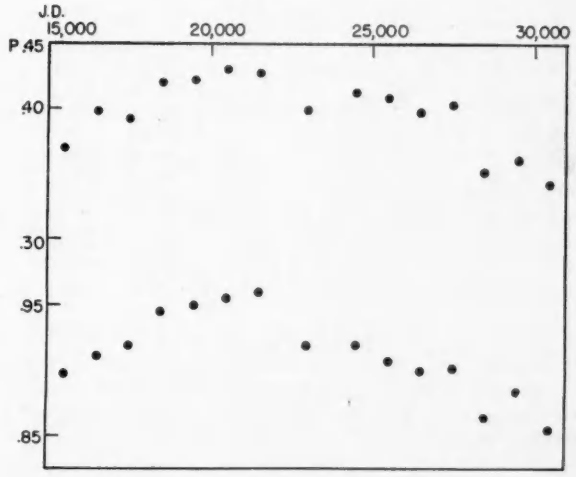

FIG. 1.—Change of period of HV 11086. Ordinates and abscissas are phases of minimum (primary above, secondary below) and Julian days.

complications that are introduced into the study of Wolf-Rayet stars by their inclusion among eclipsing systems.

II. COMPARISON STARS

The original observations were made in terms of a scale unit, which facilitates the procedures of observation and reduction. The scale units, the value of which was later determined, are almost linearly related to the international photographic magnitudes. Five plates, with exposures from 51 to 130 minutes, were used to determine the photographic magnitudes, relative to the photographic sequence determined by V. P. Gerasimovič[4] for SX Cassiopeiae, which I have independently redetermined and confirmed. Three fundamental comparison stars were used, and two others (BD+56°2795 and BD+56° 2797) furnished a check. The adopted magnitudes and their probable errors are given in

TABLE 2

COMPARISON STARS FOR HV 11086

Designation	BD	IPg	Spectrum
a	+56°2813	$8^m74 \pm 0^m04$	A3
b	+56°2815	$8.86 \pm .03$	A0
c	+56°2808	9.53 ± 0.03	.....

TABLE 3

MEAN PHOTOGRAPHIC LIGHT-CURVE OF HV 11086

Phase	IPg	No. of Obs.	Phase	IPg	No. of Obs.	Phase	IPg	No. of Obs.
0.015	9^m28	50	0.391	9^m49	20	0.747	9^m19	50
.040	9.24	50	.402	9.52	20	.775	9.24	50
.067	9.22	50	.409	9.50	20	.806	9.29	50
.094	9.20	50	.419	9.51	20	.839	9.35	50
.119	9.18	50	.436	9.45	50	.869	9.42	50
.151	9.21	50	.469	9.36	50	.892	9.42	20
.172	9.17	50	.497	9.29	50	.903	9.44	20
.194	9.17	50	.522	9.26	50	.913	9.41	20
.220	9.16	50	.549	9.24	50	.928	9.47	20
.247	9.17	50	.579	9.19	50	.936	9.40	20
.276	9.19	50	.603	9.20	50	.956	9.37	50
.306	9.23	50	.630	9.18	50	0.986	9.33	45
.335	9.34	50	.663	9.19	50			
.363	9.43	50	.692	9.18	50	Total	.....	1795
0.381	9.46	20	0.721	9.19	50			

Table 2. The color of star "c" indicates that it is not a red star, probably also around class A. The color of star "a" is consistent with its spectral class; it is slightly redder than star "b," which is the best comparison star from the standpoints of color and constancy, though not of position. On the whole, HV 11086 is situated favorably with respect to the comparison stars.

III. THE PHOTOGRAPHIC LIGHT-CURVE

I have obtained 1795 observations from individual patrol plates; each plate was estimated only once. All the observations were reduced, and the phases corrected for the change of period, by Mr. Paul Deutschkron. Table 3 contains the mean photographic

[4] *Harvard Bull.*, No. 892, 1927.

light-curve. Phases are reckoned from JD 2,400,000 as zero and are expressed in terms of the period.

The light-curve (Fig. 2) shows two well-defined minima, of approximately equal depth, and the character of a β Lyrae curve. The two halves of the light-curve are not quite similar, as may be seen from the following tabulation:

$$\text{Max}_1 = 9^m178 \qquad \text{Min}_1 = 9^m520 \qquad A_1 = 0^m342$$
$$\text{Max}_2 = 9^m170 \qquad \text{Min}_2 = 9^m470 \qquad A_2 = 0^m300$$
$$\text{Minimum} = 2422287.501 + 1^d641272\ E$$

IV. THE PHOTOVISUAL OBSERVATIONS

I have used 31 photovisual plates, most of them at about the middle of the interval covered by the photographic plates. The photovisual magnitudes of the comparison stars were not determined independently; since they are all close to spectral class A and since the photovisual plates are few in number and of low weight in quality, I have limited myself to general inspection. There is no doubt that the variation in visual light is real, though it seems to be slightly smaller than in photographic light. It is especially note-

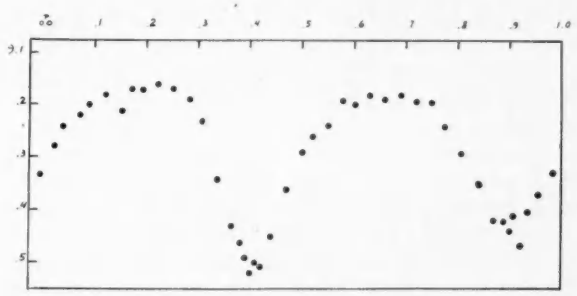

FIG. 2.—Mean light-curve of HV 11086 from 1795 photographic estimations. Ordinates and abscissas are photographic magnitudes and phases (in periods, reckoned from JD 2,400,000).

worthy that the existence of two mimima is confirmed. In this connection the observations made by Hiltner with the Yerkes 40-inch refractor should be mentioned. He seems to have been unable to detect our principal minimum (when the Wolf-Rayet component is eclipsed). It is not at all improbable that the visual and photographic light-curves of an eclipsing system such as the present may differ considerably (as has been shown, for example, for the supergiant eclipsing system SX Cassiopeiae[5]). Future detailed observations in yellow and red light will, no doubt, reveal interesting features of the system. A small over-all variation of the light-curve from cycle to cycle is not improbable.

DISCUSSION

I. GENERAL

From a consideration of the number of observations in one normal point, and the deduced mean error of ± 0.086 mag. for a single estimate, we conclude that the mean accidental error of one normal point is less than ± 0.02 mag. Errors of scale and zero point in the magnitudes of the comparison stars do not affect our mean error appreciably, though they would contribute to systematic errors.

[5] S. Gaposchkin, *Ap. J.*, **100**, 221, 1944.

II. ELLIPTICITY OF THE COMPONENTS

A first evaluation of the effective ellipticity of the components (on the assumption that they are similar in shape and that they are in alignment) was made by reducing both maxima to one by the formula

$$\Delta m = -0^{m}.007 \sin \theta ,$$

where θ is the elongation angle from the primary minimum. The effective ellipticity, z, was determined graphically, in the usual manner, to be 0.155. By rectifying all the observations with this value of z, a preliminary value of 33° was obtained for θ.

Since the two halves of the light-curve display a difference not only of maxima but of minima, I have used the two halves of the (reflected) light-curve independently in determining the ellipticity of the components. In the same graphical manner the ellipticities for the two halves of the light-curve are found to be 0.170 and 0.200 for the primary and secondary minima, respectively. As a final value for z, I have adopted the mean of 0.155

TABLE 4

RECTIFIED LIGHT-CURVE OF HV 11086

Phase	IPg	Phase	IPg	Phase	IPg	Phase	IPg
0.00°.....	9m437	13.32°.....	9m366	43.92°.....	9m186	73.08°.....	9m180
3.24.....	9.412	23.76.....	9.303	54.10.....	9.186	82.80.....	9.178
6.84.....	9.400	33.12.....	9.209	63.72.....	9.178	90.00.....	9.180

and 0.170, or 0.162. The rectified light-curve is given in Table 4. From this table the two amplitudes and the elongation angle are determined to be

$$A_1 = 0^{m}.257 ; \qquad A_2 = 0^{m}.215 ; \qquad \theta = 36° .$$

III. RELATIVE DIMENSIONS OF THE SYSTEM

It may be recalled that the system of β Aurigae, with its minima of 0.09 mag. depth, had a considerable indeterminacy in respect to the ratio of the radii. But by making the legitimate assumption that the ratio, k, is 1.00, this star became a cornerstone in the knowledge of stellar dimensions and stellar structure. The rectified minima of HV 11086 are much deeper than those of β Aurigae, but nevertheless they are far from 0.75 mag. Therefore, as in the case of the other Wolf-Rayet eclipsing variable, V 444 Cygni, we shall determine a value of k with the aid of some other data than the purely photometric results. Since the period of the star is short and the two halves of the light-curve do not differ greatly, we may, to a first approximation, adopt $k = 1.00$. Later this assumption can be modified. A few remarks must first be made concerning the nature of the problem.

Evidence accumulates of the existence, in certain eclipsing systems, of extensive rotating and expanding atmospheres or envelopes to one or even both components; the systems of β Lyrae, RY Scuti, V 444 Cygni, and SX Cassiopeiae will serve as examples. For such systems the ordinary conceptions and computations of the sizes of components are incomplete. Whether we express this idea in terms of an extraordinary limb darkening or in terms of different radii in different wave lengths is more a formal than a physical question. The Wolf-Rayet component ejects atoms with high velocity, and therefore we cannot (as N. Kosirev[6] has shown) employ the conventional law of darkening or use the ordinary conception of the "size" of the star. Nevertheless, there is no reason to

[6] *M.N.*, **94**, 430, 1934.

doubt that the radii that are obtained by the conventional discussion of our light-curve have some meaning. In what follows we shall call the radii obtained in this manner the "photographic radii."

With this restriction, we apply the formula (in the conventional notation)

$$a_0 = 1 - \lambda_1 + \frac{1 - \lambda_2}{k^2},$$

with the adopted value 1.00 for k and assuming uniform brightness. We obtain $a_0 = 0.383$ and the function $p(k, a_0) = +0.017$. Then, from the formula

$$a_1^2 = a_2^2 = \frac{\sin^2 \theta}{(1+k)^2(1 - z\cos^2\theta) - (1-z)\,[1 + k\,p(k, a_0)]^2 \cos^2\theta}$$

we find $a_1 = a_2 = 0.339A$, where a_1 and a_2 are the major axes of the components and A is the distance between their centers. From the formula

$$\cos i = a_1(1 - z)\,[1 + k\,p(k, a_0)]$$

we find that $i = 73°12'$, $\epsilon^2 = z\,\mathrm{cosec}^2\, i = 0.1769$, and $b = 0.907a$.

IV. THE ABSOLUTE DIMENSIONS

After applying the small correction to the velocity-curve, derived from the change of period, I have found from the velocities of *N* IV 4058, published by Hiltner,[3] that the W component is eclipsed at primary (deeper) minimum. The agreement between the photometric minima and the spectroscopic orbit is very good. However, although there is no doubt of the existence of the secondary minimum, which implies the existence of a secondary component of surface brightness almost equal to that of the W component, this secondary component is not seen spectroscopically: Hiltner found no trace of a second spectrum. This camouflage of one of the components is not a new phenomenon, and it seems to be associated with the existence of an extended envelope with a bright-line spectrum. Stars such as UW Canis Majoris, V 343 Scorpii, and VV Cephei have bright-line spectra of this kind; and the line spectrum of the second component is not visible, although photometrically the stars are probably equally bright.

In deriving the absolute dimensions, I have used the mass function given by Hiltner:

$$f = 4.38 \odot,$$

referring to the W component. Usually it is assumed that the spectroscopically unobserved component is the lighter. Such an assumption might find support in the high ellipticity of the components, but the latter is so sensitive to mass ratio that it is sheer optimism to use the ellipticity for determining the mass ratio.

We need not necessarily require that the spectroscopically visible component is the heavier. If we assume that the invisible one is heavier (calling it the "first" component, as being in front at primary minimum), then, for a mass ratio 1.4 we should find for the W component a mass of 10.5 ⊙ practically identical with the well-determined value of 10.2 ⊙ derived for the W component of V 444 Cygni.[7]

If the masses of the W and unseen components are 10.5 and 14.7, respectively, we can determine the ratio of the radii by an application of the statistical relationship developed for the stars of the main sequence:[8]

$$\log R = 0.82 \log \mathrm{Mass}.$$

[7] S. Gaposchkin, *Ap. J.*, **93**, 202, 1941.

[8] S. Gaposchkin, *J. R. Astr. Soc. Canada*, **33**, 233, 1939.

If this relationship is applicable to the system, the first component will be 1.33 times larger than the W component. If this ratio of radii is used in computing a_1, as above, we derive an inclination of 69°, instead of 73°, as previously obtained. To bring into agreement k, i, and the masses, we may make the ratio of the masses close to 1.2 and the value of k equal to 0.90, so that the masses are 13.9 and 16.7. Then we shall obtain, as our final value of the inclination, 73°, with which we started. Thus the relative dimensions finally adopted are as follows:

$$a_1 = 0.359\,, \qquad a_2 = 0.323\,, \qquad b_1 = 0.326\,, \qquad b_2 = 0.293\,, \qquad i = 73°\,.$$

The mass of the W component, 13.9, is still near to that of the W component of V 444 Cygni, 10.2.

Having the masses of the components, we proceed to find the distance between the centers from the value of $a_2 \sin i = 6.66 \times 10^6$ km, published by Hiltner. Here a denotes the distance from the star center to the center of gravity of the system. Then the sizes of the components are

$$a_1 = 6.58\odot \qquad b_1 = 5.97\odot \qquad R_1\,(\text{mean}) = 6.17\odot$$

$$a_2 = 5.92\odot \qquad b_2 = 5.37\odot \qquad R_2\,(\text{mean}) = 5.55\odot$$

The photographic radius of the W component is, incidentally, almost equal to that of the W component of V 444 Cygni.

V. THE ABSOLUTE MAGNITUDES

To obtain the absolute magnitudes, in addition to the radii we need to know the effective temperatures. Kosirev has shown that the effective temperature of a W star has a somewhat different meaning from that for an ordinary star. The first component is not visible spectroscopically, so that we have no idea concerning its spectral class or, consequently, its effective temperature. We can, however, approach the problem by way of the difference in surface brightness between the components, as deduced from the light-curve.

For the system V 444 Cygni, I deduced in this fashion that the effective temperature of the W component is 13,070°, in glaring contrast to the excitation temperature of about 70,000°. This effective temperature was derived on the assumption that the spectral class of the other component is B1 (T_{eff} about 20,000°), as given by O. C. Wilson[9] and on the difference in depth of the two minima. Since that time, C. S. Beals[10] has redetermined the spectrum of the second component as of class O6 (T_{eff} about 35,000°); the resulting effective temperature of the W star is raised to about 22,000°. At the time when the temperature of this W star was first deduced, I was not aware of the paper of Kosirev, in which he examines the modifications that must be introduced into the conceptions of radius and effective temperature for stars with extended envelopes. Our photographic effective temperature of 22,000° would correspond to a true effective temperature near 60,000° (the calculations referring to a star with a radius not much greater than that of the sun). The apparent discrepancy between temperature and spectrum is thus entirely removed.

The result for V 444 Cygni can be used to deduce an effective temperature for the first component of HV 11086. We assume that the photographic effective temperature is the same for the W components of the two systems (i.e., 22,000°). We can then compute the effective temperature of the first component, from the difference of the depths of the minima, as 21,000°, corresponding to a spectrum of class B1, for the "invisible" com-

[9] *Ap. J.*, **91**, 379, 1940. [10] *Pub. A.A.S.*, **10**, 304, 1943.

ponent. The absolute visual magnitudes of the two components are, then, from the formula of Russell, Dugan, and Stewart,

$$M_1 = -2.63\ ; \qquad M_2 = -2.46\ .$$

The difference in the absolute magnitudes is in the same direction as the difference in the adopted masses and is also in agreement with the difference deduced from the light-curve (0.09 mag., as compared with 0.17 mag., obtained here).

TABLE 5

COMPARISON OF TWO WOLF-RAYET STARS

	V 444 Cygni	HV 11086
Spectrum	WN 5.5	WN 6
Mass	10.2 ⊙	13.9 ⊙
Radius	5.8 ⊙	5.5 ⊙
M_{vis}	− 2.6	− 2.5

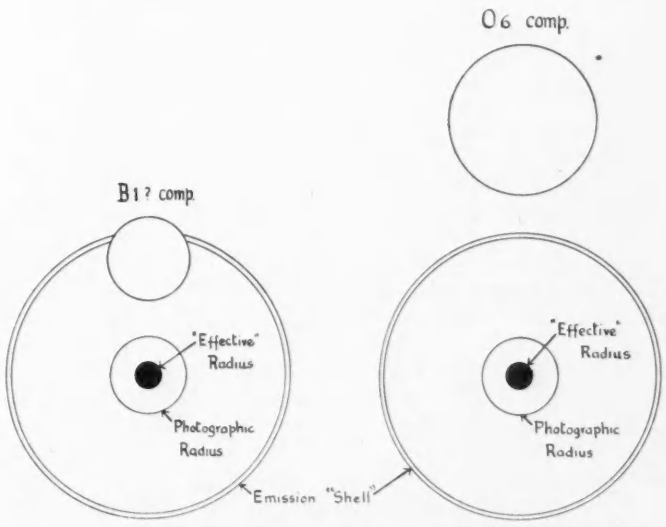

FIG. 3.—Comparison between the systems of HV 11086 (*left*) and HV 11111 (V 444 Cyg). Mean radii are represented. The sizes of the systems, the radii of the components, and the envelopes are drawn to scale. The "shell" implies the size of the sphere within which the emission lines are probably produced. The "effective radius" is that suggested by the Kosirev theory.

VI. COMPARISON WITH V 444 CYGNI

Some of the values deduced for HV 11086 were directly based on those obtained for V 444 Cygni (such as the effective temperature, and to some extent the masses); but most of the results are independent, and therefore a comparison of the two W stars is of interest. The spectroscopic work of Beals[9] tends to confirm the dimensions that I deduced for V 444 Cygni. For the ratio of luminosities he obtained 4.9, as compared with my value of 5.6; and since the Lick observations have wholly confirmed the shape of the light-curve (especially the depths of the two minima), the deduced dimensions appear

to need little modification. Though the light-curves differ greatly, the dimensions of the W components are strikingly similar, as is shown in Table 5.

The absolute magnitudes are very similar to those determined by R. F. Sanford and O. C. Wilson[11] for 8 WN stars and are about a magnitude fainter than the determination of R. E. Wilson.[12]

CONCLUDING REMARKS

If, following Kosirev, we consider that the bright lines are formed at distances of $15 \odot - 25 \odot$ from the center, we may compare the relation of the envelopes to the two systems V 444 Cygni and HV 11086. The W stars are subject to interference by components of class O6 and, computationally, B1. The dimensions of the envelopes, relative to the systems, are represented in Figure 3.

TABLE 6

ABSOLUTE DIMENSIONS OF THE SYSTEM OF HV 11086

PHOTOMETRIC ELEMENTS

$\text{Max}_1 = 9^m178$	$\text{Min}_1 = 9^m520$
$\text{Max}_2 = 9^m170$	$\text{Min}_2 = 9^m470$

Minimum = 2422287.501 + 1^d641272 E.

RELATIVE DIMENSIONS

$a_1^* = 0.359$	$b_1 = 0.326$
$a_2 = 0.323$	$b_2 = 0.293$
$L_1 = 0.52$	$L_2 = 0.48$

Ratio of radii (k)	0.90
Ratio of surface brightness	1.135
Ratio of luminosities	1.088
Inclination of orbit	73°

ABSOLUTE DIMENSIONS

	First Component	Second Component
Spectrum	B1	WN 6
Mass	16.7 ⊙	13.9 ⊙
Radius	6.2 ⊙	5.5 ⊙
M_{vis}	− 2.6	− 2.5

* The star in front at primary minimum (spectroscopically unobserved) is denoted as the first component.

An interesting phenomenon was observed by Hiltner at phases between 0^p100 and 0^p200 (our notation): A violent outburst of gases, with a velocity of about 1000 km/sec occurred on the two nights November 8 and November 13,1943. Our photographic light-curve shows a definite drop of 0.03 mag. at phase 0^p15, which may possibly be significant. Our light-curve is a summary of the effect of about 1800 nights, spread over 44 years. If our slight diminution of brightness is real, it may be associated with an outburst of cooler gases, at a time when the B component is being uncovered by the W component; and it may be found to have a physical connection with the geometrical configuration of the system.

A summary of the physical characteristics of the system is given in Table 6.

[11] *Ap. J.*, **90**, 235, 1939. [12] *Ap. J.*, **94**, 12, 1941.

THE ECLIPSING STAR AR MONOCEROTIS

CECILIA PAYNE GAPOSCHKIN
Harvard College Observatory
Received July 15, 1944

ABSTRACT

The eclipsing star AR Monocerotis, with a period of 21.208 days, has a light-curve of β Lyrae form, as determined from 1441 estimates on Harvard plates. Relative dimensions were obtained from this photographic light-curve and from a rediscussion of the visual light-curves of Florja and Lause. The relative mean radii of the K and the unknown components are 0.332 and 0.086 in photographic light, 0.265 and 0.133 in visual light. The star thus shares with SX and RX Cassiopeiae the peculiarity of possessing dimensions that apparently differ with wave length. Photographic and visual light-curves give values of the inclination of the orbit as 76.5° and 82.5°.

On the basis of the mass function determined by Sahade and Cesco and an adopted mass ratio (?/K) of $\frac{1}{4}$, radii for the K and the unknown star are found to be 22.7 ⊙ and 5.9 ⊙ in photographic and 18.1 ⊙ and 9.0 ⊙ in visual light. With assumed temperatures of 4000° and 6000° for the two stars, absolute visual magnitudes of 0.52 and 0.96 are deduced from the photographic light-curve and 1.01 and 0.06 from the visual light-curve. The photographic light-curve is considerably the better determined, and conclusions drawn from it are regarded as of the greater weight.

In the course of the systematic study of the brighter variable stars on the plates of the Harvard collection, made under a grant from the Milton Fund of Harvard University, the eclipsing star AR Monocerotis was estimated on 1441 plates by Mrs. Helen Trueblood. The observations were discussed by the writer, and a summary of the results is given in the present paper.

The most recent period, 21.208 days, given in the Schneller catalogue for 1942, was tested by means of all available minima and was found to have been correct, and sensibly constant, since JD 15,000.

Photographic magnitudes of comparison stars were determined with reference to Selected Area 123. Photovisual magnitudes of comparison stars, used by N. Florja,[1] were determined with reference to the photovisual sequence for RV Monocerotis, published by S. Gaposchkin.[2]

In the formation of the photographic light-curve, the 1075 estimates on the larger-scale patrol plates (AM camera) were first reduced (Table 2). The 366 estimates with the small-scale patrol camera (AI) were reduced separately and served as a check on the form of the light-curve (Table 3).

Two visual light-curves have been published for AR Monocerotis by N. Florja[1] and by F. Lause;[3] the former gives his comparison stars, the latter does not. At first sight the two visual light-curves seem to differ greatly. However, when Florja's step estimates are reduced by means of his own magnitudes for the comparison stars (checked by photovisual estimates on Harvard plates) his light-curve is found to agree in scale with Lause's and to differ only in zero point. An arbitary correction of 0.30 mg. was made to Lause's magnitudes, and the two light-curves were then combined (Fig. 1). The combined light-curve was used as the basis for the visual solution described below.

The relative dimensions were computed by standard methods. Both visual and photographic light-curves present difficulties. The former is not well determined, and the curves of Florja and Lause differ systematically; also, an over-all variation of brightness, as with RX Cassiopeiae,[4] is not unlikely. The photographic light-curve shows a "flash"

[1] *Pub. Sternberg Inst.*, Vol. 8, Part II, 1937.
[2] H. A., **108**, No. 1, 1939.
[3] *A.N.*, **264**, 109, 1937.
[4] S. Gaposchkin, *Ap. J.*, **100**, 230, 1944.

after primary minimum (both AM and AI curves), as in SX Cassiopeiae.[5] Both the visual difference and the photographic "flash" were arbitrarily eliminated. The relative dimensions are summarized in Table 4.

TABLE 1

COMPARISON STARS FOR AR MONOCEROTIS

BD	This Paper	Florja	IPg	HPv	Florja Vis.
−4°1924	c	.....	9^m40	.....	.....
−4°1921	b	c	10.45	9^m38	9^m38
.....	a	.....	10.94	.....	.....
−4°1918	.....	k	.....	8.42	8.56
−5°2076	.....	a	.....	9.16	9.09

TABLE 2

PHOTOGRAPHIC LIGHT-CURVE FOR AR MONOCEROTIS (AM PLATES)

Phase*	IPg	No. of Obs.	Phase	IPg	No. of Obs.	Phase	IPg	No. of Obs.
0.022	10^m22	50	0.512	10^m42	10	0.626	10^m12	50
.072	10.21	50	.522	10.68	10	.664	10.18	50
.120	10.16	50	.533	10.89	10	.709	10.14	50
.163	10.12	50	.546	10.87	10	.748	10.15	50
.209	10.06	50	.554	10.84	10	.789	10.10	50
.269	10.09	50	.561	10.70	10	.837	10.09	50
.333	10.10	50	.569	10.69	10	.882	10.12	50
.381	10.12	50	.574	10.64	10	.923	10.15	50
.425	10.16	50	.583	10.55	10	0.974	10.18	55
.470	10.19	50	.591	10.40	10			
0.495	10.25	10	0.600	10.32	10	Total	.....	1075

* Expressed in terms of the period, with JD 2,400,000 as zero.

TABLE 3

PHOTOGRAPHIC LIGHT-CURVE OF AR MONOCEROTIS (AI PLATES)

Phase*	IPg	No. of Obs.	Phase	IPg	No. of Obs.	Phase	IPg	No. of Obs.
0.035	10^m26	25	0.489	10^m21	5	0.627	10^m14	25
.111	10.15	25	.506	10.41	5	.695	10.18	25
.187	10.08	25	.524	10.64	5	.768	10.11	25
.240	10.08	25	.547	10.86	5	.844	9.98	25
.342	10.16	25	.562	10.69	5	0.934	10.16	36
.387	10.10	25	.577	10.51	5			
.460	10.17	5	.590	10.47	5	Total	.....	366
0.476	10.21	5	0.593	10.27	5			

* Expressed in terms of the period, with JD 2,400,000 as zero.

From the spectrographic study by Sahade and Cesco[6] it is found that the mass function is 0.07, and the value of $a \sin i$ is 9.2×10^6 km. Thus, if the ratio of masses is 1.00, the

[5] S. Gaposchkin, *Ap. J.*, **100**, 221, 1944.

[6] Sahade and Cesco, *Ap. J.*, **100**, 374, 1944.

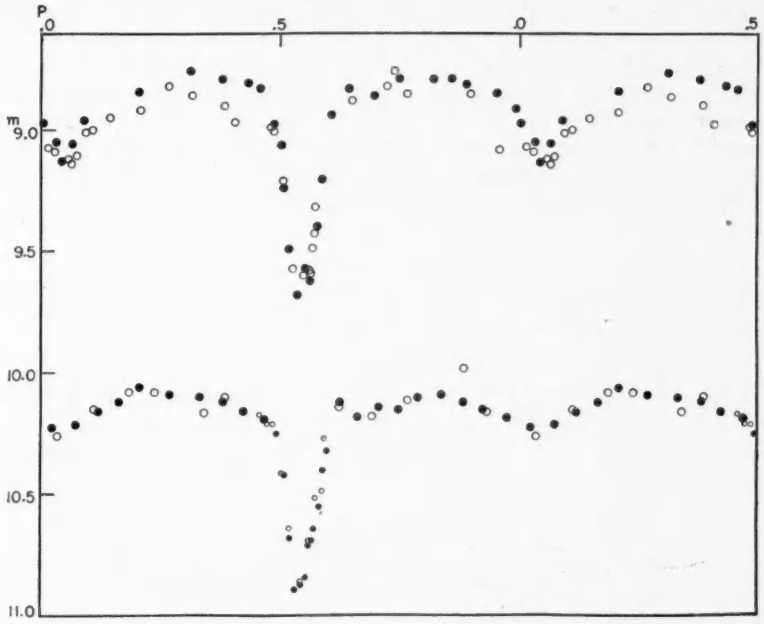

FIG. 1.—Light-curves for AR Monocerotis. *Above:* Visual: dots, Florja; circles, Lause. *Below:* Photographic: dots, AM plates (50-point and 10-point means); circles, AI plates (25-point and 5-point means). Ordinate and abscissa are magnitude and phase (reckoned from JD 2,400,000). The visual magnitudes have been reduced as described in the text.

TABLE 4

RELATIVE ELEMENTS FOR AR MONOCEROTIS

	Photographic	Visual
Maximum$_1$	$10^m.07$	$8^m.82$
Maximum$_2$	$10^m.10$	$8^m.78$
Minimum$_1$	$10^m.88$	$9^m.60$
Minimum$_2$	$10^m.24$	$9^m.14$
Amplitude$_1$	$0^m.80$	$0^m.80$
Amplitude$_2$	$0^m.16$	$0^m.34$
Ratio of radii	$0^m.26$	$0^m.50$
Duration of eclipse	$0^p.130 = 2^d.76$	$0^p.140 = 2^d.97$
Duration of totality	$0^p.023 = 0^d.478$	.....
Major axis, K star	0.344	0.278
Major axis, ? star	0.089	0.139
Luminosity, K star	0.54	0.56
Luminosity, ? star	0.46	0.44
Ratio of surface brigness (?/K)	12.8	3.11
Inclination of orbit	76.5°	82.5°

masses of K and the unknown star are 0.32 ⊙; if the ratio is $\frac{1}{2}$, the masses are 1.46 ⊙ and 0.73 ⊙, respectively; and if the ratio is $\frac{1}{4}$, they are respectively 8 ⊙ and 2 ⊙. Radii and absolute magnitudes for these three cases are summarized in Table 5. The temperatures adopted in calculating the radii are 4000° for the K star and 6000° for the unknown star, in rough conformity with its relative surface brightness. However, as was pointed out in connection with RX Cassiopeiae, a star that appears to have different radii in different wave lengths cannot be considered to have a unique effective temperature, and under

TABLE 5

RADII AND LUMINOSITIES

Mass Ratio	Photographic				Visual			
	K Component		Invisible Component		K Component		Invisible Component	
	Radius	M_{vis}	Radius	M_{vis}	Radius	M_{vis}	Radius	M_{vis}
1.00.....	9.1 ⊙	2.51	2.3 ⊙	2.05	7.2 ⊙	3.00	3.6 ⊙	2.05
0.50.....	13.6	1.63	3.5	2.09	10.9	2.12	5.4	1.16
0.25.....	22.7	0.52	5.9	0.96	18.1	1.01	9.0	0.06

such circumstances the absolute magnitudes can only be regarded as rough approximations. The approximation is, nevertheless, enough to permit us to conclude that the mass ratio $\frac{1}{4}$ is the most likely to represent the case, since it gives for the K star dimensions and luminosity that are most nearly normal for a star of this spectral type and luminosity class II.

It appears that AR Monocerotis is a giant eclipsing system that shares some of the characteristics of the remarkable systems SX Cassiopeiae and RX Cassiopeiae, notably the apparent difference of size in different wave lengths, resulting in the photographic light-curve giving a total, the visual-light curve a partial, eclipse.

REGRESSION LINES AND THE FUNCTIONAL RELATION*

FREDERICK H. SEARES[1]
Mount Wilson Observatory
Received August 11, 1944

ABSTRACT

This discussion is concerned with the linear functional relation $Y_1 = A + BX_1$, whose variables are known only through observed values X and Y, both affected by errors of measurement. The object is (1) to find A and B, (2) to reduce the values X to the system of Y (or vice versa), with results in both cases free from systematic error. A complete solution for (1) presents no particular difficulty. The solution for (2) requires the regression line $Y_c = a + b_x X$, where Y_c is a computed value and a and b_x are parameters which depend on the mean error of measurement. For observations of unequal weight, therefore, no single line suffices. This difficulty is most easily overcome by establishing a general expression for b_x as a function of B and the mean error of X. Incidentally, this relation gives at once all the characteristic properties of the regression lines, among them the fact that the lines will be strictly linear only when the frequency distribution for X (and Y) is gaussian.

I. THE PROBLEM

We have frequently to deal with measured quantities whose true values X_1 and Y_1 are known to be, or may be regarded as, connected by a linear functional relation

$$Y_1 = A + BX_1 . \tag{1}$$

Observations give, not X_1 and Y_1, but

$$X = X_1 + e_x , \qquad Y = Y_1 + e_y , \tag{2}$$

where e_x and e_y are the errors of measurement. These errors may include systematic effects, but we are here concerned only with the accidental components.

In practice, two different problems arise: (1) From a series of values of X and Y find the most probable values of the functional coefficients A and B. (2) From the measured series X find a computed series Y_c, where each Y_c is the most probable value, on the scale and zero point of Y_1, to be obtained from the corresponding X; or, more concisely stated, reduce the observations X to the system of Y. The qualification "most probable" is used in the sense defined by the least-squares criterion that the sum of the squares of the errors shall be a minimum.

The solution of this second problem, familiar enough if the values of X are all of the same weight, is given by the appropriate regression formula—that of Y on X for the conditions stated, or of X on Y if the values of Y are to be reduced to the system of X. The procedure to be followed when the observations differ in precision is less obvious, and I have seen no statement of the precautions that must then be taken to secure correct results.

The derivation of the functional coefficients A and B, free from systematic error, seems to have received even less attention;[2] and no discussion of the matter appears in any of

* *Contributions from the Mount Wilson Observatory, Carnegie Institution of Washington*, No. 698.

[1] Research associate, Carnegie Institution of Washington.

[2] The only reference to the matter that I have seen occurs in Yule and Kendall, *An Introduction to the Theory of Statistics*, 11th ed., London, 1937. On page 314 the footnote states: "In this connection we may refer to a problem for which, so far as we are aware, no general solution has been found. Given that the theoretical law relating y and x is linear, but that the sets of values given in the data are *both* subject to error, what is the unique straight line most probably (in some sense) representing the truth? The least

the available reference sources. Answers to the questions thus raised were required for the discussion in the following *Mt. W. Contr.*, No. 699.[3] Because of their general applicability, the formulae involved are derived and given here by themselves.

We begin with a change of origin such that the new co-ordinates, x, y, etc., are measured from the means $\overline{X}$, $\overline{Y}$, etc.[4] The functional relation then takes the form

$$y_1 = Bx_1 , \tag{3}$$

and the measured quantities are expressed by

$$x = x_1 + e_x , \qquad y = y_1 + e_y . \tag{4}$$

The observations are supposed to be so numerous that the algebraic means of e_x and of e_y are negligible. Hence

$$\bar{x} = \bar{y} = \bar{x}_1 = \bar{y}_1 = 0 . \tag{5}$$

Suppose, now, the observations to be grouped according to definite values—first, of x, and, second, of y (in practice, small intervals in x and y must be used). The relations between the mean values of x and of y for the two groupings define the regression lines, which may be written

$$\bar{y}_x = b_x x , \qquad \bar{x}_y = b_y y . \tag{6}$$

The subscripts indicate the basis of grouping; and the b's are proportionality factors, which, for anything we know at the moment, may vary from group to group. Moreover, equations (6) refer to the simplified problem of equal weights; that is, p_x = const., p_y = const., but p_x need not equal p_y.

Our first concern is with the coefficient B in equation (3) and the regression coefficients b_x and b_y in formulae (6). The constant A will reappear later. It will be helpful, however, to consider first certain characteristics of regression lines.

II. PROPERTIES OF REGRESSION LINES

The true values included in any one of the x groups just described are determined by the condition $x_1 = x - e_x$; hence, for that particular group as a whole

$$x = \bar{x}_1 + \bar{e}_x . \tag{7}$$

For positive and negative values of a definite e_x the corresponding true values are $x_1' = x - e_x$ and $x_1'' = x + e_x$. Since the frequencies of x_1' and x_1'' will generally differ, the positive and negative errors do not completely cancel, and $\bar{e}_x$ in equation (7) is not zero. A grouping according to x therefore involves a selection of errors in x; but, since there is no correlation between errors in x and errors in y, the corresponding values of e_y present no such selection, and $\bar{e}_y$ for the group is zero, or at least negligible. Hence $\bar{y}_x = \bar{y}_1$; and from the first of equations (6), $\bar{y}_1 = b_x x$. A quantity very nearly error-free is thus associated with a value of x that is systematically affected by disturbances of purely accidental origin.

An immediate consequence, from equations (3) and (7), is

$$b_x x = B\bar{x}_1 = B(x - \bar{e}_x) . \tag{8}$$

---

squares solutions will give us lines which, in a certain sense, are the most likely if the dependent variable is subject to errors normally distributed; but they do not yield a line which allows for errors in both variables."

[3] *Ap. J.*, **100**, 264, 1944.

[4] Note that unweighted means are to be used; otherwise the constant A will be fully eliminated only if the weights of X and Y satisfy an improbable relation.

For the systematic error $\bar{e}_x$ we have the formula[5]

$$\bar{e}_x = x - \bar{x}_1 = -\epsilon_x^2 \frac{F'(x)}{F(x)}, \tag{9}$$

where ϵ_x is the mean error of measurement in x and $F(x)$ is the frequency function of x. Hence the general equation

$$b_x = \frac{B}{x}\left[x + \epsilon_x^2 \frac{F'(x)}{F(x)}\right]. \tag{10}$$

For ordinary distributions, $F'(x) < 0$ when $x > 0$. Since $F(x)$ is essentially positive, equation (10) shows, first, that $b_x < B$; in other words, the familiar fact that the slope of the first regression line is less than that of the functional relation. Similarly, $b_y < 1/B$; hence the slope of the second line relative to the x axis exceeds B.

Equation (10) also shows that b_x will be independent of x only when the logarithmic derivative of $F(x)$ is proportional to x; that is, only when

$$\log F(x) = \pm\frac{x^2}{2k^2} + K, \tag{11}$$

where k and K are constants. $F(x)$ and $F(y)$ must therefore be exponentials in x^2 and y^2, respectively. Since the U-shaped curves corresponding to positive exponents are irrelevant, only gaussian, or normal, distributions of x and y satisfy the requirement for linear regression lines. The constant k in equation (11) is the dispersion or standard deviation for the gaussian frequency function; hence $k^2 = \overline{x^2} = \sigma_x^2$. For normal distributions of x, that is, for strictly linear regressions, equation (10) therefore reduces to

$$b_x = B\left(1 - \frac{\epsilon_x^2}{\sigma_x^2}\right). \tag{12}$$

A similar relation, of course, holds for b_y.

Equation (10) is general but is not easily applied because the logarithmic derivative of $F(x)$ must be calculated. Equation (12), however, is a practical working relation. The presupposed gaussian distribution for x may be wide of the truth, but that defect is less important than might be thought. A significant curvature in the regression lines implies a large regression effect and hence large errors of measurement; but the curvature is then likely to be masked by the errors. The linear formulae therefore have wide applicability.

Even when nonlinear, the regression lines can always be determined, given sufficient data, and used for their legitimate purpose, which for the first regression, as already explained, is the reduction of the measurements X to the system of Y. This operation involves not only adjustments for zero point and scale factor but also corrections for the probable influence of the systematic error shown in equation (8). An individual value of Y_c thus computed may be less accurate than that given by the functional coefficient B, but in the long run this will not be true; even for a single X, probability favors the result from the regression line.

[5] This equation has been independently derived by several investigators; but, as applied to errors of observation, it seems to have been first given in an article of mine (*M.N.*, **84**, 15, 1923), which grew out of a discussion by Eddington and Miss Douglas of systematic errors affecting tangential velocities. As originally derived, the equation held rigorously for gaussian distributions of x and its errors, and also for any distribution of x to terms of the third order inclusive in e, when e itself has any symmetrical distribution. Geometrical considerations suggest that the result should be wholly independent of the form of $F(x)$; and Eddington (*M.N.*, **100**, 354, 1940), by using a symbolic operator, has recently shown this to be true. K. G. Malmquist (*Medd. fran Astr. Obs. Uppsala*, No. 82, 1941) calls attention to the fact that the relation is identical with one occurring in stellar statistics derived by him in 1920. This linking of the characteristics of stars with the behavior of errors of observation arises from the circumstance that for both stars and errors the result is a consequence of combining two frequency functions.

We are thus led to a third inference to be drawn from equation (10). The coefficients b_x and b_y obviously depend on the mean errors of measurement. Hence, if the weights p_x and p_y are not constants, as hitherto supposed, the regression lines have no meaning for the data as a whole. Each X must be transformed into its equivalent Y_c by using the coefficient corresponding to the precision of X. If B can be found, equation (10) then affords an easy means of reduction which will be useful later.

III. SOLUTION FOR B, b_x, AND b_y

An expression for the functional coefficient B is given at once by equations (3) and (4). Since the errors of measurement are not correlated with the true values x_1 and y_1,[6]

$$\overline{x^2} = \overline{x_1^2} + \epsilon_x^2, \qquad \overline{y^2} = \overline{y_1^2} + \epsilon_y^2, \tag{13}$$

where the mean errors ϵ_x and ϵ_y are regarded as known. Then

$$B^2(\overline{x^2} - \epsilon_x^2) = \overline{y^2} - \epsilon_y^2. \tag{14}$$

This equation makes no assumption as to the frequency distribution of x and y or the character of the regression lines. It ignores, however, possible differences in the precision of the observations, and its relation to the least-squares criterion is obscure. We require, therefore, a more detailed analysis.

Unequal weights.—Consider, first, the general case in which not only the weights p_x and p_y differ but also the mean errors for unit weight, namely, ϵ_{0x} and ϵ_{0y}. Assume, for a moment, that true values of the variables are known. As equations of condition for B and for $1/B$, we then have

$$y = Bx_1, \qquad x = \frac{1}{B} y_1, \tag{15}$$

the weights of which are p_y and p_x, respectively. Ordinary least-squares solutions then give

$$B_x = \frac{[p_y x_1 y]}{[p_y x_1^2]}, \qquad \frac{1}{B_y} = \frac{[p_x x y_1]}{[p_x y_1^2]}. \tag{16}$$

Subscripts have been added to differentiate the two determinations of B, one corresponding to a minimum in $[p_y v_y^2]$, the other to a minimum in $[p_x v_x^2]$, where v_y and v_x are the residuals given by equations (15). Replacing x_1 by $x - e_x$ and y_1 by $y - e_y$ and noting that the sums of terms involving the first powers of the errors are negligible, we obtain

$$B_x = \frac{[p_y x y]}{[p_y x^2] - [p_y e_x^2]}, \qquad \frac{1}{B_y} = \frac{[p_x x y]}{[p_x y^2] - [p_x e_y^2]}. \tag{17}$$

The condition for simultaneous minima in $[p_y v_y^2]$ and $[p_x v_x^2]$ is $B^2 = B_x B_y$, where, it is to be noted, B_x and B_y differ in weight.

We now introduce the auxiliary quantities

$$b_x' = s_1' = \frac{[p_y x y]}{[p_y x^2]}, \qquad b_y' = \frac{1}{s_2'} = \frac{[p_x x y]}{[p_x y^2]}. \tag{18}$$

[6] The mean error of measurement—the precision—may, and often does, vary with the measured quantity. A correlation of e_x with x_1, on the other hand, would imply a preferential association of, say, large values of x_1 with positive values of e_x, whatever the precision might be, and is not to be feared. Note that the correlation involved in equation (8) is between e_x and x, not x_1.

We also write

$$[p_y e_x^2] = \left[\frac{p_y}{p_x}\right] \epsilon_{0x}^2, \qquad [p_x e_y^2] = \left[\frac{p_x}{p_y}\right] \epsilon_{0y}^2; \tag{19}$$

that is, we replace each e_x^2 by ϵ_{0x}^2/p_x, and each e_y^2 by ϵ_{0y}^2/p_y, where ϵ_{0x} and ϵ_{0y} are the mean errors corresponding to $p_x = 1$ and $p_y = 1$, respectively. Equations (17) then take the following convenient form for calculation

$$\left.\begin{aligned} R_x &= 1 - \left[\frac{p_y}{p_x}\right] \frac{\epsilon_{0x}^2}{[p_y x^2]}, \qquad R_y = 1 - \left[\frac{p_x}{p_y}\right] \frac{\epsilon_{0y}^2}{[p_x y^2]}, \qquad R = \frac{R_y}{R_x}, \\ B_x &= \frac{b_x'}{R_x}, \qquad \frac{1}{B_y} = \frac{b_y'}{R_y}, \qquad B^2 = B_x B_y = \frac{b_x' R_y}{b_y' R_x} = s_1' s_2' R. \end{aligned}\right\} \tag{20}$$

Useful check formulae may be found by inverting equations (17) and simplifying, as before. The result is

$$\frac{1}{B_x} = \frac{1}{b_x'} - \left[\frac{p_y}{p_x}\right] \frac{\epsilon_{0x}^2}{[p_y x y]}, \qquad B_y = \frac{1}{b_y'} - \left[\frac{p_x}{p_y}\right] \frac{\epsilon_{0y}^2}{[p_x x y]}. \tag{21}$$

The weights for B_x and B_y required to complete the solution for B may be obtained from equations (16), in which the denominators are the weights of the respective unknowns. Since

$$p(B_y) = \frac{1}{B_y^2} p\left(\frac{1}{B_y}\right), \tag{22}$$

we have

$$p(B_x) = [p_y x_1^2], \qquad p(B_y) = \frac{1}{B_y^2}[p_x y_1^2]. \tag{23}$$

To find B we must form the weighted geometrical mean of B_x and B_y, for which the formula is

$$\log B = \frac{Q_x \log B_x + Q_y \log B_y}{Q_x + Q_y}, \tag{24}$$

where Q_x and Q_y are the weights of $\log B_x$ and $\log B_y$, respectively. The general relation between the mean errors of a logarithm and its argument is

$$\epsilon(a) = \text{Mod } a\epsilon(\log a). \tag{25}$$

The corresponding relation between the weights is

$$p(\log a) = (\text{Mod } a)^2 p(a). \tag{26}$$

Since only relative weights are required for equation (24), we then find from formulae (26) and (23)

$$Q_x = B_x^2 p(B_x) = B_x^2 [p_y x_1^2], \qquad Q_y = B_y^2 p(B_y) = [p_x y_1^2]. \tag{27}$$

Since high accuracy in the weights is unnecessary, we may replace B_x^2 by B^2, whence $Q_x = [p_y y_1^2]$. Further, $[p_y y_1^2] = [p_y]\ \overline{p_y y_1^2}$, $[p_x y_1^2] = [p_x]\ \overline{p_x y_1^2}$, where the final factors on the right—the weighted dispersion in y_1 for two different systems of weighting—are nearly

equal. Similar considerations apply to equations (23); and we finally obtain, with sufficient accuracy,

$$Q_x = p\,(B_x) = [p_y]\,, \qquad Q_y = p\,(B_y) = [p_x]\,. \tag{28}$$

An expression for the weight or for the mean error of B itself can be found from equation (24) by the usual method; but, since B_x and B_y are nearly equal, we may use instead the formulae that apply to weighted arithmetical means. Hence for the weight, $p(B) = p(B_x) + p(B_y)$.

Equations (20), (24), and (28), with (21) as a partial check, thus cover the solution for B. As will be seen in a moment, the quantities b_x' and b_y' have the same form as the regression coefficients b_x and b_y and, in fact, are nearly equal to them.

To derive formulae for the regression coefficients themselves, we return to equations (6), which may now be written simply

$$y = b_x x\,, \qquad x = b_y y\,. \tag{29}$$

In applying the least-squares criterion to the residuals

$$v_y = y - b_x x\,, \qquad v_x = x - b_y y\,, \tag{30}$$

we must bear in mind that here both x and y are affected by errors of observation. The solutions of equations (29) are accordingly

$$b_x = s_1 = \frac{[P_y x y]}{[P_y x^2]}\,, \qquad b_y = \frac{1}{s_2} = \frac{[P_x x y]}{[P_x y^2]}\,, \tag{31}$$

where s_1 and s_2 are the slopes of the regression lines relative to the x-axis and P_y and P_x are the weights of v_y and v_x, respectively. More accurately, they are the weights corresponding to the errors $e_y' = e_y - b_{x1}e_x$ and $e_x' = e_x - b_{y1}e_y$, where b_{x1} and b_{y1} are the true values of the coefficients.

From the general expression for the weight of a function,

$$P_y = \frac{p_x p_y}{p_x + b_x^2 p_y}\,, \qquad P_x = \frac{p_x p_y}{b_y^2 p_x + p_y}\,; \tag{32}$$

or, if one of the weights, say p_y, is large relative to the other, and at the same time b_x and b_y do not differ too greatly from unity,

$$P_y = \frac{p_x}{b_x^2}\,, \qquad P_x = p_x\,. \tag{33}$$

The theoretical difficulty that formulae (32) and (33) contain b_x and b_y, which remain unknown until equations (31) have been calculated, is of no consequence; b_x' and b_y' may be used instead.

Comparison of equations (18) and (31) shows that they represent solutions of the same observation equations made with different systems of weights. The values of b_x and b_y will therefore differ but little from those of b_x' and b_y', but for the general case of unequal weights there are no simple relations connecting them. If, however, the conditions are such that equations (33) hold,

$$b_x = \frac{[p_x x y]}{[p_x x^2]}\,, \qquad b_y = \frac{[p_x x y]}{[p_x y^2]} = b_y'\,, \tag{34}$$

but there is still no means of expressing b_x in terms of b_x'.

Apparently, therefore, equations (31) must be calculated if b_x and b_y are to be found directly. But, since linear forms are used for the regression lines, the results in most cases will be only an approximation; and, although often a very good approximation, a question is raised as to whether the coefficients given by formulae (31) afford any real advantage over those found b (18), which appear during the calculation of B.

Equal weights.—For p_x = const., p_y = const., but $p_x \neq p_y$, both P_y and P_x are constant. Then from equations (31) and (18)

$$b_x = b'_x = s_1 = \frac{[xy]}{[x^2]}, \qquad b_y = b'_y = \frac{[xy]}{[y^2]}. \tag{35}$$

Further, equations (20) become

$$\left.\begin{aligned} R_x &= 1 - \frac{\epsilon_{0x}^2}{p_x \sigma_x^2}, \qquad R_y = 1 \frac{\epsilon_{0y}^2}{p_y \sigma_y^2}, \qquad R = \frac{R_y}{R_x}, \\ B_x &= \frac{b_x}{R_x}, \qquad \frac{1}{B_y} = \frac{b_y}{R_y}, \qquad B^2 = B_y B_x = \frac{b\, R_y}{b_y R_x} = s_1 s_2 R. \end{aligned}\right\} \tag{36}$$

Finally, the weights required for the combination of B_x and B_y are simply $Q_x = p_y$, $Q_y = p_x$. The regression coefficients b_x and b_y now appear automatically as steps in the calculation of B, and B itself is the geometrical mean of the slopes of the regression lines multiplied into $\sqrt{R}$.

Remarks on the solutions.—From the foregoing formulae it appears that, whatever the weights, the functional coefficient B may be found, without restrictive assumptions or approximations, by using the data either in groups or as a unit. If the weights are equal, the values of the regression coefficients b_x and b_y appear during the calculation of B. If the weights are unequal, the values of b_x and b_y obtained by treating the data as a unit, as already explained, are useless because they correspond to unknown weighted averages of p_x and of p_y and provide no means of finding the coefficients to be used with specified values of the weights. If the data are abundant, they may be segregated according to p_x, say, and discussed separately in groups.

An alternative method, applicable in all cases, is provided by equation (12). This equation and its analogue for b_y, which result from an entirely different approach to the problem, give at once

$$b_x = BR_x, \qquad b_y = \frac{R_y}{B}. \tag{37}$$

These equations are identical with expressions in formula group (36) but involve no restriction as to weights, only the usual assumption of linear regression lines; they are, in fact, explicit functions of the weights, the coefficient B, and known constants. We may therefore calculate B from equations (20), then b_x and b_y from (37) for any precision required. As a test of internal consistency it will be advantageous, however, to solve for B separately for each of several weight-groups.

For a final remark we return to equation (14), a solution for B that gives no preferential treatment to either x or y. From formulae (36), or even more directly from (17), we find for p_x = const., p_y = const.,

$$B_x = \frac{\overline{xy}}{\overline{x^2} - \epsilon_x^2}, \qquad B_y = \frac{\overline{y^2} - \epsilon^2}{\overline{xy}}, \tag{38}$$

where the relative weights are p_y and p_x, respectively. The combination $B^2 = B_x B_y$ is, in form, equation (14). To reproduce (14) numerically, however, we must suppose

$p_x = p_y = \text{const.}$ Hence, this initial solution for B satisfies the least-squares criterion only if the measurements are all of the same weight.

IV. THE ZERO-POINT CONSTANT A AND THE PARAMETER a

With the value of B available, we find from equations (1) and (2) for the constant term of the functional relation (1)

$$A = \overline{Y} - B\overline{X} . \tag{39}$$

A weighted mean is preferable, however, the weight for any A being similar in form to the first of equations (32). Aside from the influence of accidental errors, the value of A should be independent of the particular observations from which it is derived—a fact often useful in testing for the presence of systematic error.

The reduction of X to the system of Y starts from the formula $y = b_x x$. Since $y = Y - \overline{Y}$, we have the computed value

$$Y_c = b_x x + \overline{Y} . \tag{40}$$

Or, again, since $x = X - \overline{X}$,

$$Y_c = a + b_x X , \qquad a = \overline{Y} - b_x\overline{X} = A + B\overline{X}\,\frac{\epsilon_x^2}{\sigma_x^2}. \tag{41}$$

If only the values of X used to obtain B are to be reduced, equation (40) is all that is required; but, if other observations, homogeneous with the original X's, are also to be referred to the system of Y, then equations (41) are to be used. Strictly speaking, even these formulae are not applicable unless $\overline{X}$ and $\overline{Y}$ are changed accordingly. To explain this statement, consider the supplementary observation X'. Had X' and a corresponding Y' (which may not exist) been included in the original solution, the values of A and B would have differed from those actually found only by the negligible influence of accidental error. The parameter a, however, would have been increased by

$$\delta a = B\,\frac{X' - \overline{X}}{n+1}\,\frac{\epsilon_x^2}{\sigma_x^2}, \tag{42}$$

where n is the original number of observations. This change in a is always small, and wholly negligible if n is large. In practice, therefore, equations (41) will be adequate.

A convenient form for calculation is

$$r = B\,\frac{\epsilon_{0x}^2}{\sigma_x^2}, \qquad a = \frac{r\overline{X}}{p_x}, \qquad b_x = B - \frac{r}{p_x}, \qquad Y_c = a + b_x X . \tag{43}$$

The parameters a and b_x therefore appear as simple functions of the weight of X and certain constants and can therefore be tabulated with p_x as argument.

Actually, matters are not quite so simple as formulae (43) would suggest. What one usually finds is that ϵ_{0x} and ϵ_{0y}, the mean errors corresponding to unit weights, do not remain strictly constant—in other words, that the weighting system is not wholly consistent. Tests can be applied, however; and if it is known that the weights for Y, say, are reliable, or even merely that p_y is large relative to p_x, values of ϵ_{0x} can be computed for different weight-groups and compared for constancy. The segregation of the data according to p_x, as described in the preceding section, supplies the necessary material, which comprises, in particular, the residuals v_y and v_x defined by equations (30).

Mean errors for unit weight.—The general expression for the mean error of a function applied to the equation for the arithmetical mean of v_y gives

$$\epsilon^2(\bar{v}_y) = \epsilon^2(\bar{y}) + b_x^2\epsilon^2(\bar{x}),$$

whence

$$\frac{[P_y v_y^2]}{[P_y](n-1)} = \frac{\epsilon_{0y}^2}{[p_y]} + b_x^2 \frac{\epsilon_{0x}^2}{[p_x]}, \tag{44}$$

where P_y and P_x are to be found from equations (32) or (33). Rearranging terms, we find from (44) and from the similar equation based on v_x

$$\text{(from } v_y\text{)} \qquad b_x^2\epsilon_{0x}^2 = \frac{[p_x]\,[P_y v_y^2]}{[P_y](n-1)} - \frac{[p_x]}{[p_y]}\epsilon_{0y}^2, \tag{45}$$

$$\text{(from } v_x\text{)} \qquad \epsilon_{0x}^2 = \frac{[p_x]\,[P_x v_x^2]}{[P_x](n-1)} - \frac{[p_x]}{[p_y]} b_x^2\epsilon_{0y}^2. \tag{46}$$

The adopted values of ϵ_{0x} and ϵ_{0y} should satisfy these relations for all the weight-groups. If $[p_y]$ is large relative to $[p_x]$, we may calculate values of ϵ_{0x} with little interference from any uncertainty in ϵ_{0y}. With information thus gained, the tabulation of a and b_x by formulae (43) can be controlled.

Applications of the foregoing formulae will be found in the following *Contribution.*

RELATION BETWEEN COLOR INDEX AND EFFECTIVE WAVE LENGTH FROM THE OBSERVATIONS OF HERTZSPRUNG AND VANDERLINDEN*

FREDERICK H. SEARES[1] AND MARY C. JOYNER
Mount Wilson Observatory
Received August 11, 1944

ABSTRACT

The investigation is concerned, first, with a recalibration of the effective wave lengths corresponding to photographic magnitudes observed by Hertzsprung and by Vanderlinden in terms of revised color indices on the International System; second, with a comparison of the resulting functional relations between C and λ with the corresponding theoretical relation computed for black-body radiators in *Mt. W. Contr.*, No. 685.

The regression formulae for reducing the observations to the International System (Table 4 and eq. [12]), which are based on the statistical investigation in the preceding *Contribution*, No. 698, may also be used for reducing other observations by Hertzsprung (those for NGC 1647 require an additional zero-point correction) and by Vanderlinden, made under the same conditions as those of the polar stars.

The agreement of the computed and the observed relations between λ and C is shown by equations (1), (25), and (26). The theoretical range of 400 A in λ for photographic magnitudes, for the temperature interval 30,000°–3,000°, is confirmed; and the zero points agree within the inherent uncertainty—the equivalent of about 0.1 mag. in C. The computed effective wave lengths can therefore be used for all the ordinary calculations for which these quantities are required.

I. INTRODUCTION

In *Mount Wilson Contribution* No. 685[2] we have derived for black-body radiators of different temperatures the effective wave lengths corresponding to International photographic and photovisual magnitudes. For each temperature we have also calculated the color index C, the arbitrary zero point being fixed to give $C = 0$ for $T = 11{,}000°$ K. Since $C = 0$ for HD spectral type A5, the spectrum-temperature relation is in general agreement with that based on laboratory standards.

The results for photographic effective wave lengths are summarized by the formula

$$\lambda = 4242 + 195C\,, \qquad (1)$$

which for C between -0.4 and $+1.4$ ($T = 30{,}000°$–$3{,}500°$) gives no residual greater than 1 A. For $C = +1.66$ ($T = 3{,}000°$) the residual is still only 7 A. The computed change in λ for the interval 30,000°–3,000° is 400 A.

The applicability of these black-body results to stars is a matter of some consequence, since effective wave lengths are frequently required for calculations affecting stellar radiation—for example, the influence of atmospheric extinction and of selective space absorption, the definition of the characteristics of magnitude systems, etc. Equation (1) provides a simple means of comparing the theoretical results with those derived from stellar measurements.

Two series of observational data have been used for such comparisons—one by E. Hertzsprung,[3] the other by H. L. Vanderlinden.[4] Both give effective wave lengths for a

* *Contributions from the Mount Wilson Observatory, Carnegie Institution of Washington*, No. 699.

[1] Research associate, Carnegie Institution of Washington.

[2] *Ap. J.*, **98**, 310, Table 3, 1943.

[3] *Mt. W. Contr.*, No. 231; *Ap. J.*, **55**, 370, 1922; for brevity, hereafter referred to as *Polar Stars*. More detailed information on the observations and reductions is given in Hertzsprung's investigation of the Pleiades, in *Mém. de l'Acad. Roy. de Danemark, sec. des sci.*, 8me série, tome **4**, No. 4, 1923; hereafter referred to as *Pleiades*.

[4] *Etude de l'amas de Praesepe*, p. 19, Gembloux, 1933; hereafter referred to as *Praesepe*.

considerable number of polar stars whose International color indices are known. Hence, each series supplies an observed relation between λ and C for comparison with equation (1). The relations derived by Hertzsprung and by Vanderlinden require recalibration, however, since revised values of C are now available. Hertzsprung's investigation antedates the *Rome Report*,[5] which first gave the International standards. Vanderlinden's is based on the C_m standards of the *Report*, but the standards themselves can be improved in respect to accidental error with the aid of the extensive exposure-ratio observations by Baade and Malmquist and by Malmquist.[6]

The comparison of equation (1) with the corresponding stellar relations therefore requires two preliminary investigations—the revision of the values of C and the recalibration of λ in terms of the revised C's. The latter is undertaken here; the revision of the colors is given in a following *Contribution*, No. 701,[7] in order that the values of C derived from the effective wave lengths may be used with other data for a further revision of standards. It may be remarked that the recalibration provides the means of reducing to the International System other observations by Hertzsprung and by Vanderlinden, notably the important series on the Pleiades[3] and on Praesepe.[4]

II. HERTZSPRUNG'S EFFECTIVE WAVE LENGTHS

These observations, made with the 60-inch reflector at Mount Wilson on July 19–September 14, 1912, include 12 Lumière Σ plates of the polar region, among them several with multiple exposures. Standard colors, C, are available for 94 of the 129 stars measured. Hertzsprung's results are given in the form of zenith color indices, denoted by I_λ and computed from the wave lengths with the formula

$$I_\lambda = \frac{\lambda - 4216}{200}. \tag{2}$$

Since it is convenient to work with equivalent color indices instead of the wave lengths, the printed values are used as they stand. For I_λ we write simply I, or sometimes I_H.

The range in the weight of I is unusually large, roughly 100 to 1; but, since the weighting system seems to be reasonably consistent, all the observations of low weight are retained for what they may contribute. To make the system homogeneous (or nearly so) with that of the standards, Hertzsprung's weights $p(I_\lambda)$ have been divided by 64, giving p_I, the values used here. The corresponding mean error for $p_I = 1$ is $\epsilon_{0I} = \pm 0.125$ mag. (based on Hertzsprung's estimate).

The large errors of the low-weight observations imply a large regression effect; in fact, we must deal with a rather extreme example of the statistical problem discussed in the preceding *Contribution*, No. 698.[8] We require, first, the functional relation

$$C = A + BI\ , \tag{3}$$

where the constants A and B are to be determined, free from systematic disturbances arising from the accidental errors. Second, we must establish the regression formula

$$C_c = a + b_I I\ , \tag{4}$$

in which C_c is the computed color index on the International System, the "most probable" value to be found from I; and a and b_I are parameters which must be expressed as functions of the weight p_I. The quantity a, although definitely associated with I, needs

[5] *Trans. I.A.U.*, **1**, 67, 1922.

[6] *Hamburg Mitt.*, **5**, No. 21, 1925; *Lund. Medd.*, Ser. II, No. 37, 1937.

[7] *Ap. J.*, **101**, January, 1945.

[8] *Ap. J.*, **100**, 255, 1944.

no distinguishing subscript here, since the corresponding parameter for the second regression line does not appear.

Equation (3), combined with equation (2), gives the observed relation between λ and C required for comparison with the theoretical relation (1). The applicability of the computed effective wave lengths to stars turns upon the agreement at this point. Equation (4), on the other hand, provides for the reduction of the individual values of I to the system of C.

In applying the formulae of the preceding *Contribution* to the present discussion, it is to be noted that X is to be replaced by I, and Y by C, throughout. Since equation (3) is a functional relation, C and I therein are to be regarded as true values; hence, (3) is the equivalent of (1*), while (4) corresponds to the first of formulae (41*), the asterisks, here as elsewhere, denoting formulae in the preceding general discussion.

The divisions of Table 1 give the original data for the four weight-groups used for the solutions. The standard color indices C and their weights p_C, as already indicated, are taken from a following *Contribution*.[7] The values of I and p_I are from Hertzsprung's *Polar Stars*, Table II,[8] the latter modified as already explained. The average weights per star for the four groups are in Table 3, columns 7 and 8. The unweighted means of C and of I in Table 2, columns 3 and 5, are required for the calculation of $x = I - \bar{I}$ and $y = C - \bar{C}$, which are the basis of the solutions for the various coefficients.

The results given by equations (18*) and (20*), with (21*) used as check formulae, are in Table 3, columns 2–6. Strictly speaking, b_I and b_C should have been calculated with formulae (31*) and (32*) instead of (18*); but, as pointed out in the general discussion, the distinction between b_I' and b_I, etc., is largely of academic interest. Moreover, since p_C is here much larger than p_I, equations (34*) are applicable; and for b_C' and b_C, at least, the distinction disappears.

The only irregularity of any consequence appears in group III, which, as shown by the last column of Table 1, includes five observations giving residuals in excess of 0.3 mag. The corresponding value of B_C, which is seriously in error, is rejected.

The mean errors of b_I and b_C are found from the usual least-squares relations. Those for B_I and B_C then follow from the formulae connecting b_I and B_I, etc., given in group (20*). For the calculation of B and its mean error, equations (24*) and (28*) are used. With the final value of B available, A is found from formula (39*). The weights of C are such that the unweighted means from Table 2, column 3, may be used with the weighted means of I from column 7 of the same table. The resulting values of A given in column 8 agree well. The adopted values for the coefficients of equation (3) are

$$A = +0.158 \pm 0.010\,, \qquad B = +1.005 \pm 0.027\,. \tag{5}$$

The large variation of b_I with p_I is obvious from the results in Table 3, columns 2 and 7. This relationship is now to be established in greater detail with the aid of equation (12*), which may be written

$$b_I = B\left(1 - \frac{\epsilon_{0I}^2}{p_I \sigma_I^2}\right), \tag{6}$$

where σ_I is the dispersion in $x = I - \bar{I}$. The average value of ϵ_{0I} (for $p_I = 1$) corresponding to Hertzsprung's estimate, as already noted, is ± 0.125 mag. But this value should not be used without applying the test afforded by equations (45*) and (46*). These equations give for each group two values of ϵ_{0I} based on the residuals v_C and v_I defined by formulae (30*). The corresponding mean error ϵ_{0C} for the standards, which occurs in both (45*) and (46*), is also about ± 0.125 mag.; but, since the coefficients of ϵ_{0C}^2 are small, any uncertainty here is of no consequence. The results in Table 2, columns 10–12, show that ϵ_{0I} is not constant. The weighted mean for the four groups, ± 0.140 mag., is somewhat

TABLE 1

OBSERVATIONS BY HERTZSPRUNG

H.A., 48	Pg m	C	p_C	I	p_I	$C-C_o$*	H.A., 48	Pg m	C	p_C	I	p_I	$C-C_o$*
I. p_I=4.7–2.2							III. p_I=1.2–0.55						
408...	11.6	+0.35	52	+0.15	3.3	+ 4	420...	9.1	+0.12	45	+0.03	1.0	−21
197...	11.3	0.37	51	0.17	4.2	+ 4	311...	15.0	0.61	23	.14	0.58	+16
101...	10.5	0.21	51	0.21	2.7	−16	403...	14.5	0.70	28	.22	1.0	+23
320...	12.3	0.39	48	0.21	2.9	+ 2	424...	14.5	0.65	25	.39	0.75	+ 4
350...	11.0	0.25	52	0.22	3.9	−13	436...	13.6	0.56	14	.39	0.92	− 4
302...	13.0	0.49	45	0.23	2.8	+10	419...	11.4	0.43	28	.40	0.69	−18
268...	12.7	0.44	45	0.25	3.0	+ 3	159...	15.2	0.74	7	.43	1.0	+12
85...	12.6	0.57	13	0.30	2.7	+11	391...	14.6	0.74	25	.52	1.0	+ 5
284...	13.6	0.57	35	0.35	3.0	+ 7	323...	15.3	0.84	15	.56	0.56	+12
386...	10.9	0.43	49	0.35	3.8	− 7	125...	14.8	0.53	10	.57	1.0	−19
225...	12.6	0.56	45	0.39	3.2	+ 2	282...	11.9	0.56	51	.61	1.2	−19
362...	13.1	0.80	50	0.54	2.5	+11	158...	15.2	0.62	8	.63	0.86	−15
75...	11.4	0.67	53	0.65	4.0	−13	130...	15.0	0.75	12	.65	0.80	− 3
191...	14.5	0.78	26	0.66	2.3	− 2	254...	15.3	0.96	25	.65	0.55	+19
127...	14.2	0.85	46	0.66	2.6	+ 5	327...	14.6	1.15	2.8	.68	1.2	+34
152...	14.6	0.74	26	0.67	2.5	− 7	62...	11.6	0.50	26	.70	1.1	−32
227...	11.1	1.08	52	0.90	4.7	+ 2	430...	12.0	0.48	21	.71	0.89	−34
184...	11.0	1.12	52	0.93	4.6	+ 3	190...	15.3	0.84	13	.75	0.78	− 1
151...	13.7	1.12	34	1.01	3.0	− 2	324...	14.9	0.66	26	.80	0.88	−23
219...	13.2	1.16	40	1.11	3.1	− 8	103...	13.6	1.34	8.9	.81	0.91	+45
300...	13.8	1.30	42	1.17	2.3	+ 2	338...	14.7	0.85	23	.83	0.66	− 4
345...	13.8	+1.61	50	+1.50	2.2	+ 3	288...	14.6	0.99	28	.85	1.0	+ 6
							439...	14.7	1.32	17	.88	0.59	+40
							401...	14.5	+0.79	28	+0.96	1.0	−22
II. p_I=2.2–1.2							IV. p_I=0.52–0.03						
489...	13.2	+0.49	13	+0.14	1.5	+14	356...	10.7	+0.33	28	−0.03	0.47	− 2
309...	11.3	0.33	23	0.27	2.2	−11	154...	14.9	0.51	14	+0.18	.52	+ 3
263...	14.1	0.57	28	0.30	1.8	+10	342...	14.9	0.69	8	+0.19	.44	+19
426...	13.8	0.52	33	0.32	1.5	+ 2	212...	15.9	0.71	11	+0.21	.03	+16
176...	14.4	0.58	23	0.36	2.2	+ 6	295...	15.6	0.66	13	+0.28	.06	+ 7
279...	13.9	0.62	29	0.36	1.8	+ 9	262...	13.1	0.50	6	+0.56	.50	−22
134...	14.2	0.66	21	0.41	2.2	+ 9	277...	15.3	0.75	20	+0.62	.20	− 1
57...	13.0	0.60	8.4	0.43	1.9	+ 1	319...	14.4	0.77	29	+0.62	.41	+ 1
292...	13.5	0.61	35	0.44	2.2	+ 1	480...	14.8	0.91	1.5	+0.63	.30	+14
226...	14.9	0.78	19	0.51	1.5	+11	205...	16.0	0.83	7	+0.76	.12	− 2
479...	13.3	0.61	20	0.51	1.4	− 6	334...	15.2	0.82	25	+0.80	.28	− 5
174...	13.5	0.56	3.1	0.52	1.6	−11	339...	15.5	1.07	11	+0.81	.09	+19
146...	14.3	0.66	15	0.55	1.7	− 4	195...	11.4	0.96	52	+0.83	.38	+ 7
332...	14.2	0.84	4.6	0.56	1.2	+12	341...	15.2	1.10	25	+0.91	.42	+16
142...	14.5	0.74	16	0.57	1.3	+ 2	365...	15.4	0.72	16	+0.94	.16	−23
389...	13.6	0.64	36	0.60	1.8	−10	126...	15.6	1.02	7	+1.04	.12	+ 1
494...	12.6	1.05	28	0.66	1.7	+25	336...	14.9	0.85	10	+1.05	.44	−17
256...	14.6	0.85	28	0.75	2.2	− 3	358...	15.3	0.85	11	+1.09	.14	−19
248...	13.3	0.80	36	0.79	2.2	−12	218...	15.5	1.37	18	+1.12	.19	+32
265...	14.7	1.03	28	0.86	2.0	+ 5	164...	16.0	0.94	8	+1.25	.03	−20
329...	14.3	0.78	29	0.88	1.8	−22	283...	14.9	1.31	21	+1.28	.36	+15
427...	13.2	1.10	48	0.96	1.4	+ 6	368...	15.8	1.24	6	+1.28	.03	+ 8
378...	14.1	1.31	41	1.07	1.8	+14	459...	14.5	1.26	16	+1.30	.30	+10
172...	13.7	+1.48	16	+1.21	2.2	+17	139...	15.3	+1.26	11	+1.72	0.20	−14

* Unit, 0.01 mag.

larger than the preassigned value ± 0.125. The low-weight observations, however, are better than their weights would indicate.

These differences cannot be ignored in extending the sequence of values of b_I in Table 3 and in computing the values of a with equations (43*). To avoid discontinuities at the boundaries of the groups, some adjustment and smoothing is therefore necessary. Omitting details, we have for b_I and a the results in Table 4.

TABLE 2

HERTZSPRUNG, MISCELLANEOUS RESULTS

Group (1)	Pg m (2)	$\bar{C}$ (3)	$[p_C]$ (4)	$\bar{I}$ (5)	$[p_I]$ (6)	$\overline{p_I I}$ (7)	A (8)	$\overline{p_I(C-C_e)}$ (9)	$\epsilon_{0I}(v_C)$ (10)	$\epsilon_{0I}(v_I)$ (11)	ϵ_{0I} (12)
I.....	12.70	0.720	947	0.574	69.3	0.561	+0.156	−0.003	±0.139	±0.147	±0.138
II.....	13.76	.759	581	.585	43.1	.590	.166	+ .024	.164	.146	.153
III.....	14.00	.739	510	.590	20.9	.591	.145	− .012	(.300)	.177	.177
IV.....	14.84	0.893	374	0.810	6.2	0.726	+0.163	+0.017	±0.126	±0.108	±0.110
All..	.....	.....	.....	.....	.....	0.580	+0.158	.....	.....	.....	±0.140

TABLE 3

HERTZSPRUNG, COEFFICIENTS

Group (1)	b_I (2)	b_C (3)	B_I (4)	B_C (5)	B (6)	$\bar{p}_I$ (7)	$\bar{p}_C$ (8)
I.....	0.967±0.043	0.996±0.048	0.991±0.044	0.997 ±0.048	0.994±0.032	3.15	43
II.....	.903 .084	0.901 .083	1.058 .099	1.092 .085	1.078 .064	1.80	24
III.....	.697 .160	0.504 .142	1.032 .237	(1.942) .144	1.032 .237	0.87	21
IV.....	0.586±0.069	1.294±0.150	1.014±0.119	0.771 ±0.150	0.943±0.095	0.26	16
All...	.....	.....	.....	.....	1.005±0.027	.....	.....

For the mean values of p_I shown in Table 3, column 7, Table 4 reproduces the original b_I in Table 3, column 2, within 0.002. For the same weights Table 4 gives

$$a = 0.164,\ 0.203,\ 0.329,\ 0.401\ ,$$

whereas from the second of formulae (41*) and the mean values of C and of I shown in Table 2, columns 3 and 5, we find

$$a = 0.165,\ 0.231,\ 0.328,\ 0.419\ .$$

The differences between these sequences are only of the order of the uncertainty in the mean color indices. The termination of the table at $p_I = 4.0$ does not appreciably affect the reduced colors, although the computed parameters are still short of their limiting values.

The values of C_e found from the last of formulae (43*)—the equation is repeated in Table 4—or from equation (3) if $p_I > 4.0$, give the differences $C - C_e$ in the last column of Table 1. The zero points are checked by the weighted means of these differences in Table 2, column 9. Although many of the deviations from the standards are large, none is inconsistent with its weight. The only abnormality is the excessive percentage of large deviations in group III.

The foregoing results for Hertzsprung represent an average solution for all stars together. Since the observations cover an interval of 7 mag., the possibility of a magnitude error must be considered. The essential data of Table 1 were therefore regrouped according to Pg m, as shown in Table 5. The weighted means of $C - C_c$, collected in the third column of Table 6, reveal a small systematic run expressed by

$$C - C_c = +0.02\,(m - 12.0), \tag{7}$$

which applies to the interval Pg m = 9.1–14.2. For fainter stars we have

$$\left.\begin{array}{lccc} \text{Pg } m = & 14.3 & 14.4\text{–}14.7 & \geqslant 14.8\,, \\ C - C_c = & +0.04 & +0.03 & +0.02\,. \end{array}\right\} \tag{8}$$

The range of formula (7) is extended to Pg m = 6.7 with the aid of the *Göttingen Aktinometrie* stars discussed in Section IV; see equation (21).

TABLE 4

HERTZSPRUNG, PARAMETERS FOR REGRESSION LINE*

p_I	b_I				a			
	0	1	2	3	0	1	2	3
0.0	.....	0.727	0.923	0.965	0.441	0.310	0.190	0.166
0.1	0.566	.752	.928	.968	.424	.296	.187	.165
0.2	.575	.778	.932	.970	.408	.280	.185	.163
0.3	.591	.804	.937	.973	.396	.265	.182	.162
0.4	.608	.830	.941	.975	.383	.247	.179	.161
0.5	.625	.853	.946	.978	.370	.230	.177	.160
0.6	.642	.873	.950	.980	.358	.218	.175	.160
0.7	.661	.890	.954	.983	.347	.211	.173	.160
0.8	.682	.903	.958	.985	.337	.203	.171	.160
0.9	.704	.915	.962	.988	.325	.197	.168	.160
1.0	0.727	0.923	0.965	0.990	0.310	0.190	0.166	0.160

* $C_c = b_I I + a$. Corrected for magnitude error, the adopted color index for Hertzsprung, International System, is $C_H = C_c - 0.021(m - 12.0)$, (eq. [21]). For Pg $m > 14.2$, use

$$\left.\begin{array}{lccc} \text{Pg } m = & 14.3 & 14.4\text{–}14.7 & \geqslant 14.8\,, \\ C_H - C_c = & +0.04 & +0.03 & +0.02\,. \end{array}\right\} \tag{8}$$

Note that the argument p_I is one sixty-fourth of Hertzsprung's weight.

For Hertzsprung's observations of NGC 1647 an additional zero-point correction is required; see Section V.

These systematic differences are probably attributable to an imperfect elimination of the influence of the density of the spectral image on the effective wave length. They are accepted as such and applied to the values of C_c to obtain C_H, the adopted values of Hertzsprung's color indices reduced to the International System. The final deviations from the standards, $C - C_H$, appear in the next to the last column of Table 5; their weighted means for magnitude groups, in the fourth column of Table 6. Except for the first group, the agreement is now satisfactory.

For convenience, the magnitude corrections given by formulae (8) and (21) are appended to Table 4.

III. VANDERLINDEN'S EFFECTIVE WAVE LENGTHS

Except for the use of Seed 30 plates in place of Lumière Σ's, the instrumental equipment and the procedure were the same as for Hertzsprung's observations. Twenty-two

TABLE 5

HERTZSPRUNG, FINAL DEVIATIONS $C-C_H$

H.A., 48	NPS	Pg *m*	*C*	p_C	$C-C_H$*	p_I
420	10	9.1	0.12	45	−15	1.0
101	13	10.5	0.21	51	−13	2.7
356	.....	10.7	0.33	28	+ 1	0.47
386	14	10.9	0.43	49	− 5	3.8
350	.....	11.0	0.25	52	−11	3.9
184	7r	11.0	1.12	52	+ 5	4.6
227	5s	11.1	1.08	52	+ 4	4.7
197	15	11.3	0.37	51	+ 5	4.2
309	.....	11.3	0.33	23	−10	2.2
75	6s	11.4	0.67	53	−12	4.0
195	8r	11.4	0.96	52	+ 8	0.38
419	.....	11.4	0.43	28	−17	0.69
408	16	11.6	0.35	52	+ 5	3.3
62	.....	11.6	0.50	26	−31	1.1
282	17	11.9	0.56	51	−19	1.2
430	.....	12.0	0.48	21	−34	0.89
320	18	12.3	0.39	48	+ 1	2.9
85	10r	12.6	0.57	13	+10	2.7
225	7s	12.6	0.56	45	+ 1	3.2
494	.....	12.6	1.05	28	+24	1.7
268	19	12.7	0.44	45	+ 2	3.0
57	.....	13.0	0.60	8.4	− 1	1.9
302	20	13.0	0.49	45	+ 8	2.8
262	.....	13.1	0.50	6	−24	0.50
362	.....	13.1	0.80	50	+ 9	2.5
427	.....	13.2	1.10	48	+ 4	1.4
489	.....	13.2	0.49	13	+12	1.5
219	11r	13.2	1.16	40	−10	3.1
248	21	13.3	0.80	36	−15	2.2
479	.....	13.3	0.61	20	− 9	1.4
292	22	13.5	0.61	35	− 2	2.2
174	.....	13.5	0.56	3.1	−14	1.6
436	.....	13.6	0.56	14	− 7	0.92
389	.....	13.6	0.64	36	−13	1.8
284	23	13.6	0.57	35	+ 4	3.0
103	.....	13.6	1.34	8.9	+42	0.91
172	.....	13.7	1.48	16	+14	2.2
151	.....	13.7	1.12	34	− 5	3.0
345	.....	13.8	1.61	50	− 1	2.2
300	12r	13.8	1.30	42	− 2	2.3
426	.....	13.8	0.52	33	− 2	1.5
279	24	13.9	0.62	29	+ 5	1.8
378	.....	14.1	1.31	41	+10	1.8
263	25	14.1	0.57	28	+ 6	1.8
127	.....	14.2	0.85	46	+ 1	2.6
134	.....	14.2	0.66	21	+ 5	2.2
332	.....	14.2	0.84	4.6	+ 8	1.2
146	.....	14.3	0.66	15	− 8	1.7
329	.....	14.3	0.78	29	−26	1.8
176	.....	14.4	0.58	23	+ 3	2.2

* Unit, 0.01 mag.

TABLE 5—*Continued*

H.A., 48	NPS	Pg *m*	*C*	p_C	$C-C_H$*	p_I
319		14.4	0.77	29	− 2	0.41
459		14.5	1.26	16	+ 7	0.30
142		14.5	0.74	16	− 1	1.3
424		14.5	0.65	25	+ 1	0.75
401		14.5	0.79	28	−25	1.0
403		14.5	0.70	28	+20	1.0
191	8s	14.5	0.78	26	− 5	2.3
152		14.6	0.74	26	−10	2.5
327		14.6	1.15	2.8	+31	1.2
391		14.6	0.74	25	+ 2	1.0
288	26	14.6	0.99	28	+ 3	1.0
256		14.6	0.85	28	− 6	2.2
338		14.7	0.85	23	− 7	0.66
265	9s	14.7	1.03	28	+ 2	2.0
439		14.7	1.32	17	+37	0.59
125		14.8	0.53	10	−21	1.0
480		14.8	0.91	1.5	+12	0.30
283		14.9	1.31	21	+13	0.36
342		14.9	0.69	8	+17	0.44
154		14.9	0.51	14	+ 1	0.52
226		14.9	0.78	19	+ 9	1.5
324	27	14.9	0.66	26	−25	0.88
336		14.9	0.85	10	−19	0.44
311		15.0	0.61	23	+14	0.58
130		15.0	0.75	12	− 5	0.80
341		15.2	1.10	25	+14	0.42
158		15.2	0.62	8	−17	0.86
159		15.2	0.74	7	+10	1.0
334		15.2	0.82	25	− 7	0.28
139		15.3	1.26	11	−16	0.20
358		15.3	0.85	11	−21	0.14
323	10s	15.3	0.84	15	+10	0.56
254	11s	15.3	0.96	25	+17	0.55
190	28	15.3	0.84	13	− 3	0.78
277		15.3	0.75	20	− 3	0.20
365	12s	15.4	0.72	16	−25	0.16
218		15.5	1.37	18	+30	0.19
339	13s	15.5	1.07	11	+17	0.09
295		15.6	0.66	13	+ 5	0.06
126		15.6	1.02	7	− 1	0.12
368		15.8	1.24	6	+ 6	0.03
212	29	15.9	0.71	11	+14	0.03
205		16.0	0.83	7	− 4	0.12
164		16.0	0.94	8	−22	0.03

polar plates, all but four carrying multiple exposures, were taken on October 10 and 11, 1923, and July 7, 1924. The 36 standard stars observed were all used by Vanderlinden to calibrate his wave lengths. With the C_m values of the *Rome Report*[5] he obtained the regression formula

$$C=\frac{\lambda-4242}{193}=I_V, \tag{9}$$

which was then used to compute color indices for the polar standards. For uniformity with

the preceding notation these results from wave lengths we also denote by I (sometimes by I_V).

For star 1r Vanderlinden found the discordant difference $C_m - I = +0.26$. It was soon evident that, relative to the standards used here, star 345 of *H.A.*, Vol. **48,** also is

TABLE 6

HERTZSPRUNG, DEVIATIONS* FOR MAGNITUDE GROUPS

Group	Pg m	$C-C_c$	$C-C_H$	AD	$[p_I]$	No. of Stars
1	10.8	−5.7	−3.8	± 7.8	31.57	10
2	12.0	−0.2	−0.3	10.6	18.06	10
3	13.1	+1.2	−0.7	8.1	20.30	10
4	13.6	+3.2	0.0	7.8	20.13	10
5	14.1[5]	+4.1	+0.2	7.0	18.60	10
6	14.5	+3.1	+0.1	10.1	12.76	11
7	14.8	+2.0	−0.5	11.1	10.45	11
8	15.2	+2.6	+0.6	12.7	5.83	11
9	15.6	+1.9	−0.1	± 6.4	1.81	11
All	.....	+0.5	−1.0	.....	139.51	94

* Unit, 0.01 mag.

TABLE 7

OBSERVATIONS BY VANDERLINDEN

I. p_I = 19–9.1							II. p_I = 8.6–0.12						
NPS	Pg m	C	p_C	I	p_I	$C-C_V$*	NPS	Pg m	C	p_C	I	p_I	$C-C_V$*
5	6.5	0.00	25	+0.01	19	− 2	2	5.2	−0.08	18	−0.05	8.6	− 4
14	10.9	+0.43	49	0.32	19	+10	1	4.4	0.00	16	+0.06	4.5	− 7
16	11.6	0.35	52	0.32	15	+ 2	10	9.1	+0.12	45	+0.14	5.2	− 3
18	12.3	0.39	48	0.36	12	+ 2	13	10.5	+0.21	51	+0.15	5.8	+ 5
19	12.7	0.44	45	0.42	16	+ 1	12	10.1	+0.28	51	+0.28	2.4	− 1
20	13.0	0.49	45	0.45	15	+ 3	350†	11.0	+0.25	52	+0.28	8.1	− 3
17	11.9	0.56	51	0.59	12	− 3	15	11.3	+0.37	51	+0.32	3.4	+ 5
23	13.6	0.57	35	0.59	13	− 2	4s	10.3	+0.48	49	+0.49	0.12	− 1
22	13.5	0.61	35	0.62	13	− 1	7s	12.6	+0.56	45	+0.50	7.6	+ 6
24	13.9	0.62	29	0.63	9.3	− 1	25	14.1	+0.57	28	+0.54	7.4	+ 3
21	13.3	0.80	36	0.88	14	− 8	10r	12.6	+0.57	13	+0.60	4.8	− 3
8r	11.4	0.96	52	0.97	9.1	0	27	14.9	+0.66	26	+0.62	3.6	+ 4
5s	11.1	1.08	52	1.01	13	+ 8	6s	11.4	+0.67	53	+0.63	5.6	+ 4
4r	9.2	0.90	22	1.07	14	−16	28	15.3	+0.84	13	+0.79	1.1	+ 8
11r	13.2	1.16	40	1.21	14	− 4	8s	14.5	+0.78	26	+0.87	6.7	− 8
12r	13.8	1.30	42	1.32	12	− 1	26	14.6	+0.99	28	+1.02	4.5	− 2
2r	7.9	+1.57	25	+1.59	17	− 1	7r	11.0	+1.12	52	+1.04	3.2	+10

* Unit, 0.01 mag. † *H.A.*, Vol. **48.**

discordant. Both these stars are omitted from the present discussion. The data for the remaining 34 stars, segregated into two weight-groups, are in Table 7, arranged like Table 1. The coefficients and other results are collected in Tables 8 and 9, which follow the form of Tables 2 and 3. The weights p_I have been reduced to the system used for Hertzsprung by dividing Vanderlinden's values by 16.

The 2 to 1 ratio for the two values of ϵ_{0I}, Table 8, column 11, is an anomalous result for which there is no obvious explanation. Together with the average weights given in Table 9, column 7, it suggests that there is little or no gain in precision with increasing weight. The deviations from the standards $C - C_V$, grouped according to p_I, confirm this conclusion. On this account, unweighted as well as weighted solutions were made for the coefficients, without, however, any significant difference in the results, as shown by Table 9.

For the functional relation we adopt

$$C = +0.004 + 0.994I\,, \tag{10}$$

which, in effect, is simply $C = I$. In other words, Vanderlinden's color indices I are functionally identical with the standards. Since the regression effect is very small, the result

TABLE 8

VANDERLINDEN, MISCELLANEOUS RESULTS

Group (1)	Pg m (2)	$\bar{C}$ (3)	$[p_C]$ (4)	$\bar{I}$ (5)	$[p_I]$ (6)	A (7)	$\overline{p_I(C-C_V)}$ (8)	$\epsilon_{0I}(v_C)$ (9)	$\epsilon_{0I}(v_I)$ (10)	ϵ_{0I} (11)	σ_I^2 (12)
I.....	11.75	0.720	683	0.727	236.4	−0.003	−0.003	±0.211	±0.213	±0.212	0.166
II.....	11.35	0.494	617	0.487	86.62	+0.010	−0.004	±0.098	±0.100	±0.099	0.100
All..	.....	.....	.....	.....	.....	+0.004	.....	.....	.....	.....	0.133

TABLE 9

VANDERLINDEN, COEFFICIENTS

Group (1)	b_I (2)	b_C (3)	B_I (4)	B_C (5)	B (6)	$\bar{p}_I$ (7)	$\bar{p}_C$ (8)
I.....	0.935±0.034	1.047±0.037	0.957±0.034	0.948±0.037	0.953±0.025	13.9	40
II.....	1.025 .038	0.970 .036	1.051 .039	1.028 .036	1.039 .027	4.9	36
I*.....	0.989 .038	0.988 .037	1.012 .039	1.008 .037	1.010 .027	.....	.....
II*.....	0.934±0.031	1.052±0.037	0.947±0.032	0.947±0.037	0.947±0.024	.....	.....
Wtd.....	0.967±0.025	.....	.....	.....	0.994±0.018	.....	.....
Unwtd.....	0.971±0.024	.....	.....	.....	0.975±0.018	.....	.....

* Unweighted solutions.

is, practically speaking, a complete confirmation of Vanderlinden's calibration. The adjustment of the standards for accidental error has not, therefore, appreciably affected the systematic relations.

To find C_c we should ordinarily use equations (43*); but, since here we have $\bar{C} = \bar{I}$, sensibly (for all the data together both means are 0.607), we find from equations (41*)

$$C_c = I - (1 - b_I)\,(I - \bar{I})\,, \tag{11}$$

where b_I is given by equation (6). The adopted values of C_c were found with the data in Table 8, columns 11 and 12, but the mean-square dispersion $\sigma_I^2 = 0.133$ and $\epsilon_{0I} = \pm 0.125$ might equally well have been used. Further, since B is sensibly unity, these numerical data, together with equations (6) and (11), give as a general reduction formula for Vanderlinden

$$C_V = I - \frac{0.117}{p_I}(I - 0.607)\,, \tag{12}$$

where it is to be remembered that p_I is one-sixteenth of Vanderlinden's weight. C_c has been replaced by C_V, since, as will appear in a moment, there is no certain evidence of any magnitude error in C_c. The results from equations (11) and (12) are therefore accepted as final, and their deviations from the standards appear in Table 7 under the heading "$C - C_V$."

Grouped according to magnitude, these differences give the unweighted means in the third column of Table 10. For the first four groups the agreement is poor; but, since each group includes only 4 or 5 stars, the influence of accidental error may still be appreciable. On that account, the bad agreement can scarcely be accepted as evidence of a magnitude error in Vanderlinden's values of C_c. It should be noted that the agreement of C_V with the original C_m standards, as shown by the last column of Table 10, is in some respects better than with C.

TABLE 10

VANDERLINDEN, DEVIATIONS* FOR MAGNITUDE GROUPS

NPS	Pg m	$C-C_V$	AD	$[p_I]$	C_m-C_V
1, 2, 5, 2r, 10	6.6	−3.4	±3.4	54.3	−2.4
4r, 12, 4s, 13	10.0	−3.2	5.8	22.3	−3.8
14, 7r, 350, 5s	11.0	+6.2	7.8	43.3	+3.0
15, 6s, 8r, 16	11.4	+2.8	2.8	33.1	+3.2
17, 18, 10r, 7s	12.4	+0.5	3.5	36.4	+1.5
19, 20, 11r, 21	13.0	−2.0	4.0	59.0	−1.8
22, 23, 12r, 24	13.7	−1.2	1.2	47.3	−0.5
25, 8s, 26, 27, 28	14.7	+1.0	±5.0	23.3	−5.4
All			±4.2	319.0	−0.8

* Unit, 0.01 mag.

The deviations $C - C_V$ for the omitted stars are +0.26 for 1r and −0.22 for 345 of *H.A.*, Vol. **48.**

IV. GÖTTINGEN "AKTINOMETRIE" STARS

Some further information on the behavior of the observed colors of bright stars may be gained from the groups of *Aktinometrie* stars measured by Hertzsprung[9] and by Vanderlinden.[10] These stars are listed in Table 11. In the third column are the colors defined by J_P = GA Pg m − PD Vis m, where it will be noted that the final visual magnitude from *Potsdam Pub.*, Vol. **17,** has been substituted for the provisional value used in the *Aktinometrie.*

The reduction of J_P to the International System was found from 155 stars in the Mount Wilson polar catalogue[11] for which there are both GA (polar section) and PD magnitudes. The color relations are complicated and apparently not wholly independent of magnitude. The corrections used are roughly represented by

$$C_P - J_P = +0.20 - 0.10 J_P , \qquad (13)$$

in which C_P denotes the reduced color index. The principal departures from this formula are for Pg $m < 5.5$, for which the first term on the right is +0.13, and for Pg $m > 7.0$

[9] *Pleiades,* Table 11.

[10] *Praesepe,* Table 6.

[11] Seares, Ross, and Joyner, "Magnitudes and Colors of Stars North of +80°," *Carnegie Inst. of Wash. Pub. 532,* 1941.

and $J_P < 0$, for which the coefficient of J_P is about -0.2. The actual correction used for any star may be found by forming the difference $C_P - J_P$ from Table 11. The well-known dependence of J_P on right ascension for stars in the 0°–20° zone is ignored, on the assumption that it is not observational error but a consequence of space absorption.

TABLE 11

GÖTTINGEN "AKTINOMETRIE" STARS

VANDERLINDEN					HERTZSPRUNG				
GA No.	GA Pg m	J_P	C_P	$C_P - C_V$†	GA No.	GA Pg m	J_P	C_P	$C_P - C_H$†
2766*	6.39	−0.67	−0.30	−36	2766*	6.39	−0.67	−0.30	(−42)
3189	6.63	−0.51	−0.21	+ 4	2764*	5.47	−0.41	−0.19	(−53)
3237	5.88	−0.43	−0.20	+ 4	2800*	6.88	−0.40	−0.10	+35
3331	4.73	−0.42	−0.22	+21	2759*	6.17	−0.35	−0.12	−18
2764*	5.47	−0.41	−0.19	−31	2757*	7.20	−0.17	+0.06	− 6
2800*	6.88	−0.40	−0.10	−16	3040*	7.85	−0.16	+0.07	−12
2759*	6.17	−0.35	−0.12	−19	541	5.02	0.00	+0.14	−14
3327	5.33	−0.31	−0.10	+13	539	5.93	0.00	+0.19	− 7
3148	6.13	−0.21	0.00	−14	512	4.84	+0.04	+0.17	−19
3194	6.77	−0.21	+0.02	− 3	549	6.36	+0.04	+0.24	−17
3336	4.43	−0.17	−0.01	(+45)	544	6.93	+0.07	+0.23	−12
3196	6.23	−0.17	+0.04	−22	542	5.84	+0.18	+0.35	− 8
2757*	7.20	−0.17	+0.06	−21	509	6.95	+0.21	+0.37	+15
3040*	7.85	−0.16	+0.07	− 2	2814*	7.61	+0.21	+0.39	− 4
3199	7.07	+0.04	+0.22	−13	532	7.13	+0.28	+0.43	− 6
3279	5.94	+0.06	+0.25	+ 9	80	6.56	+0.58	+0.72	−35
3158	6.49	+0.07	+0.26	+13	498	4.98	+0.82	+0.86	− 1
2814*	7.61	+0.21	+0.39	+ 8	2760*	6.21	+0.94	+0.97	−13
3146	7.35	+0.23	+0.40	+11	2816*	6.73	+1.06	+1.15	+15
3241	6.55	+0.37	+0.53	+24	525	6.31	+1.07	+1.09	−10
3200	7.22	+0.37	+0.52	+27	528	5.05	+1.12	+1.12	+22
3218	7.45	+0.74	+0.87	+20	2805*	8.59	+1.14	+1.23	+24
2760*	6.21	+0.94	+0.97	+ 6	2954*	7.88	+1.22	+1.33	+15
3165	8.11	+1.00	+1.11	+ 3	2765*	7.47	+1.43	+1.51	−12
2816*	6.73	+1.06	+1.15	+23	2848	5.32	+1.46	+1.43	(+45)
2805*	8.59	+1.14	+1.23	0	3047*	8.71	+1.46	+1.54	0
2954*	7.88	+1.22	+1.33	+13	3042*	7.47	+1.75	+1.78	+24
3204	7.80	+1.26	+1.37	−11	3486*	7.64	+2.52	+2.42	+32
3274	7.89	+1.26	+1.36	− 7					
2765*	7.47	+1.43	+1.51	−14					
3047*	8.71	+1.46	+1.54	+ 6					
3391	8.21	+1.65	+1.75	+13					
3042*	7.47	+1.75	+1.78	+25					
3236	7.06	+1.77	+1.71	− 2					
3486*	7.64	+2.52	+2.42	+18					

* Observed by both Vanderlinden and Hertzsprung.

† Unit, 0.01 mag.

Our interest centers in the differences $C_P - C_V$ and $C_P - C_H$ in the last columns of the two divisions of Table 11, where, as before, C_V and C_H represent colors derived from effective wave lengths. C_V was found from the mean regression formula (b_I from Table 9)

$$C_V = 0.97 I_V + 0.02 , \qquad (14)$$

which, combined with equation (9), gives

$$C_V = \frac{\lambda - 4238}{199}. \tag{15}$$

From 34 stars we then find for Vanderlinden

$$C_P - C_V = +0.01 \pm 0.03 . \tag{16}$$

This small difference (for Pg $m = 7.0$) is in harmony with the conclusion already expressed that there is no evidence of magnitude error in Vanderlinden's color indices.

The comparison for Hertzsprung required, first, the calculation of the effective wave length from $\lambda = 3944.2l$ (l = separation of spectral images), next, the derivation of I_H from equation (2) and of C_c from Table 4; whence for 25 stars, mean Pg $m = 6.7$,

$$C_P - C_c = -0.11 \pm 0.04 , \tag{17}$$

a difference attributed to magnitude error in Hertzsprung's results.

Formulae (16) and (17) both involve the rather uncertain color correction summarized by equation (13). Further, they are based on differences that obviously are still affected by color equation. But, since both series of measures cover the entire range of color, it is not likely that the zero points are seriously disturbed. Moreover, from 14 of the 15 stars observed by both Vanderlinden and Hertzsprung (No. 2800 is discordant), we find directly for Pg $m = 7.2$

$$C_V - C_c = -0.13 \pm 0.04 , \tag{18}$$

free from any doubt affecting formula (13). Equations (16) and (18) together give

$$C_P - C_c = -0.12 \pm 0.05 , \tag{19}$$

practically the equivalent of formula (17). This agreement affords justification for accepting the difference (17) as a magnitude correction to Hertzsprung's colors at Pg $m = 6.7$. In Section II, however, we have found that $C - C_H = 0$ at Pg $m = 12.0$. Hence, assuming a linear relation, we may write

$$C_P - C_c = +0.021 (m - 12.0) . \tag{20}$$

Since C_P has been reduced to the International System, this relation is essentially the same as equation (7), already accepted as expressing the magnitude error of Hertzsprung's colors for polar stars between Pg m 9.1 and 14.2. The double check on the general relations, supplied by equations (17) and (19) and by (7) and (20), relieves somewhat any doubt raised by the relatively large mean errors affecting the various formulae.

Finally, since $C_H = C_c +$ magnitude correction, we have

$$C_P - C_H = C_P - C_c - 0.021 (m - 12.0), \tag{21}$$

the formula used to obtain the differences in the last column of Table 11. The assumption that the linear correction (20) applies over the entire magnitude interval for which formula (21) was used may not be wholly correct, but a good majority of the differences thus found are less than would have been obtained with the correction (17) used as a constant.

V. RESULTS FOR NGC 1647

An attempt to confirm the foregoing results for Hertzsprung by a comparison of his effective wave lengths[12] for stars in NGC 1647 with Mount Wilson color indices[13] has led

[12] *Mt. W. Contr.*, No. 100; *Ap. J.*, **42**, 92, 1915.

[13] Seares, *Mt. W. Contr.*, No. 102; *Ap. J.*, **42**, 120, 1915.

to a contradiction. So far as the record goes, the wave lengths are on the system used for the polar stars. Values of I were therefore computed with equation (2) and reduced to the International System with the data of Table 4. The color indices depend on polar comparisons, 5 for Pg m and 5 for Pv m. The 47 stars observed in common for which $p_I > 0$ give

$$C_{MW} - C_H = -0.27 . \qquad (22)$$

The original comparison in *Mt. W. Contr.* No. 102 gave $C_{MW} - C_H = -0.16$ for a wave-length constant of 4234 A. Substitution of the constant used here would change this difference to -0.25, practically the same as the value (22). The other variants in the reduction therefore have little influence.

This difference, however, should be zero. The mean error of C_{MW} is ± 0.06.[14] The wave lengths depend on 12 plates—6 Lumière Σ and 6 Seed 27—the latter reduced to the system of the former. The zero point of C_H therefore supposes that the 6 Lumière plates are representative of those used for the polar stars—possibly a doubtful assumption; but, even at that, much of the discrepancy is still to be accounted for. Hertzsprung's results for the Pleiades, on the other hand, as will appear in a later *Contribution*, seem to be consistent with those for the polar stars.

VI. COLOR INDEX AND EFFECTIVE WAVE LENGTH

We now return to the question raised in the Introduction as to the agreement of the observed and the computed relations between color index and effective wave length. The substitution of equation (2) and the coefficients (5) into the functional relation (3) gives for Hertzsprung's data

$$C = +0.158 + 1.005 \frac{\lambda - 4216}{200} \quad \text{(Zenith, Lumière } \Sigma) . \quad (23)$$

This relation refers to the weighted mean zero point defined by the observations of polar stars before correction for magnitude error; but, since the mean of these corrections is zero (see third column of Table 6), it also applies to the corrected colors.

Similarly, equation (9) substituted into (10) gives for Vanderlinden

$$C = +0.004 + 0.994 \frac{\lambda - 4242}{193} \quad \text{(Zenith, Seed 30)} . \quad (24)$$

The reduction of the Lumière plate to the International System (Seed 27 plate) is +30 A,[15] to be applied to the wave-length constant 4216. The color sensitivity of the Seed 30 plate may be taken as identical with that of the Seed 27. The wave-length constants in both formulae (23) and (24), however, must be increased by 23 A[16] to reduce the results from the zenith to the North Pole for comparison with the computed relation (1). Applying these corrections and simplifying, we have, for the altitude of the pole at Mount Wilson,

$$\lambda = 4237 + 199C \quad \text{(Hertzsprung)}, \quad (25)$$
$$\pm 2 \quad \pm 5.4$$

$$\lambda = 4264 + 194C \quad \text{(Vanderlinden)}, \quad (26)$$
$$\pm 2 \quad \pm 3.6$$

$$\lambda = 4242 + 195C \quad \text{(Computed)}, \quad (1)$$

[14] The probable error given originally as ± 0.035 should have been 10 per cent larger. The sampling error in the mean residual was overlooked.

[15] *Mt. W. Contr.*, No. 100, p. 5; *Ap. J.*, **42**, 96, 1915.

[16] Hertzsprung, *Polar Stars*, p. 3; Vanderlinden, *Praesepe*, p. 19.

where the effective wave lengths are for photographic magnitudes, and the magnitudes and the color indices C are on the International System.

The mean errors appended to the coefficients of C are significant, but the 2 A uncertainty indicated for the constant terms is only an expression of the internal consistency of the measures and takes no account of the much larger uncertainty arising from the observer's habit of setting on the spectral images. Hertzsprung bisected the images;[17] Vanderlinden set on the center of gravity,[18] a method which corresponds closely to the definition of the computed wave lengths. Another circumstance affecting the agreement of the two observers is the reduction of the Lumière plates to the International System. Owing to the discrepancy brought to light in Section V, the correction of 30 A may be doubtful.

The computed change of 400 A in λ for the temperature interval 30,000°–3,000° is fully confirmed. The agreement between the observed and the computed wave-length constants depends partly on the influence of departures from black-body radiation in the stars and partly on the assumption that the effective temperature of an HD A5 star ($C = 0$) is 11,000°. An error here of 1000°, however, would make a difference of only 12 A. From these details it appears that the computed wave lengths should be adequate for all calculations in which they are ordinarily required.

[17] *Pleiades*, p. 353. [18] *Praesepe*, p. 13.

COSMIC STATIC

GROTE REBER
Wheaton, Illinois
Received May 8, 1944

ABSTRACT

Cosmic static is a disturbance in nature which manifests itself as electromagnetic energy in the radio spectrum arriving from the sky. The results of a survey at a frequency of 160 megacycles per second show the center of this disturbance to be in the constellation of Sagittarius. Minor maxima appear in Cygnus, Cassiopeiae, Canis Major, and Puppis. The lowest minimum is in Perseus. Radiation of measurable intensity is found coming from the sun.

Experiments on the measurement of electromagnetic energy at radio wave lengths arriving from the sky have been conducted at Wheaton, Illinois, for a number of years. Preliminary results have already been published.[1] During the year 1943 new and improved apparatus was put into operation and considerably better data were obtained.

The electromagnetic energy is captured by the mirror shown in Figure 1 and is directed to the mouth of the drum at the focal point of the mirror. Within the drum are a pair of cone antennae. These convert the electromagnetic energy into alternating current. This current is fed from the tips of the cones up a parallel-wire transmission line to the receiver-mounting on the end of the drum. On this mounting is attached a five-stage amplifier of about 90-decibels gain over the frequency range 156–164 megacycles per second.[2] It uses type 954 acorn tubes and a circuit arrangement involving transmission-line elements. The output of the amplifier is rectified by a type 9006 diode, and the resulting direct-current voltage is fed down a concentric cable into the house, where the associated power supply and recorder equipment shown in Figure 2 are located.

It is well known that considerable amounts of random-charge voltage are generated in the grid and plate circuits of the first tube of a multistage amplifier. This background random-charge voltage will be rectified by the diode and appears as a constant direct-current voltage, V_{on}, at the end of the concentric cable. Its magnitude has been the point of much investigation and serves as a reference level for the calibration of the intensity of cosmic static phenomena. The value of V_{on} is noted on a meter before and after a set of data is taken. During the actual taking of data, V_{on} is canceled out by a small battery so that the cosmic static may be more easily perceived.

The mirror of Figure 1 is mounted on an east-west axis so that it may be pointed to any angle of declination between the limits of $-32°.5$ and $+90°$ along the north-south meridian. One of the circular tracks is calibrated in degrees. The mirror is set to point at the desired declination; and then, as the earth rotates, the mirror sweeps out a band in the sky along this particular declination. Whenever the mirror passes over a cosmic static disturbance, energy is collected, and the voltage at the end of the concentric cable increases by an amount ΔV_{on} The recorder of Figure 2 is set to a chart speed of 6 inches per hour. If no cosmic static is intercepted, the recorder will draw a straight line on the chart. If cosmic static is encountered, the pen will move up by an amount ΔV_{on}. Figure 3 shows sample charts taken at various declinations.

If no cosmic static had been intercepted, the recorder would have drawn a line of some constant slope. The magnitude of this slope is unimportant, provided the line remains

[1] G. Reber, *Proc. I.R.E.*, **28**, 68, 1940; *Ap. J.*, **91**, 621, 1940; *Proc. I.R.E.*, **30**, 367, 1942.

[2] G. Reber, *Electronic Industries*, **3**, 89–92, 1944.

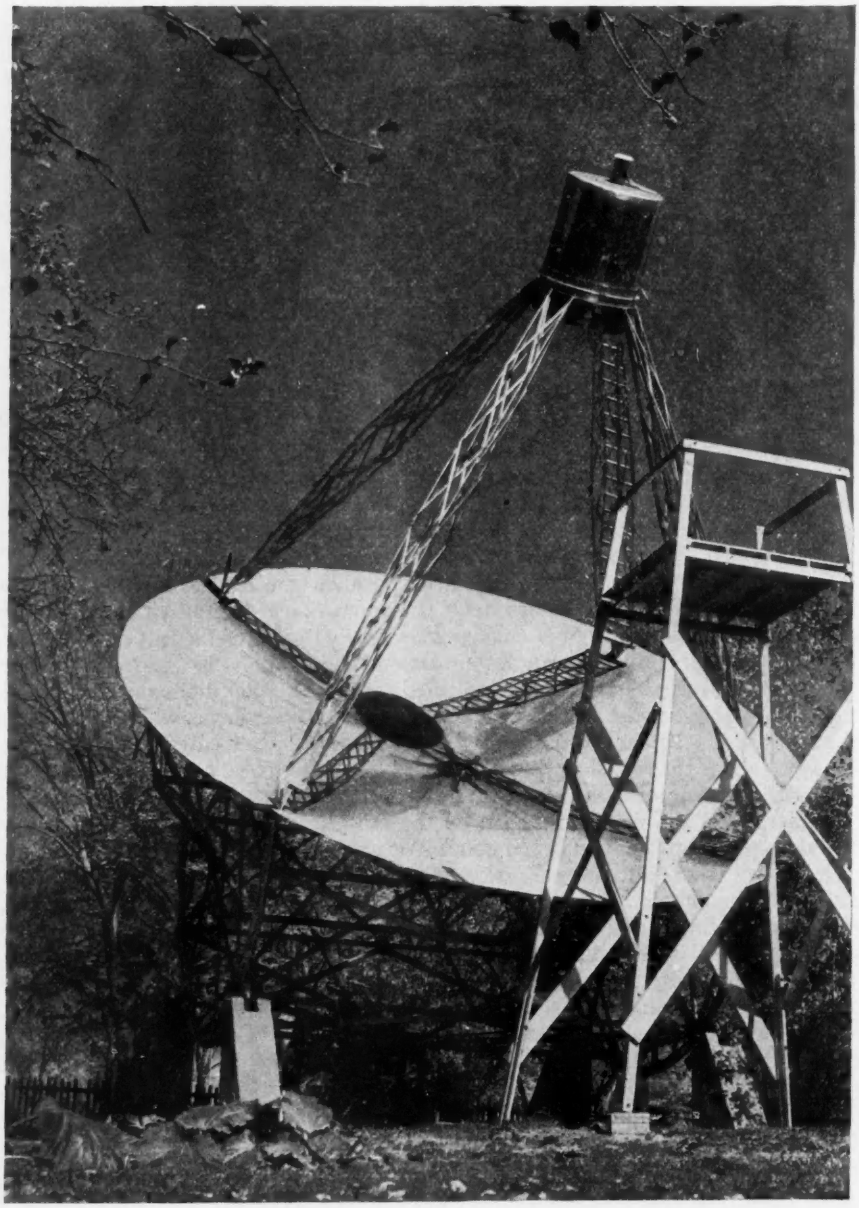

FIG. 1.—Sheet-metal mirror, 31.4 feet in diameter, 20 feet in focal length, used for collecting cosmic static

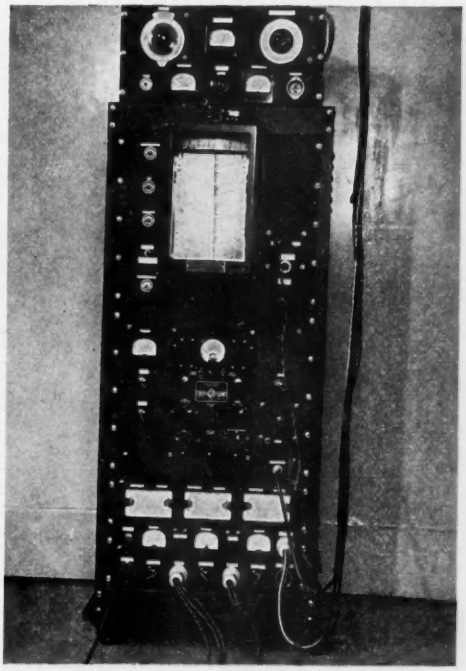

FIG. 2.—Power supply and automatic recorder for cosmic-static investigation

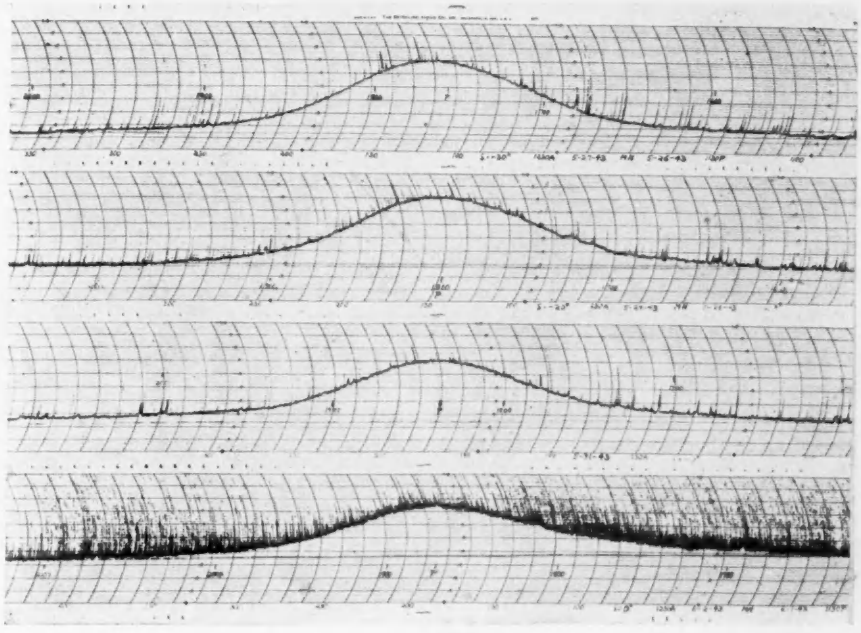

FIG. 3*a*

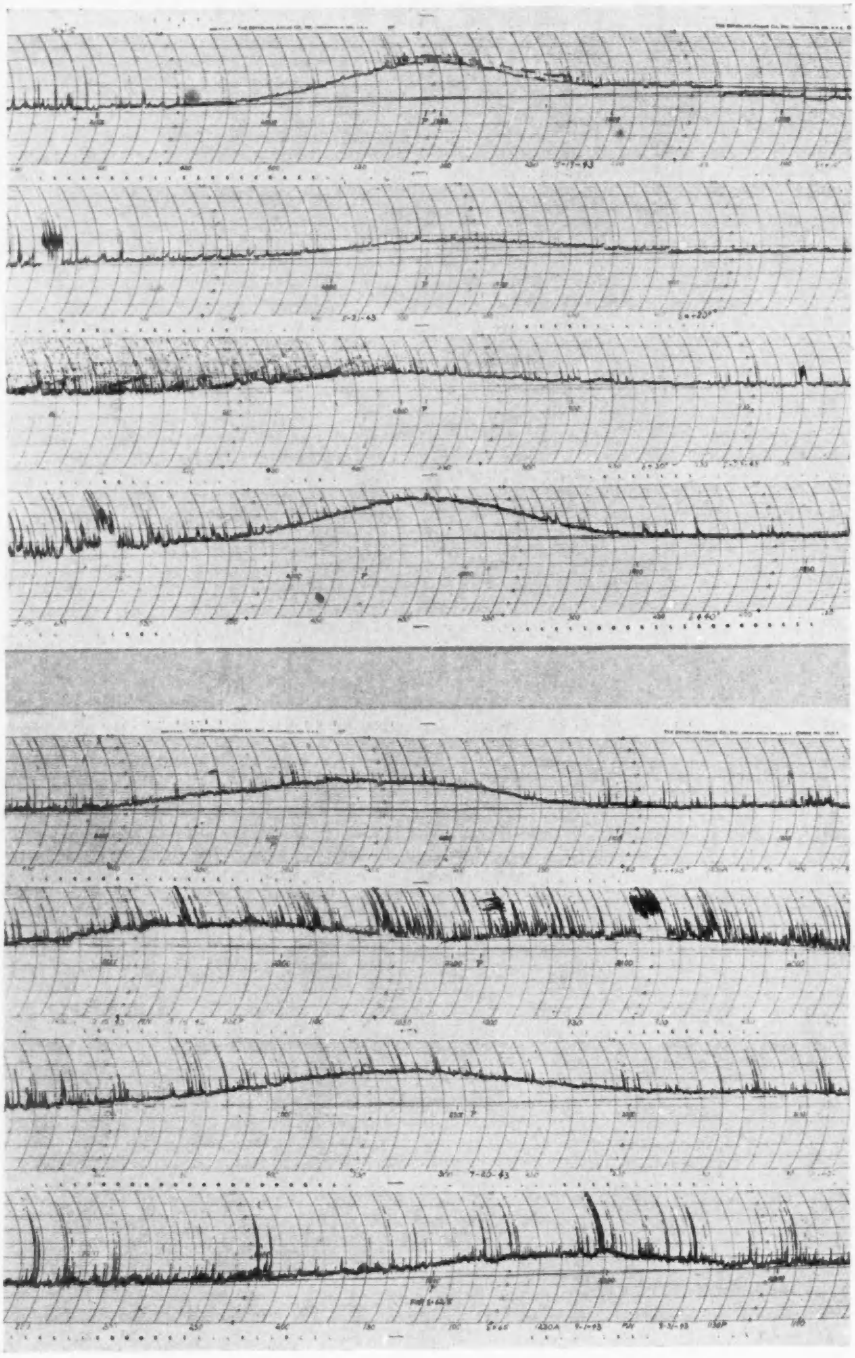

FIG. 3*b*

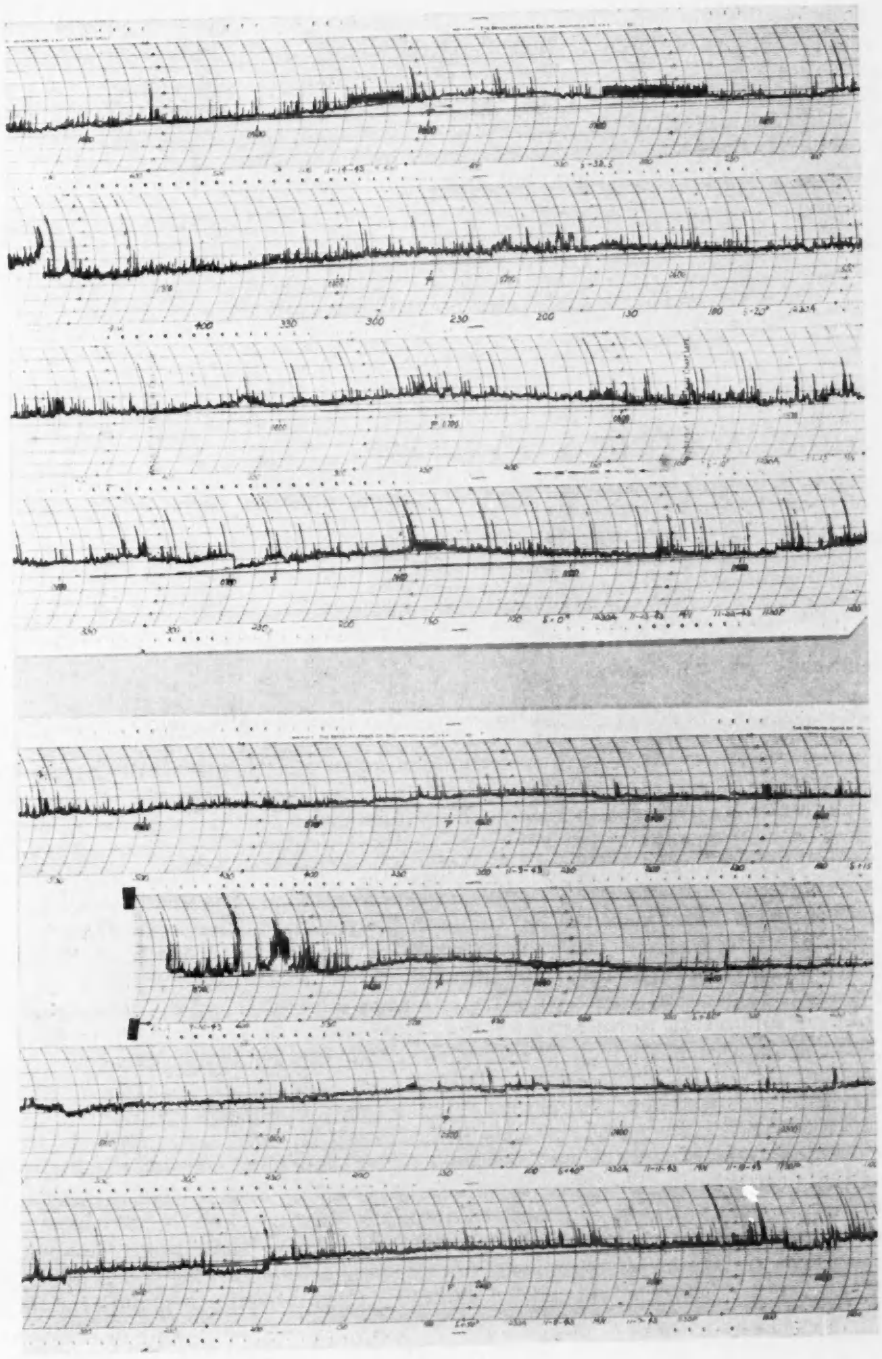

FIG. 3c

on scale for the required length of time. On the charts of Figure 3 this slope has been drawn in. The rise of the curved line above the straight one indicates cosmic static, and its magnitude is ΔV_{on}. The small peaked rises are due to the ignition noise from passing automobiles. The sharp spikes are caused by opening and closing of switches. Central Standard time is noted in the margin. Right ascension in hours is marked by short lines on the chart. The plane of the galaxy is indicated by the mark at *P*.

Referring to a previous paper,[3] the intensity of cosmic static is

$$I = \frac{2U}{E_d E_m A \phi_e \phi_m}, \tag{1}$$

where

$$U = 15.1 \times 10^{-14} \Delta \text{ watts/M.C. band},$$

$$E_d = 1.00 = \text{Drum efficiency},$$

$$E_m = 0.85 = \text{Mirror efficiency},$$

$$A = 7 \times 10^5 \text{ sq. cm.} = \text{Mirror area},$$

$$\phi_e = 8° = \text{Resolving-power in plane of electric vector},$$

$$\phi_m = 6° = \text{Resolving-power in plane of magnetic vector},$$

and

$$\Delta = \frac{\Delta V_{on}}{V_{on}}.$$

Assembling these values gives

$$I = 10.6 \times 10^{-21} \Delta \text{ watts/sq. cm., cir. deg., M.C. band}. \tag{2}$$

Several charts are taken at each declination under consideration. All charts of like declination are then worked up, the right ascension for a given intensity is determined, and the results are averaged to give mean right ascension for this intensity. About two hundred charts were obtained in 1943. The final results plotted on a flattened globe are shown in Figure 4, *a* and *b*, for the two hemispheres of the sky. The constant-intensity lines are in terms of 10^{-22} watts/sq. cm., cir. deg., M.C. band. The small numbers at the centers of major maxima are the top values in this direction. The points at declination $-48°$ in Figure 4, *a* are beyond the normal range of the collector machine. They were obtained as the result of an accident when the machine was run off the end of the track in a heavy snowstorm. It lodged with the mirror nearly vertical and the drum somewhat out of focus and resting in the service tower. These points show the general trend of the phenomena but are not of a high order of accuracy and, consequently, are connected with dashed lines.

Too little is known about the cause of this phenomenon to read a great deal from Figure 4. However, it is suggested that this disturbance is in some way connected with the amount of material in space. Since the wave length is long (1.87 meters), the absorption caused by dust is small. Therefore, the intensity is roughly indicative of the amount of material between us and the edge of the Milky Way. On this basis the various maxima point to the directions of projections from the Milky Way. These projections may be similar to the arms often photographed in other spiral nebulae. In the case of the Milky Way this general picture would call for the center toward Sagittarius, and arms in the directions of Cygnus, Cassiopeiae, and Canis Major. A minimum occurs in Perseus, indicating that we are nearest the edge of the galaxy in that direction. The maximum in lower Puppis is possibly a general rise toward the center. This region from Puppis to

[3] *Proc. I.R.E.* **30**, 376, eq. (20), 1942.

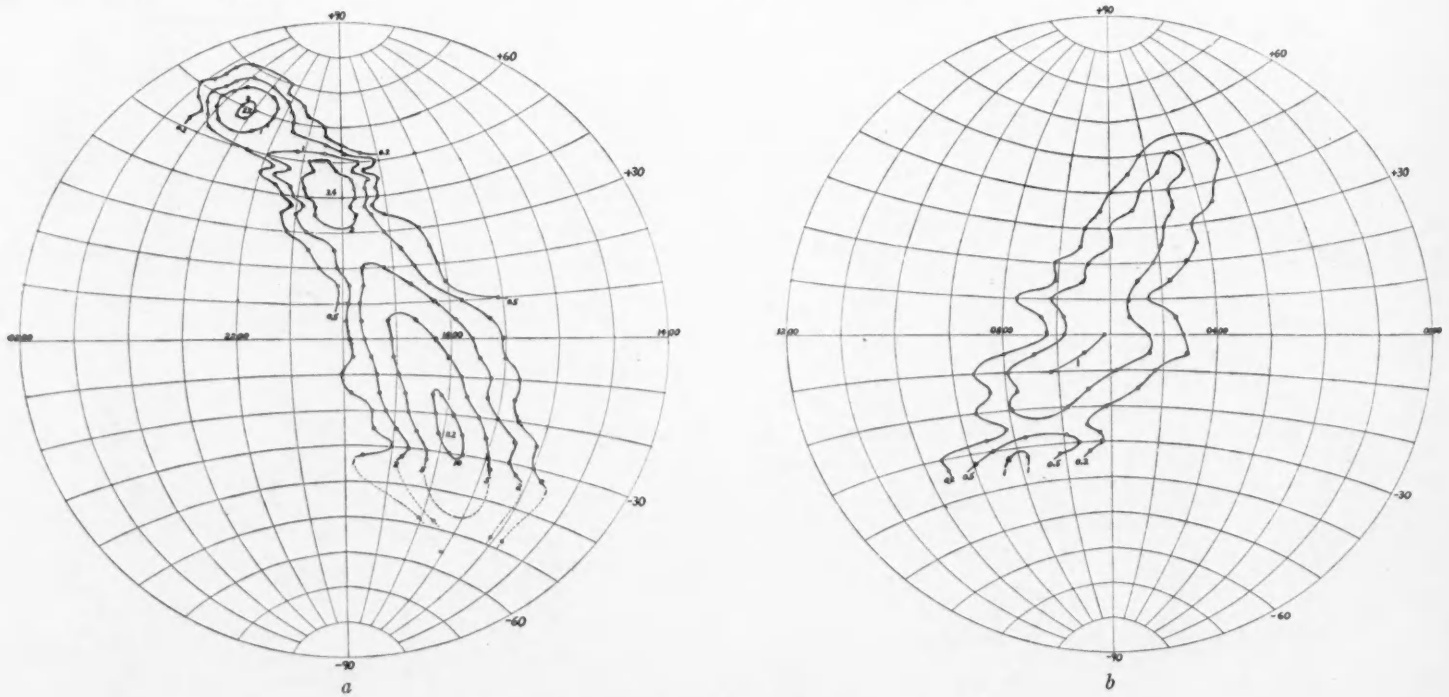

FIG. 4.—Constant intensity lines in terms of 10^{-22} watt/sq. cm./cir. deg./M.C. band

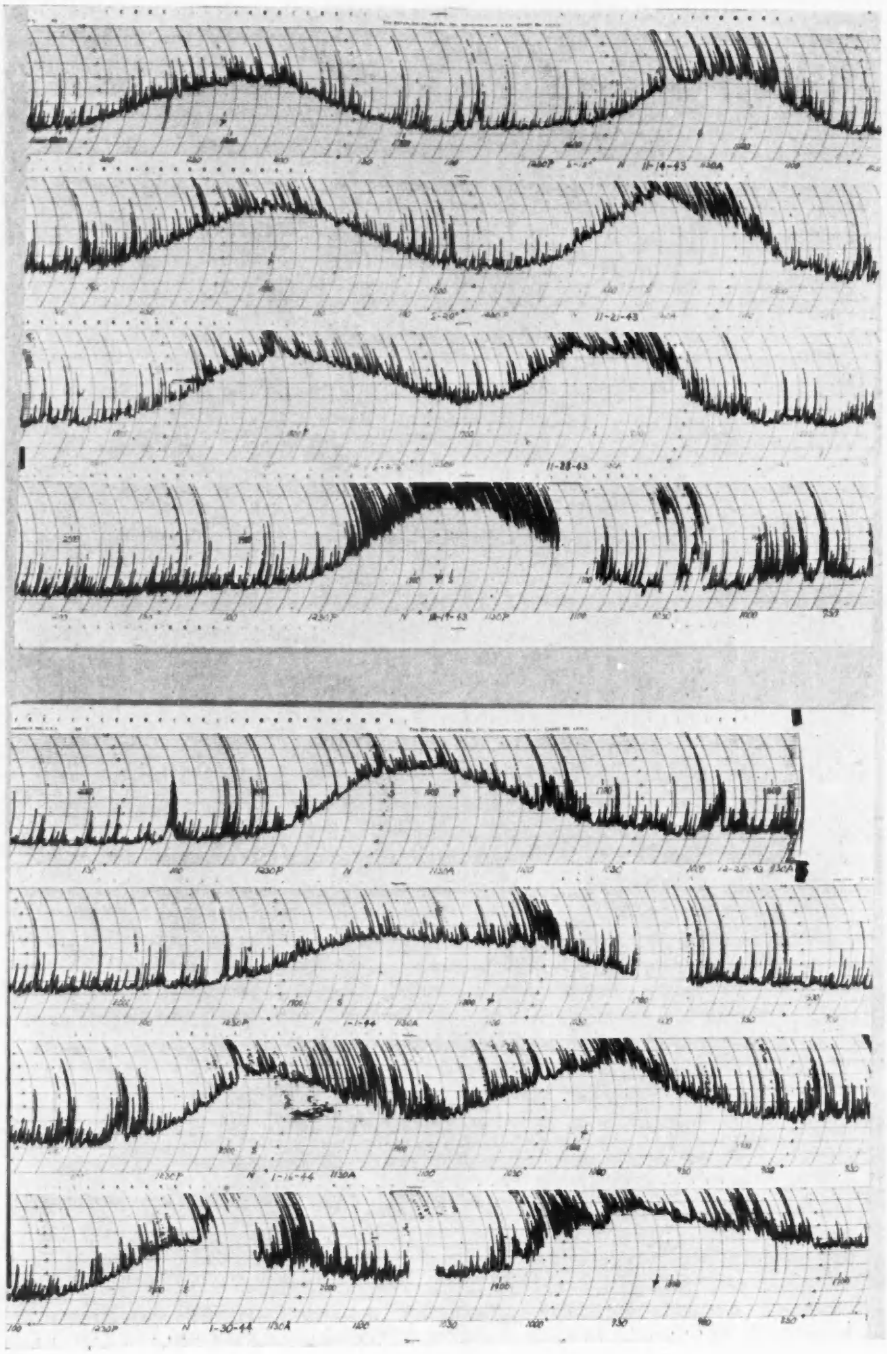

FIG. 5

Scorpius is out of reach at the latitude of Wheaton. However, it is deserving of study, as it may contain other minor maxima.

It has been suggested that this long-wave radiation could be set up in the corona of the sun. Until recently no positive evidence was available. However, the new apparatus was sufficiently stable to allow some data to be taken during the day in spite of severe automobile noise. Figure 5 shows a series of charts taken over several months as the sun passed through the center of the Milky Way. V_{on} is different on the various charts; hence they are not strictly comparable. In any case the sun had the rather surprising center intensity of 10×10^{-22} watts/sq. cm., cir. deg., M.C. band. In spite of the apparent great strength from the sun, this source must be greatly discounted when explaining the origin of cosmic static. If it were the source and the Milky Way were made of average stars like the sun, a very large area in Sagittarius would have a visible intensity equal to that of the sun. Since this is not the case, some other cause must be found to make up the difference of 20 or 30 mag.

A few other objects, such as the moon, the Pleiades, the Orion Nebula, and the spiral in Andromeda have been tested without conclusive results. The last object seems to be at the threshold of sensitivity of the present apparatus, namely, 0.2×10^{-22} watt/sq. cm., cir. deg., M.C. band. Further improved sensitivity will probably pick up a variety of other objects, and an increase in resolving-power will probably show more detail in the galactic structure.

ON THE ORIGIN OF SMOKE PARTICLES IN THE INTERSTELLAR GAS*

D. TER HAAR
Leiden, Holland
Received May 20, 1944

ABSTRACT

This paper attempts to give a theory of the formation of solid particles from the interstellar gas. After a brief outline in Section I of the present data pertaining to the interstellar gas and smoke in the region of the sun, a formula for the temperature of the smoke particles is derived, in Section III, supposing the smoke particles to be heteropolar crystalline particles.

In Section IV it is shown that if the density in the gas clouds is smaller than a certain *characteristic density*, the problem must be attacked differently from the cases in which the density is larger. In Section V the case of $\rho < \rho_{char}$ is treated. The probability for radiation capture, important in that case, is discussed in Section VI.

In Section VII the case $\rho > \rho_{char}$ is treated by a method used by Becker and Döring in their theory of the formation of liquid drops in supersaturated vapor. Now the velocity of smoke formation decreases very rapidly with increasing ρ.

The result of Sections V and VII is that there exists an optimum density for the smoke formation; this density will nearly coincide with the characteristic density.

Finally, Section VIII gives an estimate of the maximum size of the smoke particles and discusses the total smoke density in our part of the galactic system on the assumption that the condensation has stretched over a period of the order of 10^9 years. The density of the diatomic molecules is also discussed.

I. INTRODUCTION

Only a part of the mass of our galactic system is taken up by the stars. The mass of the interstellar gas and of the smoke[1] particles in that gas, taken together, is of the same order as the mass of the stars.[2] Since Eddington's original investigations[3] many papers have been published about the composition, temperature, density, etc., of the interstellar gas.[2,4,5,6] Hydrogen is by far the most abundant element.

Lindblad[7] has discussed the possibility that the solid particles have been formed by condensation from the interstellar gas. He found that the maximum size of the particles which follows from the law for the light-scattering in the smoke clouds (λ^{-1} law[8]) can be explained on the simple hypothesis that there exist particles acting as nuclei for condensation and that every atom falling on the surface of such a nucleus is caught by it, because of the low temperature (3° K) of the latter. He did not inquire into the problem of the formation of the nuclei.

That problem will be investigated in the present paper, which is partly an elaboration and partly a completion of the author's lecture at an interacademical colloquium in Utrecht.

* [This manuscript was submitted for publication by Dr. Bart J. Bok, chairman of the Committee for the Distribution of Astronomical Literature of the American Astronomical Society.—ED.]

[1] The term "smoke" for the solid interstellar particles was suggested by Mr. van de Hulst (J. H. Oort, *Nederl. Tijdschr. Natuurk.*, **10**, 238, 1943). Considering the probable process of formation, this name appears to be more adequate than that of "dust," by which they have usually been described.

[2] T. Dunham, Jr., *Proc. Amer. Phil. Soc.*, **81**, 277, 1939.

[3] *Proc. R. Soc.*, A, **111**, 424, 1926.

[4] B. Strömgren, *Ap. J.*, **89**, 529, 1939.

[5] P. Swings, *Ann. d'Ap.*, **1**, 1, 1938.

[6] E. Schönberg, *Ergeb. Exakt. Naturwiss.*, **19**, 1, 1940.

[7] *M.N.*, **95**, 20, 1934; *Nature*, **135**, 133, 1935.

[8] See, e.g., Hall, *Ap. J.*, **85**, 145, 1937.

II. SYMBOLS USED

The following symbols have been used:

$\rho(\omega)$ Density of radiation at the frequency ω
ω_0 Fundamental frequency of the crystal; $\omega_0/c = 1000$ cm^{-1}
m Reduced mass of an ion in the crystal; $m = 2.5 \cdot 10^{-23}$ gm (nitrogen atom)
e Effective charge of an ion in the crystal; $e = 10^{-10}$ e.s.u.[9]
σ Surface of an atom; $\sigma = 2 \cdot 10^{-15}$ cm^2 (surface of a graphite sphere divided by the two-thirds power of the number of atoms contained in it)
i Number of atoms in a crystal
T_i Temperature of a particle consisting of i atoms
T_{rad} Temperature of the stellar radiation;[10] $T_{\text{rad}} = 10{,}000°$
T_g Temperature of the interstellar gas; $T_g = 10{,}000°$
v Mean velocity of the hydrogen atoms in the interstellar gas;[10] $v = 1.5 \cdot 10^6$ cm sec^{-1}
ρ, ρ' Number of atoms per cm^3 in the interstellar gas
g Dilution factor of the radiation;[10] $g = 10^{-14}$
u_i Binding energy of an atom in a particle of i-atoms; $u_i = 1$ e.v.
N_i Number of crystals consisting of i-atoms
O_i Surface of one crystal of i-atoms; $O_i = i^{2/3}\sigma$
Z_i Total surface of all crystals of i-atoms; $Z_i = N_i O_i$
$2\tau_c$ Collision time; $\tau_c = 10^{-13}$ sec
γ_i, γ_i' Probability for an impinging atom to stick to the surface of a crystal
ΔE Dissociation energy of a diatomic molecule
$c_1, c_2, \ldots$ Numerical factors of order 1
$K', K'', \ldots$ Nonspecified factors
c Velocity of light; $c = 3 \cdot 10^{10}$ cm sec^{-1}
h Planck's constant; $h = 6.6 \cdot 10^{-27}$ erg sec
$\hbar$ Dirac's constant; $\hbar = h/2\pi$
k Boltzmann's constant; $k = 1.4 \cdot 10^{-16}$ erg degree^{-1}
a_i Number of colliding atoms which in 1 sec stick to 1 cm^2 of the surface of a particle of i-atoms
b_i Number of atoms which in 1 sec evaporate from 1 cm^2 of the surface of a particle of i-atoms

III. TEMPERATURE OF THE CRYSTALLINE PARTICLES

If there should be a temperature equilibrium between the atoms of the interstellar gas ($T_g = 10{,}000°$) and the diatomic, triatomic, and polyatomic particles, the number of particles consisting of i-atoms would decrease rapidly with increasing i, and condensation would be entirely out of the question. The density of the radiation in space, however, is small;[10] therefore, the emission of radiation of a polyatomic particle will not be counterbalanced by the absorption of radiation, and the temperature of the particles will decrease with increasing i. As a consequence, the conditions for the accretion process will become gradually more favorable, until, for sufficiently large i, the temperature has become so low that every atom (except probably the hydrogen and helium atoms[2]) falling upon a smoke particle is caught by it.

As a model for the smoke particles we will use heteropolar crystals, which are small, compared to the wave length of the stellar radiation. Inasmuch as there are only slight deviations from harmonic binding between the atoms, these will emit and absorb radiation approximately as one large harmonic oscillator (only the fundamental frequencies contribute). A harmonic oscillator with mass M, charge ϵ, and frequency ω absorbs and emits per second the following energies (assuming $kT \ll h\omega$; viz., only a small fraction

[9] We have taken about one-fifth of the elementary charge, corresponding to Dennison's (*Phys. Rev.*, **31**, 503, 1928) figure for *HCl*. For the actual crystals, e may be expected to be a good deal smaller.

[10] A. S. Eddington, *op. cit.*

of the radiation oscillators is in the first excited quantum state, whereas higher excitations can be neglected):

$$E_{\text{abs}} = \frac{\pi\epsilon^2}{M}\,\rho(\omega) \qquad \text{and} \qquad E_{\text{em}} = \frac{8\pi^2 h\omega^3\epsilon^2}{Mc^3}\,e^{-h\omega/kT}. \tag{1}$$

In our case we must use for particles of i-atoms: $\epsilon = ie$, $M = im$, $T = T_i$, and $\omega = \omega_0$. The radiation in interstellar space is approximately a diluted Planck radiation; therefore, the formulae (1) become

$$E_{\text{abs}} = i\,\frac{8\pi^2 e^2 h g\omega_0^3}{mc^3\,(e^{h\omega_0/kT_{\text{rad}}} - 1)} \qquad \text{and} \qquad E_{\text{em}} = i\,\frac{8\pi^2 h\omega_0^3 e^2}{mc^3}\,e^{-h\omega_0/kT_i}. \tag{2}$$

The atoms colliding with the particles and those evaporating from them are practically all hydrogen atoms; they carry with them per second the following energies:

$$E_{\text{on}} = c_1 i^{2/3}\sigma\rho v k T_g \qquad \text{and} \qquad E_{\text{off}} = c_2 i^{2/3}\sigma\rho v k T_i\,.$$

The energy balance yields the following equation:

$$c_1\sigma\rho v k T_g i^{2/3} + i\,\frac{8\pi^2 e^2 h g\omega_0^3}{mc^3}\,(e^{h\omega_0/kT_{\text{rad}}} - 1)^{-1} = c_2\sigma\rho v k T_i i^{2/3} + i\,\frac{8\pi^2 h e^2\omega_0^3}{mc^3}\,e^{-h\omega_0/kT_i}.$$

On the left-hand side the ratio of the coefficient of i to the coefficient of $i^{2/3}$ is approximately 10^{-9}; on the right-hand side their ratio is larger than 10^4 for $T_i \cong 100°$ K.

Thus, the following equation holds approximately:

$$e^{-h\omega_0/kT_i} = \frac{c_3\sigma\rho v m c^3 k T_g}{8\pi^2 e^2 h\omega_0^3}\,i^{-1/3} = \rho e^{-A} i^{-1/3}. \tag{3}$$

The ρ and v in formula (3) may be taken to refer to the hydrogen atoms in the interstellar gas, while σ, m, e, and ω_0 are quantities characteristic of the composition of the crystals (which can be safely assumed to contain little or no hydrogen). Using for all these quantities the values given in the list and using 2 cm^{-3} for ρ, we obtain from formula (3)

$$T_i = \frac{83}{1 + \frac{1}{10}\log i} \qquad \text{(the log is to the base } e\text{)}. \tag{4}$$

If we had taken for ρ a value one hundred times larger and for e a value ten times smaller, we would get: $T_i = (182/1 + \frac{1}{24}\log i)$. We are, therefore, certain that the temperature pertaining to the internal degrees of freedom of the particles is very low, even if i is not more than 2 or 3. In the region of large i the formulae for our crystal model are clearly rather different from those holding for a black body, but it seems physically justifiable to use this model for the determination of T_i in the region of i-values, where this temperature is significant for our problem.

IV. THE CONDENSATION PROCESS; CHARACTERISTIC DENSITY

Assuming that a quasi-stationary situation has been established, so that the number of particles containing a given number of atoms remains practically constant, we can express this by the equation

$$j = a_i Z_i - b_{i+1} Z_{i+1}\,. \tag{5}$$

A similar equation also occurs in Becker and Döring's theory[11] on the formation of

[11] *Ann. d. Phys.*, Ser. V, **24**, 719, 1935.

liquid drops in a supersaturated vapor. The quantity j is the number of particles "flowing through" the various particle sizes; the number of new smoke particles formed per second will clearly depend on j.

Using the condensation-evaporation picture, we obtain the following formulae[12,13] for a_i and b_i:

$$a_i = c_4 \gamma_i \rho' v' = \gamma_i e^{\alpha}, \tag{6a}$$

$$b_i = c_5 \gamma'_{i-1} \frac{m(kT_i)^2}{h^3} e^{-u_i/kT_i} = \gamma'_{i-1} e^{\beta_i - (u_i/kT_i)}. \tag{6b}$$

We see that, apart from the factor γ_i, a_i is independent of i. We may take β_i and u_i practically independent of i. The quantity b_i is still very much dependent on i through T_i appearing in the exponent.

TABLE 1

u (E.V.)	$\frac{\omega_0}{c}$ (Cm^{-1})	e (E.S.U.)	ρ_{char}
2	1000	10^{-10}	$4 \cdot 10^{6}$
		10^{-11}	$4 \cdot 10^{4}$
	2000	10^{-10}	$4 \cdot 10^{5}$
		10^{-11}	$4 \cdot 10^{3}$
1	1000	10^{-10}	$4 \cdot 10^{4}$
		10^{-11}	$4 \cdot 10^{2}$
	2000	10^{-10}	200
		10^{-11}	2
$\frac{1}{2}$	1000	10^{-10}	20
		10^{-11}	0.2
	2000	10^{-10}	$2 \cdot 10^{-5}$
		10^{-11}	$2 \cdot 10^{-7}$

The ratios b_{i+1}/a_i decrease gradually to values smaller than 1 when i increases. We can distinguish now between two cases—viz., the case where these ratios decrease from a value originally larger than 1 and the case where these ratios even from $i = 1$ onward are always smaller than 1.

Assuming all quantities appearing in our formulae to remain constant, with the exception of ρ, the first or the second case is realized according as ρ is larger or smaller than a certain *characteristic density*. We can determine this characteristic density by calculating T_i from the equation $a_i = b_{i+1}$ and then solving ρ from equation (3), putting $i = 1$. The result is

$$\log \rho_{char} = A - \frac{h\omega_0}{u}(\beta - \alpha). \tag{7}$$

Using different values for u, ω_0/c, and e, we have computed Table 1 for ρ_{char}. The value we choose for u depends on the assumption of the nature of the evaporation. If molecules

[12] The term ρ' in formula (6a) indicates the density of the atoms constituting the crystal; ρ' differs, therefore, from the ρ in formula (3) and will be much smaller.

[13] In b_i there appears $\gamma'_i - 1$ (instead of γ'_i), since the evaporation probability is dependent on the number of impinging atoms sticking to a particle of $i - 1$ atoms. Except for small i, $\gamma'_i = \gamma_i$. For the deduction of the formula for b_i see, e.g., Schäfer (*Einf. Theor. Phys.*, 2, 609, Berlin-Leipzig, 1929).

evaporate from the crystal, u may be a good deal smaller than in the case where only atoms evaporate. Since ρ_{char} will nearly coincide with the optimum density for the smoke formation (cf. Sec. VII), the conditions will be most favorable for this formation if ρ nearly coincides with ρ_{char}.

From Table 1 we see that the order of magnitude of ρ_{char} depends first of all on the choice of u. Since particles for which u is small will not be formed, because of their large evaporation, it seems probable that u has approximately the value of 1 e.v. Since the composition of the smoke particles is still less known than that of the gas, our choice for ω_0/c and e necessarily remains somewhat arbitrary.[14]

In the following sections we will treat the two cases ($\rho < \rho_{\text{char}}$ and $\rho > \rho_{\text{char}}$) as if they could be separated rigorously, although there will, of course, be a certain transition range of ρ-values.

V. FIRST CASE: $\rho < \rho_{\text{char}}$

Assuming in equation (5) the terms $b_{i+1}Z_{i+1}$ to be negligible, we get

$$j = a_i Z_i = c_6 \sigma \rho' v' \gamma_i \qquad (i = 1, 2, 3, \ldots). \quad (8)$$

As in formula (6a), ρ' is the density of the atoms constituting the crystal.

Using formula (8), we obtain

$$N_i = \frac{j}{a_i O_i} = \frac{a_1 Z_1}{a_i O_i} = \frac{\gamma_1 N_1}{\gamma_i i^{2/3}}. \quad (9)$$

Except for small values of i, we may put $\gamma_i = 1$, and formula (9) becomes

$$N_i = \gamma_1 N_1 i^{-2/3}. \quad (10)$$

We see the importance of γ_1, the probability that a diatomic molecule is formed when a collision of two atoms occurs. In ordinary chemical kinetics the formation of diatomic molecules takes place through a three-body collision. The ratio of the number of three-body collisions to that of two-body collisions is, however, only of the order 10^{-24} in interstellar space, whereas the ratio required to explain the observed smoke density would be much larger. It is, therefore, necessary to explain the formation of diatomic molecules by radiation capture (i.e., association accompanied by emission of radiation).[15]

VI. ESTIMATE OF γ_1

To estimate the probability, γ_1, of the formation of a diatomic molecule by radiation capture, we will first consider the following rough model. When the two atoms that are to form the molecule approach each other, the system will, during the collision, possess a dipole moment which varies with the time; and radiation will therefore be emitted. This emission will be calculated on a rough correspondence basis analogous to Kramers' treatment of X-ray transitions.[16]

For this purpose we assume the potential of the interaction forces of the two atoms, considered as a function of their distance apart, to have the shape shown in Figure 1, and we wish to calculate the probability of a radiation capture in the two-particle system so defined.

The relative velocity of the atoms will be a function of the time. A representative type

[14] The sublimation heats of H_2, H_2O, Ca, and BaO are 0.22, 11.26, 43, and 90 Cal., which correspond to u-values of about 0.01, 0.5, 1.9, and 4 e.v. It must be borne in mind, however, that an exact theory should demand a thorough sorting-out of the different possibilities of the building-up of a smoke particle.

[15] Swings (*Ap. J.*, **95**, 270, 1942) has also urged the necessity of taking radiation capture into consideration, but for a different purpose.

[16] *Phil. Mag.*, **46**, 836, 1923.

of this function is shown in Figure 2. The corresponding acceleration will be a function of two δ functions[17]

$$a(t) = \sqrt{\frac{2\Delta E'}{m}}\left[\delta(t+\tau_c) - \delta(t-\tau_c)\right],$$

with the Fourier analysis:

$$a(t) = \sqrt{\frac{2\Delta E}{m}}\int_{-\infty}^{+\infty} 2ie^{2\pi i\nu t}\sin 2\pi\nu\tau_c d\nu.$$

The total classical emitted radiation will formally be given by

$$\frac{2e^2}{3c^3}\int |a(t)|^2 dt = \frac{2e^2}{3c^3}\cdot\frac{16\Delta E}{m}\int_0^{\infty}\sin^2 2\pi\nu\tau_c d\nu$$

(e is an effective charge entirely comparable with the effective charge in the previous sections).

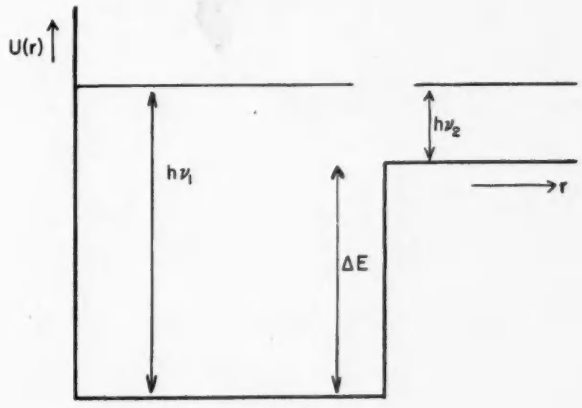

FIG. 1

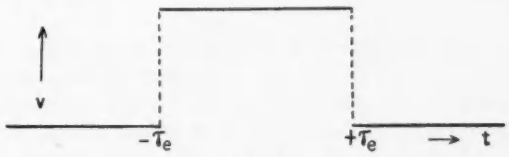

FIG. 2

Using Kramers' application of the correspondence principle,[16] we obtain an estimate for the average energy actually emitted by quantum processes by replacing the boundaries of the integral by ν_1 and ν_2.

Because $\nu_1 - \nu_2 \cong 10^{15}$ sec^{-1} and $\tau_c \cong 10^{-13}$ sec, it is permissible to replace $\sin^2 2\pi\nu\tau_c$ by its mean value $\frac{1}{2}$. At every molecule formation approximately $\frac{1}{2}h(\nu_1+\nu_2)$ is emitted. We obtain, therefore,

$$\gamma_1 \cong \frac{2e^2}{3c^3}\frac{2(\nu_2-\nu_1)}{h(\nu_2+\nu_1)}\frac{8\Delta E}{m}$$

or

$$\gamma_1 \cong \frac{32}{6\pi}\frac{\nu_2-\nu_1}{\nu_2+\nu_1}\frac{e^2}{\hbar c}\frac{\Delta E}{mc^2}. \qquad (11)$$

[17] P. A. M. Dirac, *Principles of Quantum Mechanics*, p. 72, Oxford, 1935.

For the formation of CH molecules we obtain, for instance, approximately $\gamma_1 \cong 10^{-13}$.

It should be borne in mind that the mechanism of radiation capture actually may be more complicated. In fact, when two atoms approach each other, two or more electronic states may be realized and a radiation capture may occur which is accompanied by electron transitions. According to the considerations and figures of R. S. Mulliken,[18] this will hold for CH, CN, N_2^+, CO^+, and BH (and, therefore, presumably also for CH^+; data of Herzberg, cited by Swings,[15] confirm this conclusion), but not for NH, OH, NO, and NaH. In that way, γ_1 may be much larger. A calculation of γ_1 taking into account this possibility of electronic transitions yields for CH the approximate value of 10^{-10}. It seems, however, that for other compounds (except, probably, CN) γ_1 will be much smaller.

I am greatly indebted to Professor Kramers for the following estimate of γ_1 in this case:

If $A(r)$ is the Einstein probability for the transition between the two possible electronic states of the molecule, it is easily shown that, when taking into account the dif-

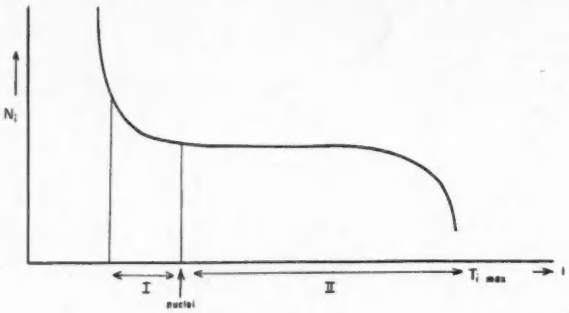

FIG. 3

ferent possibilities during a collision, the cross-section for a radiation capture will be given by

$$Q_{\text{rad}} = Q_{\text{coll}}\,\gamma_1 = f\int 4\pi r^2 A\,(r)\, e^{-U(r)/kT}\left[F\left(\sqrt{\frac{U'}{kT}}\right) - F\left(\sqrt{\frac{U}{kT}}\right)\right] dr\,. \quad (12)$$

In this formula $U(r)$ is the energy of the molecule in the upper state and $U'(r)$ that in the lower state (U and U' tend to zero for $r \to \infty$), T is the temperature of the atoms involved in the capturing process, $F(r)$ is a function which for imaginary argument is equal to zero, whereas for real positive argument it is defined by

$$F(x) = \frac{4}{\sqrt{\pi}}\int_0^x e^{-x^2} x^2 dx\,,$$

while f is the probability that, when the two atoms meet, they will find themselves in the upper electronic state under consideration.

In the case of CH the ground state $^3P(C) + {}^2S(H)$ splits into $^4\Pi$ ($g = 8$), $^2\Sigma$ ($g = 2$), $^4\Sigma$ ($g = 4$), $^2\Pi$ ($g = 4$) (the g's are the weights of the respective states). The radiation capture corresponds to $^2\Sigma \to {}^2\Pi$ transitions. Thus, f in this case equals $2/18 = 1/9$. From an inspection of the curves for $U(r)$ ($^2\Sigma$) and $U'(r)$ ($^2\Pi$), one infers that for $T \cong 10{,}000°$ the factor $e^{-U/kT}\,(F' - F)$ equals about 1 between $r = 0.5$ and $r = 1.5$ A, whereas it can be neglected for other r-values. Thus Q_{rad} becomes $\cong (4\pi/9)\, 10^{-24}\, A$ (where $r = 1$ A). With $A \cong 10^6$ sec^{-1} and $Q_{\text{coll}} \cong 1.5 \cdot 10^{-9}$, this gives for γ_1 the estimate 10^{-10} mentioned above.

[18] *Rev. Mod. Phys.*, **2**, 60, 1930.

VII. SECOND CASE: $\rho > \rho_{\text{char}}$

In this case we are in the same situation as Becker and Döring.[11] The ratios b_{i+1}/a_i decrease gradually with increasing i from a value larger than 1 to values smaller than 1. In this case a quasi-stationary situation will be established where at first N_i will decrease rapidly as a function of i until we have reached a *critical range of* i-values (this critical range appears for $b_{i+1}/a_i \cong 1$). After that N_i will decrease according to the formula: $N_i \cong K i^{-2/3}$; in the latter range the condensation predominates largely over the evaporation. The particles at the end of the critical range may indeed be considered as the nuclei for the further (easy) smoke formation (see Fig. 3). Of course, the curve representing N_i will break off somewhere in the pure condensation range, because the period over which the condensation has stretched (presumably about 10^9 years) has been too short for the formation of larger particles.

We shall now eliminate, as Becker and Döring have done (cf. their formula [7*a*] and the calculations following thereupon) $Z_2, Z_3, \ldots, Z_{n-1}$ from equations (5) by writing them in the following form:

$$\begin{aligned}
\frac{j}{a_1} &= Z_1 - Z_2\frac{b_2}{a_1}\\
\frac{jb_2}{a_2a_1} &= Z_2\frac{b_2}{a_1} - Z_3\frac{b_3b_2}{a_2a_1}\\
\frac{jb_3b_2}{a_3a_2a_1} &= Z_3\frac{b_3b_2}{a_2a_1} - Z_4\frac{b_4b_3b_2}{a_3a_2a_1}\\
&\cdots\cdots\cdots\cdots\cdots\cdots\cdots\cdots\\
\frac{jb_{n-2}\ldots b_2}{a_{n-2}a_{n-1}\ldots a_1} &= Z_{n-1}\frac{b_{n-1}\ldots b_3b_2}{a_{n-2}\ldots a_2a_1} - Z_n\frac{b_n\ldots b_2}{a_{n-1}\ldots a_1}
\end{aligned}$$

A summation of these equations gives

$$j = \frac{Z_1 - \dfrac{b_n\ldots b_2}{a_{n-1}\ldots a_1}Z_n}{\sum_{i=1}^{n-1} R_i} \cong \frac{Z_1}{\sum_{i=1}^{\infty} R_i}, \tag{13}$$

with

$$R_1 = \frac{1}{a_1}, \qquad R_i = \frac{b_2}{a_1}\frac{b_3}{a_2}\ldots\frac{b_{i-1}}{a_{i-2}}\frac{1}{a_{i-1}}. \tag{14}$$

Since the ratios b_i/a_{i-1} are at first larger than 1 and finally smaller than 1, R_i reaches a maximum for $i = i_0$, where i_0 is that particular value of i for which $b_i/a_{i-1} = 1$.

Using for a_i, b_i, and T_i the following formulae,

$$a_1 = \gamma_i e^{\alpha}, \tag{6a}$$

$$b_i = \gamma'_{i-1} e^{\beta - (u/kT_i)}, \tag{6b}$$

$$e^{-h\omega_0/kT_i} = \rho e^{-A} i^{-1/3}, \tag{3}$$

we get for R_i approximately[11] (cf. Becker and Döring)

$$R_i = e^{C(i-1)\log i_0 - Ci\log i + Ci}(\rho' v')^{-1}, \tag{15}$$

where $C = u/3h\omega_0$.

For $\sum_{i=1}^{\infty} R_i$ we get thus approximately

$$\sum_{i=1}^{\infty} R_i = c_7 i_0^{-} c_e^{c i_0} (\rho' v')^{-1} . \tag{16}$$

Since i_0 and ρ_{char} satisfy the following equations,

$$\tfrac{1}{3} \log i_0 = \frac{h\omega_0}{u}(\beta - \alpha) - A + \log \rho \tag{17}$$

and

$$\log \rho_{\text{char}} = A - \frac{h\omega_0}{u}(\beta - \alpha), \tag{7}$$

we get

$$i_0 = \left(\frac{\rho}{\rho_{\text{char}}}\right)^3, \tag{18}$$

so that we obtain for j the following formula:

$$j = c_8 \sigma \rho'^2 v' \left(\frac{\rho}{\rho_{\text{char}}}\right)^{u/h\omega_0} e^{-(u/3h\omega_0)(\rho/\rho_{\text{char}})^3} . \tag{19}$$

From formula (19) it follows that above the characteristic density the velocity of smoke formation will *decrease* with *increasing* density. Since $u/3h\omega_0$ is of the order of 1,

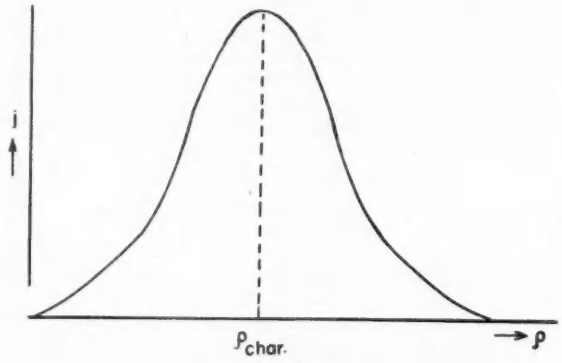

FIG. 4

we arrive at the conclusion that smoke formation will be practically absent in a system where the gas density is only a few times larger than the characteristic density. Together, formulae (8) and (19) present us with j as a function of ρ (see Fig. 4). There will exist an optimum density which will only differ from the characteristic density by a factor of 2 or 3.

VIII. MAXIMUM SIZE OF THE SMOKE PARTICLES; SMOKE DENSITY; DENSITY OF THE DIATOMIC MOLECULES

Equation (5) is, of course, not suited for the determination of the maximum size of the smoke particles reached in a given interval of time. We have instead to use the equation

$$\frac{dN_i}{dt} = a_{i-1} Z_{i-1} - a_i Z_i - b_i Z_i + b_{i+1} Z_{i+1} . \tag{20}$$

(We assume, for the sake of simplicity, that the exhaustion of the interstellar gas is negligible.)

In the condensation range we may neglect terms with b and, putting $\tau = \sigma\rho' v' t$, $\delta_i^{-1} = \gamma_i i^{2/3}$, we obtain

$$\frac{dN_i}{d\tau} = \delta_{i-1}^{-1} N_{i-1} - \delta_i^{-1} N_i . \tag{21}$$

These simultaneous differential equations can be solved.[19] For the initial conditions at $t = 0$: $N_1 = N_1^0$, $N_2 = N_3 = \ldots = 0$, the solution is

$$N_i = N_1^0 \prod_{j=1}^{i-1} \delta_j^{-1} \sum_{j=1}^{i} \frac{e^{-\delta_j^{-1}\tau}}{\prod_{k \neq j} (\delta_k^{-1} - \delta_j^{-1})} \tag{22a}$$

or

$$N_i = N_1^0 \delta_i \frac{1}{2\pi\sqrt{-1}} \oint \frac{e^{-x\tau}}{\prod_{j=1}^{i} (1 - x\delta_j)} dx , \tag{22b}$$

where the integration path is clockwise round the poles of the integrand. We see from formula (22a) that terms with $\delta_i^{-1}\tau \gg 1$ will not materially contribute to N_i; $\delta_1^{-1}\tau$ is certainly small, compared with 1 (a period $t = 10^9$ years corresponds to $\tau \cong 1000$, using for ρ': 10^{-4}, the approximate density of oxygen). Since diatomic molecules in their lowest vibration state (from eq. [4] it follows that $T_2 \cong 83°$ K) will have a chance of capturing a third atom in a purely mechanical way, γ_2 must certainly be expected to be much larger than γ_1. For the moment we shall assume $\delta_3^{-1}\tau$, $\delta_4^{-1}\tau$, etc., to be much greater than 1. About $\delta_2^{-1}\tau$ we shall decide nothing at first ($\delta_2^{-1}\tau \ll 1$ means that the density of the diatomic molecules, and therefore also the stream of larger particles developing from these molecules, is still increasing with the time). We then obtain, approximately, in the region where $|x|\delta_3 \ll 1$,

$$N_i \cong \frac{N_1^0 \delta_i}{2\pi\sqrt{-1}} \oint \frac{e^{x([1/3]i^{1/3} - \tau)}}{(1 - x\delta_1)(1 - x\delta_2)} dx . \tag{23}$$

It now follows from formula (23) (assuming $\gamma_2 \gg \gamma_1$ and $\gamma_1 < 1$) that

$$N_i \cong \frac{\gamma_1}{\gamma_i} i^{-2/3} N_1^0 (1 - e^{\gamma_2([1/3]i^{1/3} - \tau)}) \quad [1 < i < (3\tau)^3], \tag{24a}$$

$$N_i = 0 \quad [i > (3\tau)^3]. \tag{24b}$$

From formula (24a) we get

$$N_i \cong \frac{\gamma_1}{\gamma_i} i^{-2/3} N_1 \quad (\gamma_2\tau \gg 1), \tag{25a}$$

$$N_i \cong \frac{\gamma_1\gamma_2}{\gamma_i} i^{-2/3} N_1 (\tau - \tfrac{1}{3} \cdot i^{1/3}) \quad (\gamma_2\tau \ll 1). \tag{25b}$$

The maximum size is given by the following formula, which is practically equivalent to Lindblad's results:[7]

$$i_{\max} = (3\tau)^3 = (3\sigma\rho' v' t)^3 . \tag{26}$$

Using the values $\rho' = 10^{-4}$ cm^{-3} (approximate density of oxygen atoms), $t = 3 \cdot 10^{16}$ sec, $\sigma = 10^{-15}$ cm^2, we get $i_{\max} = 10^9$, which does not contradict the observed extinction law,[20] since it corresponds to a particle size of about 1000 atomic diameters, i.e., of about 2000 A.

[19] E. Rutherford, *Radioactivity*, p. 331. Cambridge, 1905.

[20] O. Struve, *Ann. d'Ap.*, **1**, 143, 1938.

The total smoke density now becomes

$$\rho_{sm} = \sum_{i=2}^{i_{max}} N_i i m$$

or

$$\rho_{sm} \cong \tfrac{3}{4} m \gamma_1 N_1 i_{max}^{4/3}, \tag{27a}$$

$$\rho_{sm} \cong \tfrac{1}{2}\tfrac{1}{0} m \gamma_1 \gamma_2 N_1 i_{max}^{5/3}. \tag{27b}$$

For the density of the diatomic molecules we get from formulae (25*a*) and (25*b*)

$$N_2 \cong \frac{\gamma_1}{\gamma_2} N_1 \qquad (\gamma_2 \tau \gg 1), \tag{28a}$$

$$N_2 \cong \gamma_1 N_1 \tau \qquad (\gamma_2 \tau \ll 1). \tag{28b}$$

These simple formulae involve the assumption that the smoke formation may be considered as due to the agglomeration of heavy atoms, all of one kind, and that this simplified picture holds even for the first steps in the process where diatomic and triatomic molecules are formed.

If we wish, on this basis, to explain the observed smoke density[7] of 10^{-26} gm cm^{-3}, we find from formula (27), assuming for the density of the heavy atoms $N_1 \cong 10^{-4}$ cm^{-3} (corresponding to $\tau \cong 10^3$),

$$\gamma_1 \cong 10^{-12}, \qquad \gamma_2 \gg 10^{-3}, \tag{29a}$$

or

$$\gamma_1\gamma_2 \cong 10^{-14}, \qquad \gamma^2 \ll 10^{-3}, \qquad \text{say} \qquad \gamma_1 \cong 10^{-10}, \qquad \gamma_2 \cong 10^{-4}. \tag{29b}$$

These values of γ_1 would both be theoretically permissible (see Sec. VI). An estimate of γ_2 has not been performed; but that $\gamma_2 \cong 10^{-2}$, or larger, seems not very likely.

For the density of the diatomic molecules we would get

$$N_2 \ll 10^{-13} \tag{30a}$$

or

$$N_2 \cong 10^{-11}. \tag{30b}$$

In both cases this density would be so small as to be practically unobservable.

Our conclusions would be substantially the same if we had chosen N_1 to be larger by a factor of 10, but this would make the linear dimensions of the maximum size of the particles also ten times larger.

An important question is: How can these results be reconciled with the observed presence of the diatomic molecules *CH*, CH^+, and *CN* in interstellar space, with densities of the order 10^{-6}? Of all the hydrides of the atoms in the beginning of the periodic system, the probability of the formation of *CH* and CH^+ by radiation capture outweighs, according to theory, by far that of the formation of the others, like *NH*, *OH*, *NaH* (see Sec. VI). This is, of course, a satisfactory result, and it seems not improbable that the first step in the coagulation process is precisely the formation of *CH* by radiation capture. For the corresponding γ_1, the theoretical estimate gives approximately 10^{-10}. The next step would be the mechanical capture of either a second hydrogen atom or some heavy atom, the capture of the former being more probable because of the larger hydrogen concentration. The corresponding γ_2 is very difficult to estimate theoretically; but from the observed *CH* density, one would find the approximate value of 10^{-7}. Indeed, for N_{CH} we have

$$\frac{dN_{CH}}{dt} = \gamma_1 N_C \sigma N_H v - \gamma_2 N_{CH} \sigma N_H v,$$

giving

$$N_{CH} = \frac{\gamma_1}{\gamma_2} N_C (1 - e^{-\gamma_2 \sigma N_H v_H t}) = \frac{\gamma_1}{\gamma_2} N_C (1 - e^{-1.35 \cdot 10^8 \gamma_2}).$$

Taking Dunham's[21] values, $N_{CH} \cong 2 \cdot 10^{-6}$ and $N_C \cong 3 \cdot 10^{-3}$, we find that the exponential term can be neglected and that

$$\gamma_2 \cong 1.5 \cdot 10^{-7} .$$

(In view of the fact that Dunham's carbon concentration is very different from the much lower concentrations given by other authors, this value is rather uncertain.)

If $C \rightarrow CH \rightarrow CH_2$ actually should be the initial steps in the smoke formation, our rough interpretation of the observed smoke density will no longer hold. First of all, we must consider more closely the subsequent steps. It is clear that these will certainly not consist in the capture of hydrogen atoms only, since these will evaporate again. Heavy atoms must necessarily now be added; a certain amount of hydrogen atoms may be added too, but their number will, at its highest, be of the same order as the number of other atoms. In a detailed theory one might try to take the capture and evaporation of hydrogen into account, but it seems safe to use the simplified picture that after CH_2 (or perhaps after CH_3 or CH_4; for simplicity we will, however, start directly after CH_2) only those atoms are captured whose density is of the same order as that of carbon.

We can now use again the differential equations (21), but with this difference: that the values of δ_1^{-1} and δ_2^{-1} are no longer equal to γ_1 and $\gamma_2 2^{2/3}$ but are larger by a factor N_H/N_C, for which we will take $3 \cdot 10^4$, corresponding to $\rho' \cong 10^{-4}$ used in formula (26); the value of τ, however, remains the same (viz., $\tau \cong 10^3$). If, now, $\delta_3^{-1}\tau$, $\delta_4^{-1}\tau$, etc., are all large, compared with unity, we would, from formula (27), using $\gamma_1 \cong 10^{-10}$, clearly get a smoke density which is too large by a factor of 10^6.

This difficulty can be overcome if we remember that the first steps of the capture of heavy atoms by the CH_2 molecule need by no means be easy, so that, even if $\delta_2^{-1}\tau$ is large compared with 1, the quantities $\delta_3^{-1}\tau$, $\delta_4^{-1}\tau$, etc., may eventually be small compared with 1. This means that, for instance, the probability for the capture of a carbon atom by CH_2 or CH_3 or C_2H_2 during a collision is still small compared to 10^{-3}, as may well be the case. It is clear that this will have a diminishing effect on the final smoke density. With $\delta_3^{-1}\tau$ and $\delta_4^{-1}\tau \ll 1$, $\delta_5^{-1}\tau$, $\delta_6^{-1}\tau$, ... $\gg 1$, we get from formula (22) for the total smoke density

$$\rho_{sm} = \left(3^5 m N_1 \tau^3 \frac{\gamma_1 \tau}{4}\right)\left(\frac{\gamma_3 3^{2/3}\tau}{5}\right)\left(\frac{\gamma_4 4^{2/3}\tau}{6}\right). \qquad (31)$$

The factor between the first parentheses is the same as the expression for ρ_{sm} in formula (27*a*).

The factors $\gamma_3\tau$ and $\gamma_4\tau$, and perhaps one or two more, may easily account for the required factor 10^{-6}.

As long as we are not better informed about the capture probabilities γ_3, γ_4, etc., it will be difficult to predict a precise value for ρ_{sm}; but there is, as yet, no particular reason to fear that the theoretical picture is in contradiction with the observations.

Some remarks may still be made about CN. This molecule is rather easily formed by radiation capture. The γ_1, corresponding to this process, should be smaller than in the case of CH, perhaps by a factor of 10 or so. The total number of CN molecules formed in the course of 10^9 years from carbon and nitrogen in the interstellar gas becomes, however, many powers of 10 smaller than the observed density ($\sim 10^{-6}$); and their formation by direct capture seems, therefore, to play an insignificant part. The presence in space of CN should perhaps be ascribed to evaporation from particles originally built up along the CH line. If this is the case, other diatomic molecules should likewise be expected.

I wish to express my thanks to Professor H. A. Kramers for his advice and constant assistance and to Professor J. H. Oort for much helpful criticism.

[21] *Pub. A.A.S.*, **10**, 123, 1941.

SOLAR CONCENTRATIONS OF THE HYDROXYL RADICAL

ROBERT J. DWYER[1]
Research Laboratory of Physics, Harvard University
Received August 14, 1944

ABSTRACT

The discrepancy between the observed and calculated concentrations of *OH* in the disk of the sun, as found by Russell, is reduced upon recalculation based upon a new measurement of the energy of dissociation of the *OH* radical.

A comparison between the calculated and observed concentrations of certain molecules on the surface of the sun was made by H. N. Russell.[2] He defined S as the concentration of molecules per unit area on the surface of the sun expressed on an arbitrary scale. Experimental values of log S were taken as 3, 2, 1, or 0 according as the lines observed were conspicuous, medium, weak, or barely visible. The theoretical values were calculated by the methods of spectroscopic thermodynamics. The results obtained, though qualitative, were satisfactory for most of the molecules considered.

Of these molecules, *OH* showed the greatest discordance. A value of 5.3 was computed for log S_{OH}, whereas the experimental value was only 3.0. Russell suggested that the discordance in the data for this radical might be due partly to the difficulties in the calibration of faint lines near λ 3000.

The calculation of Russell was made using Bates' value[3] of 5.0 electron volts for the energy of dissociation of *OH*. Since the value of log S is sensitive to this constant, it seemed worth while to recalculate log S_{OH}, using the value of 100.1 kilocalories, or 4.34 electron-volts, obtained by Dwyer and Oldenberg.[4]

The value of log S is obtained from the equation

$$\log S_{OH} = \log S_O + \log S_H - \log K_{OH} - 12.6 ,$$

in which log K_{OH} is the only term containing the dissociation energy of *OH*. The equation for calculating log K_{OH} is an involved one (eq. [3] of Russell's paper); and when the calculation is made using the new value of the dissociation energy, the result obtained for 5740° is 2.2, instead of Russell's value of 1.6. Upon substituting this new value in the above equation, the result for log S_{OH} is 4.7 instead of 5.3, the value obtained using the old dissociation energy. This is still considerably removed from the value of 3.0 obtained experimentally but is 25 per cent closer than before. The discordance is made less than that in *NH*, where the experimental value was 2.0 and the calculated value 4.0.

Tables of the free-energy function $-(G^0 - U_0^0)/T$ have been published[5] for H, O, and *OH* for temperatures up to 5000°. From these tables and the formula[6]

$$\ln K = \frac{1}{R}\Delta\left(-\frac{G^0 - U_0^0}{T}\right) + \frac{\Delta U_0^0}{RT}$$

[1] Work done while Charles A. Coffin Foundation Fellow at the Research Laboratory of Physics of Harvard University; now at Trinity College, Hartford, Connecticut.

[2] *Ap. J.*, **79**, 317, 1934.

[3] Bates, *Phys. Ber.*, **12**, 2465, 1931.

[4] *J. Chem. Phys.*, **12**, 351, 1944.

[5] Landolt Bornstein, *Physikalische Chemische Tabellen*, 3d Erg., Table 265, 1936.

[6] Glasstone, *Textbook of Physical Chemistry*, p. 866.

the value of log K may be calculated for the temperature of 4720° found on the spots. This gives 1.1 instead of Russell's 0.6; and the resulting value of log S_{OH} is 6.2, compared with Russell's 6.7. No observed value is given by Russell for the case of the spots, so that there is no experimental check at this temperature.

F. E. Roach[7] has made a calculation of log $S \cdot f$, where f is the absolute intensity factor, for several of the molecules discussed by Russell. The trend of the results, as compared with Russell's, seems to indicate lower f-values for OH than for the other molecules considered. Absolute f-values are known only for OH[4] and CN[8], and the values for OH are about a tenth of those for CN. If it is generally true that OH has smaller f-values than the other molecules considered by Russell, then the discrepancy between his observed and calculated values for OH on the disk would be still further reduced.

The author wishes to express appreciation to the Charles A. Coffin Foundation for a fellowship.

[7] *Ap. J.*, **89**, 110, 1939.

[8] White, *J. Chem. Phys.*, **8**, 79, 1939.

A REPORT ON NEW SPECTROGRAPHIC MATERIAL OF 13 CETI

CARL AUGUST BAUER
Yerkes Observatory
Received July 12, 1944

ABSTRACT

This paper is concerned principally with the measurements of 108 spectrograms of the triple system 13 Ceti, which were taken during the interval from September, 1928, through January, 1944, and with the discussion of the variations in the systemic velocity of the spectroscopic system, the absence of spectral variations, and the determination of an improved period for the spectroscopic system.

The previously found correlation between γ, which is the systemic velocity of A, and V, which is the relative radial velocity of B with respect to A, is confirmed. According to the equation $\gamma = \Gamma - \beta \cdot V$, this correlation determines new values. These values are $\Gamma = +9.4$ km/sec and $\beta = 0.25$ (mass of B/mass of the total system). This value of β gives the masses of the visual components as $M_A = 1.8 \odot$ and $M_B = 0.6 \odot$. No significant variations in the spectrum were found. From a displacement of 0.11 day of the observed phase from the predicted phase of minimum velocity, $P = 2.081877$ days.

1. The system 13 Ceti AB ($\alpha = 0^h30^m$, $\delta = -4°09'$, 1900.0) is a visual binary with A = 5.6 mag. and B = 6.4 mag., as given by R. G. Aitken.[1] According to the *Henry Draper Catalogue*,[2] the photometric magnitude of the system 13 Ceti (HD 3196) is 5.24, the color index is 0.56, the photographic magnitude is 5.80, and the spectral type is G0. According to W. J. Luyten,[3] using the value of the absolute parallax, $p = 0''.050$, which he determined, and his final elements of the visual orbit, the absolute dimensions of the system are:

$a = 4.9$ astronomical units
$q = 1.3$ astronomical units
total mass $= 2.4 \odot$

The brighter visual component A is a spectroscopic binary with the components designated A_1 and A_2. A_1 is the only star of the system which appears with certainty on the spectrograms. However, it is believed that since B is only 0.8 mag. fainter than the bright component A, it should disturb the spectrum of A_1 to some extent. The principal unsolved problem of this system is the apparently peculiar variation in the γ-velocity of the spectroscopic system. These γ-velocities do not define a velocity-curve which represents the motion of A around the center of mass of the visual system. In addition, other questions are raised by the variations in the orbital elements of the spectroscopic system and by the possibility that the light of the system may be variable.

2. The star Ho 212 = 13 Ceti AB was discovered to be a visual binary by G. W. Hough[4] in 1886. Elements of the visual orbit have been published by Aitken.[5] M. Maggini[6] has also derived the elements of the visual orbit from interferometer measures. All the visual observations given in Burnham's and Aitken's catalogues and a later observation by Van den Bos, together with the measurements of Maggini, have been rediscussed by Luyten,[7] who gives the following elements for the visual system 13 Ceti AB:

$\Omega = 24°$	$e = 0.73$
$i = +52°$	$P = 6.91$ years
$\omega = 73°$	$T = 1925.94$
$a = 0''.244$	Angles increasing

[1] *Pub. Lick Obs.*, **12**, 5, 1914.
[2] *Harvard Ann.*, **91**, 47, 1918.
[3] *Ap. J.*, **78**, 231, 1933.
[4] *A.N.*, **125**, 3, 1890.
[5] *Op. cit.* See also *Lick Obs. Bull.*, **3**, 90, 1905; **4**, 107, 1907; **11**, 60, 1923; **12**, 173, 1927.
[6] *A.N.*, **233**, 97, 1928.
[7] *Op. cit.*, p. 230.

P. Slavenas[8] used 13 Ceti as a comparison star in a photometric investigation and suspects it of being variable by 0.2 mag. with a period of 0.4692 day.

In 1907 E. B. Frost[9] found that the brighter component A of 13 Ceti was a spectroscopic binary. Since that time the observations of 13 Ceti with the Bruce spectrograph have been continued, with interruptions; and from time to time the plates have been measured and new orbital elements have been derived. P. Fox[10] derived orbital elements from 18 plates taken in 1906 and 1907. J. S. Paraskevopoulos[11] discussed this system in the light of his measurements of 25 plates taken in 1908, 1912–1913, and 1919–1920. In addition, he remeasured the 18 plates of 1906 and 1907 for which he obtained essentially the same results as Fox. A. Pogo,[12] from the much more extensive data from 110 plates taken in the period 1906–1928, published additional elements of the spectroscopic orbit and discussed the system. Luyten[13] rediscussed all the available observations of 13 Ceti up to 1928, both those concerning the visual system AB and the spectroscopic system A_1A_2. In view of the fact that some of the anomalies of this system have not been satisfactorily explained, observations of it have been continued.

3. All of the 108 spectrograms were taken with the one-prism arrangement of the Bruce spectrograph attached to the Yerkes 40-inch refractor. This combination gives about 20 A/mm at $H\delta$ (λ 4101.75). A list of the plates, together with the data and results, is given in Table 1.

The spectrograms were measured on a Gaertner machine, and the measurements were reduced with the aid of a dispersion table. The stellar and comparison lines which were measured are listed in Table 2. All these lines were measured on each plate if possible, but on a few underexposed plates one or more of these lines had to be omitted. In order to eliminate any systematic differences between the velocities derived from plates on which all star lines were measured and from plates on which not all star lines were measured, a correction was derived and applied to the velocity as given by each star line. This correction was determined from those plates on which all of the star lines were measured and was taken as the negative of the average for all such plates of the deviations of the velocity as given by each star line from the mean velocity for the plate. These corrections were determined and applied separately to the plates falling into the groups as given in Table 3, which also lists these corrections. With these corrections applied to the lines of those plates on which not all of the star lines were measured, the mean velocity was determined for each plate. This velocity was then reduced to the sun by means of the graphical method described by G. Van Biesbroeck.[14] The phases, in days, given in Table 1 are counted from $T_{\min}$ = 1906 Sept. 30.250 G.M.T. = JD 2417484.250, corresponding to the passage of the brighter component of the spectroscopic binary through the descending node. No correction was made to reduce the phases to the center of mass of the visual system or to the sun. This small correction might have slightly reduced the scatter of the points, but the effect upon the variation in the γ-velocity would have been negligible.

From the phases and velocities reduced to the sun, which are listed in Table 1, the corresponding points defining the velocity-curves were plotted, as shown in Figure 1. A velocity-curve was determined by adjusting the elements found by the method of Lehmann-Filhés until a good fit was obtained for the two well-observed seasons, 1934 and 1942. For the compromise curve finally adopted the eccentricity and the longitude of periastron are: e = 0.05 and ω = 275°. The γ-velocity for each of the eight seasons in which observations were made since 1928 was determined by adjusting this curve along the velocity axis until the best possible fit was obtained. In obtaining this fit, no shift in

[8] *A.N.*, **233**, 125, 1928.

[9] *Ap. J.*, **25**, 60, 1907.

[10] *Ap. J.*, **27**, 372, 1908.

[11] *Ap. J.*, **52**, 110, 1920.

[12] *Ap. J.*, **68**, 116, 1928.

[13] *Op. cit.*, p. 225.

[14] *Ap. J.*, **64**, 258, 1926.

TABLE 1*

RADIAL VELOCITIES OF 13 CETI

Date	U.T. Mid-exposure	Quality	Phase (Days)	Uncorr. Velocity (Km/Sec)
1928 Sept. 16	5:23	g	0.067	−27.6
Sept. 17	5:10	p	1.058	+33.3
Dec. 22	23:54	g	2.074	−29.8
Dec. 24	1:26	g	1.056	+47.4
1929 Jan. 16	0:42	g	1.125	+45.2
1932 Sept. 23	6:49	g	0.416	−10.2
Oct. 2	8:43	f	1.168	+38.3
Oct. 8	7:00	p	0.851	+23.8
1933 Aug. 24	7:59	p	0.286	−22.9
Aug. 27	10:00	g	1.288	+37.2
Sept. 8	6:00	f	0.630	+17.4
Sept. 21	7:45	f	1.211	+35.8
Sept. 29	6:01	g	0.812	+32.9
Oct. 5	6:36	g	0.590	+15.9
Oct. 14	5:26	g	1.214	+40.5
Oct. 18	6:02	f	1.075	+43.3
Dec. 25	0:44	f	0.154	−24.6
1934 July 18	8:40	g	1.462	+20.4
July 20	9:18	f	1.407	+25.5
July 21	8:25	g	0.288	−21.4
July 24	9:39	g	1.257	+38.2
July 30	8:53	f	0.980	+37.0
Aug. 1	9:29	g	0.923	+32.9
Aug. 3	8:53	p	0.816	+24.1
Aug. 17	8:05	g	0.210	−24.8
Aug. 21	9:48	g	0.117	−27.0
Sept. 26	8:29	p	0.670	+24.0
Sept. 28	7:03	g	0.530	+ 7.6
Oct. 2	6:33	f	0.345	−15.7
Oct. 2	7:32	g	0.386	− 8.7
Oct. 7	5:36	g	1.141	+42.7
Oct. 8	6:21	g	0.091	−26.2
Oct. 10	7:44	g	0.066	−26.1
Oct. 12	6:29	g	2.014	−29.1
Oct. 13	5:18	g	0.884	+31.8
Oct. 16	6:25	g	1.848	−13.1
Oct. 21	4:51	g	0.537	+ 8.6
Oct. 22	3:45	g	1.491	+18.2
Oct. 22	5:35	g	1.568	+11.9
Oct. 26	3:49	f	1.330	+33.2
Oct. 30	6:46	g	1.290	+41.2
Nov. 7	1:37	g	0.747	+24.9
Nov. 15	3:39	g	0.505	0.0
Dec. 5	1:32	g	1.680	+ 2.8
Dec. 10	23:20	g	1.342	+33.5
1940 Sept. 13	7:18	p	1.996	−22.2
Oct. 24	5:35	f	1.288	+35.4
Nov. 3	4:01	g	0.812	+31.6
Nov. 25	2:54	g	1.948	−19.7
Dec. 3	3:38	g	1.650	+ 6.6
Dec. 9	2:52	g	1.373	+26.4

* The spectrograms were obtained by several observers at the Yerkes Observatory.

TABLE 1—*Continued*

Date	U.T. Mid-exposure	Quality	Phase (Days)	Uncorr. Velocity (Km/Sec)
1941 Sept. 26	4:59	g	1.001	+42.1
Oct. 15	5:07	g	1.270	+40.8
Oct. 16	3:43	g	0.130	−27.8
Oct. 24	2:08	f	1.818	−11.9
Oct. 25	4:50	f	0.848	+30.8
Dec. 6	2:54	g	1.131	+39.4
Dec. 15	1:02	f	1.726	− 1.6
Dec. 20	2:23	f	0.536	+ 4.1
1942 Jan. 6	0:18	g	0.794	+23.7
Jan. 14	0:15	p	0.465	−10.6
1942 Sept. 27	6:09	g	0.642	+13.7
Sept. 28	5:16	g	1.605	+11.5
Oct. 6	5:42	g	1.297	+38.2
Oct. 6	6:49	g	1.343	+35.0
Oct. 7	4:40	f	0.171	−22.3
Oct. 7	5:48	g	0.219	−23.3
Oct. 7	6:53	g	0.264	−17.5
Oct. 8	4:32	g	1.166	+38.7
Oct. 8	5:45	g	1.217	+46.1
Oct. 17	8:22	p	1.998	−24.6
Oct. 19	5:25	g	1.793	− 5.3
Oct. 19	6:35	g	1.841	−10.6
Nov. 6	4:32	g	1.020	+43.2
Nov. 13	2:10	g	1.675	+ 7.4
Nov. 13	3:18	g	1.723	+ 0.7
Nov. 13	4:26	g	1.770	− 1.2
Nov. 14	1:48	g	0.578	+ 8.5
Nov. 27	2:32	g	1.118	+43.0
Nov. 27	3:43	g	1.167	+50.1
Dec. 4	2:07	g	1.855	− 7.6
Dec. 4	3:19	g	1.904	−14.9
Dec. 5	2:13	g	0.777	+27.9
Dec. 5	3:14	g	0.820	+33.3
Dec. 12	2:19	f	1.536	+20.6
Dec. 12	3:22	f	1.579	+12.9
1943 Jan. 9	0:24	g	0.310	−24.6
1943 Aug. 10	8:03	p	1.278	+32.3
Aug. 17	9:36	g	0.016	−23.9
Aug. 18	8:23	f	0.965	+31.4
Sept. 21	6:46	g	1.588	+14.1
Sept. 24	4:54	g	0.346	− 9.4
Sept. 29	7:00	p	1.271	+46.5
Oct. 6	4:28	g	1.919	−15.0
Oct. 7	5:00	g	0.859	+38.6
Oct. 12	4:24	p	1.670	+ 0.8
Oct. 20	3:56	p	1.324	+38.4
Oct. 21	4:10	f	0.252	−15.3
Oct. 22	3:41	g	1.231	+41.1
Oct. 27	3:53	g	2.076	−29.4
Oct. 29	3:28	g	1.977	−22.7
Nov. 28	2:26	p	0.706	+23.8
Dec. 5	1:02	g	1.402	+30.8
Dec. 11	3:22	g	1.253	+44.6
Dec. 20	1:27	g	1.846	−15.9
Dec. 23	23:47	g	1.613	− 7.0
1944 Jan. 3	0:02	g	1.214	+30.0
Jan. 11	0:15	p	0.896	+43.6

phase from that of the 1942 season was made except for a very small shift to the left for the early seasons (1928, 1932, 1933, and 1934), which was in the direction indicated by the improved period derived later. The resulting γ-velocities are given on the γ-axes of the velocity-curves in Figure 1.

TABLE 2

LIST OF STELLAR LINES AND COMPARISON LINES USED TO DETERMINE THE RADIAL VELOCITY

Element	Wave Length in A		Element	Wave Length in A	
	Comparison*	Star†		Comparison*	Star†
Ti	4012.39	.....	*Fe*	4260.48	.....
Fe	4045.82	4045.83	*Fe*	.....	4271.54
Fe	4063.60	4063.61	*Ti*	4274.58	.....
Fe	4071.74	4071.75	*Ti*	4318.64	.....
Ti	4078.47	.....	*Fe*	.....	4325.62
Fe	4132.06	4132.07	*Ti*	4341.38	.....
Fe	.....	4143.74	*Ti*	4344.29	.....
Ti	4163.65	.....	*Fe*	4383.55	4383.56
Fe	4202.03	.....	*Ti*	4399.77	.....
Fe	4235.94	.....	*Fe*	.....	4404.76
Fe	.....	4250.46	*Fe*	4415.12	4415.14

* Wave lengths from *Massachusetts Institute of Technology Wavelength Tables*, New York: John Wiley & Sons, Inc., London: Chapman & Hall, Ltd., 1939.

† Wave lengths from *Trans. I.A.U.*, **5**, 193, 1935, by W. S. Adams.

TABLE 3

VELOCITY CORRECTIONS FOR THE STAR LINES

Wave Length of Star Line in A	Correction to Velocity (in Km/Sec)				
	1928, 1932, and 1933	1934	1940 and 1941	1942	1943
4045.83	+1.0	+2.6	+4.4	+5.0	+3.3
4063.61	+2.0	+1.1	+1.2	+1.2	+2.0
4071.75	+1.5	+6.0	+1.7	+5.4	+4.0
4132.07	−9.1	−9.2	−6.8	−4.1	−5.3
4143.74	+1.6	−0.2	−0.8	+4.2	+3.8
4250.46	+0.5	−0.6	+1.4	−1.0	−0.6
4271.54	−1.8	−5.2	−3.9	−5.1	−4.6
4325.62	−0.5	−3.4	−5.4	−4.3	−4.2
4383.56	+6.2	+3.3	+6.7	−0.8	−0.5
4404.76	−2.2	+4.0	+0.7	+1.3	+0.6
4415.14	+0.8	+1.5	+0.7	−1.9	+1.7

4. If the γ-velocities given in Figure 1 and those determined by Pogo are plotted against the mean epoch of the observations, it is at once apparent that my γ-velocities are systematically lower than those determined by Pogo. It is very doubtful that this difference is real, for recent independent investigations indicate that the Bruce spectrograph has been giving velocities which are systematically too small by several kilo-

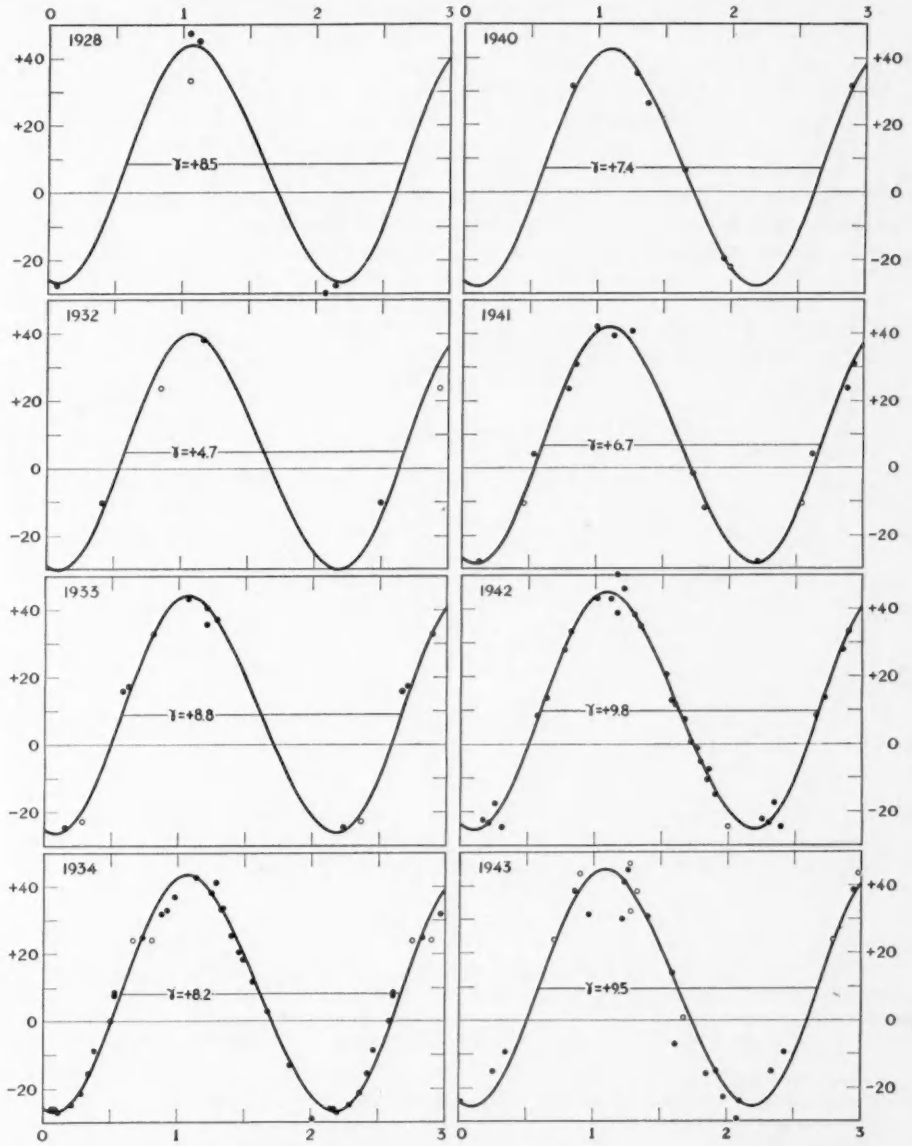

FIG. 1.—Velocity-curves of 13 Ceti. Ordinates: radial velocity in km/sec; abscissas: phase in days reckoned from T_{min} = 1906 Sept. 30.250 G.M.T. with P = 2.08186 days. Solid circles represent observations of good or fair quality, while open circles represent observations of poor quality.

meters per second.[15] Consequently, I have corrected my γ-velocities for the seasons 1940, 1941, 1942, and 1943 by adding to them 4.6 km/sec, which is the difference between the means of Pogo's seven γ-velocities that are based on more than five observations and my four γ-velocities for these seasons. No correction was applied to the seasons 1928, 1932, 1933, and 1934. Table 4 lists the γ-velocities for the eight seasons in which I had observations and, for convenient reference, the γ-velocities determined from five or more observations by Pogo.

If the γ-velocities listed in Table 4 are plotted against the phase in the visual orbit, a velocity-curve of A with respect to B is not defined. Therefore, it is better to use the method adopted by Luyten to reveal any correlation between γ and the relative radial

TABLE 4

THE γ-VELOCITIES AND THE RELATIVE RADIAL VELOCITIES OF B WITH RESPECT TO A

Epoch	V (Km/Sec)	γ (Km/Sec)	No. of Plates
1906.90	−11	+10.0	8
1907.87	− 6	+11.0	10
1908.89	− 1	+ 8.0	12
1911.72	+25	− 3.0	5
1912.97	−16	+17.0	10
1917.06	+ 6	+17.0	5
1923.72	+ 4	+18.4	15
1925.75	+29	+ 7.0	5
1926.87	−16	+13.0	6
1927.95	−10	+13.5	19

Epoch	V (Km/Sec)	γ Uncorr. (Km/Sec)	No. of Plates
1928.88	− 4.4	+ 8.5	5
1932.75	+26.6	+ 4.7	3
1933.74	−16.2	+ 8.8	9
1934.72	− 9.8	+ 8.2	28
		γ Corr. (Km/Sec)	
1940.84	−14.8	+12.0	6
1941.88	− 8.5	+11.3	10
1942.84	− 3.7	+14.4	26
1943.82	+ 1.1	+14.1	21

velocity of B with respect to A. If Γ be the true systemic velocity of AB, V the relative radial velocity of B with respect to A, γ the observed systemic velocity of A, and β the ratio of the mass of B to the mass of the total system, then we have

$$\gamma = \Gamma - \beta \cdot V \ .$$

[15] The possibility that the velocities given by the Bruce spectrograph in recent years might be influenced by a systematic error was first suggested in an investigation of ζ Tauri by J. A. Hynek and O. Struve (*Ap. J.*, **96**, 425, 1942). This revealed a systematic difference of about 2 km/sec between the velocities determined since 1940 at Yerkes and at Perkins. Subsequently, the following four independent determinations of this error have been made:

1. In an investigation of κ Cancri by O. Struve (*Ap. J.*, **99**, 216, 1944) the difference in the γ-velocities as determined from Victoria and from Yerkes plates was found to be +4.2 km/sec.

2. Recent measures by Miss J. Ringstad of the radial velocity of α Persei from 32 Yerkes plates taken in the interval from November 2, 1943, to March 26, 1944, inclusive, indicate that the correction is a function of wave length. For the mean wave length, λ 4228, of the lines which were measured in the present work, her curve indicates a correction of +6.5 km/sec.

3. The paper on 48 Librae by P. W. Merrill and R. F. Sanford (*Ap. J.*, **100**, 14, 1944) indicates a correction of +4.0 km/sec for the hydrogen lines and +8.8 km/sec for the metal lines.

4. Finally, in the present paper the correction is found to be +4.6 km/sec.

Although the dispersion among these separate determinations is rather large, the mean value, +5.6 km/sec, should furnish a fairly reliable value of the systematic correction to be applied to the velocities determined from plates taken with the Bruce spectrograph since July 15, 1940, when a different collimator and prism were installed. While testing the spectrograph on April 21, 1944, it was found that the collimator focus was in error. After proper adjustment the definition of the spectrograph was definitely improved. Measures of α Boötis by A. J. Deutsch of 22 plates taken since this change was made show that the large positive correction is no longer present. His mean gives a correction of −0.3 km/sec.

The value of V for each mean epoch is also given in Table 4. These data are plotted in Figure 2. It is important to notice that all the points in Figure 2 which have V greater than +5 km/sec are based upon five or fewer observations. In addition, the remaining points do not define well the position of the straight line $\gamma = \Gamma - \beta \cdot V$. However, I have tentatively drawn a straight line by inspection. This line gives

$$\Gamma = +9.4 \text{ km/sec} \quad \text{and} \quad \beta = 0.25 .$$

Since Luyten gives the total mass of the visual system as $M = 2.4 \odot$, the above value of β gives the following values of the individual masses: $M_A = 1.8 \odot$ and $M_B = 0.6 \odot$. For comparison, Luyten's previous values are: $\Gamma = +11$ km/sec, $\beta = 0.45$, $M_A = 1.27 \odot$, $M_B = 1.05 \odot$.

5. Previous papers have all made reference to the possibility that another star of the system, besides the bright component A_1, might be capable of leaving its record on the spectrograms. It has been suggested in particular that the visual component B, which is

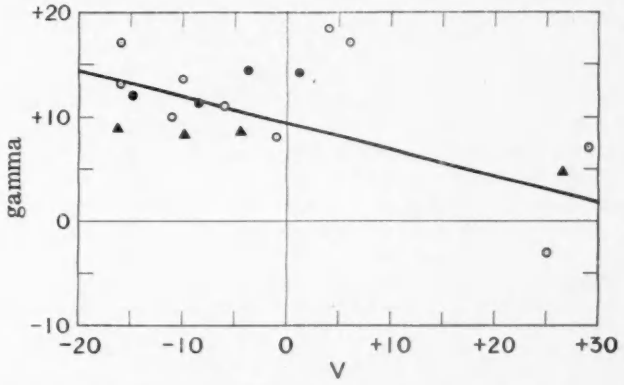

FIG. 2.—Correlation between the γ-velocity of 13 Ceti A and the relative radial velocity of B referred to A. Open circles represent Pogo's values. Triangles represent the uncorrected values, and solid circles the corrected values found in the present paper.

only 0.8 mag. fainter than A, might produce a disturbing effect upon the velocity-curves. With this problem in mind, about a dozen good plates were selected at such phases in the visual and spectroscopic systems that the relative radial velocity of B with respect to A_1 would be either near a maximum, near a minimum, or near zero. These spectrograms were compared in pairs in a Gaertner measuring machine provided with two stages. Under these circumstances, favorable to the discovery of any doubling or differing character of the lines, no significant differences were found. The range in the relative radial velocity of B with respect to A_1 is from +65 km/sec to −54 km/sec. A difference in velocity of 65 km/sec corresponds to a shift in the position of a line of 0.045 mm or 0.90 A at $H\delta$ (λ 4101.75), which would be just sufficient to show the similar lines of the two components as doubles if they were both present. However, it is still possible that spectral variations exist which were not discovered in this comparison, since it was not quite possible to realize the full difference in velocity of 65 km/sec in the selection of the pairs of plates and since the lines of the component B would necessarily be very faint even if they were well separated from the lines of A_1.

6. The period of the spectroscopic binary system 13 Ceti A, as determined by Pogo and by Luyten, is 2.08186 days. It is apparent from Figure 1 that the time of minimum velocity is shifted to the right by about 0.11 day. This corresponds to a change in the

period to $P = 2.081877$ days. The neglect of light-time introduces an uncertainty of about 3 in the last place.

7. The observations of 13 Ceti have not been distributed as evenly in the phase of the visual orbit as could be hoped for. None of the points in Figure 2 with V greater than $+5$ km/sec are based upon more than five observations. Considering this and the very favorable phase of the visual system in the next few years, it is desirable to obtain at least 15 good plates per season in 1944.8, 1945.8, and 1946.8, when V will have approximately the values $+7$, $+16$, and -19 km/sec, respectively. The very critical position of all of these points in Figure 2 can be seen at a glance. It would also be important to verify the photometric observations by Slavenas which led him to suspect that 13 Ceti was variable by 0.2 mag. with a period of 0.4692 day.

I wish to express my sincere thanks to Dr. O. Struve, who suggested this problem and who has given me valuable advice during its progress. I am also indebted to the other members of the Yerkes staff for helpful discussions and to Mrs. C. Rezek, Miss J. Ringstad, and to my wife, Grace, for aid in the computations.

THE INTERACTION OF A PROTON AND A HYDROGEN ATOM IN ITS EXCITED STATES

MARGARET K. KROGDAHL
Yerkes Observatory
Received August 15, 1944

ABSTRACT

The problem of calculating the van der Waals force between a proton and an excited hydrogen atom is considered. It is found that the energy of interaction depends essentially on the inverse second power of the nuclear separation, in contrast to the more familiar R^{-6} law. Moreover, the energy may be evaluated *exactly*, to as many orders in the perturbation as are desired.

The numerical values of the interactions are given, in atomic units, for the excited states of hydrogen as far as $n = 5$; and it is suggested how these results can be applied to astrophysical problems.

I. FORMULATION OF THE PROBLEM

1. *Introduction.*—A physical problem of considerable astrophysical interest is that of the interaction of a proton and a hydrogen atom in its various excited states; for, on account of the enormous abundance of hydrogen in stellar atmospheres, we might, on the Lorentz-Weisskopf[1] theory of collision-broadening, seek in these interactions a cause for the broadening of the hydrogen lines in stellar spectra. As is well known, the discussion of this latter problem in terms of Stark effect caused by the interatomic electric fields in the stellar atmosphere has been carried out by Struve, Pannekoek, Verwey, Unsöld, and others.[2] However, an alternative discussion of the problem in terms of the direct interactions between a proton and a hydrogen atom may prove useful in extending the current treatments of the problem. Accordingly, with this intention we shall examine in this paper the basic physical problem.

The interaction of a proton and a hydrogen atom in the ground state has recently been considered by C. A. Coulson,[3] who has shown that the interaction energy can be expressed as a power series in $1/R$ and that, further, the coefficients of the various powers of $1/R$ can be directly and explicitly evaluated. An examination of Coulson's method with a view toward extending it to the more general problem on hand revealed several interesting features of the problem which are not encountered in the simple case treated by Coulson. For this reason we shall formulate the problem anew in a completely general manner.

2. *Outline of the method.*—In considering the problem of the interaction energy, two types of forces must be distinguished: the weak interactions, which operate for large separations of the nuclei, and the forces which are connected with molecular binding. The latter are the resonance or exchange forces and are important for much smaller values of R. In this case the wave function for the electron is symmetrical with respect to the two nuclei, and the energy of the binding is proportional to e^{-2R}. However, at very large distances the exponential term becomes very small, and it is the van der Waals forces which become important.

It is assumed that during the "collision" the electron remains confined to the nucleus A (see Fig. 1) and that the nuclear separation R is always large compared to the radius

[1] V. Weisskopf, *Phys. Zs.*, **34**, 1, 1933; also H. Margenau and W. Watson, *Rev. Mod. Phys.*, **8**, 22, 1936.

[2] For an account of these investigations see A. Unsöld, *Physik der Sternatmosphären*, pp. 180–184 and pp. 286–290, Berlin, 1938.

[3] *Proc. R. Soc. Edinburgh*, A, **51**, 20, 1941.

of the hydrogen atom. Accordingly, the presence of an additional proton at B can be considered as causing small perturbations. We can expand the perturbing potential

$$V = \frac{1}{R} - \frac{1}{r'} \tag{1}$$

in spherical harmonics about AB as axis in the form

$$V = -\left\{ \frac{r}{R^2} P_1(\cos\theta) + \frac{r^2}{R^3} P_2(\cos\theta) + \dots . \right\}. \tag{2}$$

Now the wave equation pertaining to the perturbed problem is

$$(H + V - E)\psi = 0 , \tag{3}$$

where H is the Hamiltonian operator for the unperturbed hydrogen atom:

$$H = -\tfrac{1}{2}\nabla^2 - \frac{1}{r}. \tag{4}$$

The method of solving equation (3) is to seek expansions for E and ψ of the forms

$$E = E_0 + \frac{1}{R} E_1 + \frac{1}{R^2} E_2 + \dots . \tag{5}$$

and

$$\psi = \psi_0 + \frac{1}{R} \psi_1 + \frac{1}{R^2} \psi_2 + \dots , \tag{6}$$

where E_0 and ψ_0 denote the energy and wave function for the unperturbed hydrogen atom. More particularly,

$$E_0(n) = -\frac{1}{2n^2} \qquad \text{(in atomic units)} \tag{7}$$

and

$$\psi_0 = \sum_{l,\, m} a_{l,\, m} \psi_0(n, l, m) = \sum_{l,\, m} a_{l,\, m} \Phi_m(\phi) \Theta_{l,\, m}(\theta) R_{n,\, l}(r) , \tag{8}$$

where the $a_{l,\, m}$'s are certain appropriately chosen constants and[4]

$$\Phi_m(\phi) = \frac{1}{\sqrt{2\pi}} e^{im\phi} , \tag{9}$$

$$\Theta_{l,\, m}(\theta) = \sqrt{\frac{(2l+1)\,(l-m)!}{2\,(l+m)!}}\, P_l^m(\cos\theta) , \tag{10}$$

$$R_{n,\, l}(r) = -\left(\frac{2}{n}\right)^{3/2} \sqrt{\frac{(n-l-1)!}{2n\,[\,(n+l)!\,]^3}}\, e^{-\rho/2} \rho^l L_{n+l}^{2l+1}(\rho) , \tag{11}$$

and

$$\rho = \frac{2}{n} r . \tag{12}$$

[4] See, e.g., Pauling and Wilson, *Introduction to Quantum Mechanics*, p. 132, New York: McGraw-Hill Book Co., 1935.

It will be noticed that we have chosen for ψ_0 a linear combination of the n^2 linearly independent wave functions belonging to $E_0(n)$. This is because we do not yet know which particular linear combinations will lead to pure states when the perturbation is effective (see below). Then, by substituting equations (2), (5), and (6) into equation (3) and equating the coefficients of like powers of $1/R$, the following equations involving the perturbed energies and wave functions are obtained:

$$[H-E_0]\psi_0 = 0\,, \tag{13a}$$

$$[H-E_0]\psi_1 = E_1\psi_0\,, \tag{13b}$$

$$[H-E_0]\psi_2 - rP_1(\cos\theta)\psi_0 = E_1\psi_1 + E_2\psi_0\,, \tag{13c}$$

$$[H-E_0]\psi_3 - r^2P_2(\cos\theta)\psi_0 - rP_1(\cos\theta)\psi_1 = E_1\psi_2 + E_2\psi_1 + E_3\psi_0\,, \tag{13d}$$

$$\left.\begin{aligned}[H-E_0]\psi_4 - r^3P_3(\cos\theta)\psi_0 - r^2P_2(\cos\theta)\psi_1 - rP_1(\cos\theta)\psi_2 \\ = E_1\psi_3 + E_2\psi_2 + E_3\psi_1 + E_4\psi_0\,,\end{aligned}\right\} \tag{13e}$$

. . . . . .

The essence of Coulson's method is that these equations can all be solved *exactly*, to as many orders in the perturbation as are desired.

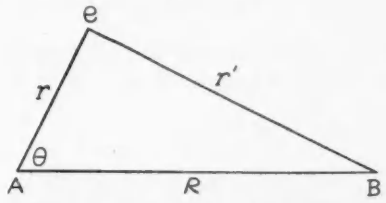

FIG. 1.—Proton and hydrogen atom

The first equation simply describes the unperturbed hydrogen atom. However, owing to the fact that the energy levels of the hydrogen atom are degenerate, the solution of equation (13*a*) can be any linear combination of the n^2 independent wave functions belonging to E_0. To begin with, therefore, we must determine the proper linear combination to use. This problem is somewhat simplified by the fact that all the equations of the perturbation are trivially separable in ϕ, so that for any n we may consider the various values of m separately. It will be seen that this means that the perturbation has the effect of removing the degeneracy with respect to m—but not that with respect to l. In other words, there will be a mixture of the states with different l's which belong to a given n and m.

Finally, the perturbed wave function is subject to two conditions, namely, that it should always be normalized correct to the order to which one is working and that it should possess no singularities.[5]

We are now in a position to consider the detailed solution of the equations (13). In accordance with the foregoing remarks, we shall carry out the discussion for the different values of m in turn. Now, for any n the greatest value of $|m|$ is $n-1$; and corresponding to this value there is only one possible value of l, namely, $n-1$. In this situation, of which the Coulson case is an example, ψ_0 contains only one term, and removal of the perturbation leaves the atom in a pure state. For all other values of m there are two or more possible values of l, corresponding to a mixture of states. Finally, it is clear that to complete the discussion for a particular value of n, say, $n = q$, we should consider all values of $|m|$ down to $|m| = n - q$.

[5] Singularities of the form $r^{-1+\epsilon}(\epsilon > 0)$ are, however, permitted.

II. THE CASE $|m| = n - 1$

3. *The first-order terms.*—Consider the simplest case, namely, $|m| = n - 1$. The unperturbed wave function, ψ_0, is simply $\psi_0(n, n-1, n-1)$ as given by equations (9), (10), and (11). Hence the first step is to multiply equation (13*b*) by ψ_0^* and integrate over the entire configuration space. Denoting by $d\tau$ the element of volume in the configuration space, we have

$$\left.\begin{aligned} \int \psi_0^* [H - E_0] \psi_1 d\tau &= E_1 \\ &= \int \psi_1 [H - E_0] \psi_0^* d\tau = 0 \end{aligned}\right\} \tag{14}$$

because of the self-adjoint property of the Hamiltonian. Hence,

$$E_1(n, n-1, n-1) = 0 , \tag{15}$$

and equation (13*b*) becomes identical with the unperturbed wave equation:

$$(H - E_0)\psi_1 = 0 . \tag{16}$$

Hence ψ_1 is an arbitrary multiple of ψ_0,

$$\psi_1 = a\psi_0 . \tag{17}$$

The condition that ψ be normalized correct to $1/R$ determines the constant a; for, in order that this may be true, we must require that

$$\int \psi_0^* \psi_1 d\tau = 0 , \tag{18}$$

from which it follows that a, and therefore also ψ_1, are zero.

4. *The second-order terms.*—Multiplying equation (13*c*) by ψ_0^* and integrating, we have

$$\int \psi_0^* [H - E_0] \psi_2 d\tau - \int r P_1(\cos\theta) \psi_0^* \psi_0 d\tau = E_2 \tag{19}$$

or

$$E_2 = -\int r P_1(\cos\theta) \psi_0^* \psi_0 d\tau . \tag{20}$$

Since the element of volume is

$$d\tau = r^2 \sin\theta dr d\theta d\phi , \tag{21}$$

the integral contains a factor

$$\int_0^\pi P_1(\cos\theta) [P_l^m(\cos\theta)]^2 \sin\theta d\theta = \int_0^\pi [\cos\theta P_l^m(\cos\theta)] P_l^m(\cos\theta) \sin\theta d\theta . \tag{22}$$

Using the relation between the associated Legendre polynomials

$$\cos\theta P_l^m(\cos\theta) = \frac{l+m}{2l+1} P_{l-1}^m(\cos\theta) + \frac{l-m+1}{2l+1} P_{l+1}^m(\cos\theta), \tag{23}$$

we can readily show that the integral in question vanishes. Hence

$$E_2(n, n-1, n-1) = 0 . \tag{24}$$

Therefore, equation (13*c*) becomes

$$(H - E_0)\psi_2 = r P_1(\cos\theta)\psi_0 , \tag{25}$$

or, more explicitly,

$$\left.\begin{aligned} -\frac{1}{2}\left\{\frac{1}{r^2}\frac{\partial}{\partial r}\left(r^2\frac{\partial\psi_2}{\partial r}\right)+\frac{1}{r^2\sin\theta}\frac{\partial}{\partial\theta}\left(\sin\theta\frac{\partial\psi_2}{\partial\theta}\right)+\frac{1}{r^2\sin^2\theta}\frac{\partial^2\psi_2}{\partial\phi^2}\right\}-\frac{\psi_2}{r} \\ -E_0\psi_2 = rP_1(\cos\theta)\psi_0\,. \end{aligned}\right\} \quad (26)$$

In view of the form which ψ_0 has, we may write

$$\psi_2 = e^{im\phi}\Psi_2\,, \quad (27)$$

where Ψ_2 now depends only on θ and r. If we neglect for the time being the normalization factor, equation (26) becomes

$$\left.\begin{aligned} -\frac{1}{2}\left\{\frac{1}{r^2}\frac{\partial}{\partial r}\left(r^2\frac{\partial\Psi_2}{\partial r}\right)+\frac{1}{r^2\sin\theta}\frac{\partial}{\partial\theta}\left(\sin\theta\frac{\partial\Psi_2}{\partial\theta}\right)-\frac{m^2}{r^2\sin^2\theta}\Psi_2\right\}-\frac{\Psi_2}{r}-E_0\Psi_2 \\ = -rP_1(\cos\theta)P_l^m(\cos\theta)\,e^{-\rho/2}\rho^l L_{n+l}^{2l+1}(\rho)\,. \end{aligned}\right\} \quad (28)$$

Introducing the variable ρ (cf. eq. [12]), we find, after some minor rearrangement of the terms,

$$\left.\begin{aligned} \frac{1}{\rho^2}\frac{\partial}{\partial\rho}\left(\rho^2\frac{\partial\Psi_2}{\partial\rho}\right)+\frac{1}{\rho^2\sin\theta}\frac{\partial}{\partial\theta}\left(\sin\theta\frac{\partial\Psi_2}{\partial\theta}\right)-\frac{m^2}{\rho^2\sin^2\theta}\Psi_2+\frac{n}{\rho}\Psi_2-\tfrac{1}{4}\Psi_2 \\ = \frac{n^3}{4}P_1(\cos\theta)P_l^m(\cos\theta)\,e^{-\rho/2}\rho^{l+1}L_{n+l}^{2l+1}(\rho)\,. \end{aligned}\right\} \quad (29)$$

Without loss of generality, we may write

$$\Psi_2 = \sum_k P_k^m(\cos\theta)\,\mathcal{R}_{n,k}(\rho)\,. \quad (30)$$

Then,

$$\left.\begin{aligned} \sum_k\left\{\frac{P_k^m}{\rho^2}\frac{d}{d\rho}\left(\rho^2\frac{d\mathcal{R}_{n,k}}{d\rho}\right)+\frac{\mathcal{R}_{n,k}}{\rho^2}\left[\frac{1}{\sin\theta}\frac{d}{d\theta}\left(\sin\theta\frac{dP_k^m}{d\theta}\right)-\frac{m^2}{\rho^2\sin^2\theta}P_k^m\right]\right. \\ \left.+\frac{n}{\rho}P_k^m\mathcal{R}_{n,k}-\tfrac{1}{4}P_k^m\mathcal{R}_{n,k}\right\} = \frac{n^3}{4}P_1(\cos\theta)P_l^m(\cos\theta)\,e^{-\rho/2}\rho^{l+1}L_{n+l}^{2l+1}\,. \end{aligned}\right\} \quad (31)$$

The quantity in brackets in the foregoing equation is equal to $-k(k+1)P_k^m(\cos\theta)$. Using this, together with equation (23), we may equate the coefficients of P_k^m on both sides of the equation. Remembering that $m = l = n-1$, we find

$$\frac{1}{\rho^2}\frac{d}{d\rho}\left(\rho^2\frac{d\mathcal{R}_{n,k}}{d\rho}\right)+\left\{-\frac{k(k+1)}{\rho^2}+\frac{n}{\rho}-\frac{1}{4}\right\}\mathcal{R}_{n,k}=0 \qquad (k\neq n) \quad (32)$$

and

$$\left.\begin{aligned} \frac{1}{\rho^2}\frac{d}{d\rho}\left(\rho^2\frac{d\mathcal{R}_{n,n}}{d\rho}\right)+\left\{-\frac{n(n+1)}{\rho^2}+\frac{n}{\rho}-\frac{1}{4}\right\}\mathcal{R}_{n,n}=\frac{n^3}{4}\frac{1}{2n-1}\,e^{-\rho/2}\rho^n L_{2n-1}^{2n-1} \\ (k=n)\,. \end{aligned}\right\} \quad (33)$$

It will be noticed that equation (32) and the homogeneous part of equation (33) are identical in form with the radial wave equation for the nth quantum state, whose solution is any multiple of

$$e^{-\rho/2}\rho^k L_{n+k}^{2k+1}.$$

Equation (33) may be solved by making the substitution

$$\mathcal{R}_{n,\,n} = e^{-\rho/2}\rho^n \sum_j c_j L_{n+j}^{2n+1}, \tag{34}$$

where the c_j's are constants to be determined. According to equation (34),

$$\mathcal{R}'_{n,\,n} = \sum_j c_j \{ e^{-\rho/2} [\rho^n (L_{n+j}^{2n+1})' + n\rho^{n-1} L_{n+j}^{2n+1}] - \tfrac{1}{2} e^{-\rho/2}\rho^n L_{n+j}^{2n+1} \} \tag{35}$$

and

$$\left.\begin{aligned} \mathcal{R}''_{n,\,n} = \sum_j c_j \{ & e^{-\rho/2} [\rho^n (L_{n+j}^{2n+1})'' + 2n\rho^{n-1} (L_{n+j}^{2n+1})' + n(n-1)\rho^{n-2} L_{n+j}^{2n+1}] \\ & - e^{-\rho/2} [\rho^n (L_{n+j}^{2n+1})' + n\rho^{n-1} L_{n+j}^{2n+1}] + \tfrac{1}{4} e^{-\rho/2}\rho^n L_{n+j}^{2n+1} \}, \end{aligned}\right\} \tag{36}$$

where the primes denote differentiation with respect to ρ. Substituting these in equation (33) and dividing through by ρ^{n-1}, we obtain

$$\sum_j c_j \{ \rho (L_{n+j}^{2n+1})'' + [2(n+1) - \rho] (L_{n+j}^{2n+1})' - L_{n+j}^{2n+1} \} = \frac{n^3}{4} \frac{1}{2n-1} \rho L_{2n-1}^{2n-1}. \tag{37}$$

This equation can be further simplified by using the differential equation for the associated Laguerre polynomials, namely,

$$\rho (L_{n+j}^{2n+1})'' + [2(n+1) - \rho] (L_{n+j}^{2n+1})' = (n - j + 1) L_{n+j}^{2n+1}. \tag{38}$$

We find

$$\sum_j c_j (n-j) L_{n+j}^{2n+1} = \frac{n^3}{4} \frac{1}{2n-1} \rho L_{2n-1}^{2n-1}. \tag{39}$$

Now, by means of the recursion formulae,

$$L_{r+1}^s \left(1 - \frac{s}{r+1}\right) + L_r^s (\rho - 1 - 2r + s) + r^2 L_{r-1}^s = 0 \tag{40}$$

and

$$L_r^s - r L_{r-1}^{s+1} + r L_{r-1}^s = 0, \tag{41}$$

we can express the product ρL_{2n-1}^{2n-1} on the right-hand side of equation (39) as a sum of Laguerre polynomials, all of order $2n+1$ and having constant coefficients. In this manner we find

$$\left.\begin{aligned} \sum_j c_j (n-j) L_{n+j}^{2n+1} = \frac{n^3}{4} \frac{1}{2n-1} \Bigg[& \frac{2(n+1)}{2n(2n+1)} L_{2n+1}^{2n+1} \\ & - \frac{1}{2n(2n+1)(2n+2)} L_{2n+2}^{2n+1} \Bigg], \end{aligned}\right\} \tag{42}$$

a relation which determines the coefficients c_j uniquely. Thus

$$-c_{n+1} = \frac{n^3}{4} \frac{1}{2n-1} \frac{2(n+1)}{2n(2n+1)} \tag{43}$$

and

$$-2c_{n+2} = -\frac{n^3}{4}\frac{1}{2n-1}\frac{1}{2n(2n+1)(2n+2)}, \tag{44}$$

and the remaining c's vanish. The solution for $\mathcal{R}_{n,n}$ can therefore be written as

$$\left.\begin{aligned}\mathcal{R}_{n,n} = \frac{n^3}{4}\frac{1}{2n-1}\,e^{-\rho/2}\rho^n\Big[-\frac{2(n^3+1)}{2n(2n+1)}L_{2n+1}^{2n+1} \\ +\frac{1}{4n(2n+1)(2n+2)}L_{2n+2}^{2n+1}\Big].\end{aligned}\right\} \tag{45}$$

Finally, in order that ψ may be normalized to the second order in $1/R$, ψ_2 must satisfy the condition

$$\int\psi_0^*\psi_2 d\tau = 0. \tag{46}$$

This requires that

$$\psi_2 = \frac{1}{\sqrt{2\pi}}\left(\frac{2}{n}\right)^{3/2}\sqrt{\frac{2n-1}{2(2n-2)!}}\,\frac{1}{\sqrt{2n[(2n-1)!]^3}}\,e^{i(n-1)\phi}P_n^{n-1}\mathcal{R}_{n,n}. \tag{47}$$

If n be put equal to 1, the foregoing equation yields the ψ_2 given by Coulson.

5. *The third-order terms.*—Multiply equation (13*d*) by ψ_0^* and integrate:

$$\int\psi_0^*[H-E_0]\psi_3 d\tau - \int r^2P_2(\cos\theta)\psi_0^*\psi_0 d\tau = E_3. \tag{48}$$

The first integral vanishes, and we are left with

$$E_3 = -\int r^2P_2(\cos\theta)\psi_0^*\psi_0 d\tau. \tag{49}$$

From the expression for ψ_0, it is readily seen that the integration over ϕ gives unity. The integration over θ is of the form

$$\int_0^\pi P_2(\cos\theta)\,[P_l^m(\cos\theta)]^2\sin\theta d\theta = \int_{-1}^{+1}P_2(z)\,[P_l^m(z)]^2 dz. \tag{50}$$

Now it may be shown that

$$\left.\begin{aligned}P_2(z)P_l^m(z) = \frac{3}{2}\frac{l+m}{2l+1}P_{l-2}^m + \frac{3}{2}\frac{l-m+1}{2l+1}\frac{l-m+2}{2l+3}P_{l+2}^m \\ +\left\{\frac{3}{2}\left[\frac{l+m}{2l+1}\frac{l-m}{2l-1}+\frac{l-m+1}{2l+1}\frac{l+m+1}{2l+3}\right]-\frac{1}{2}\right\}P_l^m,\end{aligned}\right\} \tag{51}$$

where use has been made of equation (23) and the further relation

$$\left.\begin{aligned}z^2P_l^m = \frac{l+m}{2l+1}\frac{l+m-1}{2l-1}P_{l-2}^m + \frac{l-m+1}{2l+1}\frac{l-m+2}{2l+3}P_{l+2}^m \\ +\left[\frac{l+m}{2l+1}\frac{l-m}{2l-1}+\frac{l-m+1}{2l+1}\frac{l+m+1}{2l+3}\right]P_l^m.\end{aligned}\right\} \tag{52}$$

Hence

$$\left.\begin{aligned}\int_{-1}^{+1} P_2(z)\,[P_l^m(z)]^2 dz = \left\{\frac{3}{2}\left[\frac{l+m}{2l+1}\,\frac{l-m}{2l-1}+\frac{l-m+1}{2l+1}\,\frac{l+m+1}{2l+3}\right]-\frac{1}{2}\right\}\\ \times\int_{-1}^{+1}[P_l^m(z)]^2 dz\,.\end{aligned}\right\} \tag{53}$$

The integral on the right is just canceled by the normalization factor for the Legendre polynomials (cf. eq. [10]), so that we finally have

$$E_3 = -\left\{\frac{3}{2}\left[\frac{l+m}{2l+1}\,\frac{l-m}{2l-1}+\frac{l-m+1}{2l+1}\,\frac{l+m+1}{2l+3}\right]-\frac{1}{2}\right\}\int_0^\infty r^2 R_{n,\,l}^2(r)\,r^2 dr\,. \tag{54}$$

Now the integral over r defines the mean value of r^2, so that

$$E_3 = -\left\{\frac{3}{2}\left[\frac{l+m}{2l+1}\,\frac{l-m}{2l-1}+\frac{l-m+1}{2l+1}\,\frac{l+m+1}{2l+3}\right]-\frac{1}{2}\right\}\overline{r_{n,\,l}^2}\,, \tag{55}$$

where[6]

$$\overline{r_{n,\,l}^2} = \frac{n^2}{2}[5n^2+1-3l(l+1)]\,. \tag{56}$$

Inserting the proper values of m and l, we find

$$E_3(n,\,n-1,\,n-1) = \frac{n^2}{2}(n^2-1)\,. \tag{57}$$

The van der Waals interaction between a proton and a hydrogen atom *in a pure state* is thus seen to follow essentially an R^{-3} law, in contrast to the more familiar R^{-6} law, which applies, for instance, in the case of two hydrogen atoms in the ground state. The R^{-3} law applies, however, only in this special case; and it will be seen in the next section how the degeneracy with respect to l brings about a term in E_2.

The Coulson case, $n = 1$, differs from the general pure-state case in that E_3 also vanishes. Hence for this case it becomes necessary to consider also the fourth-order terms.

Returning to equation (13*d*), we have

$$[H-E_0]\,\psi_3 - r^2 P_2(\cos\theta)\,\psi_0 = \frac{n^2}{2}(n^2-1)\,\psi_0 \tag{58}$$

or

$$\left.\begin{aligned}-\frac{1}{2}\left\{\frac{1}{r^2}\frac{\partial}{\partial r}\left(r^2\frac{\partial\psi_3}{\partial r}\right)+\frac{1}{r^2\sin\theta}\frac{\partial}{\partial\theta}\left(\sin\theta\,\frac{\partial\psi_3}{\partial\theta}\right)+\frac{1}{r^2\sin^2\theta}\frac{\partial^2\psi_3}{\partial\phi^2}\right\}-\frac{\psi_3}{r}\\ -E_0\psi_3 = r^2P_2(\cos\theta)\,\psi_0+\frac{n^2}{2}(n^2-1)\,\psi_0\,.\end{aligned}\right\} \tag{59}$$

The separation of this equation is made in exactly the same way as before. Omitting the normalization factors and writing

$$\psi_3 = e^{i(n-1)\phi}\sum_k P_k^m(\cos\theta)\,\mathfrak{F}_{n,\,k}(\rho)\,, \tag{60}$$

[6] See H. Bethe, *Handb. d. Phys.*, **24**, Part I, 286, eq. (3.21), Berlin, 1933.

we find that the functions $\mathcal{S}_{n,k}$ satisfy the equations

$$\frac{1}{\rho^2}\frac{d}{d\rho}\left(\rho^2\frac{d\mathcal{S}_{n,k}}{d\rho}\right)+\left\{-\frac{k(k+1)}{\rho^2}+\frac{n}{\rho}-\frac{1}{4}\right\}\mathcal{S}_{n,k}=0 \qquad (k\neq n-1,\ n+1), \quad (61)$$

$$\left.\begin{aligned}\frac{1}{\rho^2}\frac{d}{d\rho}\left(\rho^2\frac{d\mathcal{S}_{n,n+1}}{d\rho}\right)+\left\{-\frac{(n+1)(n+2)}{\rho^2}+\frac{n}{\rho}-\frac{1}{4}\right\}\mathcal{S}_{n,n+1}\\ =\frac{3}{2}\frac{n^4}{8}\frac{2}{(2n-1)(2n+1)}e^{-\rho/2}\rho^{n+1}L_{2n-1}^{2n-1}\end{aligned}\right\} \quad (k=n+1), \quad (62)$$

and

$$\left.\begin{aligned}\frac{1}{\rho^2}\frac{d}{d\rho}\left(\rho\frac{d\mathcal{S}_{n,n-1}}{d\rho}\right)+\left\{-\frac{n(n-1)}{\rho^2}+\frac{n}{\rho}-\frac{1}{4}\right\}\mathcal{S}_{n,n-1}\\ =-\frac{n^4}{8}\frac{n-1}{2n+1}\{\rho^2-2(n+1)(2n+1)\}e^{-\rho/2}\rho^{n-1}L_{2n-1}^{2n-1}\end{aligned}\right\} \quad (k=n-1). \quad (63)$$

Solutions of these equations in terms of Laguerre polynomials can be found exactly as in the case of ψ_2. Finally, the arbitrary constants which appear in these solutions are determined by the normalizing condition that ψ_0 and ψ_3 be orthogonal. This completes the formal discussion of the third-order terms.

6. *The fourth-order terms.*—The quantity E_4 is obtained in exactly the same way. Multiplying equation (13*e*) by ψ_0^* and integrating over the configuration space, we have

$$\int\psi_0^*[H-E_0]\psi_4 d\tau-\int r^3P_3(\cos\theta)\psi_0^*\psi_0 d\tau-\int rP_1(\cos\theta)\psi_0^*\psi_2 d\tau=E_4 \quad (64)$$

or

$$E_4=-\int r^3P_3(\cos\theta)\psi_0^*\psi_0 d\tau-\int rP_1(\cos\theta)\psi_0^*\psi_2 d\tau. \quad (65)$$

Now the first term on the right contains as a factor an integral of the type

$$\int_0^\pi P_3(\cos\theta)\,[P_l^m(\cos\theta)]^2\sin\theta d\theta=\int_{-1}^{+1}P_3(z)\,[P_l^m(z)]^2 dz. \quad (66)$$

Since

$$\int_{-1}^{+1}z^jP_k dz=0 \qquad (j=0,\ 1,\ \ldots,\ k-1), \quad (67)$$

integrals of the above type are equal to zero unless $2l\geq 3$. Thus the integral in question is zero, at least for s and p states. More generally, we have

$$\left.\begin{aligned}\int_{-1}^{+1}P_3[P_l^m]^2dz=\frac{1}{2}\int_{-1}^{+1}(5z^3-3z)[P_l^m]^2dz=\frac{5}{2}\int_{-1}^{+1}z^3[P_l^m]^2dz\\ -\frac{3}{2}\int_{-1}^{+1}z[P_l^m]^2dz;\end{aligned}\right\} \quad (68)$$

and we have already shown that

$$\int_{-1}^{+1}z[P_l^m]^2dz=0. \quad (69)$$

Moreover, it is also true that

$$\int_{-1}^{+1}z^3[P_l^m]^2dz=0, \quad (70)$$

since z^3 is an odd function of z and $[P_l^m]^2$ is an even function; and thus

$$\int_{-1}^{+1} P_3 [P_l^m]^2 d z = 0 . \tag{71}$$

It is further clear that, quite generally,

$$\int_{-1}^{+1} P_{\text{odd}} [P_l^m]^2 d z = 0 , \tag{72}$$

since P_{odd} is a sum of odd powers of z only.

Therefore,

$$E_4 = -\int r P_1 (\cos\theta) \psi_0^* \psi_2 d\tau , \tag{73}$$

or, inserting the proper expression for ψ_2 (cf. eq. [47]), we have

$$\left.\begin{aligned} E_4 = -\frac{1}{\sqrt{2\pi}} \left(\frac{2}{n}\right)^{3/2} \sqrt{\frac{2n-1}{2(2n-2)!}} \frac{1}{\sqrt{2n[(2n-1)!]^3}} \int_0^{2\pi} \Phi_{n-1}^*(\phi)\, e^{i(n-1)\phi} d\phi \\ \times \int_0^{\pi} P_1(\cos\theta)\, \Theta_{n-1,\,n-1}(\theta) P_n^{n-1}(\cos\theta) \sin\theta\, d\theta \int_0^{\infty} r R_{n,\,n-1} \mathcal{R}_{n,\,n}\, r^2 d r . \end{aligned}\right\} \tag{74}$$

Now the integration over ϕ cancels the factor $(2\pi)^{-1/2}$. Also, making use of equation (23) and carrying out the integration over θ, we have

$$E_4 = -\left(\frac{2}{n}\right)^{3/2} \frac{2n-1}{2n+1} \frac{1}{\sqrt{2n[(2n-1)!]^3}} \int_0^{\infty} r R_{n,n-1} \mathcal{R}_{n,n}\, r^2 d r . \tag{75}$$

Using the proper forms for the radial functions and expressing everything in terms of ρ, we obtain

$$\left.\begin{aligned} E_4 = \frac{n^4}{8} \frac{1}{2n+1} \frac{1}{2n[(2n-1)!]^3} \int_0^{\infty} \rho^{2n+2} e^{-\rho} L_{2n-1}^{2n-1} \left[-\frac{2(n+1)}{2n(2n+1)} L_{2n+2}^{2n+1} \right. \\ \left. + \frac{1}{4n(2n+1)(2n+2)} L_{2n+2}^{2n+1} \right] d\rho . \end{aligned}\right\} \tag{76}$$

Now the associated Laguerre polynomials have the integral property[7]

$$\left.\begin{aligned} \int_0^{\infty} \rho^p e^{-\rho} L_r^s L_{r'}^{s'} d\rho = p!\, r!\, r'! \sum_{\tau=0}^{\leq r-s,\ r'-s'} (-1)^{r+r'+\tau} \\ \times \binom{p-s}{r-s-\tau} \binom{p'-s'}{r'-s'-\tau} \binom{-p-1}{\tau} . \end{aligned}\right\} \tag{77}$$

Making use of this property and combining all the terms, we find that

$$E_4(n, n-1, n-1) = -\frac{n^4}{8}(n+1)(4n+5) . \tag{78}$$

If n be put equal to 1, the above expression gives the first coefficient in the Coulson case, namely, $-\frac{9}{4}$.

[7] See E. Schrödinger, *Collected Papers on Wave Mechanics*, p. 99, eq. (115), London: Blackie, 1928.

III. THE CASE $|m| = n - 2$

7. *The zero-order terms.*—Corresponding to the value $|m| = n - 2$ there are two possible values of l, namely, $l = n - 2$ and $l = n - 1$. In accordance with the remarks of the introductory section we let

$$\psi_0 = a\psi_0(n, n-2, n-2) + b\psi_0(n, n-1, n-2), \tag{79}$$

where the ψ_0's on the right-hand side are given by equations (9), (10), and (11), and a and b are the coefficients to be determined.

8. *The first-order terms.*—Multiplying equation (13*b*) by ψ_0^* and integrating over configuration space, we have

$$\int \psi_0^* [H - E_0] \psi_1 d\tau = E_1 \tag{80}$$

or

$$E_1 = 0 . \tag{81}$$

It will be noticed that this result is valid for *all* values of $|m|$, since it depends only on the self-adjointness of the Hamiltonian operator.

Hence, equation (13*b*) becomes

$$[H - E_0] \psi_1 = 0 . \tag{82}$$

This equation is exactly the same as equation (13*a*), and therefore it, too, is satisfied by any linear combination of $\psi_0(n, n-2, n-2)$ and $\psi_0(n, n-1, n-2)$. Thus

$$\psi_1 = a_1\psi_0(n, n-2, n-2) + b_1\psi_0(n, n-1, n-2), \tag{83}$$

where a_1 and b_1 are constants unspecified for the present but which will be determined later (see sec. 10 below).

9. *The second-order terms.*—If we insert the proper expressions for the zero- and first-order terms, equation (13*c*) becomes

$$\left.\begin{aligned} [H - E_0]\psi_2 - rP_1(\cos\theta)\,[a\psi_0(n, n-2, n-2) + b\psi_0(n, n-1, n-2)] \\ = E_2\,[a\psi_0(n, n-2, n-2) + b\psi_0(n, n-1, n-2)] . \end{aligned}\right\} \tag{84}$$

This equation involves three unknowns, namely, a, b, and E_2. Two relations between these quantities may be obtained by multiplying equation (84) by $\psi_0^*(n, n-2, n-2)$ and $\psi_0^*(n, n-1, n-2)$, respectively, and integrating over the entire configuration space. Thus, applying equation (72) and making use of the self-adjointness of H, we obtain

$$-b\int rP_1(\cos\theta)\,\psi_0^*(n, n-2, n-2)\,\psi_0(n, n-1, n-2)\,d\tau = aE_2 \tag{85}$$

and

$$-a\int rP_1(\cos\theta)\,\psi_0^*(n, n-1, n-2)\,\psi_0(n, n-2, n-2)\,d\tau = bE_2 . \tag{86}$$

The integral which appears in equations (85) and (86) can be evaluated with the aid of expressions (23) and (77); its value is $-\frac{3}{2}n$. Hence, the two equations become

$$\tfrac{3}{2}nb = aE_2 \tag{87}$$

and

$$\tfrac{3}{2}na = bE_2 . \tag{88}$$

Combining these, we obtain the secular equation for E_2:

$$\begin{vmatrix} E_2 & -\frac{3}{2}n \\ -\frac{3}{2}n & E_2 \end{vmatrix} = 0 , \tag{89}$$

whence

$$E_2 = \pm \tfrac{3}{2}n \tag{90}$$

and

$$a = \pm b . \tag{91}$$

The third relation between the unknowns is furnished by the condition that ψ_0 be normalized to unity; this requires that

$$a^2 + b^2 = 1 . \tag{92}$$

Solving equations (91) and (92), we find that

$$a = \frac{1}{\sqrt{2}}; \qquad b = \pm\frac{1}{\sqrt{2}}, \tag{93}$$

whence

$$\psi_0 = \frac{1}{\sqrt{2}}[\psi_0(n, n-2, n-2) \pm \psi_0(n, n-1, n-2)] . \tag{94}$$

Finally, the equation for ψ_2 becomes

$$\left.\begin{aligned} [H - E_0]\psi_2 - \frac{1}{\sqrt{2}} rP_1(\cos\theta)\,[\psi_0(n, n-2, n-2) \pm \psi_0(n, n-1, n-2)] \\ = \pm\frac{3}{2}\, n\, \frac{1}{\sqrt{2}}[\psi_0(n, n-2, n-2) \pm \psi_0(n, n-1, n-2)] . \end{aligned}\right\} \tag{95}$$

The discussion of this equation is postponed to a later paragraph (sec. 11 below), where it will be shown that a complete solution can be found in terms of hydrogen-like functions.

10. *The third-order terms.*—Equation (13*d*) for E_3 becomes

$$\left.\begin{aligned} [H - E_0]\psi_3 - \frac{1}{\sqrt{2}} r^2P_2(\cos\theta)\,[\psi_0(n, n-2, n-2) \pm \psi_0(n, n-1, n-2)] \\ - rP_1(\cos\theta)\,[a_1\psi_0(n, n-2, n-2) + b_1\psi_0(n, n-1, n-2)] \\ = \pm\tfrac{3}{2}n\,[a_1\psi_0(n, n-2, n-2) + b_1\psi_0(n, n-1, n-2)] \\ \pm\frac{1}{\sqrt{2}} E_3[\psi_0(n, n-2, n-2) \pm \psi_0(n, n-1, n-2)] . \end{aligned}\right\} \tag{96}$$

Again there are three unknowns to be determined: a_1, b_1, and E_3. Multiplying by $\psi_0^*(n, n-2, n-2)$ and integrating over the configuration space, we have

$$\left.\begin{aligned} -\frac{1}{\sqrt{2}}\int r^2P_2\psi_0^*(n, n-2, n-2)\,\psi_0(n, n-2, n-2)\,d\tau \\ - b_1\int rP_1\psi_0^*(n, n-2, n-2)\,\psi_0(n, n-1, n-2)\,d\tau = \pm\tfrac{3}{2}na_1 + \frac{1}{\sqrt{2}}E_3 , \end{aligned}\right\} \tag{97}$$

where use has been made of equation (72) and the fact that P_2 contains only even powers of z (cf. eq. [51]). Similarly,

$$\left.\begin{aligned} &\mp\frac{1}{\sqrt{2}}\int r^2 P_2 \psi_0^*(n, n-1, n-2)\,\psi_0(n, n-1, n-2)\,d\tau \\ &-a_1\int r P_1 \psi_0^*(n, n-1, n-2)\,\psi_0(n, n-2, n-2)\,d\tau = \pm\tfrac{3}{2}n b_1 \pm \frac{1}{\sqrt{2}}E_3 . \end{aligned}\right\} \quad (98)$$

The integrals containing P_2 can be evaluated by making use of equations (53) and (77). They have the values

$$\int r^2 P_2 \psi_0^*(n, n-2, n-2)\,\psi_0(n, n-2, n-2)\,d\tau = -\frac{n^2}{2}(n-2)(n+5) \quad (99)$$

and

$$\int r^2 P_2 \psi_0^*(n, n-1, n-2)\,\psi_0(n, n-1, n-2)\,d\tau = -\frac{n^2}{2}(n+1)(n-4). \quad (100)$$

Hence equations (97) and (98) become

$$\frac{1}{\sqrt{2}}\frac{n^2}{2}(n-2)(n+5) + \tfrac{3}{2}n b_1 = \pm\tfrac{3}{2}n a_1 + \frac{1}{\sqrt{2}}E_3 \quad (101)$$

and

$$\frac{1}{\sqrt{2}}\frac{n^2}{2}(n+1)(n-5) + \tfrac{3}{2}n a_1 = \pm\tfrac{3}{2}n b_1 \pm \frac{1}{\sqrt{2}}E_3 . \quad (102)$$

Finally, the third condition on the unknowns is imposed by the orthogonality of ψ_0 and ψ_1, which leads to the relation

$$\frac{1}{\sqrt{2}}a_1 \pm \frac{1}{\sqrt{2}}b_1 = 0 . \quad (103)$$

Equations (101), (102), and (103) may now be solved for the three unknowns. We have

$$E_3 = \frac{\begin{vmatrix} \pm\frac{3}{2}n & -\frac{3}{2}n & \frac{1}{\sqrt{2}}\frac{n^2}{2}(n-2)(n+5) \\ -\frac{3}{2}n & \pm\frac{3}{2}n & \pm\frac{1}{\sqrt{2}}\frac{n^2}{2}(n+1)(n-4) \\ \frac{1}{\sqrt{2}} & \pm\frac{1}{\sqrt{2}} & 0 \end{vmatrix}}{\begin{vmatrix} \pm\frac{3}{2}n & -\frac{3}{2}n & \frac{1}{\sqrt{2}} \\ -\frac{3}{2}n & \pm\frac{3}{2}n & \pm\frac{1}{\sqrt{2}} \\ \frac{1}{\sqrt{2}} & \pm\frac{1}{\sqrt{2}} & 0 \end{vmatrix}} = \frac{n^2}{2}(n^2-7). \quad (104)$$

In like manner it is found that

$$a_1 = \pm\frac{1}{\sqrt{2}}\frac{n}{2}(n-1); \qquad b_1 = -\frac{1}{\sqrt{2}}\frac{n}{2}(n-1). \tag{105}$$

Accordingly,

$$\psi_1 = \pm\frac{1}{\sqrt{2}}\frac{n}{2}(n-1)\,[\psi_0(n, n-2, n-2) \mp \psi_0(n, n-1, n-2)]. \tag{106}$$

In particular, it should be noted that there is only one value of E_3 corresponding to the pair of values $\pm\frac{8}{2}n$ for E_2.

11. *The function* ψ_2.—Finally, we shall show how the function ψ_2 may be obtained and that it does indeed satisfy the criteria for an acceptable wave function. After the Hamiltonian operator has been expanded, equation (95) is of the form

$$\left.\begin{aligned} -\frac{1}{2}\left\{\frac{1}{r^2}\frac{\partial}{\partial r}\left(r^2\frac{\partial\psi_2}{\partial r}\right)+\frac{1}{r^2\sin\theta}\frac{\partial}{\partial\theta}\left(\sin\theta\frac{\partial\psi_2}{\partial\theta}\right)+\frac{1}{r^2\sin^2\theta}\frac{\partial^2\psi_2}{\partial\phi^2}\right\}-\frac{\psi_2}{r} \\ +\frac{1}{2n^2}\psi_2 = \frac{1}{\sqrt{2}}rP_1(\cos\theta)\,[\psi_0(n,l,m)\pm\psi_0(n,l+1,m)] \\ \pm\frac{3}{2}n\frac{1}{\sqrt{2}}\,[\psi_0(n,l,m)\pm\psi_0(n,l+1,m)], \end{aligned}\right\} \tag{107}$$

where we shall later let m and l have the value $n-2$. Setting

$$\psi_2 = \frac{1}{\sqrt{2\pi}}e^{im\phi}\psi_2(\theta, r) \tag{108}$$

and suppressing the factor

$$\sqrt{\frac{(2l+1)(l-m)!}{2(l+m)!}}\left(\frac{2}{n}\right)^{3/2}\sqrt{\frac{(n-l-1)!}{2n[(n+l)!]^3}},$$

we have

$$\left.\begin{aligned} -\frac{1}{2}\left\{\frac{1}{r^2}\frac{\partial}{\partial r}\left(r^2\frac{\partial\Psi_2}{\partial r}\right)+\frac{1}{r^2\sin\theta}\frac{\partial}{\partial\theta}\left(\sin\theta\frac{\partial\Psi_2}{\partial\theta}\right)-\frac{m^2}{r^2\sin^2\theta}\Psi_2\right\}-\frac{\Psi_2}{r} \\ +\frac{1}{2n^2}\Psi_2 = -\left[\frac{1}{\sqrt{2}}rP_1(\cos\theta)\pm\frac{1}{\sqrt{2}}\frac{3}{2}n\right]\left[P_l^m e^{-\rho/2}\rho^l L_{n+l}^{2l+1}\right. \\ \pm\sqrt{\frac{(2l+3)(l-m+1)}{(2l+1)(l+m+1)}}\frac{1}{\sqrt{(n-l-1)(n+l+1)^3}} \\ \left.\times P_{l+1}^m e^{-\rho/2}\rho^{l+1}L_{n+l+1}^{2l+3}\right]. \end{aligned}\right\} \tag{109}$$

In terms of ρ this becomes

$$\left.\begin{aligned} \frac{1}{\rho^2}\frac{\partial}{\partial\rho}\left(\rho^2\frac{\partial\Psi_2}{\partial\rho}\right)+\frac{1}{\rho^2\sin\theta}\frac{\partial}{\partial\theta}\left(\sin\theta\frac{\partial\Psi_2}{\partial\theta}\right)-\frac{m^2}{\rho^2\sin^2\theta}\Psi_2+\frac{n}{\rho}\Psi_2-\tfrac{1}{4}\Psi_2 \\ =\left[\frac{n^3}{8}\sqrt{2}\,\rho P_1(\cos\theta)\pm 3\,\frac{n^3}{8}\sqrt{2}\right]\left[P_l^m e^{-\rho/2}\rho^l L_{n+l}^{2l+1}\right. \\ \left.\pm\sqrt{\frac{(2l+3)(l-m+1)}{(2l+1)(l+m+1)}}\frac{1}{\sqrt{(n-l-1)(n+l+1)^3}}P_{l+1}^m e^{-\rho/2}\rho^{l+1}L_{n+l+1}^{2l+3}\right]. \end{aligned}\right\} \tag{110}$$

If we write

$$\Psi_2 = \sum_k P_k^m \mathcal{R}_{n,\,k}(\rho), \tag{111}$$

then

$$\left.\begin{aligned}\sum_k P_k^m \left[\frac{1}{\rho^2}\frac{d}{d\rho}\left(\rho^2\frac{d\mathcal{R}_{n,\,k}}{d\rho}\right) - \frac{k(k+1)}{\rho^2}\mathcal{R}_{n,\,k} + \frac{n}{\rho}\mathcal{R}_{n,\,k} - \tfrac{1}{4}\mathcal{R}_{n,\,k}\right] \\ = \frac{n^3}{8}\sqrt{2}\,[\rho P_1 \pm 3]\left[P_l^m e^{-\rho/2}\rho^l L_{n+l}^{2l+1} \pm \sqrt{\frac{(2l+3)(l-m+1)}{(2l+1)(l+m+1)}}\right. \\ \left.\times\frac{1}{\sqrt{(n-l-1)(n+l+1)^3}} P_{l+1}^m e^{-\rho/2}\rho^{l+1} L_{n+l+1}^{2l+3}\right].\end{aligned}\right\} \tag{112}$$

Finally, equating the coefficients of P_k^m and remembering that $l = m$, we obtain

$$\frac{1}{\rho^2}\frac{d}{d\rho}\left(\rho^2\frac{d\mathcal{R}_{n,\,k}}{d\rho}\right) + \left\{-\frac{k(k+1)}{\rho^2} + \frac{n}{\rho} - \frac{1}{4}\right\}\mathcal{R}_{n,\,k} = 0 \qquad (k \geq l+3), \tag{113}$$

$$\left.\begin{aligned}\frac{1}{\rho^2}\frac{d}{d\rho}\left(\rho^2\frac{d\mathcal{R}_{n,\,l}}{d\rho}\right) + \left\{-\frac{l(l+1)}{\rho^2} + \frac{n}{\rho} - \frac{1}{4}\right\}\mathcal{R}_{n,\,l} \\ = \pm\frac{n^3}{8}\sqrt{2}\left[3e^{-\rho/2}\rho^l L_{n+l}^{2l+1} + \sqrt{\frac{(l+1)^2 - m^2}{(2l+1)(2l+3)}}\right. \\ \left.\times\frac{1}{\sqrt{(n-l-1)(n+l+1)^3}} e^{-\rho/2}\rho^{l+2} L_{n+l+1}^{2l+3}\right]\end{aligned}\right\} \qquad (k = l), \tag{114}$$

$$\left.\begin{aligned}\frac{1}{\rho^2}\frac{d}{d\rho}\left(\rho^2\frac{d\mathcal{R}_{n,\,l+1}}{d\rho}\right) + \left\{-\frac{(l+1)(l+2)}{\rho^2} + \frac{n}{\rho} - \frac{1}{4}\right\}\mathcal{R}_{n,\,l+1} \\ = \frac{n^3}{8}\sqrt{2}\left[\frac{l-m+1}{2l+1} e^{-\rho/2}\rho^{l+1} L_{n+l}^{2l+1} + 3\sqrt{\frac{(2l+3)(l-m+1)}{(2l+1)(l+m+1)}}\right. \\ \left.\times\frac{1}{\sqrt{(n-l-1)(n+l+1)^3}} e^{-\rho/2}\rho^{l+1} L_{n+l+1}^{2l+3}\right]\end{aligned}\right\} \qquad (k = l+1), \tag{115}$$

and

$$\left.\begin{aligned}\frac{1}{\rho^2}\frac{d}{d\rho}\left(\rho^2\frac{d\mathcal{R}_{n,\,l+2}}{d\rho}\right) + \left\{-\frac{(l+2)(l+3)}{\rho^2} + \frac{n}{\rho} - \frac{1}{4}\right\}\mathcal{R}_{n,\,l+2} \\ = \pm\frac{n^3}{8}\sqrt{2}\sqrt{\frac{(l-m+1)(l+m+2)^2}{(2l+1)(2l+3)(l+m+1)}} \\ \times\frac{1}{\sqrt{(n-l-1)(n+l+1)^3}} e^{-\rho/2}\rho^{l+2} L_{n+l+1}^{2l+3}\end{aligned}\right\} \qquad (k = l+2). \tag{116}$$

To solve these equations we first remove from the $\mathcal{R}$'s the factor $e^{-\rho/2}\rho^k$. To do this, let

$$\mathcal{R}_{n,\,k} = e^{-\rho/2}\rho^k A_{n,\,k}. \tag{117}$$

Then

$$\mathcal{R}'_{n,\,k} = e^{-\rho/2}\{\rho^k A' + k\rho^{k-1}A\} - \tfrac{1}{2}e^{-\rho/2}\rho^k A, \tag{118}$$

and

$$\left.\begin{aligned}\mathcal{R}''_{n,\,k} = e^{-\rho/2}\{\rho^k A'' + 2k\rho^{k-1}A' + k(k-1)\rho^{k-2}A\} \\ - e^{-\rho/2}\{\rho^k A' + k\rho^{k-1}A\} + \tfrac{1}{4}e^{-\rho/2}\rho^k A.\end{aligned}\right\} \tag{119}$$

After substituting these expressions in the three equations (114), (115), and (116) and dividing through by ρ^{k-1}, we are left with

$$\left.\begin{aligned}\rho A''_{n,\,l}+[2(l+1)-\rho]\,A'_{n,\,l}+(n-l-1)\,A_{n,\,l}&=\pm\frac{n^3}{8}\sqrt{2}\left[3\rho L^{2l+1}_{n+l}\right.\\&\left.+\sqrt{\frac{(l+1)^2-m^2}{(2l+1)\,(2l+3)}}\,\frac{1}{\sqrt{(n-l-1)\,(n+l+1)^3}}\,\rho^3 L^{2l+3}_{n+l+1}\right],\end{aligned}\right\}\tag{120}$$

$$\left.\begin{aligned}&\rho A''_{n,\,l+1}+[2(l+2)-\rho]\,A'_{n,\,l+1}+(n-l-2)\,A_{n,\,l+1}\\&\quad=\frac{n^3}{8}\sqrt{2}\left[\frac{l-m+1}{2l+1}\,\rho L^{2l+1}_{n+l}+3\sqrt{\frac{(2l+3)\,(l-m+1)}{(2l+1)\,(l+m+1)}}\right.\\&\qquad\left.\times\frac{1}{\sqrt{(n-l-1)\,(n+l+1)^3}}\,\rho L^{2l+3}_{n+l+1}\right],\end{aligned}\right\}\tag{121}$$

and

$$\left.\begin{aligned}&\rho A''_{n,\,l+2}+[2(l+3)-\rho]\,A'_{n,\,l+2}+(n-l-3)\,A_{n,\,l+2}=\pm\frac{n^3}{8}\sqrt{2}\\&\times\sqrt{\frac{(l-m+1)\,(l+m+2)^2}{(2l+1)\,(2l+3)\,(l+m+1)}}\,\frac{1}{\sqrt{(n-l-1)\,(n+l+1)^3}}\,\rho L^{2l+3}_{n+l+1}.\end{aligned}\right\}\tag{122}$$

Finally, putting $l = m = n - 2$ in the foregoing equations, we obtain

$$\left.\begin{aligned}&\rho A''_{n,\,n-2}+[2(n-1)-\rho]\,A'_{n,\,n-2}+A_{n,\,n-2}\\&\quad=\pm\frac{n^3}{8}\sqrt{2}\left[3\rho L^{2n-3}_{2n-2}+\frac{1}{(2n-1)^2}\,\rho^3 L^{2n-1}_{2n-1}\right],\end{aligned}\right\}\tag{123}$$

$$\left.\begin{aligned}&\rho A''_{n,\,n-1}+[2n-\rho]\,A'_{n,\,n-1}\\&\quad=\frac{n^3}{8}\sqrt{2}\left[\frac{1}{2n-3}\,\rho L^{2n-3}_{2n-2}+\frac{3}{(2n-1)\,(2n-3)}\,\rho L^{2n-1}_{2n-1}\right],\end{aligned}\right\}\tag{124}$$

and

$$\left.\begin{aligned}&\rho A''_{n,\,n}+[2(n+1)-\rho]\,A'_{n,\,n}-A_{n,\,n}\\&\quad=\pm\frac{n^3}{8}\sqrt{2}\,\frac{2n-2}{(2n-3)\,(2n-1)^2}\,\rho L^{2n-1}_{2n-1}.\end{aligned}\right\}\tag{125}$$

The last of these equations is, apart from a constant factor, identical with equation (37). Hence its solution is (cf. eq. [45])

$$\left.\begin{aligned}A_{n,\,n}=\pm\frac{n^3}{8}\sqrt{2}\,\frac{2n-2}{(2n-3)\,(2n-1)^2}&\left[-\frac{2(n+1)}{2n(2n+1)}\,L^{2n+1}_{2n+1}\right.\\&\left.+\frac{1}{4n(2n+1)\,(2n+2)}\,L^{2n+1}_{2n+2}\right]\end{aligned}\right\}\tag{126}$$

and

$$\left.\begin{aligned}\mathcal{R}_{n,\,n}=\pm\frac{n^3}{8}\sqrt{2}\,\frac{2n-2}{(2n-3)\,(2n-1)^2}\,e^{-\rho/2}\rho^n&\left[-\frac{2(n+1)}{2n(2n+1)}\,L^{2n+1}_{2n+1}\right.\\&\left.+\frac{1}{4n(2n+1)\,(2n+2)}\,L^{2n+1}_{2n+2}\right].\end{aligned}\right\}\tag{127}$$

Consider, next, equation (124). Letting

$$A_{n,\,n-1}=\sum_j c_j L_{2n+j}^{2n-1}, \tag{128}$$

we find

$$\left.\begin{aligned}\sum_j -c_j(j+1)L_{2n+j}^{2n-1}=\frac{n^3}{8}\sqrt{2}\Bigg[&\frac{1}{2n-3}\,\rho L_{2n-2}^{2n-3}\\&+\frac{3}{(2n-1)(2n-3)}\,\rho L_{2n-1}^{2n-1}\Bigg].\end{aligned}\right\} \tag{129}$$

Now, by means of the recurrence relations (40) and (41), the right-hand side of this equation can be expressed as a sum of associated Laguerre polynomials of order $2n-1$, with constant coefficients. Thus,

$$\rho L_{2n-2}^{2n-3}=-\frac{6n}{2n-1}L_{2n-1}^{2n-1}+\frac{2(n+2)}{2n(2n-1)}L_{2n}^{2n-1}-\frac{2}{2n(2n-1)(2n+1)}L_{2n+1}^{2n-1}, \tag{130}$$

and

$$\rho L_{2n-2}^{2n-1}=2nL_{2n-1}^{2n-1}-\frac{1}{2n}L_{2n}^{2n-1}, \tag{131}$$

and equation (129) becomes

$$\left.\begin{aligned}\sum_j -c_j(j+1)L_{2n+j}^{2n-1}=\frac{n^3}{8}\sqrt{2}\,\frac{1}{2n-3}\Bigg[&\frac{2n+1}{2n(2n-1)}L_{2n}^{2n-1}\\&-\frac{2}{2n(2n-1)(2n+1)}L_{2n+1}^{2n-1}\Bigg].\end{aligned}\right\} \tag{132}$$

All the coefficients c_j except c_{-1} are now uniquely determined; we have

$$\left.\begin{aligned}c_0&=-\frac{n^3}{8}\sqrt{2}\,\frac{1}{2n-3}\,\frac{2n+1}{2n(2n-1)},\\c_1&=\frac{n^3}{8}\sqrt{2}\,\frac{1}{2n-3}\,\frac{1}{2n(2n-1)(2n+1)},\end{aligned}\right\} \tag{133}$$

so that

$$\left.\begin{aligned}A_{n,\,n-1}=\frac{n^3}{8}\sqrt{2}\,\frac{1}{2n-3}\Bigg[&cL_{2n-1}^{2n-1}-\frac{2n+1}{2n(2n-1)}L_{2n}^{2n-1}\\&+\frac{1}{2n(2n-1)(2n+1)}L_{2n+1}^{2n-1}\Bigg].\end{aligned}\right\} \tag{134}$$

Consequently,

$$\left.\begin{aligned}\mathcal{R}_{n,\,n-1}=\frac{n^3}{8}\sqrt{2}\,\frac{1}{2n-3}\,e^{-\rho/2}\rho^{n-1}\Bigg[&cL_{2n-1}^{2n-1}-\frac{2n+1}{2n(2n-1)}L_{2n}^{2n-1}\\&+\frac{1}{2n(2n-1)(2n+1)}L_{2n+1}^{2n-1}\Bigg].\end{aligned}\right\} \tag{135}$$

To solve equation (123), we let

$$A_{n,\,n-2}=\sum_j c_j L_{2n+j}^{2n-3} \tag{136}$$

and obtain

$$\sum_j -c_j(j+2)L_{2n+j}^{2n-3}=\pm\frac{n^3}{8}\sqrt{2}\left[3\rho L_{2n-2}^{2n-3}+\frac{1}{(2n-1)^2}\rho^3 L_{2n-1}^{2n-1}\right]. \tag{137}$$

Also, it can be shown that

$$\rho L_{2n-2}^{2n-3} = 2nL_{2n-2}^{2n-3} - \frac{2}{2n-1} L_{2n-1}^{2n-3} - (2n-2)^2 L_{2n-3}^{2n-3} \tag{138}$$

and that

$$\left.\begin{aligned} \rho^3 L_{2n-1}^{2n-1} = {} & 2n(2n-1)^2(2n-2)^2 L_{2n-3}^{2n-3} - 6n(2n-1)^2 L_{2n-2}^{2n-3} \\ & + 12nL_{2n-1}^{2n-3} - \frac{6}{2n} L_{2n}^{2n-3}, \end{aligned}\right\} \tag{139}$$

whence

$$\left.\begin{aligned} \sum_j - c_j(j+2) L_{2n+j}^{2n-3} = \pm\frac{n^3}{8}\sqrt{2}\Big[& (2n-3)(2n-2)^2 L_{2n-3}^{2n-3} \\ & + \frac{6}{(2n-1)^2} L_{2n-1}^{2n-3} - \frac{6}{2n(2n-1)^2} L_{2n}^{2n-3}\Big]. \end{aligned}\right\} \tag{140}$$

Equating coefficients, we find that

$$\left.\begin{aligned} c_0 &= \pm\frac{n^3}{8}\sqrt{2}\,\frac{3}{2n(2n-1)^2}, \\ c_{-1} &= \mp\frac{n^3}{8}\sqrt{2}\,\frac{6}{(2n-1)^2}, \\ c_{-3} &= \pm\frac{n^3}{8}\sqrt{2}(2n-3)(2n-2)^2, \end{aligned}\right\} \tag{141}$$

and c_{-2} is arbitrary. Thus

$$\left.\begin{aligned} \mathcal{R}_{n,\,n-2} = \pm\frac{n^3}{8}\sqrt{2}\; e^{-\rho/2}\rho^{n-2}\Big[& c' L_{2n-2}^{2n-3} + (2n-3)(2n-2)^2 L_{2n-3}^{2n-3} \\ & - \frac{6}{(2n-1)^2} L_{2n-1}^{2n-3} + \frac{3}{2n(2n-1)^2} L_{2n}^{2n-3}\Big]. \end{aligned}\right\} \tag{142}$$

Finally, combining all the various functions, ψ_2 is found to be

$$\left.\begin{aligned} \psi_2 = \frac{1}{\sqrt{2\pi}}\left(\frac{2}{n}\right)^{3/2}\sqrt{\frac{2n-3}{2(2n-4)!}}\,\frac{1}{\sqrt{2n\,[(2n-2)!]^3}}\; e^{i(n-2)\phi} \\ \times [P_{n-2}^{n-2}\mathcal{R}_{n,\,n-2} + P_{n-1}^{n-2}\mathcal{R}_{n,\,n-1} + P_n^{n-2}\mathcal{R}_{n,\,n}]. \end{aligned}\right\} \tag{143}$$

Through the functions $\mathcal{R}_{n,\,n-2}$ and $\mathcal{R}_{n,\,n-1}$, ψ_2 involves two arbitrary constants, c and c', which are, in fact, the coefficients of $\psi_0(n,\, n-2,\, n-2)$ and $\psi_0(n,\, n-1,\, n-2)$. One condition on these constants is given by the requirement that ψ be normalized correct to $1/R^2$:

$$\int \psi_1^* \psi_1 d\tau + 2\int \psi_1^* \psi_2 d\tau = 0. \tag{144}$$

In addition, two further relations between the quantities c, c', and E_4 will be obtained when integrating the equation for E_4. These conditions make the problem determinate.

IV. DISCUSSION OF THE RESULTS

The solution of the perturbation equations (13) for other values of $|m|$ can be carried out exactly as in the case $|m| = n - 2$ and presents no new problems of principle. In

TABLE 1

$\|m\|$	E_0	E_1	E_2	E_3	E_4	ψ_0
$n-1$	$-\frac{1}{2n^2}$	0	0	$\frac{n^2}{2}(n^2-1)$	$-\frac{n^4}{8}(n+1)(4n+5)$	$\psi_0(n, n-1, n-1)$
$n-2$	$-\frac{1}{2n^2}$	0	$\pm\frac{3}{2}n$	$\frac{n^2}{2}(n^2-7)$		$\frac{1}{\sqrt{2}}[\psi_0(n, n-2, n-2) \pm \psi_0(n, n-1, n-2)]$
$n-3$	$-\frac{1}{2n^2}$	0	0	$\frac{n^2}{2}(n^2-1)$		$\sqrt{\frac{n-2}{2n-3}}\psi_0(n, n-3, n-3) - \sqrt{\frac{n-1}{2n-3}}\psi_0(n, n-1, n-3)$
			$\pm 3n$	$\frac{n^2}{2}(n^2-25)$		$\left\{\frac{1}{\sqrt{2}}\left[\sqrt{\frac{n-1}{2n-3}}\psi_0(n, n-3, n-3) \pm \psi_0(n, n-2, n-3) + \sqrt{\frac{n-2}{2n-3}}\psi_0(n, n-1, n-3)\right]\right.$
$n-4$	$-\frac{1}{2n^2}$	0	$\pm\frac{3}{2}n$	$\frac{n^2}{2}(n^2-7)$		$\left\{\frac{\sqrt{3}}{2}\sqrt{\frac{n-3}{2n-5}}\psi_0(n, n-4, n-4) \pm \frac{1}{2}\sqrt{\frac{n-3}{2n-3}}\psi_0(n, n-3, n-4) - \frac{1}{2}\sqrt{\frac{n-1}{2n-5}}\psi_0(n, n-2, n-4) \pm \frac{\sqrt{3}}{2}\sqrt{\frac{n-1}{2n-3}}\psi_0(n, n-1, n-4)\right.$
			$\pm\frac{9}{2}n$	$\frac{n^2}{2}(n^2-55)$		$\left\{\frac{1}{2}\sqrt{\frac{n-1}{2n-5}}\psi_0(n, n-4, n-4) \pm \frac{\sqrt{3}}{2}\sqrt{\frac{n-1}{2n-3}}\psi_0(n, n-3, n-4) + \frac{\sqrt{3}}{2}\sqrt{\frac{n-3}{2n-5}}\psi_0(n, n-2, n-4) \pm \frac{1}{2}\sqrt{\frac{n-3}{2n-3}}\psi_0(n, n-1, n-4)\right.$

TABLE 1—*Continued*

$\lvert m\rvert$	E_0	E_1	E_2	E_3	E_4	ψ_0
$n-5$	$-\frac{1}{2n^2}$	0	0	$\frac{n^2}{2}(n^2-1)$		$\sqrt{\frac{3}{2}}\sqrt{\frac{(n-4)(n-3)}{(2n-7)(2n-5)}}\psi_0(n,n-5,n-5) - \sqrt{\frac{(n-3)(n-2)}{(2n-7)(2n-3)}}\psi_0(n,n-3,n-5) + \sqrt{\frac{3}{2}}\sqrt{\frac{(n-1)(n-2)}{(2n-5)(2n-3)}}\psi_0(n,n-1,n-5)$
			$\pm 3n$	$\frac{n^2}{2}(n^2-25)$		$\sqrt{\frac{(n-2)(n-4)}{(2n-5)(2n-7)}}\psi_0(n,n-5,n-5) \pm \frac{1}{\sqrt{2}}\sqrt{\frac{n-4}{2n-5}}\psi_0(n,n-4,n-5) - \sqrt{\frac{3}{2}}\frac{1}{\sqrt{(2n-7)(2n-3)}}\psi_0(n,n-3,n-5) \mp \frac{1}{\sqrt{2}}\sqrt{\frac{n-1}{2n-5}}\psi_0(n,n-2,n-5) - \sqrt{\frac{(n-3)(n-1)}{(2n-5)(2n-3)}}\psi_0(n,n-1,n-5)$
			$\pm 6n$	$\frac{n^2}{2}(n^2-97)$		$\frac{1}{2}\sqrt{\frac{(n-2)(n-1)}{(2n-5)(2n-7)}}\psi_0(n,n-5,n-5) \pm \frac{1}{\sqrt{2}}\sqrt{\frac{n-1}{2n-5}}\psi_0(n,n-4,n-5) + \sqrt{\frac{3}{2}}\sqrt{\frac{(n-1)(n-4)}{(2n-7)(2n-3)}}\psi_0(n,n-3,n-5) \pm \frac{1}{\sqrt{2}}\sqrt{\frac{n-4}{2n-5}}\psi_0(n,n-2,n-5) + \frac{1}{2}\sqrt{\frac{(n-4)(n-3)}{(2n-5)(2n-3)}}\psi_0(n,n-1,n-5)$

each case the various matrix elements encountered in the integration of the equations can be evaluated by using equation (77) and the various recurrence relations between the Legendre polynomials. For the case $|m| = n - q$, say, the quantity E_2 is always obtained from a secular determinant of order q, while the determination of E_3 involves the solution of a symmetric determinant of order $q + 1$.

TABLE 2

n	$\|m\|$	l	E_0	E_1	E_2	E_3	E_4
1	0	0	$-\frac{1}{2}$	0	0	0	$-\frac{9}{4}$
2	1	1	$-\frac{1}{8}$	0	0	+6	−78
	0	0, 1			±3	−6	
3	2	2	$-\frac{1}{18}$	0	0	+36	−1377
	1	1, 2			$\pm\frac{9}{2}$	+9	
	0	0, 1, 2			0	+36	
					±9	−72	
4	3	3	$-\frac{1}{32}$	0	0	+120	−3360
	2	2, 3			±6	+72	
	1	1, 2, 3			0	+120	
					±12	−72	
	0	0, 1, 2, 3			±6	+72	
					±18	−312	
5	4	4	$-\frac{1}{50}$	0	0	+300	$-\frac{4687.5}{4}$
	3	3, 4			$\pm\frac{15}{2}$	+225	
	2	2, 3, 4			0	+300	
					±15	0	
	1	1, 2, 3, 4			$\pm\frac{15}{2}$	+225	
					$\pm\frac{45}{2}$	−375	
	0	0, 1, 2, 3, 4			0	+300	
					±15	0	
					±30	−900	

The first two coefficients, E_2 and E_3, have been calculated in this manner as far as $q = 5$, that is, up to and including the state $n = 5$; and there is no difficulty in principle in extending them to as high a value of n as is desired. The results, as found for the separate values of $|m|$, are given in Table 1, together with the unperturbed wave function which specifies the mixture of the states. In Table 2 will be found the numerical values of the interaction energies for the various quantum states.

The most striking fact shown by the calculations is that, because they follow essentially an R^{-2} law, the interaction energies for a hydrogen atom and a proton are very much larger than other interactions which have thus far been considered, that is to say, those in which the perturbing particle is an unexcited hydrogen atom. Moreover, the energy coefficients, especially the E_3's, increase rapidly with increasing n, a result of special significance for problems of line broadening. By way of comparison it may be recalled that for the interaction between two hydrogen atoms in the ground state, the van der Waals constant—which is the coefficient of R^{-6}—is approximately $-\frac{1}{2}a\overline{r^2_{n,l}}$, where a, the polarizability of the hydrogen atom, is 4.5 in atomic units.

The results given here for hydrogen may be applied, with a few minor changes, to ionized helium, doubly ionized lithium, etc. If Z denotes the charge on the nucleus, the perturbing potential becomes

$$V = \frac{Z}{R} - \frac{1}{r'}. \tag{145}$$

This introduces a new term in R^{-1}, as a result of which E_1 is found to be $Z - 1$. But the higher-order equations are unchanged. More important, however, is the change of the scale factor. Instead of equation (12), the relation between r and ρ is now given by

$$\rho = \frac{2Z}{n} r, \tag{146}$$

and the radial part of the unperturbed wave function contains an additional factor, $Z^{3/2}$. The result of this is that, when Z differs from 1, E_2 and E_3 must be divided by Z and Z^2, respectively.

The application of these interaction energies in the formation of stellar absorption lines will be considered in a later paper.

I wish to express my sincere thanks to Dr. S. Chandrasekhar for suggesting this problem and for many helpful discussions and criticisms.

THE INTERACTION OF A PROTON AND A HELIUM ATOM IN ITS EXCITED STATES

MARGARET KIESS KROGDAHL
Yerkes Observatory
Received September 3, 1944

ABSTRACT

The perturbations of the excited levels of helium due to the interaction with a proton are found and are compared with the displacements caused by a homogeneous electric field. It is found that, for the order of stellar densities considered, the nonhomogeneity of the fields due to the presence of such charged particles cannot be ignored. Finally, the results of the present theory are used to calculate the displacements of several triplet lines of astrophysical interest.

FORMULATION OF THE PHYSICAL PROBLEM

1. *Introduction.*—The Stark effect of the helium lines in early-type stellar spectra has been studied by various writers, including Struve,[1] Foster and Douglas,[2] and Adams and Merrill.[3] In the physical discussions relating to this problem extensive use has been made of the investigations of J. S. Foster[4] on the Stark effect of the helium lines under the action of homogeneous electric fields. However, these discussions have not always been completely satisfactory—as in the case of the line λ 4469.96, identified by Struve as arising from the forbidden transition 2 p—4f among the ortholevels. Thus laboratory investigations have shown that this line, which is of zero intensity for zero field strengths, becomes progressively shifted toward the violet as the field strength increases. On the other hand, this line appears in stellar spectra at the position for zero field strength. However, it may be pointed out that the conditions under which the Stark effect appears in stellar spectra are not strictly comparable with those under which it is produced in the laboratory; for in stellar spectra the Stark effect arises from the influence of charged particles—principally protons—and the electric fields caused by charged particles are nonhomogeneous, in contrast to the laboratory fields which are homogeneous. It is therefore of interest to examine in what way the nonhomogeneity of the fields modifies the present theoretical expectations. It will be seen that this effect is not negligible.

2. *Formulation of the quantum mechanical problem.*—The potential which acts on a helium atom, due to the presence of a near-by proton, is

$$V = \frac{2}{R} - \frac{1}{r_1'} - \frac{1}{r_2'} \tag{1}$$

or[5]

$$\left.\begin{aligned} V = &-\frac{r_1}{R^2} P_1(\cos\theta_1) - \frac{r_1^2}{R^3} P_2(\cos\theta_1) - \dots . \\ &-\frac{r_2}{R^2} P_1(\cos\theta_2) - \frac{r_2^2}{R^3} P_2(\cos\theta_2) - \dots , \end{aligned}\right\} \tag{2}$$

[1] *Observatory*, **61**, 53, 1938, and the references given in this paper.

[2] *M.N.*, **99**, 150, 1939.

[3] *Ap. J.*, **97**, 98, 1943.

[4] *Proc. R. Soc.*, A, **114**, 47, 1927.

[5] See the preceding paper (*Ap. J.*, **100**, 311, eq. [2]).

where R, r_1', and r_2' are the distances from the proton to the helium nucleus and to the two electrons, respectively. Thus, to find the displacements of the helium lines caused by the action of nonhomogeneous fields, we must consider the perturbation problem involving a proton and a helium atom in its excited states.

Now the wave function for an excited state of helium can be written, in a first approximation, as

$$\Psi = \frac{1}{\sqrt{2}} [u_1(1)\, u_{n,\, l,\, m}(2) \pm u_1(2)\, u_{n,\, l,\, m}(1)], \tag{3}$$

where the u's denote the normalized hydrogen wave functions for each of the two electrons, the electron 1 under the influence of an effective nuclear charge 2, and the electron 2 under the influence of an effective nuclear charge 1. The energy corresponding exactly to a wave function of this type is just the sum of the hydrogen-like energies for the two electrons, namely,

$$E = -2 - \frac{1}{2n^2} \quad \text{(atomic units)}; \tag{4}$$

and hence in this approximation the excited levels of helium are degenerate. However, it is known that this is not strictly the case and that the various term values of helium corresponding to the same quantum number n for the outer electron are separated by small but finite amounts. On the other hand, these term separations become progressively smaller with increasing l, that is, the difference between a d and an f term is much smaller than that between the s and p terms for the same value of n; and in this sense the energy levels for the higher values of l might be considered to be "partially degenerate." Hence the small differences between the energy levels can be regarded as the result of an intra-atomic perturbation which tends to remove the degeneracy inherent in the use of the hydrogen-like functions. Accordingly, we shall begin on the supposition that the problem of the intra-atomic perturbation has already been solved and shall say that, corresponding to the wave functions (3), the values of the perturbations in energy are given by the *observed* energy differences between the helium levels.

This, then, is the situation with regard to the unperturbed helium atom. For the problem at hand, there is superposed upon this an external perturbation of the form (2), due to the proton; and it is necessary to determine in what way the combination of atomic and external perturbations acts to modify the energy levels of the helium atom. From the principles of the general perturbation theory for the degenerate case, it may be expected that, when the helium levels are "semidegenerate," the external perturbation will tend to remove the degeneracy and may be more important in this case than for levels already well separated by the atomic perturbation.

From the astrophysical standpoint it is of primary interest to know how the external perturbation varies with the distance R, or, equivalently, with the average density of the protons. If R is very large, the external perturbation will be small, and the main effect must necessarily be that of the atomic perturbation. On the other hand, as R decreases, the external perturbation must become relatively more important. Moreover, as R varies, the different terms of the external perturbation (2) become of different magnitudes relative to each other,[6] and we need to know which of the terms are dominant for the range of atmospheric densities.

The question of the precise value of R to be used in these calculations is a little difficult to settle, as it is affected by any uncertainty in the value adopted for the density of protons in the atmosphere. However, an idea of the order of magnitude of the distances involved can be obtained by adopting as the average density of protons

$$\log n_P = 14.48\,, \tag{5}$$

[6] However, as $R \to \infty$, the dominant term arises from the "nonhomogeneous" term in $P_2(\cos\theta)$ (see § 3 below).

as given by Unsöld for the B0 star τ Scorpii.[7] Assuming that the value of R effective in the perturbation is the same as the average distance between particles, we obtain

$$R \simeq 1.6 \times 10^3 \text{ atomic units} . \tag{6}$$

Hence we may say that the distances of primary interest will be roughly of the order of 10^3–10^4 atomic units.

3. *The interaction of a proton and a helium atom as* R *becomes infinite.*—It is clear that as R approaches infinity the principal term in the perturbation must come from the diagonal matrix elements of the external perturbation (2). Now the first term in the series which gives a nonvanishing diagonal matrix element is the one in $P_2(\cos\theta)$. Since this term is due to the nonhomogeneity of the field, it gives at once a rough indication of the role which the fields due to a charged particle may be expected to play. More particularly, we have

$$\left.\begin{aligned}\Delta E_{n,l,m} \simeq -\frac{1}{2R^3}\int [\, r_1^2 P_2(\cos\theta_1) + r_2^2 P_2(\cos\theta_2)\,]\,[u_1(1)\,u_{n,l,m}(2) \\ \pm u_1(2)\,u_{n,l,m}(1)\,]^* \times [u_1(1)\,u_{n,l,m}(2) \pm u_1(2)\,u_{n,l,m}(1)\,]\,d\tau_1 d\tau_2 .\end{aligned}\right\} \tag{7}$$

Now it can be shown that, because of the indistinguishability of the two electrons, the terms in u_1 have no effect on the matrix element and that in making such integrations it is necessary to consider only the outer electron. Thus,

$$\Delta E_{n,l,m} = -\frac{1}{R^3}\int r^2 P_2(\cos\theta)\, u^*_{n,l,m} u_{n,l,m} d\tau . \tag{8}$$

The matrix elements are therefore of the same type as those considered in the preceding paper and can be evaluated in the manner described there (cf. eqs. [49] and [55] in the preceding paper).

It is of interest to have the numerical values of these matrix elements for a number of excited states of helium. These are given in Table 1, as far as $n = 6$ for the outer electron. The sign of the matrix element gives the direction of the shift ΔE; if the shift is negative, the energy is *lowered* by the perturbation, and vice versa. In particular, if we consider the 4f level, we find

$$\Delta E_{4f} \simeq -\frac{96}{R^3} + O(R^{-4}) . \tag{9}$$

In other words, for this case the nonhomogeneous term causes a lowering of the 4f level, which tends to shift the 2p–4f line toward the *red*. Hence it may be expected that for large values of R, i.e., low densities, the violet shift predicted for this line on the basis of laboratory data will be somewhat compensated by a red shift due to the nonhomogeneity of the field.

THE QUANTUM MECHANICAL PROBLEM

We proceed now to a discussion of the more general case.

4. *The case* n = *2.*—Consider, first, the simplest case of orthohelium, namely, that for which the outer electron has the quantum number $n = 2$. Corresponding to this there are essentially two states, 1s2s and 1s2p, which are separated from the energy (4) by known amounts, which will be called ϵ_1 and ϵ_2, respectively. If the discussion is limited to the case $m = 0$,[8] then the two wave functions corresponding to these energies are

$$\Psi_1 = \frac{1}{\sqrt{2}}[u_1(1)\,u_{2,0,0}(2) - u_1(2)\,u_{2,0,0}(1)\,] \tag{10}$$

[7] *Ap. J.*, **100**, 105, 1944.

[8] This is the only value of m for which *all* the levels corresponding to a given n are included. Moreover, levels for which $m = 0$ generally correspond to the strongest transitions and are affected the most by external perturbations.

and

$$\Psi_2 = \frac{1}{\sqrt{2}} [u_1(1)\, u_{2,1,0}(2) - u_1(2)\, u_{2,1,0}(1)], \tag{11}$$

respectively. Now, in terms of the general perturbation theory, this situation can be described by saying that the matrix corresponding to the "atomic" perturbing potential is already in the diagonal form:

$$\begin{pmatrix} \epsilon_1 & 0 \\ 0 & \epsilon_2 \end{pmatrix}.$$

To add to this the external perturbation, it is necessary to find the various matrix elements of the potential (2), construct the new matrix representing the sum of the two perturbations, and reduce it again to the diagonal form.

Let us denote by ξ, η, and ζ the matrix elements of V which contain P_1, P_2, and P_3, respectively, and keep for the time being only terms up to the fourth order in $1/R$.

TABLE 1

n, l, m	$R^3\Delta E_{n,l,m}$	n, l, m	$R^3\Delta E_{n,l,m}$	n, l, m	$R^3\Delta E_{n,l,m}$	n, l, m	$R^3\Delta E_{n,l,m}$
2, 0, 0	0	4, 0, 0	0	5, 0, 0	0	6, 0, 0	0
2, 1, 0	−12	4, 1, 0	−240	5, 1, 0	− 600	6, 1, 0	−1260
2, 1, 1	+ 6	4, 2, 0	−144	5, 2, 0	$-\frac{2700}{7}$	6, 2, 0	$-\frac{5868}{7}$
3, 0, 0	0	4, 3, 0	− 96	5, 3, 0	− 300	6, 3, 0	− 696
3, 1, 0	−72	4, 1, 1	+120	5, 4, 0	$-\frac{1500}{7}$	6, 4, 0	$-\frac{3960}{7}$
3, 2, 0	−36	4, 2, 1	− 72	5, 1, 1	+ 300	6, 5, 0	− 420
3, 1, 1	+36	4, 3, 1	− 72	5, 2, 1	$-\frac{1350}{7}$	6, 1, 1	− 630
3, 2, 1	−18	4, 2, 2	+144	5, 3, 1	− 225	6, 2, 1	$-\frac{2934}{7}$
3, 2, 2	+36	4, 3, 2	0	5, 4, 1	$-\frac{1275}{7}$	6, 3, 1	− 522
				5, 2, 2	$+\frac{2700}{7}$	6, 4, 1	$-\frac{3366}{7}$
				5, 3, 2	0	6, 5, 1	− 378
				5, 4, 2	$-\frac{600}{7}$	6, 2, 2	$+\frac{5868}{7}$
						6, 3, 2	0
						6, 4, 2	$-\frac{1584}{7}$
						6, 5, 2	− 252

Some of the matrix elements vanish because of the orthogonality property of the Legendre polynomials. The secular equation for the total perturbation is

$$\begin{vmatrix} \epsilon_1 + \frac{\eta_{11}}{R^3} - \lambda & \frac{\xi_{12}}{R^2} + \frac{\zeta_{12}}{R^4} \\ \frac{\xi_{12}}{R^2} + \frac{\zeta_{12}}{R^4} & \epsilon_2 + \frac{\eta_{22}}{R^3} - \lambda \end{vmatrix} = 0. \tag{12}$$

When expanded, correct to the fourth order in $1/R$, this becomes

$$(\epsilon_1 - \lambda)(\epsilon_2 - \lambda) + (\epsilon_2 - \lambda)\frac{\eta_{11}}{R^3} + (\epsilon_1 - \lambda)\frac{\eta_{22}}{R^3} - \frac{\xi_{12}^2}{R^4} = 0, \tag{13}$$

where it may be noted that the ζ matrix elements are absent.

In the discussion of this equation it is convenient to choose $\epsilon_2 = 0$, which means only that it is agreed to refer all the perturbations to this level instead of to that specified by equation (4). In this scheme of reference, ϵ_1 becomes just the difference in energy between the two levels. Hence the equation for λ becomes

$$\lambda^2 - \lambda\left(\epsilon_1 + \frac{\eta_{11}}{R^3} + \frac{\eta_{22}}{R^3}\right) + \epsilon_1 \frac{\eta_{22}}{R^3} - \frac{\xi_{12}^2}{R^4} = 0. \tag{14}$$

The quantity ϵ_1 is the observed difference between the orthohelium levels 1s2s and 1s2p;[9] its sign is negative, and, expressed in atomic units of energy,

$$\epsilon_1 = -0.0420653 . \tag{15}$$

For the necessary matrix elements we obtain the values

$$\xi_{12}^2 = 9 ; \qquad \eta_{11} = 0 ; \qquad \eta_{22} = -12 ; \tag{16}$$

and equation (14) becomes

$$\lambda^2 - \lambda\left(-0.0420653 - \frac{12}{R^3}\right) + 0.0420653 \times \frac{12}{R^3} - \frac{9}{R^4} = 0 . \tag{17}$$

Although this is a simple quadratic, the constants involved differ too much in order of magnitude to warrant use of the usual formal solution. Thus, if $R = 10^3$, which is probably near the lower limit for values of astrophysical interest, the quantity $12/R^3$ is about 10^6 times smaller than ϵ_1 and is at least 1000 times larger than the quantity $9/R^4$. Another way of looking at the situation is to note that the constant terms are equal for a value of R equal to 18 atomic units, which is well below the range of interest. Hence we are justified in neglecting the R^{-4} term in this case and in writing the solutions of the equation as

$$\lambda_1 = \epsilon_1 = -0.0420653 \tag{18}$$

and

$$\lambda_2 = -\frac{12}{R^3} . \tag{19}$$

The meaning of these solutions is that the external perturbation does not affect the first, or s, level at all and that it lowers the second, or p, level by the amount $12/R^3$. Moreover, it is seen that the perturbation of these levels is caused only by the nonhomogeneity of the field. We shall return to the discussion of these solutions in the final paragraph, where it will be shown how they affect lines arising from these levels.

5. *The case* n = *3.*—Consider next the set of levels corresponding to the value $n = 3$ for the outer electron. Again taking $m = 0$, we have to consider the s, p, and d states, for which the hydrogen wave functions are $u_{3,0,0}$, $u_{3,1,0}$, and $u_{3,2,0}$. Constructing the secular determinant exactly as before and keeping only terms up to $1/R^4$, we obtain

$$\begin{vmatrix} \epsilon_1 + \frac{\eta_{11}}{R^3} - \lambda & \frac{\xi_{12}}{R^2} + \frac{\zeta_{12}}{R^4} & \frac{\eta_{13}}{R^3} \\ \frac{\xi_{21}}{R^2} + \frac{\zeta_{21}}{R^4} & \epsilon_2 + \frac{\eta_{22}}{R^3} - \lambda & \frac{\xi_{23}}{R^2} + \frac{\zeta_{23}}{R^4} \\ \frac{\eta_{31}}{R^3} & \frac{\xi_{32}}{R^2} + \frac{\zeta_{32}}{R^4} & \epsilon_3 + \frac{\eta_{33}}{R^3} - \lambda \end{vmatrix} = 0 , \tag{20}$$

or, expanding and choosing $\epsilon_3 = 0$,

$$\left.\begin{aligned} -\lambda^3 + \lambda^2\left[\epsilon_1 + \epsilon_2 + \frac{\eta_{11}}{R^3} + \frac{\eta_{22}}{R^3} + \frac{\eta_{33}}{R^3}\right] - \lambda\left[\epsilon_1\epsilon_2 + \epsilon_2\frac{\eta_{11}}{R^3} + (\epsilon_1 + \epsilon_2)\frac{\eta_{33}}{R^3} + \epsilon_1\frac{\eta_{22}}{R^3}\right. \\ \left. + \frac{\xi_{12}^2}{R^4} + \frac{\xi_{23}^2}{R^4}\right] + \epsilon_1\epsilon_2\frac{\eta_{33}}{R^3} - \epsilon_1\frac{\xi_{32}^2}{R^4} = 0 . \end{aligned}\right\} \tag{21}$$

[9] See, e.g., Bacher and Goudsmit, *Atomic Energy States*, p. 220, New York: McGraw-Hill Book Co., 1932.

The necessary matrix elements have the values

$$\eta_{11}=0\,;\qquad \eta_{22}=-72\,;\qquad \eta_{33}=-36\,;\qquad \xi_{12}^2=54\,;\qquad \xi_{32}^2=27\,; \tag{22}$$

and the energy differences, derived from the observed term values, are

$$\epsilon_1=-0.0130552\,;\qquad \epsilon_2=-0.0024471\,. \tag{23}$$

Again the large difference in the relative orders of magnitude of the different terms is present; and we can obtain a measure of the relative importance of the R^{-3} and R^{-4} terms by equating the sum of the constant terms to zero. Thus we find that for $R = 300$ atomic units the two terms are equally important; while for $R = 10^3$ the $1/R^3$ term certainly makes the main contribution. Hence the solutions of the equation are simply

$$\lambda_1=\epsilon_1=-0.0130552\,, \tag{24}$$

$$\lambda_2=\epsilon_2-\frac{72}{R^3}=-0.0024471-\frac{72}{R^3}\,, \tag{25}$$

and

$$\lambda_3=-\frac{36}{R^3}\,, \tag{26}$$

meaning that the p and d levels are both lowered by slight amounts. Again the perturbation is caused by the nonhomogeneity of the field.

6. *The case* n = 4.—The secular equation governing the perturbations for the $n = 4$ level is

$$\begin{vmatrix} \epsilon_1+\frac{\eta_{11}}{R^3}-\lambda & \frac{\xi_{12}}{R^2}+\frac{\zeta_{12}}{R^4} & \frac{\eta_{13}}{R^3} & \frac{\zeta_{14}}{R^4} \\ \frac{\xi_{21}}{R^2}+\frac{\zeta_{21}}{R^4} & \epsilon_2+\frac{\eta_{22}}{R^3}-\lambda & \frac{\xi_{23}}{R^2}+\frac{\zeta_{23}}{R^4} & \frac{\eta_{24}}{R^3} \\ \frac{\eta_{31}}{R^3} & \frac{\xi_{32}}{R^2}+\frac{\zeta_{32}}{R^4} & \epsilon_3+\frac{\eta_{33}}{R^3}-\lambda & \frac{\xi_{34}}{R^2}+\frac{\zeta_{34}}{R^4} \\ \frac{\zeta_{41}}{R^4} & \frac{\eta_{42}}{R^3} & \frac{\xi_{43}}{R^2}+\frac{\zeta_{43}}{R^4} & \epsilon_4+\frac{\eta_{44}}{R^3}-\lambda \end{vmatrix}=0\,. \tag{27}$$

If ϵ_4 is chosen to be zero, this becomes, to the fourth order in $1/R$,

$$\begin{aligned} &\lambda^4-\lambda^3\left[\epsilon_1+\epsilon_2+\epsilon_3+\frac{\eta_{11}}{R^3}+\frac{\eta_{22}}{R^3}+\frac{\eta_{33}}{R^3}+\frac{\eta_{44}}{R^3}\right]+\lambda^2\left[\epsilon_2\epsilon_3+\epsilon_1\epsilon_3+\epsilon_1\epsilon_2+(\epsilon_2+\epsilon_3)\right. \\ &\left.\times\frac{\eta_{11}}{R^3}+(\epsilon_1+\epsilon_3)\frac{\eta_{22}}{R^3}+(\epsilon_1+\epsilon_2)\frac{\eta_{33}}{R^3}+(\epsilon_1+\epsilon_2+\epsilon_3)\frac{\eta_{44}}{R^3}-\frac{\xi_{23}^2}{R^4}-\frac{\xi_{12}^2}{R^4}-\frac{\xi_{34}^2}{R^4}\right] \\ &-\lambda\left[\epsilon_1\epsilon_2\epsilon_3+\epsilon_2\epsilon_3\frac{\eta_{11}}{R^3}+\epsilon_1\epsilon_3\frac{\eta_{22}}{R^3}+\epsilon_1\epsilon_2\frac{\eta_{33}}{R^3}+(\epsilon_2\epsilon_3+\epsilon_1\epsilon_3+\epsilon_1\epsilon_2)\frac{\eta_{44}}{R^3}-\epsilon_3\frac{\xi_{12}^2}{R^4}\right. \\ &\left.-\epsilon_1\frac{\xi_{23}^2}{R^4}-(\epsilon_1+\epsilon_2)\frac{\xi_{34}^2}{R^4}\right]+\epsilon_1\epsilon_2\epsilon_3\frac{\eta_{44}}{R^3}-\epsilon_1\epsilon_2\frac{\xi_{34}^2}{R_4}=0\,. \end{aligned} \tag{28}$$

The three energies corresponding to the atomic perturbation are found to be

$$\epsilon_1 = -0.0052603\,; \qquad \epsilon_2 = -0.0010725\,; \qquad \epsilon_3 = -0.0000362\,; \tag{29}$$

and the various matrix elements occurring in equation (28) are

$$\left.\begin{aligned} &\eta_{11} = 0\,, \qquad \eta_{22} = -240\,, \qquad \eta_{33} = -144\,, \qquad \eta_{44} = -96\,; \\ &\xi_{12}^2 = 180\,, \qquad \xi_{23}^2 = 115.2\,, \qquad \xi_{34}^2 = 64.8\,. \end{aligned}\right\} \tag{30}$$

To obtain a measure of the relative sizes of the different terms, we have the equation

$$\epsilon_1\epsilon_2\epsilon_3 \frac{\eta_{44}}{R^3} = \epsilon_1\epsilon_2 \frac{\xi_{34}^2}{R^4} \tag{31}$$

or

$$R = \frac{\xi_{34}^2}{\eta_{44}\epsilon_3}. \tag{32}$$

Upon inserting the numerical values, we find that

$$R \simeq 18{,}600\,. \tag{33}$$

This means that for values of R up to 18,600 atomic units the R^{-4} term is more important than the term in R^{-3} in determining the effect of the external perturbation on the f level. The reason for this large value of R is the extreme smallness of the energy difference, ϵ_3, which shows how the external perturbation becomes more important as the levels tend to be "semidegenerate." Thus we are no longer justified in ignoring the $1/R^4$ terms as was done in the previous cases.

Substituting the matrix elements (30) into equation (28), we obtain

$$\left.\begin{aligned} &\lambda^4 - \lambda^3\left[\epsilon_1+\epsilon_2+\epsilon_3 - \frac{240}{R^3} - \frac{144}{R^3} - \frac{96}{R^3}\right] + \lambda^2\left[\epsilon_2\epsilon_3 + \epsilon_1\epsilon_3 + \epsilon_1\epsilon_2 - \frac{240}{R^3}(\epsilon_1+\epsilon_3)\right. \\ &\left. - \frac{144}{R^3}(\epsilon_1+\epsilon_2) - \frac{96}{R^3}(\epsilon_1+\epsilon_2+\epsilon_3) - \frac{360}{R^4}\right] - \lambda\left[\epsilon_1\epsilon_2\epsilon_3 - \epsilon_1\epsilon_3\left(\frac{240}{R^3}+\frac{96}{R^3}\right)\right. \\ &\left. - \epsilon_1\epsilon_2\left(\frac{144}{R^3}+\frac{96}{R^3}\right) - \frac{96}{R^3}\epsilon_2\epsilon_3 - \frac{180}{R^4}\epsilon_3 - \frac{64.8}{R^4}(\epsilon_1+\epsilon_2) - \frac{115.2}{R^4}\epsilon_1\right] \\ &- \frac{96}{R^4}\epsilon_1\epsilon_2\epsilon_3 - \frac{64.8}{R^4}\epsilon_1\epsilon_2 = 0\,. \end{aligned}\right\} \tag{34}$$

Again, because of the different orders of magnitude of the quantities involved, it is not feasible to apply the usual methods of solution; but the following procedure appears to be adequate. If we make the substitution

$$q_1 = \epsilon_1\,; \qquad q_2 = \epsilon_2 - \frac{240}{R^3}\,; \qquad q_3 = \epsilon_3 - \frac{144}{R^3}\,; \qquad q_4 = -\frac{96}{R^3}\,, \tag{35}$$

equation (34) can be written in the form

$$\left.\begin{aligned} (\lambda - q_1)(\lambda - q_2)(\lambda - q_3)(\lambda - q_4) = \frac{360}{R^4}\lambda^2 - \left[\frac{180}{R^4}(\epsilon_1+\epsilon_3) + \frac{64.8}{R^4}\epsilon_2\right]\lambda \\ + \frac{64.8}{R^4}\epsilon_1\epsilon_2 \end{aligned}\right\} \tag{36}$$

or, more simply,

$$\Pi(\lambda - q_i) = \frac{1}{R^4}(c_2\lambda^2 + c_1\lambda + c_0), \tag{37}$$

where

$$\left.\begin{aligned} c_2 &= 360\,, \\ c_1 &= -180(\epsilon_1+\epsilon_3) - 64.8\epsilon_2\,, \\ c_0 &= 64.8\epsilon_1\epsilon_2\,. \end{aligned}\right\} \tag{38}$$

and

Since the right-hand side of equation (37) is a very small quantity, we may write

$$\lambda_i = q_i + \Delta q_i\,, \tag{39}$$

where Δq_i is small. Then, neglecting the powers of all small quantities, we obtain

$$\Delta q_i \prod_{i\neq j}(q_i - q_j) \simeq \Delta q_i \prod_{i\neq j}(\epsilon_i - \epsilon_j) \simeq \frac{1}{R^4}(c_2\epsilon_i^2 + c_1\epsilon_i + c_0), \tag{40}$$

whence

$$\Delta q_i \simeq \frac{1}{R^4}\frac{c_2\epsilon_i^2 + c_1\epsilon_i + c_0}{\prod_{i\neq j}(\epsilon_i - \epsilon_j)}. \tag{41}$$

If $i = 1$, we have

$$\Delta q_1 = \frac{1}{R^4}\frac{360\epsilon_1^2 - [180(\epsilon_1+\epsilon_3) + 64.8\epsilon_2]\epsilon_1 + 64.8\epsilon_1\epsilon_2}{\epsilon_1(\epsilon_1-\epsilon_2)(\epsilon_1-\epsilon_3)}. \tag{42}$$

Combining all the terms of the above expression, we obtain

$$\Delta q_1 = \frac{1}{R^4}\frac{180}{\epsilon_1 - \epsilon_2}. \tag{43}$$

Hence,

$$\lambda_1 = \epsilon_1 + \frac{1}{R^4}\frac{180}{\epsilon_1-\epsilon_2} = \epsilon_1 - \frac{42982}{R^4}, \tag{44}$$

signifying that the energy of the s level is lowered by $42982/R^4$ atomic units. Likewise we find that

$$\lambda_2 = \epsilon_2 - \frac{240}{R^3} - \frac{68183}{R^4}, \tag{45}$$

$$\lambda_3 = \epsilon_3 - \frac{144}{R^3} - \frac{1678891}{R^4}, \tag{46}$$

and

$$\lambda_4 = -\frac{96}{R^3} + \frac{1790055}{R^4}. \tag{47}$$

Thus the p and d levels are lowered in energy, and the f level is lowered or raised depending on whether R is greater or less than 18,600 atomic units.

It can be shown by an analysis similar to the above that the terms in $1/R^5$ are negligible in comparison to the $1/R^4$ terms. The only important matrix elements containing $P_4(\cos\theta)$ are those along the principal diagonal, and hence they may be regarded as small corrections to the $1/R^3$ terms.

DISCUSSION OF THE LINE SHIFTS

The results of the preceding section can be directly applied to calculate the theoretical displacements of several helium lines of astrophysical interest, as a function of the quantity R. Many of these lines arise from one of the first levels considered, namely, 1s2p, which was found to be lowered by an amount equal to $12/R^3$. Hence, the shift of any line starting from this level is given by the difference between the displacement of the upper level and the displacement $-12/R^3$. The shifts of these lines, measured in atomic units of energy, are given in Table 2; positive shifts are to the violet, and those with a minus sign are to the red.

Two lines are of special interest, namely, λ 4713 and λ 4470. For the first of these, coming from the 2p−4s transition, the shifts due to the R^{-3} and R^{-4} terms are opposite

TABLE 2

λ	Notation	Shift	Remarks
5876	2p−3d	$-\frac{24}{R^3}$	Shift due to nonhomogeneity of field
4713	2p−4s	$+\frac{12}{R^3}\left(1-\frac{3582}{R}\right)$	Shifts to red if $R<3582$; to violet if $R>3582$
4518	2p−4p	$-\frac{228}{R^3}\left(1+\frac{299}{R}\right)$	Shift predominantly due to nonhomogeneity of field
4472	2p−4d	$-\frac{132}{R^3}\left(1+\frac{12720}{R}\right)$	Nonhomogeneity of field adds significantly to shift toward red
4470	2p−4f	$-\frac{84}{R^3}\left(1-\frac{21310}{R}\right)$	Shifts to red if $R>21{,}310$; to violet if $R<21{,}310$

TABLE 3

R	Compensation by R^{-3} Term (Percentage)	R	Compensation by R^{-3} Term (Percentage)
10^3	4.7	10^4	47
2×10^3	9.4	1.5×10^4	70
5×10^3	23	2×10^4	94
7×10^3	33		

in sign and combine to produce zero shift for $R = 3582$ atomic units. As we have seen, this is well within the region of astrophysical interest; and the nonhomogeneity of the field certainly cannot be ignored.

The second line, whose apparent lack of displacement is of considerable interest in connection with the B stars, arises from the forbidden transition 2p−4f. Here also the two terms are of opposite sign and combine to produce zero shift for $R = 21{,}310$. This value of R is quite large compared to the estimate of § 2; and if R is of the order of 10^3–10^4, the resultant shift from the perturbation considered here is to the violet. However, it is of interest to see the relative effects of the $1/R^3$ and $1/R^4$ terms on the displacement, for different values of R. This is given in Table 3, which gives the relative compensation by the term in $1/R^3$, which shifts to the red. It is apparent that, even if R is in the thousands, this compensation is not negligible. Finally, in order to account for the displacement of this line in terms of this theory alone, we should have to increase the effective value of R by a factor of approximately 10. Assuming that the effective R is the same as the mean distance between protons, this would mean that the density of these atmos-

pheres should decrease by a factor of 10^3. However, it is not at all impossible that the effective value of R to be adopted is appreciably larger than the average distance between protons.[10] If the effective R were three times as great as the average distance between protons, a decrease in density by a factor of 30 would be required.

So far we have considered only the transitions $m = 0 \rightarrow m = 0$. For transitions involving other values of m the discussion can be carried out in a similar manner. But without going into details it is clear from our discussion in §§ 3 and 4 that the displacements of the levels with $n = 2$ and $n = 3$ will be given predominantly by the nonhomogeneity term in R^{-3} for the values of R of astrophysical interest.[11] In other words, for these levels the displacements will be given with entirely sufficient accuracy by the values in Table 1. However, the situation with regard to levels with $n = 4$ is somewhat different. But in view of the earlier remarks concerning the levels with $n = 2$ and $n = 3$ it is apparent that we may now also consider transitions to the levels $(4, l, 0)$ from lower levels having m different from 0. Thus, considering the 4f level, in addition to the transition $(4, 3, 0) \rightarrow (2, 1, 0)$, we may also consider the transition $(4, 3, 0) \rightarrow (2, 1, \pm 1)$. For these transitions the shift will be given by (cf. Table 1 and eq. [47])

$$\left.\begin{aligned} \Delta E([4, 3, 0] \rightarrow [2, 1, \pm 1]) &= -\frac{102}{R^3} + \frac{1790055}{R^4} \\ &= -\frac{102}{R^3}\left(1 - \frac{17550}{R}\right). \end{aligned}\right\} \tag{48}$$

Since the two terms are now equal for $R = 17{,}550$, the compensation due to the R^{-3} term is somewhat greater for these transitions than that given in Table 3. In addition, the decrease in the effective value of R from 21,310 to 17,550 means that the decrease in density for zero shift can be cut down by a factor of 2. That is, instead of the factors 10^3 and 30 given in the preceding paragraph, we should have 500 and 15, respectively.

In any case, it will be seen from Tables 2 and 3 that the $1/R^3$ term is certainly not negligible for any of these lines, for the order of atmospheric densities which is involved.

I wish to thank Dr. S. Chandrasekhar for suggesting this problem and for many helpful discussions of the physical principles involved in its solution.

[10] It should be further pointed out that the effective R can be different for different lines, depending on the magnitudes of the interaction energies.

[11] It should, however, be pointed out that as far as the levels (2, 1, 1) and (3, 2, 2) are concerned, we have *only* the nonhomogeneity term in R^{-3}.

THE GENERALIZED COWLING MODEL

MARJORIE HALL HARRISON
Yerkes Observatory
Received July 28, 1944

ABSTRACT

Stellar models are considered in which the ratio of the mean molecular weight in the core to the mean molecular weight in the envelope varies from 1 to 2. It is found that, as μ_c/μ_e increases, the fraction of the mass and radius inclosed in the convective core decreases, while the total radius and luminosity of the configuration increases.

In examining the evolution of the main-sequence stars it appears useful to consider stellar models in which the convective core and the point-source envelope have different mean molecular weights; for, as the nuclear reaction takes place predominantly only in the convective core, we may expect the mean molecular weight of this region gradually to increase. With an increase in the molecular weight, we can no longer let the mean molecular weight μ_c, in the core be equal to μ_e, the mean molecular weight in the envelope.

In an investigation carried out by M. Schonberg and S. Chandrasekhar[1] two values of the ratio μ_c/μ_e were considered, namely, $\mu_c/\mu_e = 1$ (the standard Cowling model) and $\mu_c/\mu_e = 2$. It is now proposed to determine the effect of intermediate values on the fraction of the mass and radius inclosed in the convective core and the total radius and luminosity of the configuration.

We shall consider a composite model made up of a central core described by the Lane-Emden function of index $n = \frac{3}{2}$ and a point-source envelope. In constructing this model the method used was that proposed by Chandrasekhar;[2] in such a configuration the values of the temperature, pressure, and mass of the core should be identical at the interface, along with the condition that the effective polytropic index n attain the value 1.5 at the interface. We then have

$$P(r_i)_c = P(r_i)_e\,; \qquad T(r_i)_c = T(r_i)_e\,; \qquad M(r_i)_c = M(r_i)_e\,; \qquad n = 1.5\,, \quad (1)$$

where P, M, and T denote the total pressure, the mass within the radius r, and the temperature, respectively; c refers to the core, e to the envelope, and i to the interface.

Introducing the homology invariant quantities u and v defined as in Chandrasekhar's *Stellar Structure* (pp. 146 ff.), we have for the conditions at the interface:

$$u_i = \frac{4\pi\rho_e(r_i)\, r_i^3}{M_e(r_i)}\,\frac{\mu_c}{\mu_e}\,; \qquad v_i = \frac{2}{5}\,\frac{GM_e(r_i)\,\rho_e(r_i)}{r_i P_e(r_i)}\,\frac{\mu_c}{\mu_e}\,. \quad (2)$$

The Fairclough[3] solutions of the Lane-Emden equation of index $\frac{3}{2}$ were used for the regions of the star inside $r = r_i$. The regions outside $r = r_i$ will be governed by the same equations as for the point-source model with negligible radiation pressure. Seven integrations (due to Miss I. Nielsen) for the point-source model with solar values of L, M, and R, and $\mu = 1$ and $\log \kappa_0 = 24.992$, 24.892, 24.792, 24.692, 24.592, 24.492 and 24.392, respectively, were available.

For the various values of μ_c/μ_e assumed, a series of parallel curves, determined by the right-hand sides of the equations (2), were obtained in the uv-plane; and it was found by

[1] *Ap. J.*, 96, 161, 1942.

[2] *An Introduction to the Study of Stellar Structure*, p. 352, Chicago, 1939.

[3] *M.N.*, 92, 645, 1931–32.

interpolation that point-source envelopes could be fitted to convective cores for the values of log κ_0 given in Table 1.

In Table 2 the quantities

$$q = \frac{r_i}{R} \quad \text{and} \quad \nu = \frac{M(r_i)}{M},$$

which give the fraction of the radius and the mass occupied by the convective core, are tabulated. The boundary of the configuration is reached at $\xi = \xi_1$, and $\psi = \psi_1$.

TABLE 1

μ_c/μ_e	log κ_0	μ_c/μ_e	log κ_0
1.0	24.737	1.4	24.929
1.1	24.817	1.6	24.961
1.2	24.871	1.8	24.982
1.3	24.905	2.0	24.992

TABLE 2

μ_c/μ_e	q	ν	ξ_1	ψ_1	$\frac{2}{5}\frac{\xi_1}{\psi_1}\mu_c$	$\frac{L_0}{\left[\frac{2}{5}\frac{\xi_1}{\psi_1}\mu_c\right]^{1/2}} \times 10^{-25}$
1.0	0.171	0.150	7.06	3.15	0.897	0.576
1.1	.152	.137	8.07	3.62	0.981	.662
1.2	.138	.126	9.06	4.10	1.060	.722
1.3	.126	.114	10.10	4.73	1.110	.763
1.4	.114	.101	11.35	5.56	1.144	.794
1.6	.100	.089	13.40	6.82	1.258	.815
1.8	.091	.083	15.12	7.88	1.382	.816
2.0	0.087	0.081	16.2	8.74	1.483	0.806

Assuming that the central temperature remains constant during the evolution, we can use the following relation to determine the effect of increasing μ_c/μ_e on the radius of the star:

$$T_c = \frac{2}{5}\frac{\xi_1}{\psi_1}\frac{\mu_c H}{k}\frac{GM}{R} \tag{3}$$

or

$$R = \frac{2}{5}\mu_c\frac{\xi_1}{\psi_1}\frac{H}{k}\frac{GM}{T_c}. \tag{4}$$

The variation in R will thus be governed only by the factor $2\mu_c\xi_1/5\psi_1$ if T_c is assumed to remain constant. This factor is tabulated in Table 2.

For a homologous family of stellar configurations based on Kramers' law of opacity, the luminosity is given by a formula of the form

$$L = L_0\frac{M^{5.5}}{\kappa_0 R^{0.5}}\mu_e^{7.5}, \tag{5}$$

where L_0 is a characteristic constant of the family which can be obtained directly from the integrations. If L, M, and R are expressed in solar units in the foregoing equation, then

$$L_0 = (\kappa_0)_{\text{int}}. \tag{6}$$

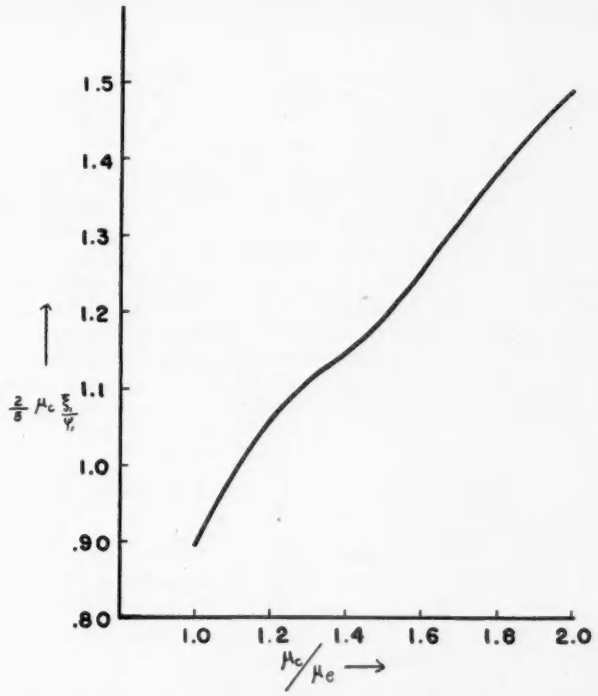

FIG. 1.—The curve illustrates the variation in the radius for constant central temperature as a function of the ratio of the mean molecular weight in the core to the mean molecular weight in the envelope. The ordinates represent the radius in certain units appropriate for the problem.

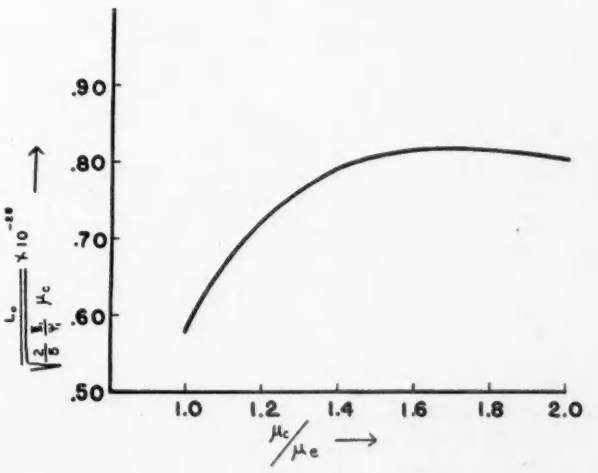

FIG. 2.—The curve illustrates the variation in the luminosity for constant central temperature as a function of the ratio of the mean molecular weight in the core to the mean molecular weight in the envelope. The ordinates represent the luminosity in certain units appropriate for the problem.

Combining equations (5) and (6) we have,

$$L = \frac{L_0}{\left[\frac{2}{5}\frac{\xi_1}{\psi_1}\right]^{1/2} \mu_c^{1/2}} \left[\frac{k}{GH}\right]^{0.5} \frac{1}{\kappa_0} M^5 T_c^{0.5} \mu_e^{7.5}. \tag{7}$$

It is clear from equation (7) that, if the central temperature is assumed constant, the variation in the luminosity will be governed by the factor $L_0[\frac{2}{5}\xi_1\mu_c/\psi_1]^{-1/2}$; this factor is tabulated in the last column of Table 2.

The variation of the radius and the luminosity of a star for varying μ_c/μ_e and for constant central temperature is illustrated in Figures 1 and 2. It is seen that as the hydrogen is transformed into helium the fraction of the radius occupied by the convective core decreases from 0.171 to 0.087 and the mass contained in the core decreases from 0.150 to 0.081, while the radius of the configuration increases by a factor of 1.65. At the same time the luminosity increases until it reaches a maximum at approximately $\mu_c/\mu_e = 1.8$ and then starts to decrease slowly; over the whole range the luminosity increases by a factor of 1.40.

I wish to express my thanks to Dr. S. Chandrasekhar for suggesting this problem and for many helpful discussions.

AN APPROXIMATE SOLAR MODEL ON BETHE'S LAW OF ENERGY GENERATION

N. R. SEN AND U. R. BURMAN
Department of Applied Mathematics, University of Calcutta
Received September 8, 1944

ABSTRACT

Bethe's law of energy generation on the carbon cycle, taken along with the stellar equations of equilibrium, gives, for an assigned central temperature and composition, two central densities, ρ_{c_1} and ρ_{c_2}, such that for a central density $\rho_c < \rho_{c_1}$ there can be only a radiative transfer of energy and for $\rho_c > \rho_{c_2}$ all stellar models will be entirely convective, with no radiative envelope. A stellar model of the convective radiative type is possible only for a single ρ_c lying between ρ_{c_1} and ρ_{c_2}. A stellar model with a central temperature of $T_c = 20.2 \times 10^6$ K and an H_2 content of 35 per cent, has been worked out and found to be in close agreement with the sun.

I. INTRODUCTION

Stellar models of the convective-radiative type have been considered, especially after the formulation of the recent energy-generation law by Bethe,[1] to be the most suitable of the configurations for description of the physical conditions within stars of the main sequence. Blanch, Lowan, Marshak, and Bethe[2] have recently calculated the temperature-density distribution in the sun by integrating the stellar equations from the boundary, using the observed values of the mass, radius, and luminosity of the sun as boundary values. It has been found that such a model, starting as a radiative one from the boundary, changes, shortly before arriving at the center, into a convective one and that it can be constructed only when its H_2 content is taken to be 35 per cent (*He* content = zero). About 98 per cent of the total heat energy of the model obtained after completing the solution was found to be generated within the convective core according to Bethe's law. But when the total luminosity was calculated from the temperature-density field of the solution by Bethe's law of energy generation, it came out to be about one hundred times the observed luminosity with which the integration was started. More recently Hoyle and Lyttleton[3] have worked out the internal constitution of the stars from the point of view of Bethe's law. They have approximated the exact exponential law of Bethe by a power law, which has simplified their calculations considerably and enabled them to arrive at certain similitude relations involving L, M, and R of stars. They have not, however, considered the variation of the guillotine factor with density and temperature while calculating the radiative envelope. In the present paper we have constructed a stellar model of the convective-radiative type based on Bethe's law of energy generation in its strict form and have taken into consideration the variation of the guillotine factor with density and temperature, which may serve as an approximate solar model.

II. METHOD OF PROCEDURE

In the solar model constructed by Blanch, Lowan, Marshak, and Bethe, referred to above, Bethe's law of energy generation is not included in the boundary-value problem solved. It is used subsequently to calculate the luminosity from the density-temperature distribution given by the solution of the boundary-value problem. We have formulated the problem here as follows: Given the usual stellar equations *and* Bethe's law of energy generation, and with assigned composition and central temperature, to find the solution

[1] *Phys. Rev.*, **55**, 434, 1939. [2] *Ap. J.*, **94**, 37, 1941. [3] *M.N.*, **102**, 177, 1942.

satisfying the external boundary condition $\rho \to 0$, $T \to 0$, simultaneously. We know the problem admits of only one solution. The method of procedure here has been to find the appropriate central density, ρ_c, which will give us the required solution. It may be noted that Bethe's law is included in the present formulation of the boundary-value problem.

Suppose we start the integration from the center with a given central temperature, say about 20,000,000° (usual for the "standard model") and an H_2 content of 35 per cent (*He* content = 0), and study the cores that are formed for varying central densities. For small radiation pressure the convective core may be regarded as a Lane-Emden polytrope of index $n = 3/2$. To find the stage where convection ceases and a radiative gradient is established, we must know the luminosity, L. This L may be calculated from Bethe's formula by making use of the density-temperature distribution of the 3/2 polytrope. After performing a series of integrations for the core with varying central densities, we have found that there exist two values, ρ_{c_1} and ρ_{c_2} ($\rho_{c_1} < \rho_{c_2}$), dependent on the assumed central temperature and composition—values such that, if the central density $\rho_c < \rho_{c_1}$, the configuration is entirely radiative, there being no convective core (without meaning, however, that the corresponding solution is suitable as a stellar model satisfying the external boundary conditions). For $\rho_{c_1} < \rho_c < \rho_{c_2}$ the core will be convective for a distance, after which the temperature gradient will change into a radiative one. But for $\rho_c > \rho_{c_2}$ we obtain an all-convective configuration, there being no radiative envelope at all. In this last case, for every $\rho_c > \rho_{c_2}$ there will be an all-convective stellar model, which will be a 3/2 polytrope. It is not thereby meant that the generation of energy would in such cases extend up to the surface. Such stellar bodies, if they exist, would have fairly high central densities.

A convective-radiative configuration will correspond to a case $\rho_{c_1} < \rho_c < \rho_{c_2}$. But every value of ρ_c within this range will not furnish a significant solution satisfying the external boundary conditions of the radiative envelope. We have determined the significant ρ_c by trial integrations. The foregoing behavior of the solutions for a given central temperature and composition and for varying values of ρ_c is quite general for all central temperatures, at least of the order of 20,000,000°. The existence of the limits ρ_{c_1} and ρ_{c_2} can be analytically proved. We have also verified the existence of all-convective models by several numerical integrations.

In the present paper we have confined ourselves to the calculation of stellar configurations, assuming the "standard-model" central temperature of about 20,000,000°, the generally accepted H_2 content of 35 per cent (*He* content = 0), and Bethe's formula in its strict form

$$\epsilon = \epsilon_0 \rho T^{-2/3} e^{-B/T^{1/3}}, \tag{1}$$

where ϵ_0 is a constant involving the H_2 content and B is a physical constant having the value

$$B = 56 \times (2 \cdot 10^7)^{1/3}.$$

Further, the opacity formula of Kramers,

$$\kappa = \frac{\kappa_0}{t} \frac{\rho}{T^{3.5}}, \tag{2}$$

has been used with Strömgren's table for the guillotine factor t.[4]

III. THE EQUATIONS

We start with the stellar equations of equilibrium in the usual notations,

$$\frac{dP}{dr} = -\frac{GM(r)}{r^2}\rho; \tag{3}$$

$$\frac{dp_r}{dr} = -\frac{\kappa\rho}{c}\frac{L(r)}{4\pi r^2}, \tag{4}$$

[4] S. Chandrasekhar, *An Introduction to the Study of Stellar Structure*, p. 269, Chicago: University of Chicago Press, 1939.

with

$$P = \frac{k}{\mu H}\rho T + \tfrac{1}{3}aT^4; \qquad p_r = \tfrac{1}{3}aT^4$$

and

$$\frac{dM(r)}{dr} = 4\pi\rho r^2; \qquad (5) \qquad \frac{dL(r)}{dr} = 4\pi\rho r^2\epsilon. \qquad (6)$$

The values of κ and ϵ are given by formulae (2) and (1), respectively.

For the present we shall be interested in temperatures for which the contribution of electron scattering to the opacity is negligible. The guillotine factor t is a function of the density and temperature. Numerical tables for t have been given by Strömgren[4] and recently by Morse.[5] In our calculations Strömgren's table has been used. As we shall be dealing with configurations with negligible radiation pressure, we shall take the convective core to be a 3/2-polytrope. For integration it is convenient to reduce the equations (3)–(6) to the forms (cf. Chandrasekhar, *op. cit.* pp. 352–354)

$$\frac{d}{d\xi}(\sigma\theta) = -\frac{5}{2}\frac{\sigma\psi}{\xi^2}; \qquad (7) \qquad \frac{d\theta}{d\xi} = -\frac{Q}{t}\frac{\sigma^2\theta^{-6.5}l}{\xi^2}; \qquad (8)$$

$$\frac{d\psi}{d\xi} = \sigma\xi^2; \qquad (9) \qquad \frac{dl}{d\xi} = \sigma^2\theta^{-2/3}e^{-b/\theta^{1/3}}\xi^2 \qquad (10)$$

by the substitutions

$$r = a\xi, \qquad \rho = \rho_c\sigma, \qquad T = T_c\theta, \qquad M(r) = M_0\psi, \qquad L(r) = L_0 l \qquad (11)$$

if a, ρ_c, T_c, M_0, L_0 satisfy the relations

$$a^2 = \frac{5k}{8\pi\mu GH}\frac{T_c}{\rho_c}; \qquad (12) \qquad M_0 = 4\pi\rho_c a^3; \qquad (13) \qquad L_0 = 4\pi\epsilon_0\rho_c^2 T_c^{-2/3}a^3 \qquad (14)$$

and

$$Q = \frac{\kappa_0 L_0}{16\pi}\frac{3}{ac}\frac{\rho_c^2}{aT_c^{7.5}}; \qquad (15) \qquad b = \frac{B}{T_c^{1/3}}. \qquad (16)$$

The constant κ_0 in the opacity formula (2) is connected with the H_2 and He contents X and Y, respectively, by the relation

$$\kappa_0 = 3.9\times 10^{25}(1+X)(1-X-Y). \qquad (17)$$

As we have assumed that the He content $= 0$, we put $Y = 0$ and take for κ_0 the value

$$\kappa_0 = 3.9\times 10^{25}(1-X^2). \qquad (18)$$

With the known density-temperature relation ($\sigma = \theta^{3/2}$) for the 3/2-polytrope we can integrate equation (10) and obtain

$$l(\xi) = \int_0^{\xi}\theta^{7/3}e^{-b/\theta^{1/3}}\xi^2 d\xi \qquad (19)$$

as the value of the luminosity in units of L_0 at any desired distance ξ. The total luminosity, $L(\xi)$, in terms of the central density and temperature will have the form

$$L(\xi) = 4\pi\epsilon_0\left(\frac{5k}{8\pi\mu GH}\right)^{3/2}T_c^{5/6}\rho_c^{1/2}l(\xi). \qquad (20)$$

[5] *Ap. J.*, 92, 27, 1940.

We have to distinguish between two cores. There will be a convective core on the surface of which the temperature gradient will change and the radiative envelope will begin. We shall describe later how this core is to be determined. Besides, there is an energy core within which the whole of the energy generation takes place. The boundary of this latter core will be reached when we arrive at a sensibly constant value of l in course of integration. We shall see below that these two cores are not identical; and, in general, the energy core will be slightly larger than the convective core for Bethe's law.

IV. EXISTENCE OF THE LIMITS ρ_{c_1} AND ρ_{c_2}

In this section we shall show that for a given central temperature and composition the two limiting densities, ρ_{c_1} and ρ_{c_2}, mentioned in Section II, exist. The existence of the first limit, ρ_{c_1}, has been shown by one of the authors in a previous paper.[6] He limited his discussions to a central temperature of $T_c = 20 \times 10^6$ K and adopted the value of ϵ_0 originally given by Bethe. But the method of determination of this limit is generally applicable. We now proceed to prove the existence of the second limit, ρ_{c_2}.

An adiabatic temperature gradient is characterized by the following relation:[7]

$$\frac{dT}{T} = \frac{\Gamma_2 - 1}{\Gamma_2} \frac{dP}{P} = \gamma_{\text{ad}} \frac{dP}{P}, \tag{21}$$

where

$$\Gamma_2 = 1 + \frac{(4 - 3\beta)(\gamma - 1)}{\beta^2 + 3(\gamma - 1)(1 - \beta)(4 + \beta)}, \tag{22}$$

with β and γ having their usual meanings. For negligible radiation pressure $\beta \sim 1$.

From equations (3) and (4) we obtain by division

$$\frac{dT}{T} = \gamma_{\text{rad}} \frac{dP}{P}, \tag{23}$$

where

$$\gamma_{\text{rad}} = \frac{1}{16\pi cG} \frac{\kappa L(r)}{M(r)} \frac{P}{p_r}. \tag{24}$$

A stable convective gradient exists so long as

$$\gamma_{\text{ad}} < \gamma_{\text{rad}}, \tag{25}$$

which is equivalent to the relation

$$\frac{4(\Gamma_2 - 1)}{\Gamma_2} < \frac{1}{4\pi cG} \frac{L(r)}{M(r)} \frac{\kappa P}{p_r}. \tag{26}$$

If p_r be small compared to P, we obtain, using the value of κ given by equations (2) and (17),

$$\kappa \frac{P}{p_r} = 3.9 \times 10^{25} \left(\frac{3k}{2aH}\right)(1 + X)(1 - X - Y)(1 + 3X + \tfrac{1}{2}Y) \frac{\rho^2}{T^{6.5}} \frac{1}{l}. \tag{27}$$

In writing this equation we have replaced μ by $2/(1 + 3X + \frac{1}{2}Y)$ and the guillotine factor l by an average value $\bar{l}$. The mass $M(r)$ here refers to the polytrope $n = 3/2$ (the radiation pressure being negligible) and is given by the well-known expression

$$M(\xi) = 4\pi \rho_c a^3 \left(-\xi^2 \frac{d\theta}{d\xi}\right).$$

[6] U. R. Burman, *Proc. Nat. Inst. Sci., India*, **8**, 306, 1942.

[7] Chandrasekhar, *op. cit.*, p. 223.

Using equation (20) for the luminosity, we obtain

$$\frac{L(\xi)}{M(\xi)} = \epsilon_0 \rho_c T_c^{-2/3} \frac{1}{\left(-\xi^2 \frac{d\theta}{d\xi}\right)} I(\xi, T_c), \tag{28}$$

where $I(\xi, T_c)$ stands for the same integral as for l in equation (19). Hence in terms of θ and ξ variables the condition (26) for the stability of the convective gradient takes the form

$$\frac{4(\Gamma_2 - 1)}{\Gamma_2} < \frac{A}{l} \rho_c^3 f(X, Y) J(\xi, T_c), \tag{29}$$

where

$$A = 3.9 \times 10^{25} \left(\frac{3k}{2aH}\right) \frac{\epsilon_0'}{4\pi cG}, \tag{30}$$

$$f(X, Y) = X(1+X)(1-X-Y)(1+3X+\tfrac{1}{2}Y), \tag{31}$$

$$J(\xi, T_c) = \frac{1}{\theta^{7/2}\left(-\xi^2 \frac{d\theta}{d\xi}\right)} \frac{I(\xi, T_c)}{T_c^{43/6}}. \tag{32}$$

Since the H_2 content X occurs as a factor in the expression for ϵ_0 in the energy-generation formula (1), we have in the foregoing $\epsilon_0 = \epsilon_0' X$. To consider the case of no helium, we take $Y = 0$ and replace $f(X, Y)$ by

$$f(X) = X(1-X^2)(1+3X). \tag{33}$$

This function $f(X)$ vanishes for $X = 0$ and $X = 1$ and possesses a maximum near about $X = 0.7$. As we are working with negligible radiation pressure ($\beta \sim 1$), we may take Γ_2 to be practically constant. Taking the ratio of the specific heats, $\gamma = 5/3$, we write the value of $4(\Gamma_2 - 1)/\Gamma_2$ as 1.6. The function $J(\xi, T_c)$ given by equation (32) can be calculated for an assigned T_c and for different values of ξ. The results of numerical computations of the function $J(\xi, T_c)$ for two values of T_c, viz., $T_{c_1} = 20 \times 10^6$ K and $T_{c_2} = 21 \times 10^6$ K, are plotted against ξ in Figure 1. These curves each have a minimum with two sides going upward. The function $4(\Gamma_2 - 1)/\Gamma_2$ is represented by a straight line parallel to the ξ-axis, and this line will generally lie above the previous curves. It is evident that for the chosen value of l, and given X, a value of ρ_c may be so taken that the displaced curves represented by the right-hand side of equation (29) will lie entirely above the line $4(\Gamma_2 - 1)/\Gamma_2$. For such a value of ρ_c the inequality (29) will not be violated, and consequently convection will prevail throughout. The minimum value of ρ_c (for given T_c and X) for which the configuration will be all convective will be that one for which the corresponding displaced curve just touches the Γ_2 line. From Figure 1 it will also be clear that this critical minimum value of ρ_c for an all-convective configuration will be lower, the higher the central temperature T_c, the composition remaining unaltered.

So far, we have been speaking of the effect of variation of the central density ρ_c in equation (29) for a given central temperature of T_c and for composition X. We now suppose X to vary, T_c remaining unaltered. Now $f(X)$ has a maximum value (about 1.1). Taking this maximum value of $f(X)$, it is clear that we can find a value of ρ_c, say ρ_c', for which the curve represented by the right-hand side of equation (29) will just touch the Γ_2 line. Consequently, for any $\rho_c > \rho_c'$ it will generally be possible to obtain an all-convective configuration simply by varying the H_2 content X, for an assigned T_c.

Further, owing to the existence of the maximum of $f(X)$, the same minimum value ρ_{c_2}

of ρ_c mentioned above will exist for two different compositions, the central temperature, however, remaining the same. It may be noticed that the function $f(X, Y)$ has no other maximum than at $(X = 0.7, Y = 0)$, mentioned above, so that when the *He* content is not negligible this particular feature may not arise.

V. INTEGRATION OF THE EQUATIONS

We now proceed to the integration of the equations given in Section III. It has been stated before that for a given T_c and H_2 content (*He* content = 0) there exists only one significant ρ_c giving a stellar model satisfying Bethe's law and the boundary conditions. In consideration of the standard model and other ideas regarding the constitution of a star like the sun, we have undertaken two integrations for $T_c = 20 \times 10^6$ K, $T_c = 20.2 \times 10^6$ K, an H_2 content of 0.35, and $\mu = 1$. The significant central density has been

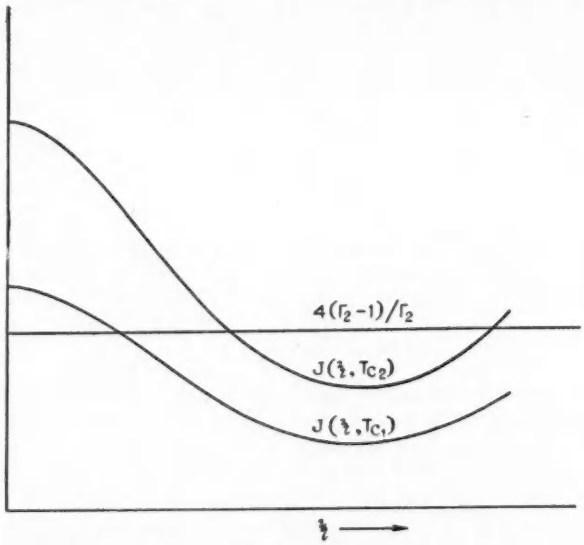

FIG. 1.—These curves show the variation of $J(\xi, T_c)$ with ξ for central temperatures T_{c_1} and T_{c_2} $(T_{c_1} < T_{c_2})$. The function $4(\Gamma_2 - 1)/\Gamma_2$ is represented by a straight line. The right-hand side of inequality (29) will be represented by a bodily upward shift of the curves. Only the left wings of the displaced curves above the Γ_2 line will be significant. A suitable value of ρ_c will shift the curves to touch or lie entirely above the Γ_2 line.

found after a number of trial integrations. The method of calculation of the luminosity function has been shown in equation (19).

To satisfy the external boundary conditions, viz., $\sigma \to 0$ and $\theta \to 0$, simultaneously, we have followed the method of Cowling.[8] The convective core is broken up arbitrarily at a definite value of $\xi = \xi_i$. The continuity of the temperature gradient $(d\theta/d\xi)$ at the interface $\xi = \xi_i$ then determines the coefficient Q in equation (8), l being calculated from equation (19). The elimination of L_0 between equations (14) and (15) gives an equation in which every member is known except ρ_c. The terminating of the convective core arbitrarily at $\xi = \xi_i$ corresponds to this value of the central density. Although the convective core ends at this distance ξ_i, the energy core may still continue, that is to say, l may not still attain a constant value. We now proceed with the numerical integration of equations (7)–(10). The function l is found to attain a constant value quite early, when the energy core ends. Equation (10) is now dropped and the integration continued. By trial

[8] *Ibid.*, p. 351.

the value of ξ_i is so determined that the boundary conditions ($\sigma \to 0$ and $\theta \to, 0$ simultaneously) are satisfied. It is found that only one such ξ_i can be obtained, which means that for a given T_c and H_2 content there is only one ρ_c giving a stellar model consistent with Bethe's law.

Our first integration was for $T_c = 20 \times 10^6$ K, in which case the luminosity L was found to be somewhat below the solar value. It was then found by trial that a central

TABLE 1

DISTRIBUTION OF TEMPERATURE, DENSITY, MASS, AND LUMINOSITY IN A STELLAR MODEL WITH $T_c = 20.2 \times 10^6$ K, $\mu = 1$, $X = 0.35$, $\epsilon_0 = 2.4 \times 10^{29}$

ξ	$T \cdot 10^{-6}$	ρ	ψ	$l \cdot 10^{25}$
0	20.20	45.50	0	0
1.1250	16.32	33.05	0.3930	0.3742
1.15	16.16	32.57	0.4162	0.3760
1.20	15.86	31.58	0.4649	0.3785
1.25	15.56	30.53	0.5161	0.3800
1.30	15.27	29.46	0.5696	0.3815
1.4	14.70	27.25	0.6830	0.3828
1.5	14.16	25.00	0.8036	0.3837
1.6	13.64	22.74	0.9294	0.3840
1.7	13.15	20.55	1.059	0.3840
1.8	12.69	18.44	1.190	.....
1.9	12.27	16.43	1.321	.....
2.0	11.89	14.56	1.450	.....
2.2	11.24	11.29	1.699	.....
2.4	10.77	8.61	1.928	.....
2.6	10.43	6.52	2.133	.....
2.8	10.18	4.95	2.314	.....
3.0	10.02	3.81	2.470	.....
3.2	9.83	3.00	2.608	.....
3.4	9.60	2.39	2.726	.....
3.6	9.29	1.90	2.829	.....
3.8	9.08	1.42	2.918	.....
4.0	8.53	1.02	2.994	.....
4.2	7.88	0.738	3.054	.....
4.4	7.29	0.530	3.098	.....
4.6	6.65	0.379	3.132	.....
4.8	6.01	0.262	3.158	.....
5.0	5.40	0.179	3.181	.....
5.2	4.82	0.119	3.200	.....
5.4	4.27	0.0800	3.216	.....
5.6	3.77	0.0547	3.228	.....
5.8	3.27	0.0381	3.235	.....
6.0	2.76	0.0268	3.240	.....
6.2	2.23	0.0188	3.244	.....
6.4	1.74	0.0131	3.247	.....
6.6	1.25	0.0091	3.248	.....
6.7	1.01	0.0046	3.248	.....

temperature of $T_c = 20.2 \times 10^6$ K gives a closer agreement with the observed solar luminosity. The mass then becomes slightly greater than the solar value. Results of integration of this latter case, $T_c = 20.2 \times 10^6$ K, are given in Table 1. The integration is stopped at the distance $\xi = 6.7$, where the temperature $T \sim 1.10^6$ K, the density $\rho \sim 0.005$ gm/cm^3, and the rest of the radius is calculated by Strömgren's method.[9] The original integration was carried out in about a hundred steps, of which about forty are

[9] *Zs. f. Ap.*, **2**, 345, 1931.

inserted in the table. It may be noted that the convective core occupies 14.4 per cent of the total radius and incloses 12 per cent of the mass of the star, and, further, that only about 3 per cent of the total energy is generated within the radiative envelope.

In the case of $T_c = 20 \times 10^6$ K the integration is stopped at $\xi = 5.9$. Extrapolation by Strömgren's method then gives the complete radius $R = 7.2 \times 10^{10}$ cm. The mass and luminosity are given by $M = 2.0 \times 10^{33}$ gm and $L = 3.0 \times 10^{33}$ ergs/sec.

VI. CONCLUSIONS

With a central temperature of $T_c = 20.2 \times 10^6$ K and an H_2 content of 0.35 per cent (He content = 0), there exists one stellar model, which, while strictly obeying Bethe's law, gives $L = 3.7 \times 10^{33}$ ergs/sec, $M = 2.12 \times 10^{33}$ gm., and $R = 8 \times 10^{10}$ cm. The corresponding central density ρ_c equals 45.5 gm/cm ^{3}. These are in fairly good agreement with the solar values.

Our further integrations have shown that for nearly the same composition an increase in T_c would considerably increase L, which is very sensitive to T_c. An increase in the H_2 content X will also cause an increase in L. But if we confine ourselves to the composition $X = 0.35$, which is widely held, it appears that the approximate solar model should have a temperature of about 20,000,000°, the same as suggested by the "standard model." On the other hand, the "standard-model" central density should be considered to be too high. A composite convective-radiative model for a star like the sun definitely demands a lower value of the central density, probably somewhat below 50 gm/cm^3.

Speculations regarding sources which might lead to a better agreement of the model with the sun are possible in different directions. The most obvious suggestion seems to be the giving-up of the idea of 35 per cent H_2 content in the composition of the solar material. A higher percentage of H_2 alone or an admixture of H_2 and He with a slightly higher central temperature may lead to a better result. For the central temperature we have assumed that the contribution of electron scattering to the opacity is certainly negligible, but the guillotine factor in Kramers' opacity formula is too complicated to be properly taken account of in numerical calculations. We have not made use of Morse's table (expected to be more accurate) for the guillotine factor, which differs considerably from Strömgren's table; instead, the latter has been used exclusively in our calculations. The opacity factor will not greatly influence the luminosity value in our calculations, since it really adds to the advantage of integration from inside. Although we have used Bethe's formula in its strict form, it may, however, be pointed out that the constant in the formula which is in part due to the assumption regarding the composition of the materials taking part in the carbon-cycle reaction has considerable influence on the calculations. A large variation of this constant may lead to widely different results and even to a failure of the model.

ON THE RADIATIVE EQUILIBRIUM OF A STELLAR ATMOSPHERE. IV

C. U. Cesco, S. Chandrasekhar, and J. Sahade
Yerkes Observatory
Received August 31, 1944

ABSTRACT

In this paper the solution to the problem of line formation given in an earlier paper is obtained in its numerical form in the first three approximations. Tables for computing the residual intensity are given.

1. *Introduction.*—In an earlier paper[1] the "standard case" in the theory of the formation of stellar absorption lines has been considered and the solution obtained in the form

$$I_i = I(\mu_i) = b_\nu \left\{ \sum_{a=1}^{n} \frac{L_a e^{-k_a t}}{1+\mu_i k_a} + \mu_i + \frac{a_{\nu_0}}{b_\nu} + t \right\} \quad (i = \pm 1, \ldots, \pm n), \quad (1)$$

where the μ_i's represent the Gaussian division of the interval $(-1, +1)$, the k_a's the n positive roots of the equation

$$1 = (1-\lambda) \sum_{j=1}^{n} \frac{a_j}{1-\mu_j^2 k^2}, \quad (2)$$

and the L_a's $(a = 1, \ldots, n)$ the n constants of integration to be determined by the boundary conditions

$$\sum_{a=1}^{n} \frac{L_a}{1-\mu_i k_a} + \frac{a_{\nu_0}}{b_\nu} = \mu_i \qquad (i = 1, \ldots, n). \quad (3)$$

Furthermore, in solution (1), t denotes the total optical depth, λ is a constant related to the ratio of the line to the continuous absorption coefficient (cf. II, eq. [87]) and which depends on the frequency in the line considered, and a_{ν_0} and b_ν are two constants which represent the coefficients in a Taylor expansion of the Planck intensity B_{ν_0}, valid near $t = 0$:

$$B_{\nu_0} = a_{\nu_0} + b_\nu t. \quad (4)$$

In this paper we propose to study this solution in greater detail.

2. *The formula for the residual intensity.*—We shall first derive the formula for the residual intensity. This is defined by

$$r = \frac{F_\nu(0)}{F_c(0)}, \quad (5)$$

where $F_\nu(0)$ denotes the emergent flux at the frequency considered and $F_c(0)$ the intensity of the background in the continuous sprectrum. Since

$$F = 2\int_{-1}^{+1} I \mu d\mu, \quad (6)$$

[1] S. Chandrasekhar, *Ap. J.*, **100**, 76, 1944. Referred to hereafter as "II."

we can write, in the approximation in which solution (1) is valid,

$$F = 2\sum_{-n}^{n} I_j \mu_j a_j . \tag{7}$$

Substituting for the I_j's according to equation (1), we obtain

$$F = \tfrac{4}{3} b_\nu \left\{ 1 - \frac{3\lambda}{1-\lambda} \sum_{a=1}^{n} \frac{L_a}{k_a} e^{-k_a t} \right\}. \tag{8}$$

Accordingly, for the emergent flux we have

$$F_\nu(0) = \tfrac{4}{3} b_\nu \left\{ 1 - \frac{3\lambda}{1-\lambda} \sum_{a=1}^{n} \frac{L_a}{k_a} \right\}. \tag{9}$$

To obtain the emergent flux $F_c(0)$ corresponding to the background continuum, we have to pass to the limit $\lambda = 1$ and $\eta = 0$ in the foregoing equation. But the result can be obtained more readily by starting with the equation of transfer appropriate for this case; for the resulting equation then admits of an elemental integration, and we obtain

$$F_c(0) = a_{\nu_0} + \tfrac{2}{3} b_{\nu_0} , \tag{10}$$

where it should be noted that the quantity b_{ν_0} [$= b_\nu (1+\eta)$] is now defined in terms of the expansion

$$B_{\nu_0} = a_{\nu_0} + b_{\nu_0} \tau , \tag{11}$$

τ denoting the optical depth for the continuous opacity only. Combining equations (9) and (10), we have

$$r = \frac{b_\nu}{b_{\nu_0}} \frac{1 - \dfrac{3\lambda}{1-\lambda} \displaystyle\sum_{a=1}^{n} \frac{L_a}{k_a}}{\dfrac{1}{2} + \dfrac{3}{4} \dfrac{a_{\nu_0}}{b_{\nu_0}}} . \tag{12}$$

Since equation (4) is to be regarded as a Taylor expansion valid near $t = 0$, we can readily find an explicit expression for b_ν / a_{ν_0}. Clearly,

$$\frac{b_\nu}{a_{\nu_0}} = \left(\frac{1}{B_{\nu_0}} \frac{dB_{\nu_0}}{dt} \right)_{T=T_0} \quad \text{and} \quad \frac{b_{\nu_0}}{a_{\nu_0}} = \left(\frac{1}{B_{\nu_0}} \frac{dB_{\nu_0}}{d\tau} \right)_{T=T_0} , \tag{13}$$

where T_0 denotes the boundary temperature. Using Milne's well-known relation

$$T^4 = T_0^4 (1 + \tfrac{3}{2} \tau) , \tag{14}$$

we derive

$$\frac{b_\nu}{a_{\nu_0}} = \frac{3}{8} u \frac{e^u}{e^u - 1} \left(\frac{d\tau}{dt} \right) = \frac{3}{8} u \frac{e^u}{e^u - 1} \frac{1}{1+\eta} , \tag{15}$$

where

$$u = \frac{h\nu_0}{kT} . \tag{16}$$

Equation (12) can now be re-written as

$$r = \frac{1}{1+\eta} \frac{1 - \dfrac{3\lambda}{1-\lambda} \displaystyle\sum_{a=1}^{n} \frac{L_a}{k_a}}{\dfrac{1}{2} + 2\,\dfrac{1}{u}\,\dfrac{e^u - 1}{e^u}}; \tag{17}$$

or, writing

$$\mathfrak{L}_a \doteq \lambda L_a; \qquad x = \frac{1}{u}\,\frac{e^u - 1}{e^u}, \tag{18}$$

we have

$$r = \frac{1}{1+\eta} \left\{ \frac{1 - \dfrac{3}{1-\lambda} \displaystyle\sum_{a=1}^{n} \frac{\mathfrak{L}_a}{k_a}}{\tfrac{1}{2} + 2x} \right\}. \tag{19}$$

The $\mathfrak{L}_a$'s are now determined by the conditions

$$\sum_{a=1}^{n} \frac{\mathfrak{L}_a}{1 - \mu_i k_a} = \lambda\mu_i - \tfrac{8}{3}\lambda(1+\eta)x \quad (i = 1, \ldots, n). \tag{20}$$

Now equations (2) and (20) allow us to derive values of k_a and $\mathfrak{L}_a$ for all values of $\lambda < 1$. To obtain the limiting form of the solution for $\lambda = 1$, we proceed as follows: It can be readily shown that, as $\lambda \to 1$, the characteristic roots k_i tend to

$$\frac{1}{\mu_i}[1 - \tfrac{1}{2}(1-\lambda)\,a_i] \qquad (\lambda \to 1). \tag{21}$$

From this we derive

$$\mathfrak{L}_i \to \tfrac{1}{2}\lambda a_i(\mu_i - \tfrac{8}{3}[1+\eta]\,x)\,(1-\lambda) \qquad (\lambda \to 1), \tag{22}$$

and the formula for r becomes

$$r = \frac{\tfrac{1}{2} + 4x \displaystyle\sum_{i=1}^{n} a_i\mu_i}{\tfrac{1}{2} + 2x}. \tag{23}$$

Since $\displaystyle\sum_{i=1}^{n} a_i\mu_i$ tends to $\frac{1}{2}$ as $n \to \infty$, $r \to 1$ as the order of approximation increases. Hence the departure of $\displaystyle\sum_{i=1}^{n} a_i\mu_i$ from $\frac{1}{2}$ is an index of the accuracy of our approximation.

3. *Numerical results.*—The numerical forms for the first three approximations to the solution have been worked out for various values of λ and x and for the most important case: $\epsilon = 0$ or $\lambda = (1+\eta)^{-1}$.

But before we tabulate these solutions, we may note here the equations that determine the characteristic roots in the first three approximations. They are:

$$k^2 = 3\lambda, \tag{24}$$

$$\mu_1^2\mu_2^2k^4 - \{\tfrac{1}{3} + \lambda[\mu_1^2 + \mu_2^2 - \tfrac{1}{3}]\}k^2 + \lambda = 0, \tag{25}$$

and

$$\left.\begin{aligned} \mu_1^2\mu_2^2\mu_3^2k^6 - \{\lambda[\mu_1^2\mu_2^2 + \mu_1^2\mu_3^2 + \mu_2^2\mu_3^2] + (1-\lambda)\,[\tfrac{1}{3}(\mu_1^2 + \mu_2^2 + \mu_3^2) - \tfrac{1}{5}]\}k^4 \\ + \{\lambda[\mu_1^2 + \mu_2^2 + \mu_3^2 - \tfrac{1}{3}] + \tfrac{1}{3}\}k^2 - \lambda = 0. \end{aligned}\right\} \tag{26}$$

In Table 1, the resulting roots k_a for various values of λ are tabulated.

In Tables 2, 3, and 4 we have tabulated the residual intensity as derived after the evaluation of the necessary constants.

TABLE 1

VALUES OF k

λ	First Approximation (k_1)	Second Approximation		Third Approximation		
		k_1	k_2	k_1	k_2	k_3
0.05	0.387298	2.01257	0.379497	3.24943	0.379484	1.23255
0.10	0.547723	2.05519	0.525560	3.29669	0.525430	1.24087
0.20	0.774597	2.14577	0.711876	3.39312	0.710456	1.26096
0.30	0.948683	2.24183	0.834508	3.49150	0.829085	1.28609
0.40	1.09545	2.34138	0.922637	3.59119	0.909563	1.31607
0.50	1.22474	2.44271	0.988751	3.69160	0.964672	1.34962
0.60	1.34164	2.54448	1.03980	3.79227	1.00260	1.38474
0.70	1.44914	2.64575	1.08012	3.89279	1.02909	1.41957
0.80	1.54919	2.74589	1.11259	3.99286	1.04801	1.45283
0.90	1.64317	2.84450	1.13917	4.09225	1.06192	1.48385
0.95	1.68819	2.89315	1.15071	4.14163	1.06752	1.49843
1.00	1.73205	2.94134	1.16126	4.19078	1.07242	1.51238

TABLE 2

VALUES OF r GIVEN BY THE FIRST APPROXIMATION

λ	x												
	0.1	0.125	0.15	1/6	0.175	0.20	0.225	0.25	0.275	0.3	0.325	1/3	0.35
0.05	0.1790	0.1952	0.2093	0.2178	0.2218	0.2330	0.2429	0.2519	0.2600	0.2674	0.2741	0.2762	0.2802
0.10	0.2671	0.2862	0.3030	0.3131	0.3178	0.3310	0.3428	0.3534	0.3630	0.3717	0.3797	0.3822	0.3870
0.20	0.4013	0.4221	0.4404	0.4513	0.4564	0.4707	0.4835	0.4950	0.5054	0.5149	0.5235	0.5262	0.5315
0.30	0.5104	0.5309	0.5488	0.5595	0.5646	0.5786	0.5912	0.6025	0.6127	0.6220	0.6305	0.6332	0.6383
0.40	0.6057	0.6250	0.6418	0.6519	0.6567	0.6699	0.6817	0.6924	0.7020	0.7108	0.7188	0.7213	0.7261
0.50	0.6917	0.7094	0.7248	0.7341	0.7385	0.7506	0.7614	0.7712	0.7800	0.7880	0.7954	0.7977	0.8021
0.60	0.7710	0.7868	0.8006	0.8089	0.8128	0.8237	0.8334	0.8421	0.8500	0.8572	0.8638	0.8658	0.8698
0.70	0.8450	0.8588	0.8709	0.8782	0.8816	0.8910	0.8995	0.9071	0.9140	0.9203	0.9260	0.9278	0.9313
0.80	0.9148	0.9265	0.9368	0.9429	0.9458	0.9538	0.9610	0.9675	0.9733	0.9786	0.9835	0.9850	0.9880
0.90	0.9810	0.9906	0.9989	1.0039	1.0063	1.0129	1.0187	1.0240	1.0288	1.0331	1.0371	1.0383	1.0407
0.95	1.0130	1.0214	1.0288	1.0333	1.0354	1.0412	1.0464	1.0510	1.0553	1.0591	1.0626	1.0637	1.0658
1.00	1.0442	1.0516	1.0580	1.0619	1.0637	1.0688	1.0733	1.0774	1.0810	1.0844	1.0874	1.0884	1.0902

TABLE 3

VALUES OF r GIVEN BY THE SECOND APPROXIMATION

λ	x												
	0.1	0.125	0.15	1/6	0.175	0.20	0.225	0.25	0.275	0.3	0.325	1/3	0.35
0.05	0.1729	0.1884	0.2021	0.2103	0.2141	0.2248	0.2344	0.2430	0.2508	0.2578	0.2643	0.2663	0.2702
0.10	0.2559	0.2741	0.2899	0.2995	0.3040	0.3164	0.3275	0.3376	0.3466	0.3549	0.3624	0.3648	0.3693
0.20	0.3822	0.4014	0.4182	0.4282	0.4330	0.4461	0.4579	0.4685	0.4780	0.4868	0.4947	0.4972	0.5020
0.30	0.4855	0.5038	0.5198	0.5294	0.5339	0.5465	0.5577	0.5678	0.5770	0.5853	0.5929	0.5953	0.5998
0.40	0.5766	0.5933	0.6078	0.6166	0.6207	0.6321	0.6423	0.6515	0.6598	0.6674	0.6743	0.6765	0.6806
0.50	0.6598	0.6744	0.6872	0.6948	0.6984	0.7084	0.7174	0.7255	0.7328	0.7394	0.7454	0.7473	0.7510
0.60	0.7374	0.7497	0.7604	0.7669	0.7699	0.7784	0.7859	0.7927	0.7988	0.8044	0.8095	0.8111	0.8142
0.70	0.8107	0.8205	0.8291	0.8343	0.8367	0.8435	0.8495	0.8549	0.8599	0.8643	0.8684	0.8697	0.8722
0.80	0.8805	0.8878	0.8942	0.8980	0.8998	0.9048	0.9093	0.9133	0.9170	0.9203	0.9233	0.9242	0.9261
0.90	0.9475	0.9522	0.9563	0.9587	0.9599	0.9631	0.9660	0.9686	0.9709	0.9730	0.9750	0.9756	0.9768
0.95	0.9801	0.9835	0.9864	0.9882	0.9890	0.9913	0.9934	0.9952	0.9969	0.9984	0.9998	1.0003	1.0011
1.00	1.0122	1.0142	1.0160	1.0170	1.0175	1.0189	1.0202	1.0213	1.0223	1.0232	1.0240	1.0243	1.0248

It may be of interest to compare these solutions with that derived by the more familiar Milne-Eddington approximation of setting $K = \frac{1}{3} J$. We have[2] in this approximation:

$$F = \tfrac{4}{3} b_{\nu_0} \frac{\sqrt{\lambda} + \frac{8}{\sqrt{3}} x}{\frac{1}{\sqrt{\lambda}} + \frac{2}{\sqrt{3}}}. \tag{27}$$

In Table 5 the comparison between this solution and the ones obtained in this paper is made.

TABLE 4

VALUES OF r GIVEN BY THE THIRD APPROXIMATION

λ	x				
	0.1	1/6	0.25	1/3	0.35
0.05	0.1722	.....	0.2419	.....	0.2690
0.10	0.2544	.....	0.3355	.....	0.3670
0.20	0.3794	0.4248	0.4645	0.4928	0.4976
0.30	0.4815	.....	0.5622	.....	0.5936
0.40	0.5717	.....	0.6446	.....	0.6729
0.50	0.6542	.....	0.7174	.....	0.7419
0.60	0.7313	.....	0.7836	.....	0.8040
0.70	0.8042	.....	0.8451	.....	0.8610
0.80	0.8739	.....	0.9028	.....	0.9141
0.90	0.9409	.....	0.9576	.....	0.9641
0.95	0.9736	.....	0.9841	.....	0.9881
1.00	1.0057	.....	1.0100	.....	1.0116

TABLE 5

COMPARISON WITH EDDINGTON'S APPROXIMATION
(Standard Case: $\lambda = 0.20$)

x	Eddington's Approximation	First Approximation	Second Approximation	Third Approximation
0.100	0.3575	0.3746	0.3568	0.3541
1/6	.4786	.5014	.4758	.4719
0.250	.6299	.6600	.6246	.6193
1/3	.7813	.8186	.7734	.7666
0.350	0.8115	0.8503	0.8032	0.7961

[2] Eddington, *M.N.*, **89**, 620, 1929.

THE RADIAL VELOCITIES OF THE PLEIADES*

BURKE SMITH AND OTTO STRUVE
Yerkes and McDonald Observatories
Received June 30, 1944

ABSTRACT

The radial velocities of 71 stars have been determined from 237 spectrograms. Sixty-nine stars are regarded as members of the cluster. The mean velocity for all 69 stars is $+4.08 \pm 0.68$ (m.e.) km/sec. If the stars are divided into two groups, according to rotational velocity, 50 of low rotation give $+5.19 \pm 0.70$, while 19 of high rotation give $+1.17 \pm 1.41$ km/sec. No explanation is offered for this systematic difference. The largest range in velocity for any star is 54 km/sec (No. 13). This star and No. 33, having a range of 45 km/sec, are regarded as spectroscopic binaries, while 8 other stars are suspected. The questions of internal motions and of spatial differences in the velocities are briefly discussed.

Nearly all of the brighter stars in the Pleiades have exceptionally broad and ill-defined lines in their spectra. The radial velocities determined from these stars are very uncertain. Those which are listed in Moore's catalogue[1] show a considerable amount of scatter. Very few radial velocities have been published for the fainter members of the cluster, although there have been numerous investigations of their proper motions. Trumpler[2] has recently published a mean velocity of + 7 km/sec for an unspecified number of stars in the cluster, which probably include many of the stars discussed in this paper. Pearce presented at the June, 1944, meeting of the American Astronomical Society results from measurements made at Victoria. These were not available to us until after the completion of this paper. From measurements of the brighter stars in the cluster he found, on the average, +7.86 km/sec.

The present investigation was undertaken in order to determine an independent value for the radial velocity of the Pleiades, using for this purpose not only the brighter stars but also those of intermediate brightness—to about magnitude 9.0. We were especially interested in finding whether the cluster contains a large percentage of spectroscopic binaries of considerable range, as does, for example, the galactic cluster NGC 6231. Finally, an attempt was to be made to discover whether there exist any spatial differences in the radial velocities of the various cluster stars or any differences depending upon the physical characteristics of the members.

The present discussion gives the results of measurements of 237 spectrograms of 71 stars.[3] Of the 237 spectrograms, 230 were taken with the quartz spectrograph attached to the 82-inch McDonald reflector, giving a dispersion of 55 A/mm at $H\gamma$; 4 were taken at McDonald with the $f/2$ glass spectrograph, giving a dispersion of 78 A/mm (Nos. 4066, 4067, 4068, 4069); and 3 were taken with the Bruce one-prism spectrograph attached to the 40-inch telescope of the Yerkes Observatory, giving a dispersion of 26 A/mm at $H\gamma$ (Nos. 12629, 12630, 12640). At least 2 spectrograms per star were obtained.

Of the 71 stars, one (our No. 23) is Hertzsprung No. 310,[4] and another (our No. 22) is

* *Contributions from the McDonald Observatory, University of Texas*, No. 97.

[1] *Pub. Lick Obs.*, **18**, 1932.

[2] *Pub. A.S.P.*, **56**, 68, 1944.

[3] The shell spectrum of Pleione has been omitted in this investigation, since it has been dealt with in a recent paper by Struve and Swings (*Ap. J.*, **97**, 426, 1943). It is not certain that the velocity of the shell spectrum is identical with the velocity of the cluster.

[4] *Mem. Acad. R. Sci. Denmark*, Ser. VIII, **4**, No. 4, 1923.

not listed as a member. The remaining 69 stars were taken from Trumpler's list of members of the cluster.[5] Most of the stars on our program were of photographic magnitude 9.0 or brighter, and only 8 were fainter. The faintest star (our No. 1) is of magnitude 10.1.

Three stars in our list are marked by Trumpler as "uncertain members," and 4 as "probable members." The radial velocities for these stars are as follows:

TRUMPLER'S "PROBABLE" CLUSTER MEMBERS

Our No.	Trumpler's No.	Plates	Velocity
66	S 142	2	− 7.0
59	S 26	2	+28.1
60	47	2	+ 1.2
64	S 115	2	+ 5.6

TRUMPLER'S "UNCERTAIN" CLUSTER MEMBERS

Our No.	Trumpler's No.	Plates	Velocity
69	S 177	2	+ 7.7
58	S 25a	2	− 6.3
63	S 84	2	+ 7.4

On the basis of these velocities, only No. 59 can be excluded as a background star. This star has been omitted from the following discussion, as has also star No. 22, which is not a member of the cluster, according to Trumpler. This leaves a total of 69 stars.

The wave lengths of the stellar lines used in determining the radial velocities for the A-type stars are taken from the papers by W. W. Morgan[6] and O. Struve.[7] For the B-type stars the wave lengths were taken from H. Kühlborn.[8] For the F-type stars the wave lengths of Adams and Harper were used,[9] together with data from other sources. Nearly all the plates were measured separately by Struve and by Smith, and the two measurers independently chose the star lines and their wave lengths.

Table 1 gives the average radial velocity of each star. The stars are numbered consecutively in column 1, and those which are in the outer parts of the cluster are listed separately at the end of the table. Some of these stars are as far as 3° from Alcyone. The photographic magnitudes are taken from Trumpler (except Nos. 22 and 23), and the spectral types are from the *Henry Draper Catalogue*. The "grade" denotes the estimated quality of the spectrum, which depends upon the number of lines suitable for measurement and their quality. Grade 1 represents the best quality. The rotational velocity at the equator in km/sec was estimated from the observed widths of the lines. Table 2 gives the mean results for all plates from the measures of Smith and of Struve.

[5] *Lick Obs. Bull.*, **10**, 110, 1921.

[6] *Pub. Yerkes Obs.*, **7**, Part III, 1935.

[7] *Ap. J.*, **90**, 699, 1939.

[8] *Veröff U.-Sternw. Berlin-Babelsberg*, **12**, Part I, 1938.

[9] *Trans. I.A.U.*, **5**, 193, 1935.

TABLE 1

RADIAL VELOCITIES FOR THE PLEIADES

Star	HD	Trumpler No.	α (1900)	δ (1900)	Mag. (Pg.)	Sp.	Vel. (Km/Sec)	m.e.	Plates	Grade	Rot. (Km/Sec)
1....	23061	R11	$3^h36^m58^s$	+24° 10'.5	10.1	F8	+ 7.2	± 1.1	3	1	0
2....	23157	50	37 46	23 19.9	8.3	A5	− 4.0	8.0	4	1	0
3....	23156	51	37 46	24 3.5	8.4	A5	+ 8.4	2.4	4	1	25
4....	23194	74	38 3	24 14.4	8.2	A2	+ 1.1	3.7	4	1	0
5....	23246	121	38 29	24 4.8	8.4	A5	+ 2.7	2.5	4	2	150
6....	23288	139	38 51	23 58.5	5.3	B5	+ 4.3	2.5	4	3	250
7....	23302	148	38 56	23 47.9	3.6	B5p	+14.9	11.5	3	3	200
8....	23289	149	38 57	22 57.3	9.3	F5	+ 6.9	1.9	4	1	0
9....	23326	163	39 10	23 23.3	9.3	F5	+ 8.7	4.6	3	2	0
10....	23325	162	39 10	23 57.0	8.8	A0	+ 8.7	1.8	4	1	75
11....	23324	166	39 12	24 31.5	5.7	B8	− 1.2	9.5	4	3	150
12....	23338	170	39 15	24 9.2	4.2	B5	+ 3.2	3.3	3	3	150
13....	23351	180	39 23	24 36.5	9.5	F5	+ 1.8	12.3	4	1	0
14....	23361	195	39 30	23 43.3	8.2	A3	+10.1	3.9	3	2	100
15....	23375	208	39 37	24 9.0	8.9	A2	+11.3	2.1	4	1	50
16....	23387	215	39 41	24 1.4	7.3	B9	+ 4.0	1.8	5	1	0
17....	23408	231	39 52	24 3.3	3.8	B5	+ 5.1	1.6	6	2	25
18....	23410	234	39 55	22 50.1	6.9	A0	+ 2.6	1.7	3	2	100
19....	23409	235	39 55	23 43.6	8.0	A0	+ 6.9	2.4	4	2	75
20....	23432	240	39 57	24 14.5	5.7	B8	− 0.2	2.6	5	3	150
21....	23441	247	40 5	24 12.9	6.3	B9	− 1.0	5.7	6	3	200
22....	23463	*	40 17	23 53.1	9.2	K2	− 8.7	.....	2	1	0
23....	23464	310†	40 18	22 49.0	8.3	G0	− 4.0	0.6	4	1	0
24....	23479	281b	40 19	23 52.7	8.7	A3	− 6.2	5.5	4	2	150
25....	23480	286	40 23	23 38.2	4.2	B5	+ 4.1	.....	2	3	300
26....	23489	295	40 30	23 56.6	7.4	A0	+ 3.1	1.9	4	2	50
27....	23512	311	40 39	23 18.8	8.5	A0	− 0.8	10.0	3	1	50
28....	23513	331	40 46	22 48.0	9.8	F8	− 2.4	9.5	3	1	0
29....	23568	354	41 2	24 12.6	6.7	B9	− 4.4	4.7	4	3	150
30....	23567	359b	41 5	24 30.6	9.0	A2	+ 9.6	4.8	3	1	50
31....	23585	365	41 8	23 41.1	8.6	A2	+ 4.7	2.9	3	2	75
32....	23607	390	41 23	23 49.8	8.4	A0	+ 5.9	2.3	3	1	0
33....	23629	395	41 24	23 48.4	6.3	A0	+ 5.6	10.2	4	2	100
34....	23632	397	41 25	23 29.6	6.9	A0	+ 2.4	2.2	3	3	150
35....	23628	399	41 26	24 16.7	7.8	A0	− 3.4	6.7	4	2	100
36....	23631	402	41 28	23 36.3	7.2	B9	+ 2.9	5.9	3	1	0
37....	23643	410	41 31	23 22.1	7.9	A0	+ 8.2	1.9	3	3	100
38....	23630	414	41 32	23 47.8	2.8	B5p	+ 9.1	6.7	3	3	250
39....	23642	413	41 32	23 58.8	6.8	B9	+14.6	10.5	3	1	0
40....	23733	493	42 16	24 0.6	8.5	A3	+ 7.8	3.0	3	2	100
41....	23753	506	42 26	23 6.8	5.4	B8	−14.4	9.5	3	3	300
42....	23763	518	42 33	24 2.3	7.0	A0	+14.2	3.2	3	1	50
43....	23791	551	42 49	22 57.2	8.6	A3	+ 2.0	2.7	3	1	50
44....	23850	594	43 13	23 44.8	3.6	B8	+ 1.7	.....	2	3	250
45....	23863	607	43 16	23 34.9	8.3	A2	+ 4.9	3.9	4	3	100
46....	23872	613	43 19	24 5.4	7.6	A0	+ 3.2	3.7	4	3	250
47....	23873	622	43 24	24 4.5	6.5	B9	+ 1.4	1.5	5	1	25
48....	23886	629	43 29	23 56.5	8.1	A0	+11.4	5.5	4	1	75
49....	23912	651	43 37	23 4.5	9.5	F8	+ 4.7	1.0	4	2	100
50....	23924	670	43 46	23 2.2	8.3	A2	+ 6.7	3.0	4	1	0
51....	23923	671	43 47	23 24.4	6.0	B8	+ 1.8	5.1	6	3	250
52....	23948	688	43 59	24 2.7	7.5	A0	+ 6.3	2.3	5	1	25
53....	23964	697	44 2	23 32.7	6.8	B9	+ 5.7	6.3	5	1	0
54....	24076	791	44 56	23 39.5	7.0	A0	+ 3.4	5.0	4	2	50
55....	24132	848	45 29	24 13.0	9.1	A5	+ 8.7	±3.9	4	2	75

* Magnitude from *Henry Draper Catalogue*.

† Hertzsprung's number and magnitude; see footnote 4.

TABLE 1—*Continued*

Star	HD	Trumpler No.	α (1900)	δ (1900)	Mag. (Pg.)	Sp.	Vel. (Km/Sec)	m.e.	Plates	Grade	Rot. (Km/Sec)
56....	22578	S23	$3^h32^m49^s$	+22°20′.0	6.7	A0	0.0	.....	2	3	150
57....	22614	S25	33 10	24 22.6	7.1	A0	− 1.4	.....	2	1	0
58....	22615	S25a	33 12	20 35.4	6.5	A0	− 6.3	.....	2	1	0
59....	22637	S26	33 23	21 31.1	7.4	A0	+28.1	.....	2	2	50
60....	23155	47	37 45	24 45.8	7.7	A2	+ 1.2	.....	2	2	75
61....	23388	S76	39 42	20 56.0	7.8	A3	+ 0.1	.....	2	3	50
62....	23402	S78	39 47	22 22.9	8.1	A0	+ 8.9	.....	2	3	150
63....	23430	S84	40 0	25 5.2	8.3	A0	+ 7.4	.....	2	1	75
64....	23664	S115	41 47	25 4.6	8.5	A2	+ 5.6	.....	2	1	25
65....	23852	S137	43 18	22 18.2	7.9	A0	+ 2.4	.....	2	1	75
66....	23913	S142	43 45	22 13.7	6.9	B9	− 7.0	.....	2	3	150
67....	23950	S149	44 2	21 56.4	6.0	B9	+13.9	.....	2	3	75
68....	24178	S165	45 56	25 41.9	7.9	A0	+ 3.6	.....	2	2	75
69....	24368	S177	47 33	25 23.1	6.3	A0	+ 7.7	.....	2	1	0
70....	24711	S185	50 32	22 51.6	8.5	A0	+15.8	.....	2	1	25
71....	24899	S194	52 23	23 47.7	7.1	B9	+ 9.4	.....	2	1	0

From Table 1 the following mean values have been derived:

Unweighted mean of all (69) stars	+4.08	±0.68 m.e.
Unweighted mean of all (31) stars of grade 1	+5.15	±0.99
Unweighted mean of all (17) stars of grade 2	+4.09	±1.01
Unweighted mean of all (21) stars of grade 3	+2.50	±1.45
Unweighted mean of all (50) stars of rotational velocity 0–100 km/sec	+5.19	±0.69
Unweighted mean of all (19) stars of rotational velocity 150–300 km/sec	+1.17	±1.41

In Figure 1 the radial velocities are plotted according to photographic magnitude. The open circles represent the 19 stars of large rotational velocity. The diagram suggests that the brighter stars, of the 19, have larger positive velocities than the fainter ones; but this may be entirely accidental. It should be remembered that the bright B-type stars are the ones that are most difficult to measure. There is no physical explanation of the systematic difference of 4 km/sec between the stars of large and those of small rotation. It is possible, though unlikely, that blends in the spectra of the high-rotation A and late B stars influence the results.

The Lick catalogue of radial velocities[1] lists 11 stars which are also in our list. A comparison of the measured velocities in the two lists is shown in Table 3. Using those stars for which the Lick catalogue contains more than 3 observations and those for which McDonald has more than 2 observations, the mean difference for the remaining 5 stars is

$$\text{Lick Catalogue } \textit{minus} \text{ McDonald} = +0.2 \text{ km/sec}.$$

In view of the fact that nearly all the stars in Table 3 have poor lines, this determination of the systematic difference carries little weight.

Of the 69 stars discussed, 8 are known or suspected, according to Trumpler, to be visual binaries, and one is a triple star. The radial velocities of these stars appear to be normal. In this investigation no stars were found with two spectra, and the greatest range in velocity for a single star (our No. 13) was 54 km/sec. It is perhaps surprising that there are so few spectroscopic binaries of large range in velocity. This may indicate that the masses of the stars are relatively small, and it does not necessarily prove that binaries are infrequent. There are 17 stars for which the observed range in velocity is

TABLE 2

RADIAL VELOCITIES FOR INDIVIDUAL SPECTROGRAMS

Star	Plate No.	Date	U.T.	Quality	V (Km/Sec)	Lines
1.....	1001	1941 Nov. 4	9:09	f	+ 8.5	12
	1273	1942 Jan. 22	2:17	f	+ 4.7	9
	2502	1943 Sept. 13	7:15	f	+ 8.3	6
2.....	1036	1941 Nov. 7	3:09	g	+ 4.1	22
	1326	1942 Jan. 27	3:12	g	+10.3	11
	2000	1943 Mar. 8	5:27	g	−25.0	7
	2427	Sept. 4	8:01	g	− 5.2	14
3.....	1002	1941 Nov. 4	9:55	g	+13.4	15
	1085	10	8:39	p	+ 2.9	6
	1274	1942 Jan. 22	2:52	g	+10.7	12
	2428	1943 Sept. 4	8:31	f	+ 6.5	9
4.....	1003	1941 Nov. 4	10:25	g	+ 7.0	11
	1086	10	9:26	f	− 8.5	9
	1275	1942 Jan. 22	3:15	g	− 2.1	17
	2429	1943 Sept. 4	9:08	g	+ 7.9	13
5.....	1004	1941 Nov. 4	11:01	g	− 0.6	10
	1062	9	7:16	g	− 1.2	8
	1276	1942 Jan. 22	3:39	g	+ 7.6	9
	2430	1943 Sept. 4	10:00	g	+ 5.0	10
6.....	1026	1941 Nov. 6	.....	f	+ 9.7	3
	1087	10	9:50	f	+ 0.9	7
	1272	1942 Jan. 22	1:48	g	+ 7.6	8
	2431	1943 Sept. 4	10:37	g	− 1.2	7
7.....	12629	1941 Oct. 24	4:26	p	+33.8	2
	1327	1942 Jan. 27	3:24	p	+14.9	3
	1366	31	1:45	f	− 4.1	6
8.....	987	1941 Nov. 3	11:44	g	+ 3.2	13
	1324	1942 Jan. 27	1:48	p	+11.8	4
	1346	28	2:47	g	+ 3.2	9
	2432	1943 Sept. 4	11:18	f	+ 9.2	12
9.....	1999	1943 Mar. 8	5:01	g	+ 1.4	10
	4066	Sept. 1	10:07	g	+16.4	11
	4067	1	10:41	g	+ 8.4	10
10.....	1037	1941 Oct. 7	3:58	g	+ 7.4	13
	1278	1942 Jan. 22	4:17	g	+ 5.6	13
	1297	24	6:21	g	+ 8.5	12
	2438	Sept. 5	7:51	g	+13.4	13
11.....	1027	1941 Nov. 6	8:38	f	+ 2.1	6
	1279	1942 Jan. 22	4:41	p	+14.5	6
	1367	31	1:49	p	−27.2	3
	2439	1943 Sept. 5	8:32	f	+ 5.9	7
12.....	12630	1941 Oct. 24	5:00	p	− 0.4	2
	1281	1942 Jan. 22	5:35	g	+10.5	9
	1368	31	2:56	g	− 0.5	9
13.....	1047	1941 Nov. 8	8:50	g	+ 0.9	16
	1280	1942 Jan. 22	5:16	p	+30.3	8
	2440	1943 Sept. 5	9:21	g	+ 0.3	15
	2513	14	7:27	f	−24.1	4

TABLE 2—*Continued*

Star	Plate No.	Date	U.T.	Quality	V (Km/Sec)	Lines
14.....	1058	1941 Nov. 9	4:19	g	+ 9.5	6
	1282	1942 Jan. 22	5:57	f	+16.9	4
	2441	1943 Sept. 5	10:28	f	+ 4.0	6
15.....	1038	1941 Nov. 7	5:06	g	+ 6.5	14
	1283	1942 Jan. 22	6:40	g	+11.8	14
	2442	1943 Sept. 5	10:27	g	+11.2	15
	2514	14	8:41	g	+15.8	15
16.....	1005	1941 Nov. 4	11:29	f	+ 2.5	4
	1061	9	6:42	g	+ 4.6	7
	1361	1942 Jan. 29	4:47	g	− 1.8	5
	2450	1943 Sept. 6	8:56	g	+ 8.1	5
	2515	14	9:25	g	+ 6.6	6
17.....	1298	1942 Jan. 24	6:41	g	+ 5.8	7
	1363	29	7:09	g	+ 4.3	11
	1364	31	1:05	g	+ 6.9	11
	1369	31	3:03	g	− 2.0	11
	1383	Feb. 1	0:58	g	+ 7.6	6
	1384	1	1:13	g	+ 8.1	12
18.....	984	1941 Nov. 3	9:14	f	+ 1.2	7
	1312	1942 Jan. 25	6:22	f	+ 6.2	4
	2453	1943 Sept. 6	9:29	f	+ 0.5	8
19.....	1012	1941 Nov. 5	5:48	p	+ 0.8	4
	1078	10	4:30	f	+11.4	5
	2449	1943 Sept. 6	8:16	f	+ 4.3	9
	2516	14	10:03	g	+11.0	8
20.....	1006	1941 Nov. 4	11:39	p	+ 4.9	6
	1299	1942 Jan. 24	6:47	f	− 0.7	7
	1370	31	3:13	g	− 9.4	5
	2451	1943 Sept. 6	9:06	f	+ 3.6	7
	2517	14	10:32	f	+ 0.6	8
21.....	1007	1941 Nov. 4	11:47	f	+10.0	8
	1300	1942 Jan. 24	6:55	f	+10.1	6
	1360	29	2:16	g	− 2.4	6
	1371	31	3:19	f	−26.3	5
	2452	1943 Sept. 6	9:15	g	+ 5.6	7
	2518	14	10:37	f	− 2.8	8
22.....	1997	1943 Mar. 8	4:18	g	−15.0	12
	4068	Sept. 1	10:59	g	− 2.4	11
23.....	985	1941 Nov. 3	9:52	f	− 2.9	13
	1345	1942 Jan. 28	1:47	f	− 3.9	14
	2454	1943 Sept. 6	10:05	f	− 5.5	12
	2519	14	11:13	p	− 3.8	12
24.....	1059	1941 Nov. 9	5:40	g	− 4.9	10
	1359	1942 Jan. 29	1:40	f	− 6.0	11
	1998	1943 Mar. 8	4:35	p	−19.0	7
	4069	Sept. 1	11:12	g	+ 5.2	10
25.....	1347	1942 Jan. 28	3:17	p	− 5.7	3
	1372	31	4:36	f	+14.0	6

TABLE 2—*Continued*

Star	Plate No.	Date	U.T.	Quality	V (Km/Sec)	Lines
26.....	1039	1941 Nov. 7	5:55	g	+ 8.5	7
	1060	9	6:22	g	+ 2.4	9
	2462	1943 Sept. 7	7:26	g	+ 0.3	7
	2520	14	11:57	g	+ 1.2	7
27.....	983	1941 Nov. 3	8:29	f	+ 4.3	7
	1329	1942 Jan. 27	3:51	p	−19.9	4
	2463	1943 Sept. 7	8:23	g	+13.2	7
28.....	986	1941 Nov. 3	10:51	g	+ 8.6	9
	1348	1942 Jan. 28	3:52	f	+ 6.7	8
	2455	1943 Sept. 6	11:05	f	−22.6	3
29.....	1029	1941 Nov. 6	9:01	f	− 2.2	5
	1088	10	10:02	f	− 6.6	4
	1380	1942 Jan. 31	4:51	p	−14.8	2
	2456	1943 Sept. 6	11:45	f	+ 6.0	8
30.....	1040	1941 Nov. 7	6:33	g	+ 3.2	12
	1337	1942 Jan. 27	6:48	f	+ 6.6	8
	2493	1943 Sept. 12	8:44	g	+19.0	17
31.....	974	1941 Nov. 2	7:27	g	+ 6.6	15
	1333	1942 Jan. 27	5:19	g	− 1.1	10
	2494	1943 Sept. 12	9:28	g	+ 8.5	15
32.....	959	1941 Oct. 29	10:09	g	+ 6.4	12
	1050	Nov. 8	11:22	g	+ 9.4	19
	1336	1942 Jan. 27	6:06	g	+ 1.9	17
33.....	958	1941 Oct. 29	8:59	f	+17.8	8
	979	Nov. 3	6:22	g	+28.3	8
	1335	1942 Jan. 27	8:59	f	−16.8	7
	2506	1943 Sept. 13	11:22	f	− 6.7	8
34.....	981	1941 Nov. 3	7:05	f	+ 3.1	7
	1331	1942 Jan. 27	4:36	f	− 1.6	8
	2465	1943 Sept. 7	10:09	g	+ 5.8	8
35.....	1030	1941 Nov. 6	9:39	f	−14.0	3
	1049	8	10:19	f	− 3.7	7
	2468	1943 Sept. 7	11:38	g	+15.6	3
	2507	13	11:41	g	−11.4	11
36.....	980	1941 Nov. 3	6:44	g	− 9.2	13
	1332	1942 Jan. 27	4:49	g	+10.1	12
	2466	1943 Sept. 7	10:43	g	+ 7.9	12
37.....	982	1941 Nov. 3	7:41	f	+12.0	7
	1330	1942 Jan. 27	4:19	f	+ 5.7	4
	2464	1943 Sept. 7	9:30	g	+ 6.8	10
38.....	12640	1941 Oct. 25	9:05	f	+10.4	4
	1334	1942 Jan. 27	5:42	g	+19.4	9
	1373	31	3:40	f	− 2.5	7
39.....	960	1941 Oct. 29	11:00	g	+16.3	7
	1048	Nov. 8	9:48	g	+30.9	9
	2467	1943 Sept. 7	11:11	g	− 3.5	10

TABLE 2—*Continued*

Star	Plate No.	Date	U.T.	Quality	V (Km/Sec)	Lines
40.....	990	1941 Nov. 4	2:41	g	+11.3	10
	1069	9	11:38	g	+ 1.5	10
	2503	1943 Sept. 13	8:34	g	+10.6	11
41.....	1028	1941 Nov. 6	8:46	f	−34.1	4
	1341	1942 Jan. 27	7:35	f	− 6.2	6
	1374	31	3:46	f	− 2.8	4
42.....	991	1941 Nov. 4	3:26	f	+13.9	7
	1338	1942 Jan. 27	7:20	f	+19.6	4
	2495	1943 Sept. 12	11:14	g	+ 9.1	9
43.....	999	1941 Nov. 4	8:08	g	+ 7.2	15
	1349	1942 Jan. 28	4:38	g	− 1.8	15
	2496	1943 Sept. 12	11:48	g	+ 0.5	17
44.....	1340	1942 Jan. 27	7:30	f	+ 3.8	8
	1375	31	3:50	f	− 0.4	7
45.....	977	1941 Nov. 2	10:54	g	+ 5.0	9
	1362	1942 Jan. 29	6:02	f	+14.8	7
	1994	1943 Mar. 8	3:26	g	− 2.3	6
	2505	Sept. 13	10:54	g	+ 2.0	8
46.....	992	1941 Nov. 4	3:45	f	+ 9.5	3
	1065	9	9:05	f	− 7.1	9
	1995	1943 Mar. 8	3:44	f	+ 4.8	6
	2485	Sept. 8	11:11	f	+ 5.5	4
47.....	1000	1941 Nov. 4	8:31	g	− 4.2	7
	1064	9	5:52	g	+ 2.9	5
	1377	1942 Jan. 31	4:03	p	+ 4.0	4
	1996	1943 Mar. 8	3:53	g	+ 2.5	8
	2484	Sept. 8	10:55	f	+ 1.7	5
48.....	993	1941 Nov. 4	4:18	g	− 1.7	9
	1066	9	9:29	g	+10.4	12
	1993	1943 Mar. 8	3:03	g	+14.1	9
	2483	Sept. 8	10:33	g	+22.7	11
49.....	997	1941 Nov. 4	7:02	g	+ 7.4	9
	1350	1942 Jan. 28	5:24	g	+ 3.2	6
	2481	1943 Sept. 8	9:05	f	+ 4.9	6
	2702	Nov. 16	2:58	g	+ 3.3	11
50.....	998	1941 Nov. 4	7:43	g	+ 8.9	12
	1351	1942 Jan. 28	6:07	g	+ 0.3	12
	2482	1943 Sept. 8	10:00	g	+ 3.8	13
	2703	Nov. 16	4:01	g	+13.8	14
51.....	1031	1941 Nov. 6	10:10	f	− 4.2	6
	1089	10	10:15	f	+15.6	7
	1378	1942 Jan. 31	4:17	f	−16.7	5
	2032	1943 Mar. 10	3:56	p	+ 2.0	6
	2479	Sept. 8	7:58	f	− 0.1	6
	2704	Nov. 16	3:55	g	+14.5	7
52.....	994	1941 Nov. 4	4:49	f	+ 6.9	4
	1067	9	9:54	f	− 0.7	7
	2030	1943 Mar. 10	3:19	g	+ 9.3	7
	2480	Sept. 8	8:13	g	+11.7	5
	2713	Nov. 17	2:26	g	+ 4.5	6

TABLE 2—*Continued*

Star	Plate No.	Date	U.T.	Quality	V (Km/Sec)	Lines
53.....	976	1941 Nov. 2	9:53	g	− 8.9	9
	1090	10	10:24	g	+16.4	5
	2031	1943 Mar. 10	3:40	g	+12.6	9
	2478	Sept. 8	7:42	g	−12.7	12
	2715	Nov. 17	4:07	g	+21.2	7
54.....	996	1941 Nov. 4	6:22	f	+ 0.5	8
	1342	1942 Jan. 27	7:44	f	− 4.7	5
	2035	1943 Mar. 10	4:13	f	+17.6	4
	2477	Sept. 8	7:20	f	0.0	6
55.....	995	1941 Nov. 4	5:37	f	+ 7.0	9
	1068	9	10:39	f	+ 8.6	6
	2504	1943 Sept. 13	9:46	f	+18.1	7
	2714	Nov. 17	3:14	f	+ 0.9	9
56.....	1021	1941 Nov. 6	5:20	f	+ 5.1	4
	1073	10	2:45	f	− 5.1	8
57.....	1025	1941 Nov. 6	8:19	g	−21.4	5
	1354	1942 Jan. 28	7:40	f	+18.7	4
58.....	1019	1941 Nov. 6	4:38	g	− 4.5	11
	1071	10	2:20	g	− 8.1	16
59.....	1020	1941 Nov. 6	4:59	f	+21.4	4
	1072	10	2:35	f	+34.9	4
60.....	1024	1941 Nov. 6	7:48	p	−13.8	4
	1075	10	3:13	f	+16.3	4
61.....	1023	1941 Nov. 6	7:00	f	− 3.1	4
	1082	10	6:52	g	+ 3.4	4
62.....	1022	1941 Nov. 6	6:00	p	+ 9.6	3
	1077	10	4:03	f	+ 8.3	6
63.....	1045	1941 Nov. 8	5:45	g	+ 5.1	13
	1076	10	3:38	g	+ 9.6	10
64.....	1046	1941 Nov. 8	7:14	g	+10.8	15
	1353	1942 Jan. 28	7:14	f	+ 0.5	5
65.....	1018	1941 Nov. 6	3:57	p	+ 3.1	5
	1079	10	4:58	f	+ 1.7	8
66.....	1017	1941 Nov. 6	3:14	f	−26.5	3
	1080	10	5:26	f	+12.5	4
67.....	1016	1941 Nov. 6	2:57	p	+34.3	2
	1057	9	3:26	f	− 6.5	9
68.....	1033	1941 Nov. 6	11:07	p	+ 2.6	3
	1084	10	7:50	f	+ 4.7	4
69.....	1032	1941 Nov. 6	10:26	g	+11.1	13
	1083	10	7:20	g	+ 4.3	12
70.....	1044	1941 Nov. 8	4:13	g	− 1.0	10
	1352	1942 Jan. 28	6:37	p	+32.6	7
71.....	1043	1941 Nov. 8	3:17	g	+10.2	7
	1355	1942 Jan. 28	7:55	g	+ 8.6	4

more than 30 km/sec. Only 10 of these have spectra of grades 1 and 2, and they may be suspected of being spectroscopic binaries. These are our Nos. 2, 13, 27, 28, 33, 39, 53, 57, 60, and 70. Only 2 of these, namely, Nos. 13 and 33, appear to be established with certainty because of the good accordance between the results of the two measurers. The scarcity in the Pleiades of binaries with large amplitudes is the principal conclusion of our investigation.

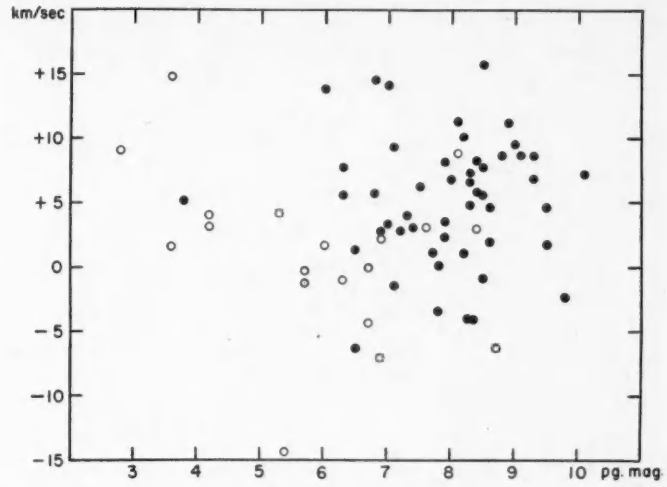

FIG. 1

TABLE 3

COMPARISON WITH LICK CATALOGUE OF RADIAL VELOCITIES

Our No.	Lick Catalogue		McDonald Obs.		Difference (Lick *minus* McDonald)
	Vel.	Plates	Vel.	Plates	
6	+ 2.2	17	+ 4.3	4	− 2.1
7	+11.9	14	+14.9	3	− 3.0
11	+24.8	1	− 1.2	4	+26.0
12	+ 5.4	17	+ 3.2	3	+ 2.2
17	+ 7.8	92	+ 5.1	6	+ 2.7
20	− 2.0	1	− 0.2	5	− 1.8
21	− 3.9	1	− 1.0	6	− 2.9
25	+ 6.8	12	+ 4.1	2	+ 2.7
38	+10.3	18	+ 9.1	3	+ 1.2
41	+ 8	3	−14.4	3	+22.4
44	+ 9.3	16	+ 1.7	2	+ 7.6

It is known from theoretical considerations that the internal motions in the Pleiades cluster must be small. Titus[10] found a mean internal space velocity for the Pleiades of ± 0.59 km/sec. In order to test whether there is any evidence of internal motions in the radial velocities, we have selected from Table 1 all stars of grades 1 and 2 which are not suspected of being spectroscopic binaries, which have small rotational velocities, and

[10] *A.J.*, **47**, 25, 1938.

which have more than 2 plates. This group of 29 stars gives an average mean error of ± 2.94 km/sec for one star. The individual mean errors in Table 1 were computed by means of Schlesinger's formula,[11] which makes an appropriate statistical correction when the number of observations is small. The unweighted mean radial velocity of the 29 stars is $+5.74 \pm 0.77$ (m.e.) km/sec. The mean error of a single star, computed from the departures (Star *minus* Mean), is ± 4.14 km/sec. The difference between the external and

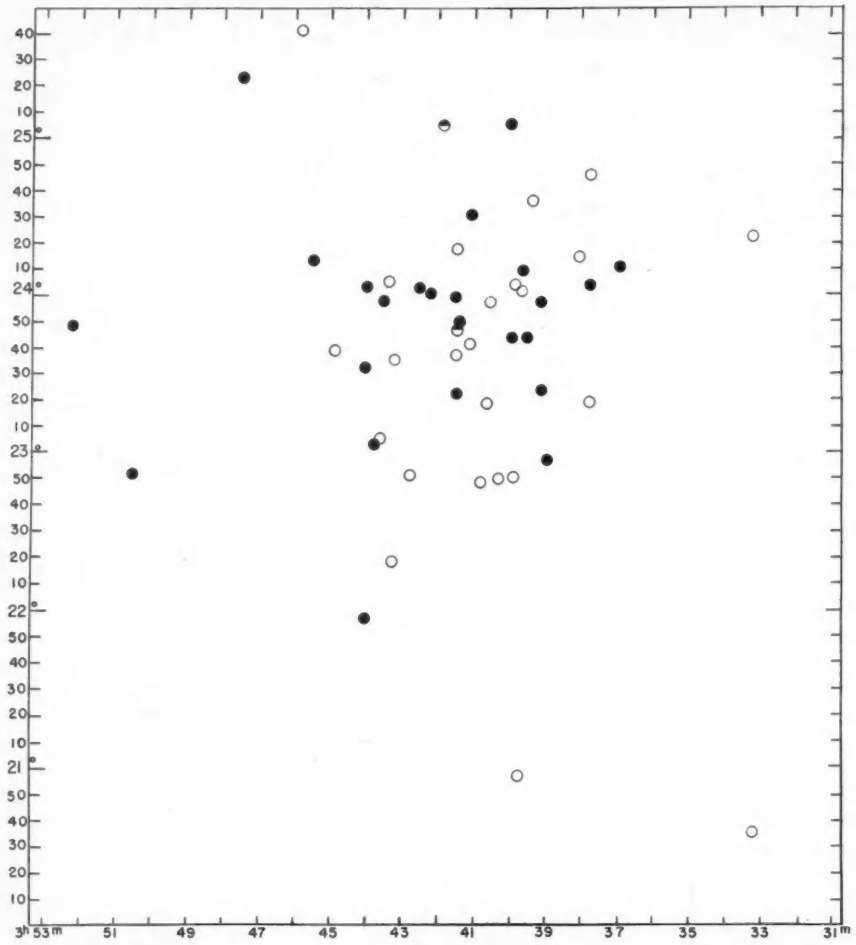

FIG. 2

internal mean errors of 1.2 km/sec suggests that there may exist internal motions of the order of 1 km/sec. This is sufficiently close to the theoretical value deduced by Titus.

An attempt was made to test whether there is evidence of rotation or of a spatial change in the velocities resulting from group motion. The median velocity for the 50 stars of low rotation, namely, +5.6 km/sec, was taken as the velocity of the center of gravity of the cluster. Figure 2 shows the location of these stars. Solid circles indicate positive residuals, and open circles negative residuals. Half-filled circles indicate the posi-

[11] *A.J.*, **46**, 161, 1937.

tions of the two stars, Nos. 33 and 64, which have zero residuals. There are no conspicuous differences in the residuals depending upon position.

If a straight line is drawn approximately through the geometrical center of the cluster, near Alcyone, at an angle of 25° west from the meridian, the residuals on the northeast side are slightly more positive than those on the southwest side. The mean velocities for four zones running parallel to this dividing line are shown in the upper part of Table 4. The lower part of the table gives the mean velocities for four zones oriented at right angles to those of the upper part.

The width of the zones was chosen so that there are roughly the same number of stars in each zone. Zones II and III are ½° in width on either side of the dividing line.

TABLE 4

	Zone I	Zone II	Zone III	Zone IV
	Zones at 25° from the Meridian			
No. of stars	10	12	17	11
Velocity	+7.3	+7.0	+5.1	+1.4
M.e.	±1.3	±1.2	±0.8	±1.9
	Zones at 115° from the Meridian			
No. of stars	15	12	12	11
Velocity	+4.1	+5.2	+7.0	+4.7
M.e.	±1.5	±1.2	±1.6	±1.3

TABLE 5

Character of Spectrum	No. of Stars	Mean (Struve *minus* Smith)
Grade 1	30	+0.9 km/sec
Grade 2	16	−1.8
Grade 3	14	−0.5
All	60	−0.15

We do not regard this effect as sufficiently pronounced to suggest that it be considered physically real, in the absence of much-needed additional material.

Our mean velocity for the cluster, as determined from stars of good spectral characteristics, is +5.2 km/sec. This is approximately 2 km/sec less than Trumpler's value and 2.5 km/sec less than Pearce's recent determination. A possible systematic error of our radial velocities may arise from the following sources: (1) a personal error of one or of both measurers; (2) a spurious shift due to blends or to incorrect identifications of the stellar lines; (3) systematic effects arising from the method of reduction, the curvature correction, etc.; and (4) faulty adjustment of the spectrograph or the effect of coma in producing unsymmetrical comparison lines.

In order to test the first source, we have compared the results of Struve and of Smith in Table 5. The differences are negligible for the mean of all stars.

The second source of error was carefully investigated for the measures by Struve. Since many Pleiades have but few lines, the probability of including blends is considerable. Table 6 gives all lines used by Struve with their wave lengths, for which there were at least three measures: the mean departures (line *minus* plate mean); the mean errors of one measurement of each line; the mean error of the systematic departure for each line; and the number of times the line was measured in the entire series. Twenty-eight measures of 21 additional lines were omitted in the tabulation because their effect is negligible. Since the omission of one residual, Δ, shifts the mean for the remainder of the series by $\Delta/(n-1)$, it is easy to verify that no appreciable change can be brought about by omitting

TABLE 6

STAR LINES USED BY O. STRUVE

Element	Wave Length	Mean Residual	ϵ	ϵ_0	n
Si II blend	3856.74	−37.6	±10.3	± 6.4	4
He I	4471.48	−15.4	27.3	10.3	11
Hε	3970.08	−14.2	20.9	3.4	59
Fe I	4045.82	−13.0	15.0	2.3	66
He I	4026.19	−12.4	23.0	8.6	11
Sr II	4077.71	− 8.8	22.3	4.2	44
Ca I	4226.73	− 8.4	18.8	2.4	95
Fe I	4071.74	− 6.7	15.3	3.1	39
H 10	3797.90	− 5.5	18.0	2.0	86
Fe I	4063.57	− 4.4	11.2	2.0	48
Hγ	4340.47	− 3.6	18.9	1.6	216
Si II	3862.60	− 1.8	9.5	6.9	3
Ti II	4289.84	− 1.5	16.0	2.8	51
Si II	4128.05	− 1.1	5.0	2.8	5
Hζ	3889.05	− 0.2	16.4	2.1	92
Ca II	3933.675	+ 0.5	13.7	1.3	164
Hδ	4101.745	+ 3.4	17.5	1.5	208
Hη	3835.39	+ 6.2	18.8	2.5	90
Si II	3856.025	+ 6.6	9.0	4.6	6
Fe I	4005.25	+ 6.8	15.0	2.5	55
Fe II	4351.79	+ 6.9	16.0	6.0	11
Sr II	4215.52	+ 9.1	19.0	5.0	23
Fe II	4233.175	+ 9.1	25.1	4.4	50
Mg II	4481.24	+10.4	20.5	1.9	176
Fe I	4383.55	+10.6	18.9	7.1	11
Fe I	3997.40	+14.6	11.0	6.9	4
Sc II	4314.09	+18.4	18.5	4.5	27
Ni II	4067.05	+18.5	15.6	4.0	24
Si II	4130.88	+32.4	±22.9	±14.2	4
Total					1683

those lines whose mean residuals are excessive. For example, omitting the first line (λ 3856.74) would shift the entire series by only +0.1 km/sec. Omitting all lines whose mean residuals exceed ± 10 km/sec would shift the result for the series by −0.6 km/sec. If, however, we should omit only those lines whose residuals are in excess of ± 10.5 km/sec, the mean of the series would be shifted by +0.7 km/sec. It is clear that in this manner small shifts of the order of 1 km/sec in the final mean can perhaps be accounted for. But it does not seem possible to explain a systematic difference of 2 km/sec.

The third and fourth sources were investigated together by means of measurements of a number of stars of constant radial velocity. Most of these spectra were obtained at approximately the same time as the spectra of the Pleiades and with identical adjustments

of the spectrograph. The stars were chosen from spectral classes A and F, and the methods of measurement and reduction were precisely the same as those used for the Pleiades. The results are summarized as follows:

53 standard stars: Lick *minus* Struve $= -1.1 \pm 0.7$ (m.e.)

21 standard stars: Lick *minus* Smith $= -1.4 \pm 1.5$ (m.e.)

The effect is in the *opposite* sense to that required for bringing our mean value of the Pleiades into harmony with Trumpler's and Pearce's results. We have preferred not to apply this correction because its mean error is of the same order of magnitude as the correction itself.

Although it is disconcerting that we have not been able to trace the cause of the difference between our mean radial velocity of the Pleiades and those of other workers, it is perhaps not impossible that several small *accidental* effects have combined to give this result. This is not contradicted by the values of the mean errors, which range from ± 0.7 to ± 1.4 km/sec, depending upon how the stars are arranged in groups. In view of the absence of any perceptible systematic errors in our work, we believe that it is best to present our measurements as they were obtained, despite this difference.

We are indebted to Dr. Gerard P. Kuiper for having suggested this investigation.

THE SPECTROSCOPIC ORBIT OF AR MONOCEROTIS*

JORGE SAHADE AND CARLOS U. CESCO
McDonald and Yerkes Observatories
Received July 15, 1944

ABSTRACT

This star is interesting because at primary eclipse the K0 component, whose spectrum is the only one observed, is in front. $P = 21.207$ days, $\gamma = +14.1$ km/sec; $K = +32.2$ km/sec; $e = 0.17$, $\omega = 102°$, $f(m) = 0.07\odot$. The emission lines of *Ca* II share the velocity variations of the K0 component.

The star HD 57364 (Sp. K0) = BD−4°1915 (8.8 mag.) = A. G. Strb. 2635 (8.8 mag.) was found to be an eclipsing binary in 1931 by C. Hoffmeister,[1] who described it as probably a "δ Cephei star with a period of a few days." It was provisionally designated as 55.1931. The spectrograms—twenty-nine in number—were taken on 103a-0 emulsion, using the Cassegrain quartz spectrograph of the 82-inch reflecting telescope of the McDonald Observatory, which gives a dispersion of 40 A/mm at λ 3933.

TABLE 1

STAR LINES USED FOR DETERMINATION OF THE RADIAL VELOCITIES

Fe I	3952.73	*Ti* II	4290.22
Fe I	4005.25	*Fe* I	4325.77
Fe I	4045.82	*Hγ*	4340.46
Fe I	4063.29	*Sc* II	4374.51
Fe I	4071.75	*Fe* I	4383.55
Hδ	4101.74	*Fe* I	4404.77
Fe I	4143.87	*Fe* I	4415.16
Sr II	4215.54	*Fe* I	4422.60
Ca I	4226.73	*Fe* I	4435.01
Fe I	4260.48	*Mg* II	4481.26

The observations (some of which were made by Dr. O. Struve and Dr. Helen Steel) were obtained during the months of January, February, and March, 1944, and cover almost three consecutive cycles of the variable. The exposure time, with fair seeing, was 90 minutes, with a slit width of 0.075 mm; but when the weather conditions were not very good, the time was increased to 120 minutes or even longer.

The determinations of radial velocity were obtained by measuring the lines listed in Table 1; they were selected from the list which Struve gives[2] for the G2 component of U Cephei. Sometimes the quality of the spectrograms did not allow us to measure all the lines, but the total number of measured lines was never less than ten. The radial velocities are indicated in Table 2 and plotted in Figure 1; "p" indicates a very poor plate, weighted one-half in the computation of the normal places.

In plotting the measurements we have adopted 21.207 days as the period—a value that was determined by Lause[3] from his estimation of magnitudes, which is 0.002 day shorter than the one previously found by Florja.[4] Lause gives for the time of the minimum JD 2426606.585 +21.207 E.

* *Contributions from the McDonald Observatory, University of Texas*, No. 98.

[1] *A.N.*, **242**, 129, 1931.

[2] *Ap. J.*, **99**, 222, 1944.

[3] *A.N.*, **264**, 105, 1937.

[4] *Sternberg Astr. Inst. Pub.*, **8**, 2, 1937.

In order to determine the preliminary elements, we drew a velocity-curve to satisfy the plotted measurements and applied the Wilsing-Russell method to twelve values read off at points of the curve at intervals of 30°. This gave us the following results:

$e = 0.17$ $\quad T =$ phase 10.930
$\omega = 99.28°$ $\quad \gamma = +13.8$ km/sec
$K = +31.3$ km/sec

The final elements and their probable errors were derived from a least-squares solution, applying the method of Schlesinger, and are shown in Table 3. For this purpose the ob-

TABLE 2

RADIAL VELOCITIES

PLATE	DATE	U.T.	PHASE (IN DAYS)	VELOCITY* (IN KM/SEC)	O−C	RADIAL VELOCITIES DERIVED FROM EMISSION LINES	
						H	K
CQ 3056	1944 Mar. 17	4:37	0.602	+24.3	+3.9	.....	.....
2935	Feb. 25	7:30	0.930	+21.6	−0.9	.....	.....
2830	4	4:49	1.025	+22.7	−0.5	.....	+21.4
2939	26	5:28	1.845	+24.1	−4.3	.....	.....
2949	29	7:46	4.941	+41.2	−2.0	.....	.....
2957	Mar. 1	4:54	5.821	+42.2	−2.7	+53.4	+47.9
2839†	Feb. 9	8:27	6.176	+49.2	+4.0	.....	.....
2965†	Mar. 2	4:47	6.816	+41.0	−3.7	.....	+53.7
2757p	Jan. 20	5:37	7.265	+49.7	+6.1	.....	.....
2765	21	9:38	8.432	+37.8	+0.4	.....	.....
2972	Mar. 4	5:42	8.854	+38.4	+4.6	.....	.....
2868	Feb. 12	6:55	9.112	+24.9	−6.4	.....	+32.9
2770	Jan. 22	6:54	9.318	+28.8	−0.3	+19.7	+32.8
2981	Mar. 5	6:58	9.907	+18.7	−3.5	.....	.....
2876	Feb. 13	8:12	10.166	+25.3	+6.5	.....	.....
2884	14	7:58	11.156	+ 5.0	−0.5	.....	.....
2779	Jan. 24	8:43	11.394	+ 3.9	+1.5	.....	.....
2785	25	7:21	12.337	−10.8	−2.4	.....	.....
3000	Mar. 8	4:37	12.809	− 8.7	+3.9	−13.8	+0.2
3006	10	7:20	14.923	−14.8	+4.3	.....	.....
2797	Jan. 28	4:17	15.210	−20.9	−2.3	.....	.....
3014	Mar. 11	5:16	15.836	−21.2	−4.3	− 6.7	− 8.1
2803	Jan. 29	6:30	16.302	−12.5	+2.6	.....	−12.7
3023	Mar. 12	6:03	16.869	−14.4	−2.1	−13.2	− 7.0
2810p	Jan. 30	7:58	17.363	−13.6	−4.1	.....	.....
2815	31	5:32	18.262	+ 1.7	+5.6	.....	− 7.4
3043	Mar. 14	3:55	18.780	+ 5.3	+5.8	.....	− 4.2
3049	15	5:45	19.857	+ 0.2	−6.7	.....	.....
2932	Feb. 24	6:20	21.088	+14.5	−1.0	.....	.....

* The groups indicated by the braces correspond to each normal place.
† Average of two measures.

servations were grouped in ten normal places, for which the phases are the averages of those for the individual plates and for which the δV are the average differences O − C between the observed velocities and those given by the preliminary orbit. Each normal place was given a weight equal to the square root of the number of observations. The probable error of one plate is ±2.6 km/sec.

The spectrum corresponds to type K0 (Pl. XIV) and does not show an appreciable change in the different phases. It shows rather broad single emissions of H and K in the *Ca* II lines; and the radial velocities derived from them agree well with those of the primary star, as is shown in Table 2. This suggests that the K0 star is surrounded by an envelope of calcium gas, which is probably excited by the secondary star. This fact is similar to that found by Joy[5] in WW Draconis, where the emissions of H and K in the *Ca* II lines

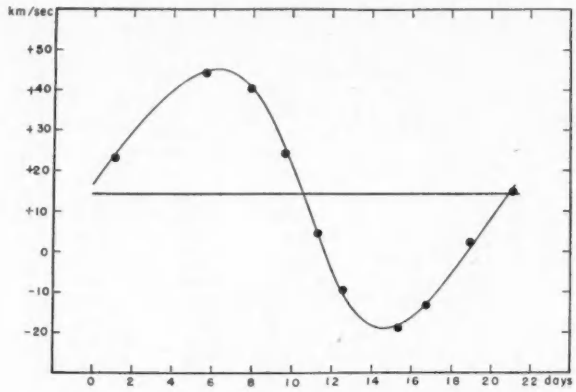

FIG. 1.—Velocity-curve of AR Monocerotis

TABLE 3

ORBITAL ELEMENTS

P = 21.207 days (assumed)	γ = +14.1 ± 0.64 km/sec
K = +32.2 ± 0.40 km/sec	$a \sin i$ = 9,300,000 km
ω = 102° ± 4.1°	$\frac{m_2^3 \sin^3 i}{(m_1 + m_2)^2}$ = 0.07 ⊙
e = 0.17 ± 0.013	
T = phase 11.1 ± 0.23 = JD 2426617.7	

are "displaced in the same direction as the absorption lines of the secondary component," which is also of K0 spectral type. In our case the few values of the radial velocity derived from the measures of the emission lines suggest that its range in velocity would be about the same as that of the K0 star, but the curve itself would be shifted a few kilometers in the direction of the positive velocities.

The principal minimum of the system corresponds to the branch of increasing velocities; hence, in the principal eclipse the K0 star whose spectrum we observe is in front. The luminosity criteria which Morgan, Keenan, and Kellman suggest in their *Atlas of Stellar Spectra* indicate that the primary star belongs to luminosity class II; i.e., it is a giant star.

The time of principal mid-eclipse, determined from the elements of the velocity-curve by the condition $v + \omega = 270°$, is phase 20.724 days, a value that agrees with Lause's light-elements within the error of the determination of periastron passage.

[5] *Ap. J.*, **94**, 407, 1941.

PLATE XIV

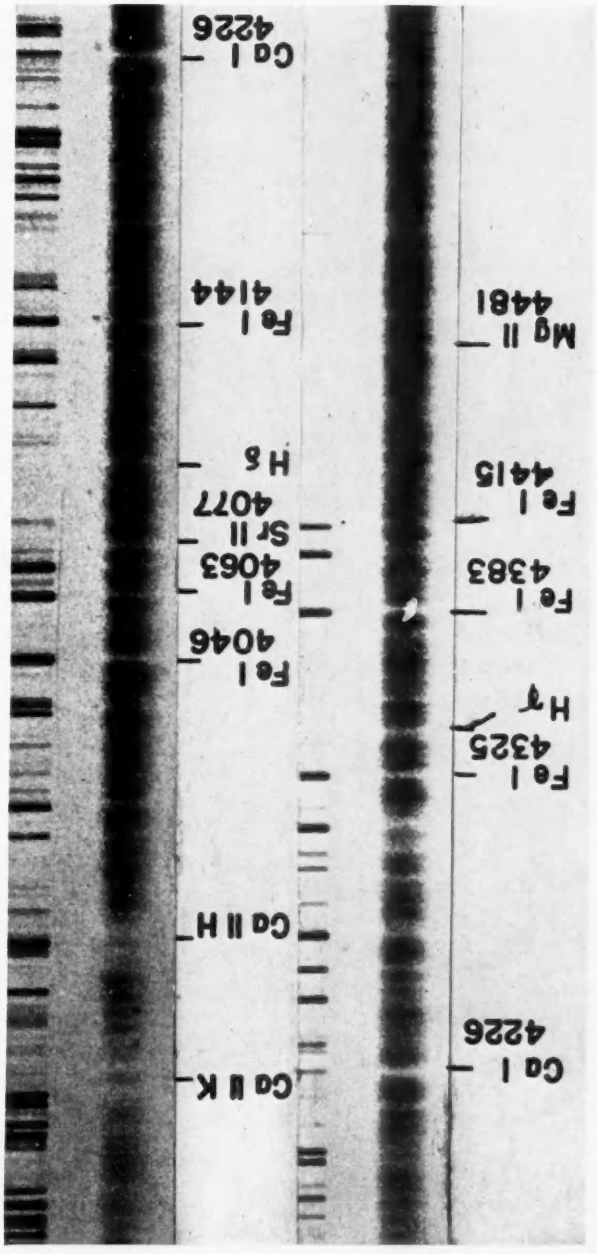

SPECTRUM OF AR MONOCEROTIS

A few of the spectrograms of AR Monocerotis which reach far into the ultraviolet show an increase of the intensity of the continuum and some H lines, which suggest that the fainter component may be of an earlier type.

Dr. Cecilia Payne Gaposchkin[6] has made a photometric study of this star and has kindly shown us the results before publication. The ratio of the surface brightnesses obtained from the photographic light-curve suggests that the secondary star would be of type F, and that obtained from the visual light-curve suggests that the fainter star would be of type G. If we assume that the fainter component is an F-type or G-type star, we find from the mass function and from $i = 80°$,[6] respectively,

$$m_K = 7.1\odot \qquad \text{or} \qquad m_K = 3.8\odot ,$$

if $m_F = 1.8\odot$ or $m_G = 1.2\odot$, these being mean values for spectral types F and G from the Russell diagram and the mass-luminosity curve.

We are indebted to Dr. Otto Struve for suggesting this problem and for many valuable discussions during our work. We also want to thank him and Dr. Helen Steel for obtaining some of the spectrograms and Dr. Cecilia Payne Gaposchkin for showing us her photometric results.

[6] *Ap. J.*, **100**, 251, 1944.

TITAN: A SATELLITE WITH AN ATMOSPHERE*

GERARD P. KUIPER[1]
McDonald and Yerkes Observatories
Received August 21, 1944

ABSTRACT

Recently the ten largest satellites in the solar system, as well as Pluto, were observed spectroscopically. Only Titan was found to have an atmosphere of sufficient prominence to be detected, but Triton and Pluto require further study. The composition of Titan's atmosphere is similar to that of Saturn, although the optical thickness is somewhat less.

The presence of gases rich in hydrogen atoms on a small body like Titan is surprising and indicates that the atmosphere was formed after Titan had cooled off. Similar arguments, though less compelling, may be advanced for analogous conclusions in regard to the formation of the atmospheres of Mars, Venus, and the earth.

I. OBSERVATIONS

During a short stay at the McDonald Observatory during the winter of 1943–1944 the ten largest satellites of the solar system were observed with a one-prism spectrograph attached to the 82-inch reflector. Pluto had been observed twice on an earlier occasion. Panchromatic film was used, sensitive below 6600 A. The dispersion was 340 A/mm at $H\gamma$. With this combination the methane absorptions of the major planets are well shown (Pl. XV); but many lesser absorptions are, of course, lost. When Titan's spectrum was found to contain the methane absorption bands, a number of plates with higher dispersion were taken. Because of the limited time available, no exhaustive study of the subject could be made at this time.

The spectra presented here consist of several groups. Plate XV shows low-dispersion spectra on panchromatic film; Plate XVI, low-dispersion spectra on infrared film; Plate XVII, medium-dispersion spectra on panchromatic film; Plate XVIII, medium-dispersion spectra on infrared plates; and Plate XIX, medium-dispersion spectra in the photographic, as well as the infrared, regions. In all cases planetary spectra, taken under similar conditions, have been added for comparison.

In addition to the major planets and the moon, the following objects were observed with low dispersion in the panchromatic region: Jupiter I, II, III, and IV; Saturn's satellites Titan, Rhea, Tethys, and Dione; Neptune's satellite Triton; and Pluto. Some of the spectra are shown in Plate XV. The methane absorption at 6190 A is striking in the three spectra of Titan shown, in marked contrast to that of Rhea and with the satellites of Jupiter. The results on Tethys and Dione were also definitely negative, but Triton may show a trace of the 6190 A band of methane. This object will be further investigated, as well as Pluto, for which two spectra were obtained with the dispersion of 720 A/mm at $H\gamma$. It is certain, however, that if Triton and Pluto have a methane atmosphere the absorptions are very much weaker than for Neptune and probably weaker than for Jupiter and Titan.

Plate XVI shows the objects for which infrared spectra of low dispersion were obtained. The most striking feature is the 7260 A band of methane. It is clearly present on Titan but is not present on the satellites of Jupiter or on the ring of Saturn. Because of field curvature the spectrograph used here required film, and the available 1N film appeared to be about two hundred times slower than panchromatic film. This condition restricted the infrared series of Plate XVI to the brighter objects.

* *Contributions from the McDonald Observatory, University of Texas*, No. 99.

[1] This paper was completed while the author was on leave of absence for war research at the Radiation Laboratory, O.S.R.D., Cambridge, Massachusetts.

PLATE XV

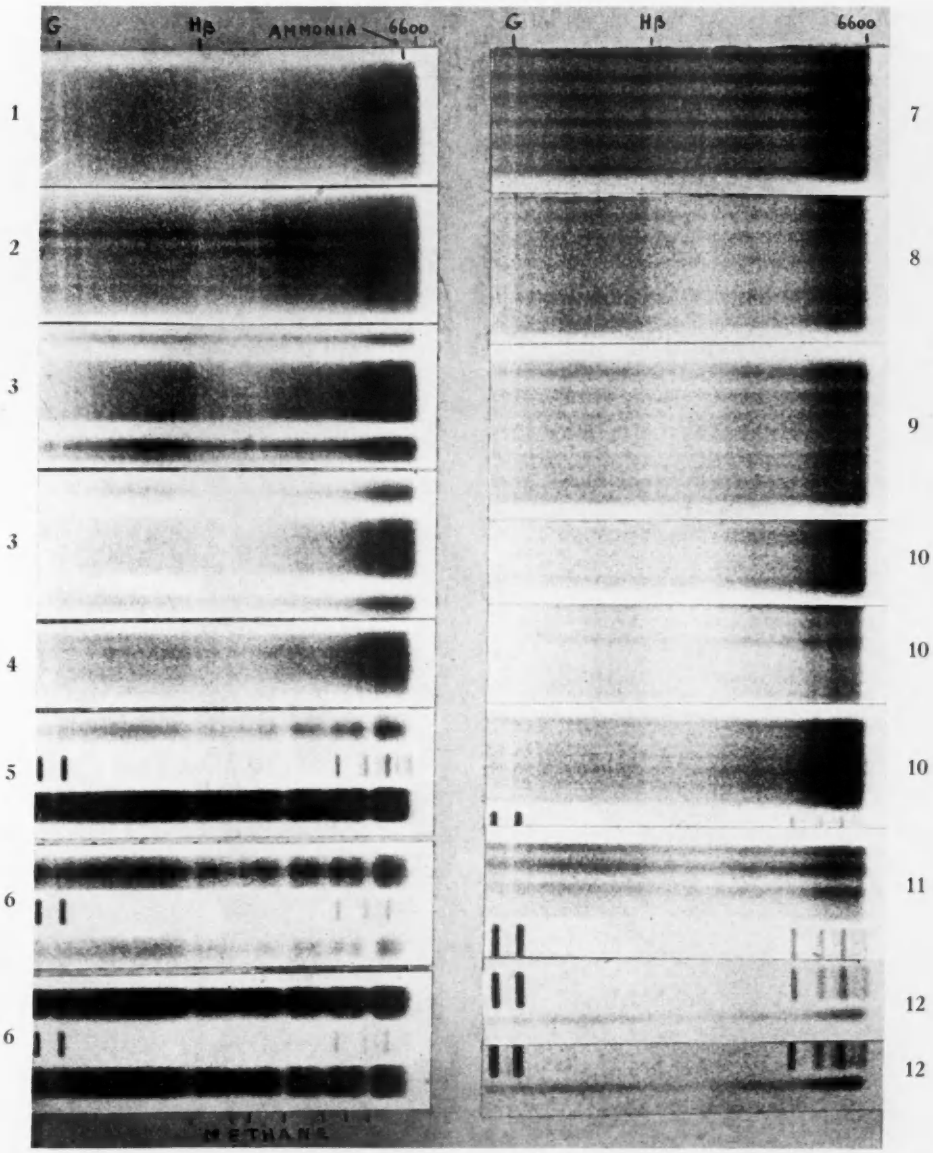

LOW-DISPERSION SPECTRA ON PANCHROMATIC FILM

1. Jupiter, equator
2. Jupiter, through poles (belts show)
3. Saturn and ring
4. Saturn, through poles
5. Uranus
6. Neptune
7. Jupiter II
8. Jupiter III
9. Jupiter IV
10. Titan
11. Rhea
12. Triton

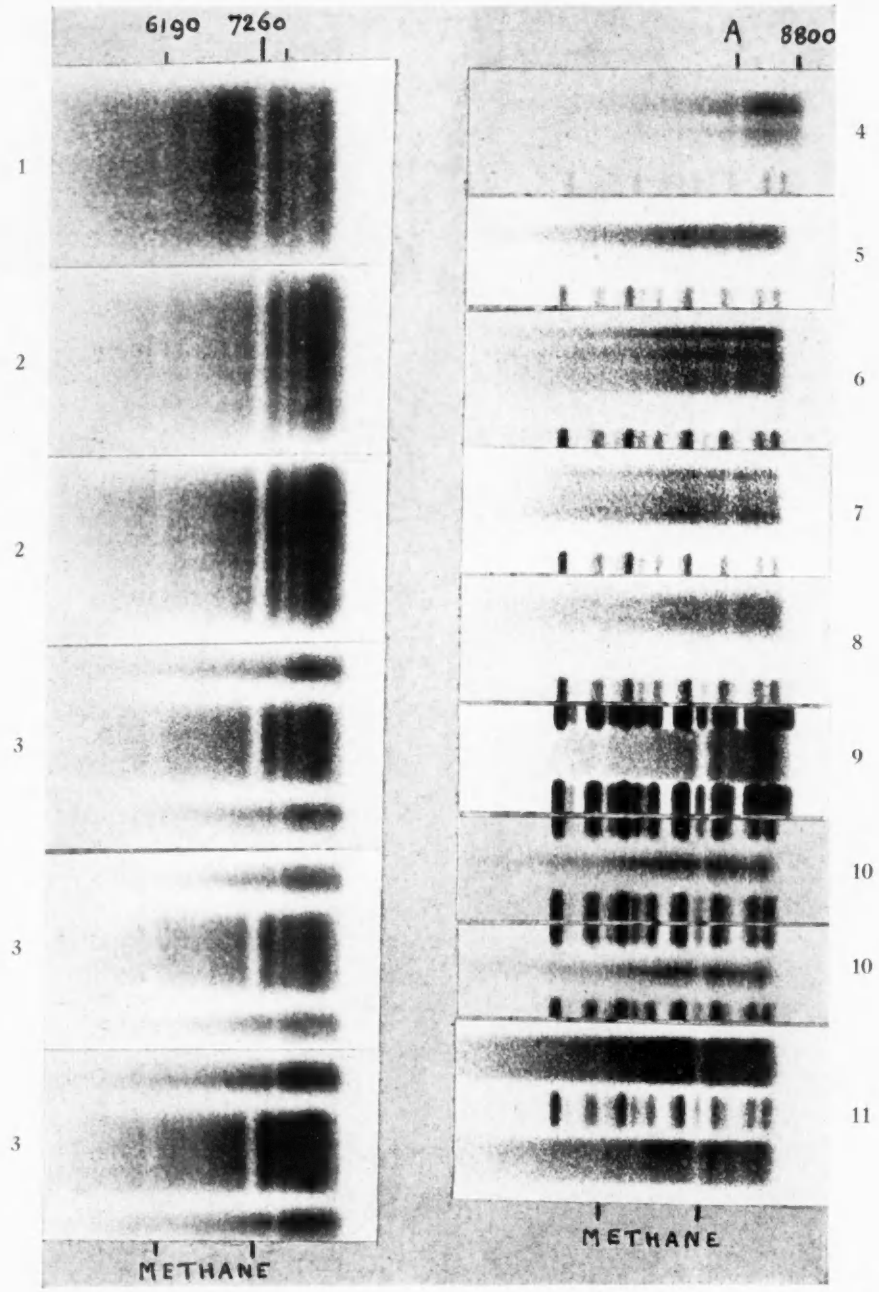

LOW-DISPERSION SPECTRA ON INFRARED FILM

1, 2. Jupiter
3. Saturn and ring
4, 5. Jupiter I
6. Jupiter II
7. Jupiter III
8. Jupiter IV
9. Saturn
10. Titan
11. Jupiter

The sensitivity-curve of the emulsion used in exposures 2, 3, 4, and 9 is somewhat different from the others.

PLATE XVII

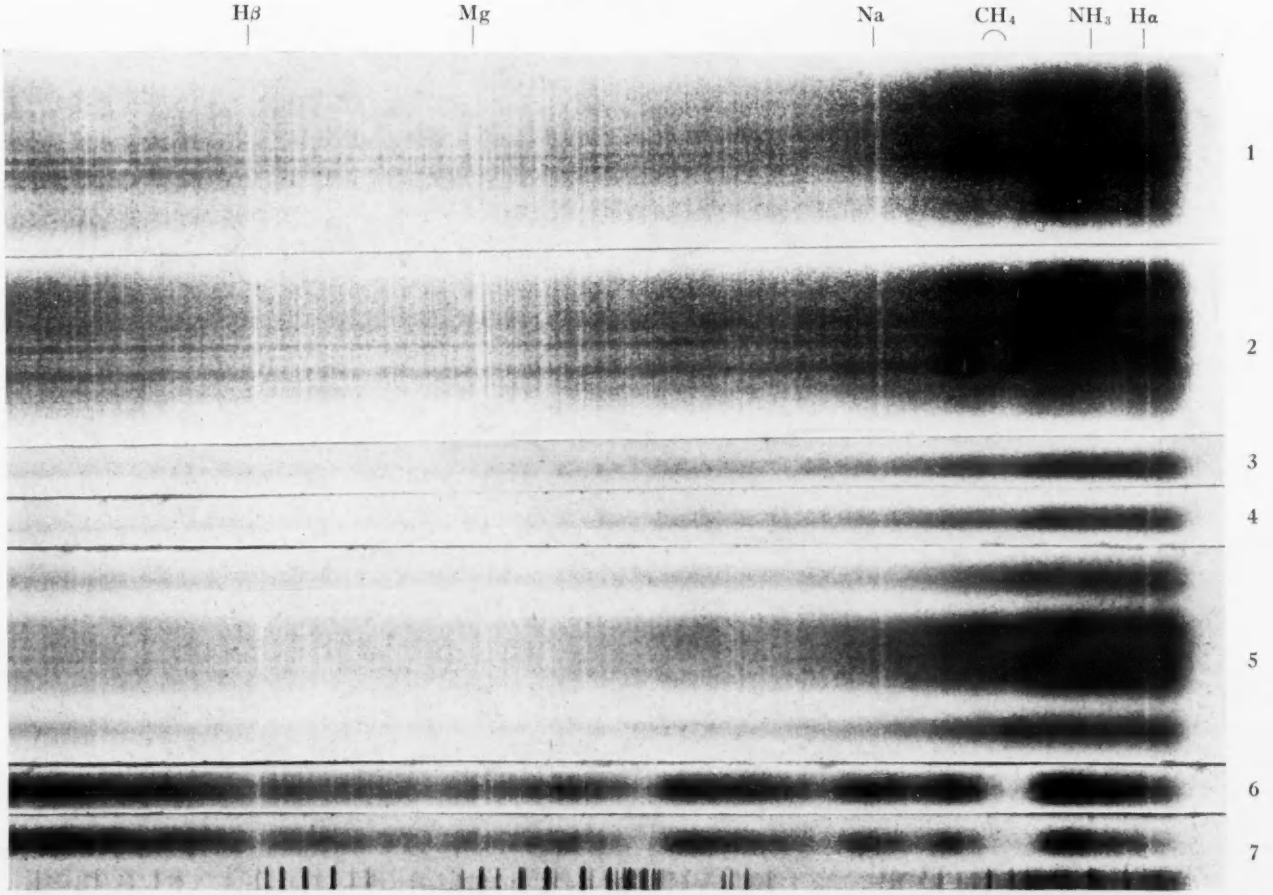

MEDIUM-DISPERSION SPECTRA ON PANCHROMATIC FILM

1, 2. Jupiter 3, 4. Titan 5. Saturn and ring 6. Uranus 7. Neptune

PLATE XVIII

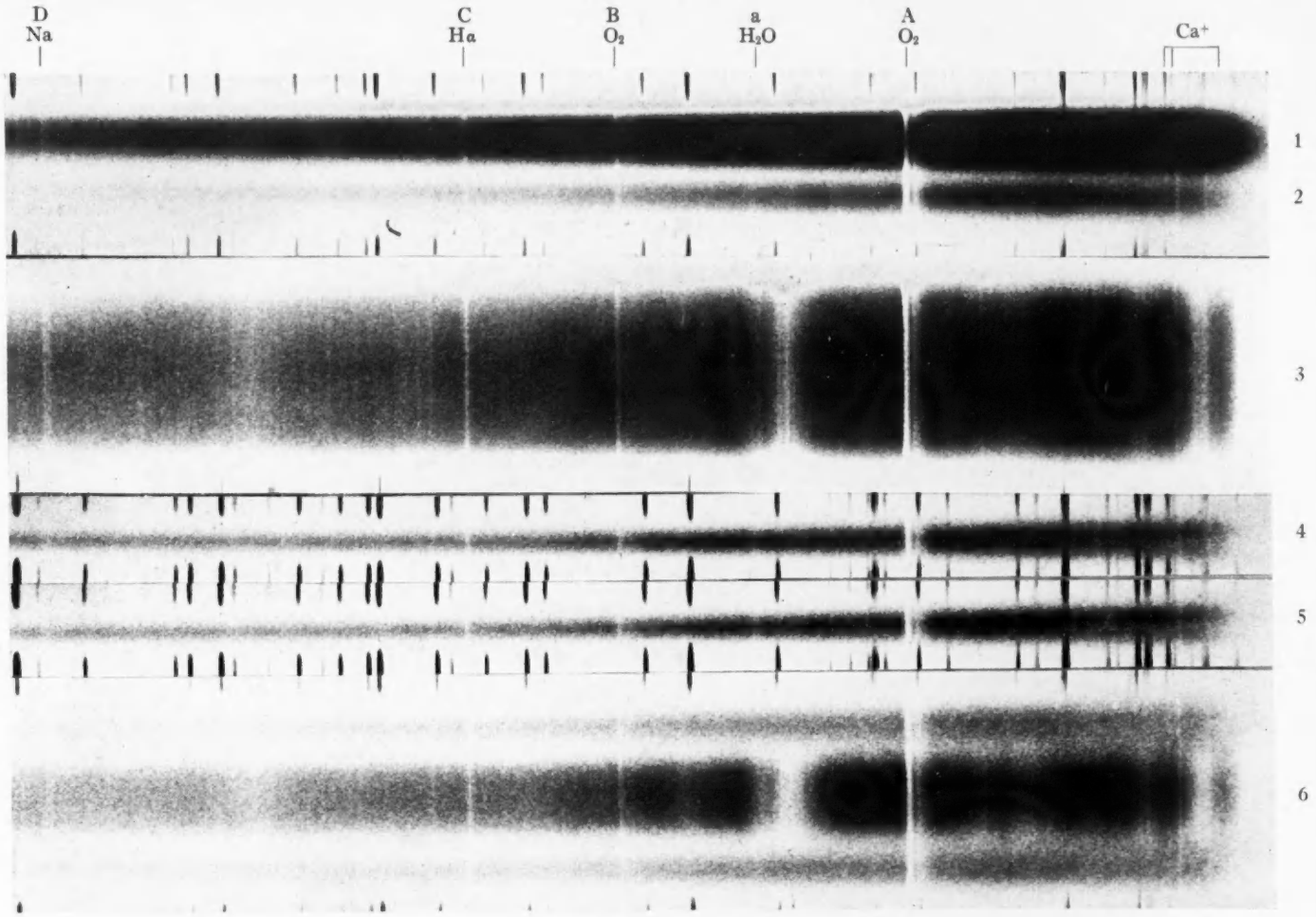

MEDIUM-DISPERSION SPECTRA, INFRARED PLATES

1, 2. Mars 3. Jupiter 4, 5. Jupiter III 6. Saturn and ring

1, 2. Mars 3. Jupiter 4, 5. Jupiter III 6. Saturn and ring

PLATE XIX

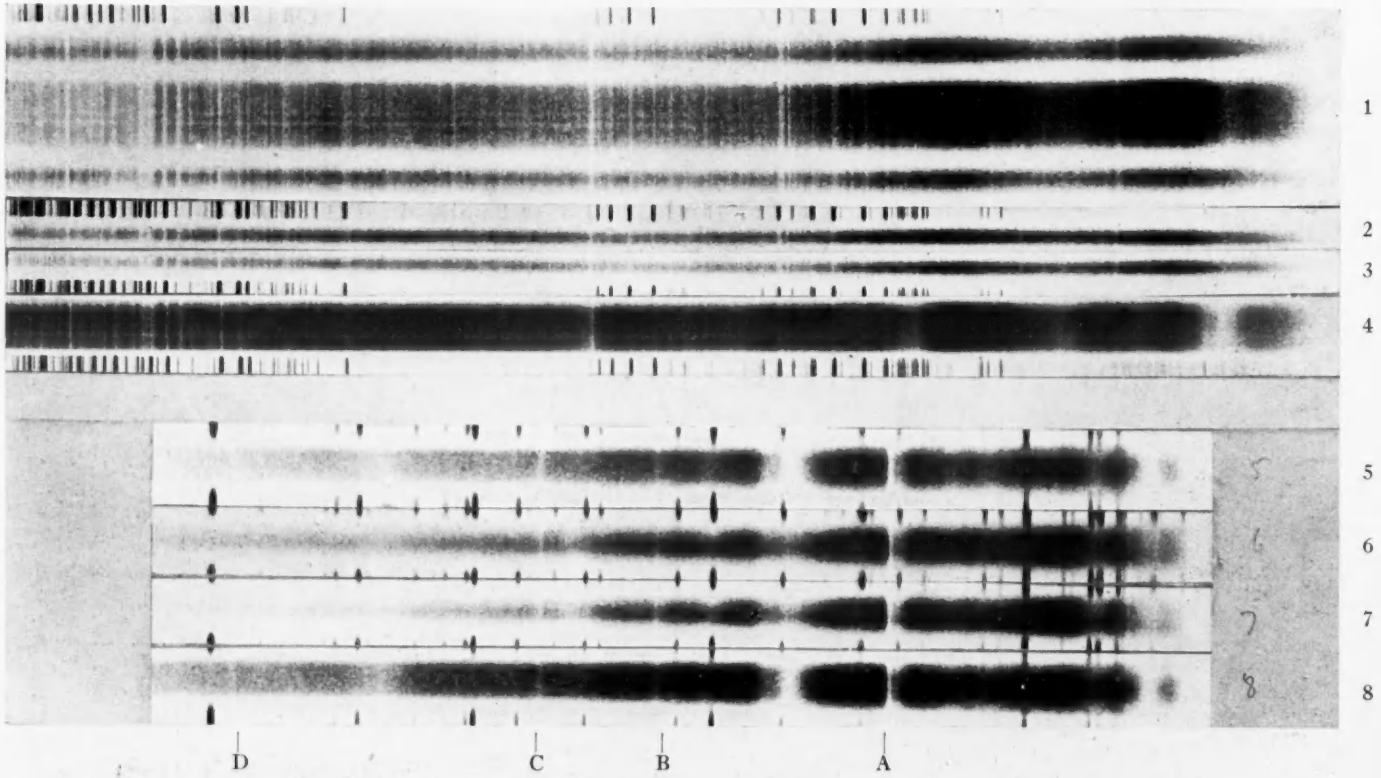

MEDIUM-DISPERSION SPECTRA

1–4. Saturn, Titan, and Uranus, visual region 5, 8. Saturn, infrared 6, 7. Titan, infrared

Plate XVII shows in the center two spectra of Titan (reproduced from the same negative), with spectra of the major planets added for comparison. The large Cassegrain spectrograph was used, with two quartz prisms and a curved plateholder. The dispersion is about 60 A/mm at $H\gamma$. The width of the methane band is so great that the larger dispersion in Plate XVII, as compared to Plate XV, does not lead to a corresponding increase of visibility. The rings of Saturn show the true solar spectrum.

With the aid of a photometer constructed by Dr. E. Dershem some density measures were made from 6000 to 6600 A on spectra of both Saturn and Titan. The density-curves are very similar but show that the methane band λ 6190 A is slightly shallower on Titan. The presence of the ammonia band at λ 6400 A is suspected, but additional plates are needed for a final answer.

The spectra of Plate XVIII were obtained on Eastman 1N plates and with glass prisms. The dispersion is about 26 A/mm at $H\gamma$ and about 140 A/mm at 7000 A. The spectrograph had not been used in the infrared before and was not designed for this region. The definition is remarkably good, although some astigmatism is apparent from the vertical dimensions in the spectra. The comparison spectrum is neon. The 1N plates were ten times faster than the film used in Plate XVI; an additional factor of 6 was gained by hypersensitization in an ammonia bath. In this manner the exposure times required in the infrared for an orange-colored light-source (Mars, Titan) were only about three-fourths of the times required in the red with the same spectrograph.

The objects shown in Plate XVIII are Mars (two exposures), Jupiter, Jupiter III (two prints of the same negative), and Saturn with its ring; the region covered is from 5800 to 8800 A. The plates were not hypersensitized. It is seen that Jupiter III does not show any trace of the methane or the ammonia bands. Its spectrum was obtained in 100 minutes, with the slit width somewhat increased.

Finally, Plate XIX shows two sets of spectra. The upper half is similar to Plate XVII but shows Titan in the photographic region compared to Saturn and Uranus. The only visible deviation from the solar spectrum is the λ 6190 A band of methane, as is seen from a comparison with Saturn's rings.

The lower half of Plate XIX shows Titan in the infrared (two central spectra, derived from one negative), compared to Saturn (two outer spectra). Quartz prisms were used, which gave a slightly lower dispersion in the infrared and a corresponding gain in speed (dispersion 60 A/mm at $H\gamma$ and about 200 A/mm at 7000 A). The plates of Saturn were not ammoniated; the exposure times were 5 and 15 minutes. These plates were kindly taken by Dr. Struve after the writer had left. The Titan plate was ammoniated; the exposure time was 4 hours. The same wide slit was used for both Titan and Saturn.

On the whole, there appears to be a close resemblance between the spectrum of Titan and that of Saturn; but the methane bands on Titan are definitely weaker. There appear to be some anomalous intensity ratios, as, for example, in the double band near λ 7200 A; but further plates are needed for a closer study.

The color contrast between Titan and Saturn shown by the spectra is striking. This is in agreement with telescopic observation, which shows Titan to be orange, like Mars. Saturn, in turn, is more yellow than its ring, as is shown by Plates XVIII (bottom) and XIX (top), a fact previously noted by V. M. Slipher.[2]

Thus, with the reservation stated regarding Triton, it appears that Titan is the only satellite in the solar system having an atmosphere detectable with the means here employed. It is of special interest that this atmosphere contains gases that are rich in hydrogen atoms; such gases had previously been associated with bodies having a large surface gravity. We shall return to this point later. The total thickness of the atmosphere is comparable to, but somewhat less than, that of the observable layers of Saturn and Jupiter, for which Slipher and Adel estimate 0.5 mile-atmospheres of methane gas.[3]

[2] "George Darwin Lecture," *M.N.*, **93**, 657, 1933.

[3] Th. Dunham, Jr., *Pub. A.S.P.*, **51**, 272, 1939.

It is somewhat surprising to find the statement by J. H. Jeans:[4] "An atmosphere has been observed on Titan," and his reference to "the suspected atmospheres on two of Jupiter's satellites." The writer has been unable to find an astronomical source for these statements. Apparently, they are not based on spectroscopic observations and have not been generally accepted, since other writers [5,6,7] make no mention of them. It is difficult to see how ordinary visual observations could have ascertained the presence of an atmosphere on bodies less than 1″ in diameter; in fact, such a thing would seem impossible.

II. MASSES OF THE OBSERVED OBJECTS

Dr. Dirk Brouwer has been kind enough to select from the various published mass determinations the ones that are, in his judgment, the most reliable. He made this compilation in February, 1944. With Dr. Brouwer's permission his list is reproduced in Table 1 of this paper.

Dr. Brouwer made the following additional comments:

> The mass of Rhea is practically unknown. There is an estimate by H. Struve of the ratio Rhea/Saturn = 1/250,000, but I would not give this any weight. Woltjer's mass of Titan is still the best. The masses of Tethys and Dione are quoted from G. Struve. H. Struve for Tethys and Woltjer for Dione had arrived at essentially the same masses. . . . . There is no dynamical determination of the masses of the Uranus satellites. . . . . Alden's mass of Triton is to be used; he had the use of a very accurate ephemeris.
>
> The mass of Pluto is very well determined by its perturbation on Neptune. The same mass satisfies the modern latitude observations [of Neptune] and gives a reasonable residual in longitude for the pre-discovery observations by Lalande in 1795. In practically all my work I have used 0.25×10^{-5}, but any mass between 0.25 and 0.35×10^{-5} will satisfy the observational material nearly equally well. The Lalande residual is improved by the larger mass, but oneshould not stress this too much. There remains for 1795 a residual in latitude of about −1″.5, that cannot be removed by any reasonable adjustment of the orbital elements of Neptune or the mass of Pluto, and a mass of 0.25×10^{-5} would leave only a slightly larger residual in longitude.

III. DISCUSSION

Table 2 shows, for the planets and the satellites, the quantities which determine the stability of the atmospheres. The masses, radii, and densities are expressed in terms of the earth; the data were taken from Table 1 and from Russell, Dugan, and Stewart's *Astronomy*. Radii followed by a colon were derived from magnitudes and assumed albedos.

The computed densities are in some cases improbably low. It may be assumed that the adopted albedos and possibly the magnitudes are responsible for these abnormal results. Since we are dealing with a group of presumably similar small bodies, the assumption of a constant density may be less dangerous than the assumption of constant albedo; moreover, for equal errors in the assumed values the radii are more accurately determined from the densities than from the albedos. Also, the use of the (uncertain) magnitude is avoided.

Table 2 gives two lines for satellites whose computed densities differ considerably from 0.5 times the earth (2.76 times water), the average value adopted for small satellites. Except perhaps for Jupiter III and IV, for which the diameters were measured, the lower entries are probably closer to the truth.

The case of Pluto is puzzling. Either the mass is much smaller, and in reality resembles that of Triton, or the albedo is low and the planet presents a disk of about 0″.5. This point must be cleared up before the stability of an atmosphere can be discussed.

[4] *Dynamical Theory of Gases* (4th ed.), p. 348, Cambridge, 1925.

[5] Russell, Dugan, and Stewart, *Astronomy*, 1926–27.

[6] H. N. Russell, *The Solar System and Its Origin*, 1935.

[7] Th. Dunham, Jr., "Knowledge of the Planets in 1938," *Pub. A.S.P.*, **51**, 253, 1939.

The velocity of escape is given by

$$V_{esc} = \sqrt{\frac{2GM}{R}} = \sqrt{\frac{M}{R}} \times 11.3 \text{ km/sec}, \tag{1}$$

in which both M and R are expressed in terms of the earth. This quantity is listed numerically in Table 2, fifth column.

An atmosphere becomes unstable during astronomical intervals if the root-mean-square velocity of the molecules, V_m, becomes an appreciable fraction of V_{esc} (say, more than one-fifth, a value examined by Jeans).

$$V_m \propto \sqrt{\frac{T}{\mu}}, \tag{2}$$

if T is the Kelvin temperature and μ the molecular weight of the gas.

TABLE 1

Object	Mass of Satellite / Mass of Primary	Mass / Mass of Sun $\times 10^7$	Authority
J I	0.0000381 ± 30 (p.e.)	0.364	De Sitter*
J II	248 ± 5	0.237	De Sitter*
J III	817 ± 10	0.780	De Sitter*
J IV	509 ± 40	0.486	De Sitter*
Tethys	1 ÷ 876,400	0.00326	G. Struve†
Dione	1 ÷ 541,300	0.00529	G. Struve†
Titan	1 ÷ 4033	0.709	Woltjer‡
Triton	0.00128 ± 23 (p.e.)	0.66	Alden§
Pluto	.....	28 ± 8 (p.e.)	Nicholson and Mayall‖
Pluto	.....	25 ± 3	Brouwer, ¶, ††
Pluto	.....	30 ± 3	Wylie**, ††

* W. de Sitter, "George Darwin Lecture, 1931," *M.N.*, **91**, 706, 1931.

† G. Struve, *Pub. Berlin-Babelsberg*, **6**, Part IV, 56, 1930.

‡ J. Woltjer, Jr., *Ann. Leiden*, **16**, Part III, 66, 1928.

§ H. L. Alden, *A.J.*, **50**, 110, 1943.

‖ S. B. Nicholson and N. U. Mayall, *Ap. J.*, **73**, 1, 1931; *Mt. W. Contr.*, No. 417. Based upon longitudes only; i.e., depends principally upon Lalande's 1795 observations.

¶ D. Brouwer, *Pub. A.A.S.*, **10**, 8, 1940.

** L. R. Wylie, *A.J.*, **49**, 101, 1941.

†† Based upon both longitudes and latitudes; essentially the same material. Wylie used Newcomb's tables; Brouwer, a numerical integration. The latter differs extremely little from the tables. From a discussion of various solutions with different weighting I would consider 28 ± 3 the best result.

The value of T varies greatly through the solar system, roughly as $r^{-1/2}$, if r is the distance to the sun. Therefore, by using the parameter, $V_{esc} \cdot r^{1/4}$ (cf. Table 2, col. 7), we have eliminated the temperature effect on the stability. Since the variation in $\sqrt{\mu}$ is probably not large ($CH_4 = 16$; $NH_3 = 17$; $N_2 = 28$; $O_2 = 32$; $CO_2 = 44$) the figures in the last column of Table 2 are a suitable basis for comparison.

The order of decreasing atmosphere stability appears to be: Jupiter, Saturn, Neptune, Uranus, earth, Venus, Triton, Mars, Titan, J III, J IV, J I, J II, Mercury, moon, etc.

Excepting Triton, for which no atmosphere has yet been established, we find that atmospheres drop out between Titan and Jupiter III. Both boundary-line cases have been well observed.

Jeans has shown that an atmosphere is stable for astronomical periods if $V_m < 0.2\ V_{esc.}$ For Titan the right-hand member of this inequality is 1.06 km/sec when reduced to $r=1$. The value of V_m will depend on the albedo and the rate of rotation. Assuming the limiting cases of no rotation and vanishing albedo, the temperature at $r=1$ equals 392° K.[8] The corresponding upper limit of V_m is 0.78 km/sec for CH_4, 0.76 km/sec for NH_3, and 0.47 km/sec for CO_2; but for H_2 it is 2.20 km/sec. Evidently the gases revealed by the spectroscope are stable components of the atmosphere, but hydrogen would escape in a matter of days.

TABLE 2

Body	Mass ⊕	Radius ⊕	Mean Density ⊕	V_{esc} (Km/Sec)	r	$V_{esc} \cdot r^{1/4}$ (Km/Sec)
Earth	1.00	1.00	1.00	11.3	1.00	11.3
Moon	0.0122	0.273	0.60	2.4	1.00	2.4
J I	0.0121	0.293	0.48	2.3	5.20	3.5
J II	0.0079	0.247	0.52	2.0	5.20	3.1
J III	0.0259	0.404	0.39	2.9	5.20	4.3
		0.373	0.50	3.0		4.5
J IV	0.0161	0.406	0.24	2.2	5.20	3.4
		0.318	0.50	2.5		3.8
Titan	0.0235	0.33	0.65	3.0	9.54	5.3
Rhea	0.00038:	0.137:	0.15:	0.60	9.54	1.1
		0.091	0.50	0.73		1.3
Dione	0.00018	0.094:	0.21:	0.49	9.54	0.9
		0.071	0.50	0.56		1.0
Tethys	0.00011	0.102:	0.10:	0.37	9.54	0.6
		0.060	0.50	0.48		0.8
Triton	0.022	0.39:	0.37:	2.7	30.1	6.3
		0.35	0.50	2.8		6.6
Pluto	0.93:	0.4:	.....	.....	.....	.....
Venus	0.81	0.973	0.88	10.3	0.723	9.5
Mars	0.108	0.531	0.72	5.1	1.524	5.7
Mercury	0.04	0.39	0.67	3.6	0.387	2.9
Jupiter	316.9	10.95	0.24	61.	5.20	92.
Saturn	94.9	9.02	0.13	36.6	9.54	64.
Uranus	14.7	4.00	0.23	21.7	19.2	45.
Neptune	17.2	3.92	0.29	23.7	30.1	55.

The stability of Titan's atmosphere would be endangered by a substantial increase in its temperature. Doubling it, i.e., raising it from 100°–125° K to 200°–250° K, would already jeopardize the permanence of CH_4; a still greater increase would cause a very rapid dissipation. Consequently, if Titan has gone through a period with a high surface temperature, as is commonly assumed to be true for all bodies in the solar system, then *it follows that Titan's atmosphere was formed subsequent to that period.* With almost equal force this conclusion follows for Mars, and to a lesser extent for Venus and the earth. In each of these cases all or nearly all of the atmosphere must have escaped from the crust after the crust was essentially cooled off.

The composition of Titan's atmosphere is in striking contrast to that of the earth

[8] Russell, Dugan, and Stewart, *op. cit.*, p. 541.

(N_2, O_2, H_2O, etc.) and of Venus (CO_2). Also, as we have seen, under terrestrial temperatures Titan's atmosphere would rapidly dissipate. On the other hand, the same factors indicate a genetic relationship to Saturn (or the other major planets). They make it highly probable that Titan was formed within the Saturn system and show definitely that Titan was not a product of capture from an (elliptical) orbit extending to the interior regions ($r \ll 5$) of the solar system.

As has been remarked above, the color of Titan is orange, in marked contrast with Saturn and its other satellites or with Jupiter and its satellites. It seems likely that the color is due to the action of the atmosphere on the surface itself, analogous to the oxidation supposed to be responsible for the orange color of Mars.[6]

It has recently been suggested that the atmosphere on Titan was predicted theoretically. Actually, as we have remarked, an observation of doubtful status preceded the theoretical discussion and was used to substantiate it. The nature of the problem is such that a complete theory of the origin of the solar system would be required before it could be predicted which bodies would have atmospheres and what their composition would be. Such a theory does not exist. The kinetic theory of gases can be used only to *deny* the existence of an atmosphere of specified composition on bodies which are too small or too hot at present. An affirmative statement would have to be based on the history of the case. In fact, something is learned about this history from the somewhat unexpected result that Titan has an atmosphere.

THE WOLF-RAYET TYPE SPECTROSCOPIC BINARY HD 152270*

OTTO STRUVE
Yerkes and McDonald Observatories
Received September 10, 1944

ABSTRACT

The broad emission feature of *C* III, *C* IV, and *He* II at λλ 4647–4686 shows oscillations in wave length with $P = 8.82$ days. If the velocity-curve is interpreted as binary motion, the elements are $K = 167.5$ km/sec, $e = 0.24$, $\omega = 10°$, and T = phase 1.3 days = JD 2431212.25. The velocity of the system is uncertain because the normal wave length of the blended emission feature is not known. The central absorptions of the *H* lines also vary in radial velocity in the same period of 8.82 days. The phase of variation is opposite to that of the emission feature. The scatter of the measures is very large, and some of it is probably real. The elements adopted for the corresponding velocity-curve are $\gamma = -44$ km/sec, $K = 45$ km/sec, $e = 0.24$, $\omega = 190°$, and T = phase 1.3 days. It is possible, but not certain, that the velocity-curve from the absorption lines represents the motion of the second component of the binary.

In a recent paper[1] the Wolf-Rayet star HD 152270 was announced as a spectroscopic binary of considerable range in radial velocity. The spectrum of this star[2] is WC6+, according to P. Swings,[3] who has given a complete description of the spectroscopic features. The spectrum is characterized by a very intense emission band at λ 4647, which is a blend of several lines of *C* III and *C* IV. The band terminates abruptly on the violet edge, where it is bordered by a strong violet absorption line of considerable strength and width. On the red side the λ 4647 emission band is blended with a somewhat weaker emission band, due to *He* II 4686. The rest of the spectrum in the ordinary photographic region shows only a faint continuous spectrum with a number of weak and very broad emission bands, all of which are too diffuse for measurement. The *H* emission bands have central absorptions, as have also the Pickering lines of *He* II and probably several lines of *He* I. Attention was first directed to these central absorptions by Mrs. C. Payne-Gaposchkin.[4] Swings[5] has summarized several attempts to explain these lines and has concluded that they do not come from a stationary outer shell because there is no indication of the dilution effect in the *He* I lines. Nor does it appear probable to Swings that they come from the underlying nucleus of the WR star, because that would require the ionization of the nucleus to be lower than that of the shell. But Swings leans toward the idea that the central absorptions are produced in the WR star and not in the atmosphere of some other star.

At the present time we know the orbits of only two other Wolf-Rayet stars.[6] Both stars belong to the nitrogen sequence. The star HD 152270 is the first member of the carbon sequence to be investigated as a spectroscopic binary. Its emission lines are broad and correspond to a velocity of expansion of the order of 2000 km/sec. The star is a member of the galactic cluster NGC 6231.

* *Contributions from the McDonald Observatory, University of Texas*, No. 100.

[1] *Ap. J.*, **100**, 199, 1944.

[2] $\alpha = 16^h47^m.3$; $\delta = -41°40'$ (1900); Sp., Oa; mag. ptm., 6.72.

[3] *Ap. J.*, **95**, 112, 1942.

[4] *Harvard Bull.*, No. 844, p. 16, 1927, and No. 874, p. 24, 1930.

[5] *Op. cit.*, p. 127.

[6] HD 193576, investigated by O. C. Wilson (*Ap. J.*, **91**, 379, 1940; **95**, 402, 1942) and HD 214419, investigated by W. A. Hiltner (*Ap. J.*, **99**, 273, 1944).

Because of the blended character of the emission at λ 4647 and the unsymmetrical character of the combined feature due to *C* III, *C* IV, and *He* II, the spectrograms were measured with the Zeiss blink-comparator of the Yerkes Observatory. This instrument is

TABLE 1

RADIAL VELOCITIES OF HD 152270

Plate	1944	U.T.	JD	Phase in Days	Vel. Em. 4647 + x	Vel. Abs. $H\gamma$
			2431+			
3077	Apr. 30	10:43	210.95	0.00	+217 km/sec	− 53 km/sec
3091	May 1	8:30	211.85	0.90	+306	− 80
3113	2	8:04	212.84	1.89	+189	− 92
3141	5	9:44	215.91	4.96	− 10	− 40
3152	6	8:55	216.87	5.92	− 11	+ 13
3523	Jul. 21	4:03	292.67	2.34	+184	− 66
3529	25	3:34	296.65	6.32	− 11	− 52
3530	25	3:40	296.65	6.32	0	− 3
3537	26	3:21	297.64	7.31	+ 97	+ 1
3538	26	3:32	297.65	7.32	+ 48	+ 12
3540	27	4:20	298.68	8.35	+155	0
3541	27	4:29	298.69	8.36	+ 89	− 57
3544	28	3:18	299.64	0.49	+309	− 98
3545	28	3:25	299.64	0.49	+320	−145
3551	29	3:12	300.63	1.48	+363	−126
3552	29	3:20	300.64	1.49	+251	− 15
3559	30	3:27	301.64	2.49	+170	− 53
3560	30	3:32	301.65	2.50	+151	− 42
3564	31	2:28	302.64	3.49	+133	− 43
3565	31	2:34	302.65	3.49	+ 54	− 9
3569	Aug. 1	2:26	303.60	4.45	+ 35	+ 6
3570	1	2:38	303.61	4.46	− 10	− 32
3574	2	2:20	304.60	5.45	− 32	− 77
3575	2	2:27	304.61	5.46	− 61	− 70
3580	3	2:19	305.60	6.45	+ 20	− 21
3581	3	2:25	305.60	6.45	− 48	− 36
3585	4	2:22	306.60	7.45	+ 27	+ 28
3586	4	2:28	306.60	7.45	+ 1	− 51
3591	5	2:20	307.60	8.45	+169	− 97
3593	5	2:54	307.62	8.47	+177	−120
3595	6	2:25	308.60	0.63	+213	− 37
3598	9	2:18	311.60	3.63	+ 11	+ 1
3599	9	2:24	311.60	3.63	+ 4	−144
3602	10	3:35	312.65	4.68	− 4	.....
3603	10	3:43	312.66	4.69	− 4	.....
3604	11	2:16	313.59	5.62	− 35	+ 12
3605	11	2:22	313.60	5.63	+ 3	− 7
3609	13	2:14	315.59	7.62	+ 25	− 23
3610	13	2:20	315.60	7.63	+ 40	− 46
3614	14	2:37	316.61	8.64	+145	−114
3615	14	2:45	316.61	8.64	+281	−168
3617	16	3:01	318.63	1.84	+322	.....
3618	16	3:10	318.63	1.84	+270	.....
3620	16	4:33	318.69	1.90	+282	−134

equipped with a micrometer at the eyepiece. The plate CQ 3530 of July 25, 1944, was adopted as a standard; and the velocities in Table 1 for the emission feature refer to it as zero point. Since the normal wave length of the blended structure is not known, these velocities are all relative. Hence they are designated in Figure 1 and in Table 2 as $x +$ velocity. Similarly, the velocity of the system is also relative and is designated as $x + \gamma$.

The absorption velocities depend upon $H\gamma$ and were obtained in the usual manner. They are not affected by an uncertainty in zero point. But it must be emphasized that, while these absorption lines are mostly due to H, there is no way to estimate the effect of blending with *He* II. Hence the velocity of the system determined from the absorption lines is

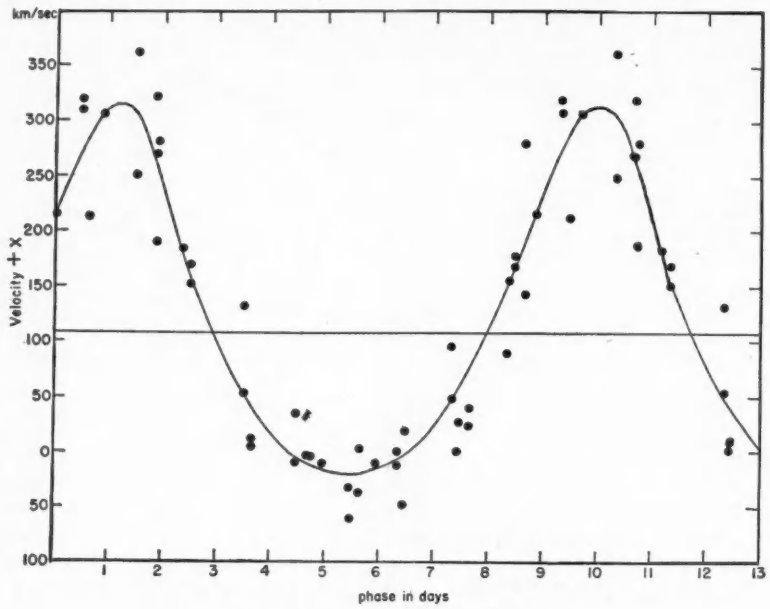

FIG. 1.—Velocity-curve from emission lines

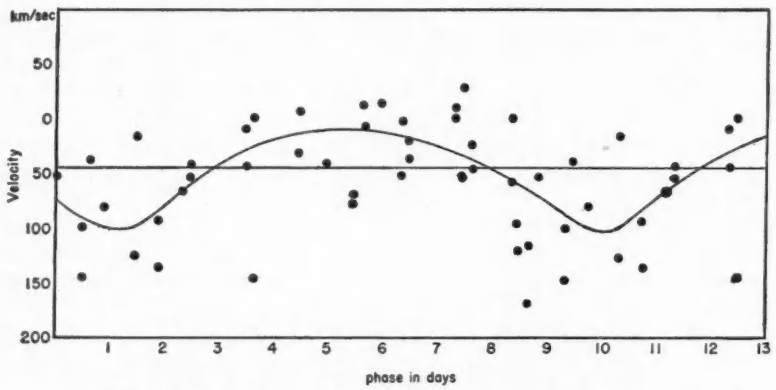

FIG. 2.—Velocity-curve from central hydrogen absorption lines

also uncertain and should not be used for a comparison with the velocity of the cluster NGC 6231, which is −29.1 km/sec. My plates are not suitable for the measurement of *He* II 4200 and *He* II 4541. An effort should be made to obtain these lines on plates of greater contrast than the emulsion used in this work (Eastman 103aO).

The velocity-curves for emission and absorption are shown in Figures 1 and 2, respectively. The period used was 8.82 days. It should be remembered that, because of the low

southern declination of this star, the observations were all made near the meridian. It is therefore not possible to eliminate periods in the vicinity of 1 day. The spectrograms used in this work were taken with the quartz Cassegrain spectrograph of the McDonald Observatory and a 500-mm camera giving a linear dispersion of 40 A/mm at λ 3930. The exposure times were approximately 5 minutes, and the star was carefully trailed along the slit in order to make the spectra as independent of the seeing as possible. The zero point in phase was arbitrarily assumed to be JD 2431210.95 = 1944, April 30, 10:43 U.T.

The two velocity-curves are clearly opposite to one another in phase. Despite the large scatter in the absorption velocities, which is probably in part real, this conclusion is quite

TABLE 2

ORBITAL ELEMENTS OF HD 152270

Element	Emission	Absorption
P	8.82 days	8.82 days
γ	$+108-x$ km/sec	-44 km/sec
K	167.5 km/sec	45 km/sec
e	0.24	0.24
T	Phase 1.3 days	Phase 1.3 days
ω	$+10°$	$+190°$

safe. It suggests that the absorption lines may belong to the second component of the binary, which would then be an absorption O-type star. But I am not certain that this interpretation is correct. It is my impression that the absorption lines are too deep to be explained in this manner. For example, in the illustration given by Swings[7] the absorption line at $H\beta$ cuts into the emission band in a manner which suggests that this band itself experiences absorption—not only the weak underlying background of continuous spectrum. But perhaps this impression is deceptive. It will be necessary to obtain accurate measurements of the residual central intensities of the absorption lines before this question can be answered.

The approximate orbital elements derived from the two velocity-curves are given in Table 2.

[7] *Op. cit.*, Pl. V, star 6.

RECENT PROGRESS IN ASTROPHYSICS

"PHYSICAL CHARACTERISTICS OF THE ATMOSPHERES OF SUPERGIANTS OF CLASSES cB5 TO cA3"
BY G. A. SHAJN

Bulletin No. 7 of the Abastumani Astrophysical Observatory on Mount Kanobili in the Caucasus contains, among other important papers, an article by Shajn which is closely related to recent investigations by Pannekoek, Beals, and the reviewer. It was first pointed out by Pannekoek[1] that the contours of the *H* absorption lines in α Cygni and in the Cepheid variables lead to values of the surface gravity g_{eff} which are about one hundred times smaller than the values *g* computed with the help of the masses and the radii of the stars. This extremely important consideration suggests that a large part of the reversing layers of early-type supergiants may be supported against gravity by radiation pressure, and Shajn points out that a slight disturbance of the physical conditions in the stars might even produce expanding atmospheres similar to those of novae or of P Cygni-type stars. In a somewhat similar manner Beals has stressed the probable relationship between such stars as α Cygni, P Cygni, and the Wolf-Rayet group of objects. Similar ideas have been discussed by the reviewer.

Shajn devotes the first section of the paper to a critical analysis of Pannekoek's argument. He has measured the contours of $H\gamma$ and $H\delta$ in seven supergiants and has derived from these values of g_{eff} which range from 1.0 to 1.4. The theory of Verwej, which was used in these determinations, considers only the so-called statistical Stark effect. Recent investigations by Mrs. Krogdahl show that collisional broadening is also important. However, it is almost certain that the theory of Verwej gives approximately correct values of g_{eff}. For stars of the main sequence his curves certainly give values which agree with those derived from the mass and the radius. Hence it is safe to suppose that Shajn's determinations of g_{eff} are correct as to order of magnitude. But the question arises next whether the masses of the supergiants are known with sufficient precision. Shajn remarks that Pearce's star—a spectroscopic binary of type cB9—has a mass which is consistent with the mass-luminosity relation. Nor does it seem possible that the absence of *H* wings in the supergiants can be caused by low abundance of hydrogen, because the jump at the Balmer limit in these stars is approximately normal.

The second section of the paper is apparently a greatly condensed account of a detailed investigation of the equivalent widths in supergiants and main-sequence stars. As an example of the character of the results, Shajn gives a comparison of α Cygni (cA2) and ε Serpentis (dA2). He concludes that (1) all the lines of the neutral atoms *Fe* I, *Mg* I, *Cr* I, *Ni* I, *Co* I, and *Ca* I are stronger in the dwarfs; (2) the lines of the ions *Fe* II, *Si* II, *Ti* II, *Cr* II, *Ni* II, and *Mg* II are much stronger in the supergiants; and (3) the resonance lines of *Sr* II, *Ba* II, *Ca* I, *Cr* I, and *Mn* I are much stronger in the dwarfs. Qualitatively these differences agree with the conclusion that α Cygni is more luminous than ε Serpentis. But quantitatively, according to Shajn, they support the value of between 50 and 100 for the ratio g/g_{eff} obtained from the *H* lines. This conclusion is borne out by the entire appearance of the supergiant spectra. They differ far more radically from the spectra of main-sequence stars than the spectra of G-type giants differ from those of G-type dwarfs. And yet the dynamical values of *g* are about 10^3 and 10^4 in the first case

[1] *B.A.N.*, No. 301, 1937.

and 10^3 and $10^{4.4}$ in the second. It is clear that the dynamical value of g does not serve to characterize the absorption-line spectra of the early-type supergiants.

Perhaps the most significant part of Shajn's paper deals with the radial velocities of a selected group of early-type supergiants. He concludes that, since an appreciable portion of the reversing layers of these stars is suspended against gravity by general and monochromatic radiation pressure, it is possible that there exists a tendency for these layers to expand. It is also possible that the rate of expansion might not be the same for all elements. For 47 c stars chosen from the list by Merrill, 4 stars observed by Harper, and 1 star observed by Young, Shajn made a solution for solar motion and galactic rotation, retaining the K-term in his equation. The result was $K = -6.8 \pm 1.8$ km/sec. Several other solutions were made by him with the same material but with assumed positions for the solar apex and the galactic center. The result was $K = -5.3 \pm 1.1$ km/sec. Shajn next included in his solution all those stars of spectral classes B5–A7 which were used by R. E. Wilson[2] in his study of the luminosities of the nonvariable c stars. Shajn finds $K = -4.9 \pm 1.5$ km/sec. Wilson's result, using all c stars of classes cB–cM (205 in

TABLE 1

Star	Radial Velocity *Ca* II *minus H, He*	
	Uncorrected	Corrected
β Ori	−5.4±0.8	−4.6
67 Oph	−5.0±1.1	+0.2
4 Lac	+2.2±0.8	−4.5
2 Hev	−4.6±1.1	−5.0
σ Cyg	−0.6±0.8	+2.9
α Cyg	−2.5±0.5	−1.5
η Leo	+1.0±0.9	+0.2

number), was $K = -2.00 \pm 0.80$ km/sec. Shajn sees in this evidence of a change in K with spectral type. The probable existence of a negative K-effect among the supergiants of early type is an interesting and unexpected result. It should certainly be tested with the help of new material.

Shajn has next determined from his own spectrograms the difference in radial velocity obtained from the *Ca* II lines and from the lines of *H* and *He* I. The results are given in the second column of Table 1. He has also attempted to correct these differences for the influence of the interstellar lines of *Ca* II. These corrected values are given in the third column. The conclusion is that "at least for several supergiants, cB7–cA2, systematic negative displacements for K and H may be considered as highly probable." In terms of McCrea's theory[3] this would suggest a density of not more than 10^8 or 10^9 particles per cubic centimeter. Incidentally, Shajn points out that the radial velocities of the two components of β Orionis do not support the contention of an expanding atmosphere in the supergiant. Shajn finds +21.0 for the supergiant and +16.9 km/sec for the faint B5 component. Moore lists +23.6 for the former, while Sanford gives +19.1 for the latter.

O. Struve

[2] *Ap. J.*, **93**, 212, 1941. [3] *M.N.*, **95**, 509, 1935.

NOTES

A CHANGE IN THE SPECTRUM OF 39 ϵ CAPRICORNI

In 1943 McLaughlin[1] described this star (MWC 373 = HD 205637; $\alpha = 21^h31^m.5$, $\delta = -19°54'$ [1900]; mag. 4.7; Sp. B5pe) as follows:

> The spectrum is characterized by well-defined hydrogen emission lines with strong sharp central absorption and by variable enhanced metallic absorption lines, which emerged to visibility in 1929, faded in 1931, remained absent through 1935, and reappeared previous to September, 1936. The metallic lines were present from 1936 to 1939, absent 1941–1942. *The sharp central absorption of the hydrogen lines remains unchanged.* $V = R$ at $H\beta$.

The Yerkes spectrograms of ϵ Capricorni, which extend as far back as 1915, agree with this description. It is, therefore, of special interest that the sharp absorption cores of *H*, which are of the shell-type, have suddenly disappeared. They were present on September 8, 1944, and were not distinctly seen October 12, 18, 20, and 26. A closer inspection of our plates shows that the shell absorption cores of *H* were very strong in 1943, until at least December 19, and were only slightly weaker on July 25, 1944. A plate taken on August 4 shows the *H* cores somewhat weaker. The double emission lines at $H\beta$ were well visible in 1942 but were not seen clearly on any plates taken in 1943 or 1944. At the present time the spectrum is that of an ordinary B3nn star ($H\alpha$ has not been observed) without emission lines. The absorption line *Mg* II 4481, which was frequently observed in the past, and which had an intermediate width between the *He* I lines and the sharp, variable metallic lines, is not now visible. As in some other stars of the same type, this line of intermediate diffuseness belongs to the variable shell spectrum and not to the underlying rapidly rotating reversing layer.

It should be noted that Miss Cannon[2] had observed changes in the *H* absorption lines prior to 1900.

O. Struve
A. J. Deutsch

Yerkes Observatory
October 27, 1944

[1] *Ap. J.*, **98**, 164, 1943.

[2] *Harvard Ann.*, **28**, 183, 1897.

INDEX TO VOLUME 100

INDEX TO SUBJECTS

Absorption Coefficient, Some Remarks on the Negative Hydrogen Ion and Its. *S. Chandrasekhar* . . . 176

Absorption Continuum of the Negative Oxygen Ion, On the. *Rupert Wildt and S. Chandrasekhar* . . . 87

Andromeda Nebula, The Resolution of Messier 32, NGC 205, and the Central Region of the. *W. Baade* . . . 137

Bethe's Law of Energy Generation, An Approximate Solar Model on. *N. R. Sen and U. R. Burman* . . . 347

B-Type Stars, Studies of Faint. II. *Daniel M. Popper* . . . 94

α^2 Canum Venaticorum, Doubly Ionized Rare Earths in. *P. Swings* . . . 132

39ϵ Capricorni, A Change in the Spectrum of. *O. Struve and A. J. Deutsch* . . . 390

RX Cassiopeiae, The Eclipsing System. *Sergei Gaposchkin* . . . 230

SX Cassiopeiae, The Eclipsing System. *Sergei Gaposchkin* . . . 221

13 Ceti, A Report on New Spectrographic Material of. *Carl August Bauer* . . . 302

Color Index and Effective Wave Length from the Observations of Hertzsprung and Vanderlinden, Relation between. *Frederick H. Seares and Mary C. Joyner* . . . 264

Comets 1940c and 1942g, Comparison of the λ 3883 *CN* Band in the Spectra of. *Andrew McKellar* . . . 69

Cosmic Static. *Grote Reber* . . . 279

Cowling Model, The Generalized. *Marjorie Hall Harrison* . . . 343

V 444 Cygni, Provisional Elements of the Eclipsing Binary. *Henry Norris Russell* . . . 213

V 444 Cygni, A Study of the Wolf-Rayet Eclipsing Binary HD 193576= . *Zdeněk Kopal* 204

31 Cygni, The Spectroscopic Binary. *Julie M. Vinter Hansen* . . . 8

Eclipsing Binary HD 193576 = V 444 Cygni, A Study of the Wolf-Rayet. *Zdeněk Kopal* . 204

Eclipsing Binary V 444 Cygni, Provisional Elements of the. *Henry Norris Russell* . . . 213

Eclipsing Star AR Monocerotis, The. *Cecilia Payne Gaposchkin* . . . 251

Eclipsing Star BD Virginis, The. *Cecilia Payne Gaposchkin* . . . 186

Eclipsing System RX Cassiopeiae, The. *Sergei Gaposchkin* . . . 230

Eclipsing System SX Cassiopeiae, The. *Sergei Gaposchkin* . . . 221

Eclipsing Variable HV 11086 = HD 214419, The Wolf-Rayet. *Sergei Gaposchkin* . . . 242

Effective Wave Length from the Observations of Hertzsprung and Vanderlinden, Relation between Color Index and. *Frederick H. Seares and Mary C. Joyner* . . . 264

Galaxies, Two New Members of the Local Group of, NGC 147 and NGC 185. *W. Baade* . 147

η Geminorum, The Spectrographic Orbit and Light-Variations of. *Dean B. McLaughlin and Suzanne E. A. Van Dijke* . . . 63

Helium Anomaly in ϕ Persei, The. *J. A. Hynek* . . . 151

Helium Atom in Its Excited States, The Interaction of a Proton and a. *Margaret Kiess Krogdahl* . . . 333

Hydrogen Atom in Its Excited States, The Interaction of a Proton and a. *Margaret K. Krogdahl* . . . 311
Hydroxyl Radical, Solar Concentrations of the. *Robert J. Dwyer* . . . 300
Interaction of a Proton and a Helium Atom in Its Excited States, The. *Margaret Kiess Krogdahl* . . . 333
Interaction of a Proton and a Hydrogen Atom in Its Excited States, The. *Margaret K. Krogdahl* . . . 311
Interstellar Gas, On the Origin of Smoke Particles in the. *D. ter Haar* . . . 288
Jupiter, Orbit of the Ninth Satellite of. *Seth B. Nicholson* . . . 57
48 Librae, Spectroscopic Observations of. *Paul W. Merrill and Roscoe F. Sanford* . . . 14
Lunar Atmosphere, An Upper Limit for the Mass of the. *Otto Struve* . . . 104
Messier 32, NGC 205, and the Central Region of the Andromeda Nebula, The Resolution of. *W. Baade* . . . 137
AR Monocerotis, The Eclipsing Star. *Cecilia Payne Gaposchkin* . . . 251
AR Monocerotis, The Spectroscopic Orbit of. *Jorge Sahade and Carlos U. Cesco* . . . 374
BN Monocerotis: An N-Type Variable. *Frank K. Edmondson and Henry Giclas* . . . 1
Negative Hydrogen Ion, On the Absorption Continuum of the. *Rupert Wildt and S. Chandrasekhar* . . . 87
Negative Hydrogen Ion and Its Absorption Coefficient, Some Remarks on the. *S. Chandrasekhar* . . . 176
NGC 147 and NGC 185, Two New Members of the Local Group of Galaxies. *W. Baade* . 147
NGC 205, and the Central Region of the Andromeda Nebula, The Resolution of Messier 32. *W. Baade* . . . 137
NGC 6231, Radial Velocities of Twenty Stars of Early Type in and near the Galactic Cluster. *O. Struve* . . . 189
Parallaxes with the 60- and 100-Inch Reflectors, The Photographic Determination of Stellar: Nineteenth Series. *Adriaan van Maanen* . . . 55
h Persei, The Proper Motion of the Cluster. Investigations on Proper Motion. XXIII. *Adriaan van Maanen* . . . 31
ϕ Persei, The Helium Anomaly in. *J. A. Hynek* . . . 151
Pleiades, The Radial Velocities of the. *Burke Smith and Otto Struve* . . . 360
Polarizing Monochromator, Effect of Temperature on the Wave Length of a Transmission Band of the Interference. *Edison Pettit* . . . 128
Proper Motion, Investigations on. XXIII. The Proper Motion of the Cluster *h* Persei. *Adriaan van Maanen* . . . 31
Proton and a Helium Atom in Its Excited States, The Interaction of a. *Margaret Kiess Krogdahl* . . . 333
Proton and a Hydrogen Atom in Its Excited States, The Interaction of a. *Margaret K. Krogdahl* . . . 311
Radial Velocities of the Pleiades, The. *Burke Smith and Otto Struve* . . . 360
Radial Velocities of Twenty Stars of Early Type in and near the Galactic Cluster NGC 6231. *O. Struve* . . . 189
Radiative Equilibrium of a Stellar Atmosphere, On the. II. *S. Chandrasekhar* . . . 76
Radiative Equilibrium of a Stellar Atmosphere, On the. III. *S. Chandrasekhar* . . . 117

Radiative Equilibrium of a Stellar Atmosphere, On the. IV. *C. U. Cesco, S. Chandrasekhar, and J. Sahade* 355
Rare Earths in α^2 Canum Venaticorum, Doubly Ionized. *P. Swings* 132
Regression Lines and the Functional Relation. *Frederick H. Seares* 255
Reviews:
Bok, Bart J., and Frances W. Wright. *Basic Marine Navigation* (J. Cuffey) . . . 115
Pierce, Newton L., and John Q. Stewart. *Marine and Air Navigation* (Oliver Justin Lee) 115
Stewart, John Q., and Newton L. Pierce. *Marine and Air Navigation* (Oliver Justin Lee) 115
Wright, Frances W., and Bart J. Bok. *Basic Marine Navigation* (J. Cuffey) 115
Satellite with an Atmosphere, A: Titan. *Gerard P. Kuiper* 378
Satellite of Jupiter, Orbit of the Ninth. *Seth B. Nicholson* 57
Scorpii, A. Unsöld's Work on the Spectrum of the B0 Star. *Otto Struve* 105
Solar Model on Bethe's Law of Energy Generation, An Approximate. *N. R. Sen and U. R. Burman* 347
Spectra of Comets 1940c and 1942g, Comparison of the λ 3883 *CN* Band in the. *Andrew McKellar* 69
Spectrographic Material of 13 Ceti, A Report on New. *Carl August Bauer* 302
Spectrographic Orbit and Light-Variations of η Geminorum, The. *Dean B. McLaughlin and Suzanne E. A. Van Dijke* 63
Spectroscopic Binary HD 152270, The Wolf-Rayet Type. *Otto Struve* 384
Spectroscopic Binary 31 Cygni, The. *Julie M. Vinter Hansen* 8
Spectroscopic Observations of 48 Librae. *Paul W. Merrill and Roscoe F. Sanford* . . . 14
Spectroscopic Orbit of AR Monocerotis, The. *Jorge Sahade and Carlos U. Cesco* . . . 374
Spectroscopic Orbit of BD Virginis, The. *Otto Struve, Carlos U. Cesco, and Jorge Sahade* . 181
Spectrum of the B0 Star τ Scorpii, A Unsöld's Work on the. *Otto Struve* 105
Spectrum of 39ϵ Capricorni, A Change in the. *O. Struve and A. J. Deutsch* 390
Stellar Atmosphere, On the Radiative Equilibrium of a. II. *S. Chandrasekhar* 76
Stellar Atmosphere, On the Radiative Equilibrium of a. III. *S. Chandrasekhar* . . . 117
Stellar Atmosphere, On the Radiative Equilibrium of a. IV. *C. U. Cesco, S. Chandrasekhar, and J. Sahade* 355
Stellar Models, Partially Degenerate. *Gordon W. Wares* 158
Sunspot Belts, Note on the Latitude Variation of the. *W. Gleissberg* 219
Sunspot Maximum, Note on the Epoch of the Next. *W. Gleissberg* 114
Supergiants of Classes cB5 to cA3, Physical Characteristics of the Atmospheres of, by G. A. Shajn. *O. Struve* 388
Titan: A Satellite with an Atmosphere. *Gerard P. Kuiper* 378
Variable, An N-Type: BN Monocerotis. *Frank K. Edmondson and Henry Giclas* . . . 1
BD Virginis, The Eclipsing Star. *Cecilia Payne Gaposchkin* 186
BD Virginis, The Spectroscopic Orbit of. *Otto Struve, Carlos U. Cesco, and Jorge Sahade* . 181
White Dwarf L 462-56 = LDS 275, Note on the Double. *W. J. Luyten* 202
Wolf-Rayet Eclipsing Binary HD 193576 = V 444 Cygni, A Study of the. *Zdeněk Kopal* 204
Wolf-Rayet Eclipsing Variable HV 11086 = HD 214419, The. *Sergei Gaposchkin* . . 242
Wolf-Rayet Type Spectroscopic Binary HD 152270, The. *Otto Struve* 384

INDEX TO AUTHORS

BAADE, W. NGC 147 and NGC 185, Two New Members of the Local Group of Galaxies . 147

BAADE, W. The Resolution of Messier 32, NGC 205, and the Central Region of the Andromeda Nebula 137

BAUER, CARL AUGUST. A Report on New Spectrographic Material of 13 Ceti 302

BURMAN, U. R., and N. R. SEN. On an Approximate Solar Model on Bethe's Law of Energy Generation 347

CESCO, C. U., S. CHANDRASEKHAR, and J. SAHADE. On the Radiative Equilibrium of a Stellar Atmosphere. IV 355

CESCO, CARLOS U., and JORGE SAHADE. The Spectroscopic Orbit of AR Monocerotis . . 374

CESCO, CARLOS U., OTTO STRUVE, and JORGE SAHADE. The Spectroscopic Orbit of BD Virginis 181

CHANDRASEKHAR, S. On the Radiative Equilibrium of a Stellar Atmosphere. II . . . 76

CHANDRASEKHAR, S. On the Radiative Equilibrium of a Stellar Atmosphere. III . . . 117

CHANDRASEKHAR, S. Some Remarks on the Negative Hydrogen Ion and Its Absorption Coefficient 176

CHANDRASEKHAR, S., C. U. CESCO, and J. SAHADE. On the Radiative Equilibrium of a Stellar Atmosphere. IV. 355

CHANDRASEKHAR, S., and RUPERT WILDT. On the Absorption Continuum of the Negative Oxygen Ion 87

CUFFEY, J. Review of: *Basic Marine Navigation*, Bart J. Bok and Frances W. Wright . 115

DEUTSCH, A. J., and O. STRUVE. A Change in the Spectrum of 39ϵ Capricorni . . . 390

DWYER, ROBERT J. Solar Concentrations of the Hydroxyl Radical 300

EDMONDSON, FRANK K., and HENRY GICLAS. BN Monocerotis: An N-Type Variable . . 1

GAPOSCHKIN, CECILIA PAYNE. The Eclipsing Star AR Monocerotis 251

GAPOSCHKIN, CECILIA PAYNE. The Eclipsing Star BD Virginis 186

GAPOSCHKIN, SERGEI. The Eclipsing System RX Cassiopeiae 230

GAPOSCHKIN, SERGEI. The Eclipsing System SX Cassiopeiae 221

GAPOSCHKIN, SERGEI. The Wolf-Rayet Eclipsing Variable HV 11086 = HD 214419. . 242

GICLAS, HENRY, and FRANK K. EDMONDSON. BN Monocerotis: An N-Type Variable . 1

GLEISSBERG, W. Note on the Epoch of the Next Sunspot Maximum 114

GLEISSBERG, W. Note on the Latitude Variation of the Sunspot Belts 219

HARRISON, MARJORIE HALL. The Generalized Cowling Model 343

HYNEK, J. A. The Helium Anomaly in ϕ Persei 151

JOYNER, MARY C., and FREDERICK H. SEARES. Relation between Color Index and Effective Wave Length from the Observations of Hertzsprung and Vanderlinden . . . 264

KOPAL, ZDENĚK. A Study of the Wolf-Rayet Eclipsing Binary HD 193576 = V 444 Cygni 204

KROGDAHL, MARGARET K. The Interaction of a Proton and a Hydrogen Atom in Its Excited States 311

KROGDAHL, MARGARET KIESS. The Interaction of a Proton and a Helium Atom in Its Excited States 333

KUIPER, GERARD P. Titan: A Satellite with an Atmosphere 378

LEE, OLIVER JUSTIN. Review of: *Marine and Air Navigation*, John Q. Stewart and Newton L. Pierce 115

LUYTEN, W. J. Note on the Double White Dwarf L 462-56 = LDS 275 202

MCKELLAR, ANDREW. Comparison of the λ 3883 *CN* Band in the Spectra of Comets 1940c and 1942g 69

MCLAUGHLIN, DEAN B., and SUZANNE E. A. VAN DIJKE. The Spectrographic Orbit and Light-Variations of η Geminorum 63

MERRILL, PAUL W., and ROSCOE F. SANFORD. Spectroscopic Observations of 48 Librae . 14

NICHOLSON, SETH B. Orbit of the Ninth Satellite of Jupiter 57

PETTIT, EDISON. Effect of Temperature on the Wave Length of a Transmission Band of the Interference Polarizing Monochromator 128

POPPER, DANIEL M. Studies of Faint B-Type Stars. II 94

REBER, GROTE. Cosmic Static 279

RUSSELL, HENRY NORRIS. Provisional Elements of the Eclipsing Binary V 444 Cygni . 213

SAHADE, J., C. U. CESCO, and S. CHANDRASEKHAR. On the Radiative Equilibrium of a Stellar Atmosphere. IV 355

SAHADE, JORGE, and CARLOS U. CESCO. The Spectroscopic Orbit of AR Monocerotis . 374

SAHADE, JORGE, OTTO STRUVE, and CARLOS U. CESCO. The Spectroscopic Orbit of BD Virginis 181

SANFORD, ROSCOE F., and PAUL W. MERRILL. Spectroscopic Observations of 48 Librae . 14

SEARES, FREDERICK H. Regression Lines and the Functional Relation 255

SEARES, FREDERICK H., and MARY C. JOYNER. Relation between Color Index and Effective Wave Length from the Observations of Hertzsprung and Vanderlinden . . . 264

SEN, N. R., and U. R. BURMAN. On an Approximate Solar Model on Bethe's Law of Energy Generation 347

SHAJN, G. A. Recent Progress in Astrophysics 388

SMITH, BURKE, and OTTO STRUVE. The Radial Velocities of the Pleiades 360

STRUVE, O. "Physical Characteristics of the Atmospheres of Supergiants of Classes cB5 to cA3," by G. A. Shajn 388

STRUVE, O. Radial Velocities of Twenty Stars of Early Type in and near the Galactic Cluster NGC 6231 189

STRUVE, OTTO. A. Unsöld's Work on the Spectrum of the B0 Star τ Scorpii 105

STRUVE, OTTO. An Upper Limit for the Mass of the Lunar Atmosphere 104

STRUVE, OTTO. The Wolf-Rayet Type Spectroscopic Binary HD 152270 384

STRUVE, OTTO, CARLOS U. CESCO, and JORGE SAHADE. The Spectroscopic Orbit of BD Virginis 181

STRUVE, O., and A. J. DEUTSCH. A Change in the Spectrum of 39ϵ Capricorni . . . 390

STRUVE, OTTO, and BURKE SMITH. The Radial Velocities of the Pleiades 360

SWINGS, P. Doubly Ionized Rare Earths in α^2 Canum Venaticorum 132

TER HAAR, D. On the Origin of Smoke Particles in the Interstellar Gas 288

UNSÖLD, A. Recent Progress in Astrophysics 105

VAN DIJKE, SUZANNE E. A., and DEAN B. MCLAUGHLIN. The Spectrographic Orbit and Light-Variations of η Geminorum 63

VAN MAANEN, ADRIAAN. Investigations on Proper Motion. XXIII. The Proper Motion of the Cluster *h* Persei 31

VAN MAANEN, ADRIAAN. The Photographic Determination of Stellar Parallaxes with the 60- and 100-Inch Reflectors. Nineteenth Series 55

VINTER HANSEN, JULIE M. The Spectroscopic Binary 31 Cygni 8

WARES, GORDON W. Partially Degenerate Stellar Models 158

WILDT, RUPERT, and S. CHANDRASEKHAR. On the Absorption Continuum of the Negative Oxygen Ion 87

DEC 5 1944

VOLUME 100 NUMBER 3

THE ASTROPHYSICAL JOURNAL

AN INTERNATIONAL REVIEW OF SPECTROSCOPY AND ASTRONOMICAL PHYSICS

Founded in 1895 by GEORGE E. HALE *and* JAMES E. KEELER

Edited by

PAUL W. MERRILL
Mount Wilson Observatory of the Carnegie Institution of Washington

HARLOW SHAPLEY
Harvard College Observatory Cambridge, Massachusetts

J. H. MOORE
Lick Observatory University of California

OTTO STRUVE
Yerkes Observatory of the University of Chicago

NOVEMBER 1944

THE ECLIPSING SYSTEM SX CASSIOPEIAE . . . . . *Sergei Gaposchkin* 221
THE ECLIPSING SYSTEM RX CASSIOPEIAE . . . . . *Sergei Gaposchkin* 230
THE WOLF-RAYET ECLIPSING VARIABLE HV 11086 = HD 214419 . *Sergei Gaposchkin* 242
THE ECLIPSING STAR AR MONOCEROTIS . . . . . *Cecilia Payne Gaposchkin* 251
REGRESSION LINES AND THE FUNCTIONAL RELATION . . . *Frederick H. Seares* 255
RELATION BETWEEN COLOR INDEX AND EFFECTIVE WAVE LENGTH FROM THE OBSERVATIONS OF HERTZSPRUNG AND VANDERLINDEN
Frederick H. Seares and Mary C. Joyner 264
COSMIC STATIC . . . . . *Grote Reber* 279
ON THE ORIGIN OF SMOKE PARTICLES IN THE INTERSTELLAR GAS *D. ter Haar* 288
SOLAR CONCENTRATIONS OF THE HYDROXYL RADICAL . . . *Robert J. Dwyer* 300
A REPORT ON NEW SPECTROGRAPHIC MATERIAL OF 13 CE TI *Carl August Bauer* 302
THE INTERACTION OF A PROTON AND A HYDROGEN ATOM IN ITS EXCITED STATES . . . . . *Margaret K. Krogdahl* 311
THE INTERACTION OF A PROTON AND A HELIUM ATOM IN ITS EXCITED STATES . . . . . *Margaret Kiess Krogdahl* 333
THE GENERALIZED COWLING MODEL . . . . . *Marjorie Hall Harrison* 343
AN APPROXIMATE SOLAR MODEL ON BETHE'S LAW OF ENERGY GENERATION
N. R. Sen and U. R. Burman 347
ON THE RADIATIVE EQUILIBRIUM OF A STELLAR ATMOSPHERE. IV
C. U. Cesco, S. Chandrasekhar, and J. Sahade 355
THE RADIAL VELOCITIES OF THE PLEIADES . . . . *Burke Smith and Otto Struve* 360
THE SPECTROSCOPIC ORBIT OF AR MONOCEROTIS *Jorge Sahade and Carlos U. Cesco* 374
TITAN: A SATELLITE WITH AN ATMOSPHERE . . . . . *Gerard P. Kuiper* 378
THE WOLF-RAYET TYPE SPECTROSCOPIC BINARY HD 152270 . . *Otto Struve* 384
RECENT PROGRESS IN ASTROPHYSICS
"PHYSICAL CHARACTERISTICS OF THE ATMOSPHERES OF SUPERGIANTS OF CLASSES cB5 TO cA3" BY G. A. SHAJN . . . . . *O. Struve* 388
NOTES
A CHANGE IN THE SPECTRUM OF 39 ε CAPRICORNI . . . *O. Struve and A. J. Deutsch* 390
INDEX 391

THE UNIVERSITY OF CHICAGO PRESS
CHICAGO, ILLINOIS, U.S.A.

November 1944 Vol. 100, No. 3

THE ASTROPHYSICAL JOURNAL

AN INTERNATIONAL REVIEW OF SPECTROSCOPY AND ASTRONOMICAL PHYSICS

Edited by

PAUL W. MERRILL
Mount Wilson Observatory of the Carnegie Institution of Washington

HARLOW SHAPLEY
Harvard College Observatory
Cambridge, Massachusetts

J. H. MOORE
Lick Observatory
University of California

OTTO STRUVE
Yerkes Observatory of the University of Chicago

With the Collaboration of the American Astronomical Society

Collaborating Editors:

1942-44
CECILIA H. PAYNE GAPOSCHKIN
Harvard College Observatory

H. N. RUSSELL
Princeton University

F. H. SEARES
Mount Wilson Observatory

1943-45
S. B. NICHOLSON
Mount Wilson Observatory

D. B. McLAUGHLIN
University of Michigan

J. A. PEARCE
Dominion Astrophysical Observatory, Victoria

1944-46
JOEL STEBBINS
Washburn Observatory

A. N. VYSSOTSKY
Leander McCormick Observatory

W. W. MORGAN
Yerkes Observatory

The Astrophysical Journal is published bimonthly by the University of Chicago at the University of Chicago Press, 5750 Ellis Avenue, Chicago, Illinois, during July, September, November, January, March, and May. ¶The subscription price is $10.00 a year; the price of single copies is $2.00. Orders for service of less than a full year will be charged at the single-copy rate. ¶Postage is prepaid by the publishers on all orders from the United States and its possessions, Argentina, Bolivia, Brazil, Chile, Colombia, Costa Rica, Cuba, Dominican Republic, Ecuador, Guatemala, Haiti, Republic of Honduras, Mexico, Morocco (Spanish Zone), Nicaragua, Panama, Paraguay, Peru, Rio de Oro, El Salvador, Spain (including Balearic Islands, Canary Islands, and the Spanish Offices in Northern Africa; Andorra), Spanish Guinea, Uruguay, and Venezuela. ¶Postage is charged extra as follows: for Canada and Newfoundland, 42 cents on annual subscriptions (total $10.42); on single copies, 7 cents (total $2.07); for all other countries in the Postal Union, 96 cents on annual subscriptions (total $10.96), on single copies 16 cents (total $2.16). ¶Patrons are requested to make all remittances payable to The University of Chicago Press, in United States currency or its equivalent by postal or express money orders or bank drafts.

The following are authorized agents:

For the British Empire, except North America, India, and Australasia: The Cambridge University Press, Bentley House, 200 Euston Road, London, N.W. 1, England. Prices of yearly subscriptions and of single copies may be had on application.

Claims for missing numbers should be made within the month following the regular month of publication. The publishers expect to supply missing numbers free only when losses have been sustained in transit, and when the reserve stock will permit.

Business correspondence should be addressed to The University of Chicago Press, Chicago 37, Illinois.

Communications for the editors and manuscripts should be addressed to: Otto Struve, Editor of THE ASTROPHYSICAL JOURNAL, Yerkes Observatory, Williams Bay, Wisconsin.

Line drawings and photographs should be made by the author, and all marginal notes such as co-ordinates, wave lengths, etc., should be included in the cuts. It will not be possible to set up such material in type.

One copy of the corrected galley proof should be returned as soon as possible to the editor, Yerkes Observatory, Williams Bay, Wisconsin. Authors should take notice that the manuscript will not be sent to them with the proof.

The cable address is "Observatory, Williamsbay, Wisconsin."

The articles in this journal are indexed in the *International Index to Periodicals*, New York, N.Y.

Applications for permission to quote from this journal should be addressed to The University of Chicago Press, and will be freely granted.

Entered as second-class matter, July 31, 1940, at the Post-Office at Chicago, Ill., under the act of March 3, 1879.
Acceptance for mailing at special rate of postage provided for in United States Postal Act of October 3, 1917, Section 1103, amended February 28, 1925.

[PRINTED IN U.S.A.]

THE PHILOSOPHY OF PHYSICAL SCIENCE

by Sir Arthur Eddington

Eddington here develops the principles of philosophic thought associated with the modern advances of science. He examines the principles of relativity and quantum and presents a general philosophical outlook which he believes a scientist can accept. *"A book like Eddington's is a spiritual necessity."*—New York Times Book Review. $2.50

PHYSICS AND PHILOSOPHY

by Sir James Jeans

This book discusses that territory which forms a borderland between physics and philosophy, and which has become increasingly important through recent developments in physics. The book touches on questions which closely concern human life, questions of free-will, determinism, and the nature of existence.

"There is no more eloquent, interesting or persuasive expositor of what may be called the science of philosophy than Sir James Jeans, and this latest book of his will for that reason be welcomed by those who want questions about the nature of things answered."—New York Times Book Review. $2.75

COSMIC RAYS

by Robert A. Millikan

This book surveys the history of research in cosmic rays and discusses the methods and machinery that have been used. Twenty-four illustrations, including remarkable cloud-chamber photographs, are a feature of the book. *"A clear account of the remarkable research and stimulating theories pertaining to cosmic rays, that will be read with profit not only by specialists in the field, but also by others."*—Scientific Book Club Review. $2.50

CAMBRIDGE UNIVERSITY PRESS

THE MACMILLAN COMPANY

60 Fifth Avenue, New York 11, N.Y.

THE flashing colors of a diamond and the clear tints of a rainbow had been seen by countless people before Sir Isaac Newton asked, "How are these colors formed?"

His memoir on "Opticks" records the answer in a quaintly worded Theorem: "The light of the sun consists of rays differently refrangible." This conclusion, based on many experiments with crude glass prisms and a pencil of sunlight slanting into a shuttered room, laid the foundation of all spectroscopy. Further, it led Newton to invent the reflecting telescope, because he thought that his prismatic colors would make an achromatic lens forever impossible.

Today, Sir Isaac Newton's successors are exploring new worlds of astronomy, chemistry, metallurgy, photography and vision with lenses and prisms in instruments of constantly increasing accuracy. Many of these modern explorers—in industry, education and the armed forces—have called on Perkin-Elmer for help in blazing new trails in optical science.

This exchange of ideas with leaders in the sciences plus war-inspired production methods will enable Perkin-Elmer to incorporate in postwar scientific optical instruments extra refinements that will open up new avenues of investigation.

WHAT PERKIN-ELMER MAKES

Custom-built optical instruments for industrial analysis, control, inspection.

New optical devices to solve specific problems, such as the all-purpose infrared spectrometer.

Special elements: fine lenses, prisms, flats, photographic objectives, interferometer plates, retardation plates, Cornu prisms, Rochon prisms, Nicol prisms.

Perkin-Elmer is now 100% in war work, but after the war will resume manufacture of such peace-time products as Schmidt cameras, refracting and reflecting telescopes, equatorial mountings, oculars, direct-vision prisms, polarizing eye pieces, and other equipment.

THE PERKIN-ELMER CORPORATION

GLENBROOK · CONN.